

Cell and Tissue Response to Osteoinductive Calcium Phosphate Architecture

NOEL DAVISON

Cell and Tissue Response to Osteoinductive Calcium Phosphate Architecture

NOEL DAVISON



THESES COMMITTEE

CHAIRMAN

Prof. Dr. J.W.M. Hilgenkamp

PROMOTER

Prof. Dr. Joost D. de Bruijn

ASSISTANT PROMOTER

Dr. Florence Barrère-de Groot

MEMBERS

Prof. Dr. Clemens A. van Blitterswijk

Prof. Dr. Pascal Jonkheijm

Prof. Dr. Vincent Everts

Prof. Dr. Pierre Layrolle

Prof. Dr. John A. Jansen

Dr. Pamela Habibovic

Dr. Moyo C. Kruyt

Cover image: fluorescent micrograph of a human osteoclast resorbing osteoinductive calcium phosphate (Chapter 6). Captured by Bas ten Harkel and Noel Davison.

Cover art and graphic design by Mateusz Kus.

Photography of the author by Rens Roosloot.

Research conducted in this thesis was fully supported by:



Financial support of this thesis was generously provided by:



Anna
Fonds

MIRA
BIOMEDICAL TECHNOLOGY
AND TECHNICAL MEDICINE

CELL AND TISSUE RESPONSE TO
OSTEOINDUCTIVE CALCIUM PHOSPHATE ARCHITECTURE

DISSERTATION

to obtain

the degree of doctor at the University of Twente,

on the authority of the rector magnificus

Prof. Dr. H. Brinksma

on account of the decision of the graduation committee,

to be publicly defended

on Wednesday November 19th, 2014 at 14:45

by

Noel Lee Davison

born December 9th, 1983

in Portland, Oregon, United States of America

P R O M O T E R

Prof. Dr. Joost D. de Bruijn

A S S I S T A N T P R O M O T E R

Dr. Florence Barrère-de Groot

© 2014 by Noel L. Davison. All rights reserved. No part of this document may be reproduced or transmitted in any form or by any means without prior written permission of the author.

ISBN: 978-90-365-3773-5

For Dad,

For Mom,

For Aria,

For Grandma and Grandpa: A-roop, A-roop!

CONTENTS

CHAPTER 1	8
General introduction	
CHAPTER 2	42
In vivo performance of microstructured calcium phosphate comprised in novel water-free carriers	
CHAPTER 3	66
Influence of surface microstructure and chemistry on osteoinduction and osteoclastogenesis by biphasic calcium phosphate discs	
CHAPTER 4	92
Submicron-scale surface architecture of tricalcium phosphate directs osteogenesis in vitro and in vivo	
CHAPTER 5	120
Liposomal clodronate inhibition of osteoclastogenesis and osteoinduction by submicrostructured beta-tricalcium phosphate	
CHAPTER 6	146
Osteoclast resorption of beta-tricalcium phosphate controlled by surface architecture	
CHAPTER 7	172
General discussion	
CHAPTER 8	192
Perspectives and future directions	
SUMMARY	208
ACKNOWLEDGEMENTS	212



M.C. Escher - Metamorphose III 1968
© The M.C. Escher Company, B.V. All rights reserved.

CHAPTER 1

General introduction

1 MODERN BIOMATERIAL DESIGN

Thanks to advances in biomaterial science, when certain tissues such as bone are damaged due to trauma or disease, biomaterials can be used in the clinic to repair the damage. Fifty years ago when biomaterials were first being intensively researched, the focus in their design was primarily biocompatibility to avoid rejection by the body [1]. Later, the goal was to design biomaterials to integrate with the body, and in the case of bone graft substitutes, later be degraded so that newly formed tissue could naturally take the place of the implant over time. Now, the modern view is that biomaterials should stimulate specific cellular responses to restore healthy tissue function where it has been lost [2,3]. To meet this goal, clinicians require biomaterials, such as bone graft substitutes or artificial skin, to be “smarter” in order to not only to avoid rejection by the body and provide a suitable substrate to support cell adhesion but also stimulate cell proliferation, differentiation, and specialized function. This aspect of a biomaterial to serve as an instructive cellular substrate or “scaffold” is integral to the field of regenerative medicine as it aims to stimulate the body’s own repair capacity to restore damaged tissue [4].

By studying how the body regenerates itself without clinical intervention, nature provides useful clues as to how to design biomaterials to stimulate and support the repair process. Cell and tissue morphogenesis during regeneration is heavily dictated by cues from cells’ own microenvironment, made up by the extracellular matrix (ECM) that fills the space between them. The ECM comprises both structural and matricellular proteins that provide specific signals to the cells, particularly during wound healing. Structural proteins such as collagen and fibrin provide a rigid, fibrous substrate for cells to adhere and migrate. Matricellular proteins such as osteopontin and tenascins transmit cellular signals to promote macrophage infiltration during early inflammation after injury, as well as subsequent reepithelialization for wound healing [5].

Cells form their own microenvironment by secreting various biomolecules such as proteins (e.g., collagen, vitronectin), carbohydrates (e.g., hyaluronan, chondroitin sulfate), and protein-carbohydrate complexes (e.g., aggrecan, decorin) that make up the ECM. In turn, the ECM gives shape, form, and mechanical properties to a given tissue. Moreover, it provides the substrate for cells to adhere, proliferate, and function [5]. In a powerful example of how instructive the ECM is to the function of the cells it contains, Uygun et al. (2010) showed that if a decellularized rat liver matrix is repopulated with donor liver cells, the tissue-engineered recellularized organ regains normal liver function and can be effectively transplanted [6].

A biomimetic approach to modern biomaterial design draws inspiration from natural ECM from a standpoint of chemical composition as well as physical structure. For instance, polymers can be functionalized with peptides that contain the same amino acid motifs of natural ECM proteins to promote cell adhesion through integrin binding. Long polymer chains can also be functionalized with peptide linkages so that they can be degraded in the body by specific enzyme proteases similar to how native ECM can be cellularly remodeled. These polymers can then be electrospun resulting in nano-scale fibers similar to the dimensionality of ECM structural proteins [7]. Likewise, calcium phosphates currently used as bone graft substitutes possess similar chemical composition to bone mineral and can be designed with an interconnected macro/micropore network evocative of bone architecture (e.g., trabeculae, lacunae, and canaliculi) that ensconce bone cells and allow for blood vessel perfusion [8,9]. As numerous investigators have already showed, biomaterial chemistry and physical structure – especially on similar size scales as cells themselves – both play important roles in their function in the body (Figure 1) [10]. These two material properties will be repeatedly tested throughout the course of this thesis in an effort to design better bone graft substitutes.

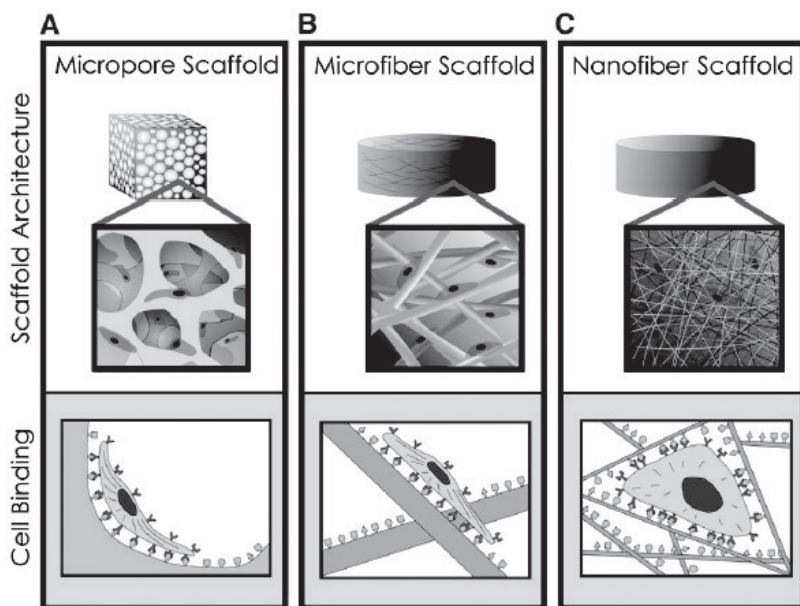


Figure 1. Architecture of biomaterial scaffolds. Scaffolds can be designed with micro-scale features such as pores and fibers (A, B) or nano-scale features such as nanofibers (C) (top row). The material surfaces adsorb serum proteins (yellow dots) that allow cell adhesion through integrin binding (red wishbones) (bottom row). Adapted from Stevens MM, George JH. Science 2005;310:1135–8.

2 BONE AND ITS REPAIR

The Yin and Yang of bone homeostasis

Bone tissue is created by osteoblasts and destroyed by osteoclasts through the cyclical process of bone remodeling. In order to maintain bone volume, bone deposition and resorption are tightly coupled [11]. In fact, in healthy adults, bone is typically deposited by osteoblasts precisely where it was first resorbed by osteoclasts, which is made possible by the membrane-bound and soluble signals produced by both cell types that regulate the other's migration, differentiation, and activity. Bone remodeling and coupling allows the body to add bone mass where it is needed (e.g., for skeletal growth and strength or bone repair), restructure it where more mechanical rigidity is necessary, and efficiently decrease it where it is not needed in a balanced system of anabolism and catabolism [12].

According to ancient Chinese philosophy and traditional medicine, Yin and Yang forces are necessary for natural balance because of their opposite nature. Despite their opposition, Yin paradoxically contains the seed of Yang, and Yang contains the seed of Yin; hence, each gives rise to the genesis of the other. Allegorically, bone formation by osteoblasts is balanced by bone resorption by osteoclasts, and each cell type regulates the differentiation of the other to maintain bone homeostasis (Figure 2).

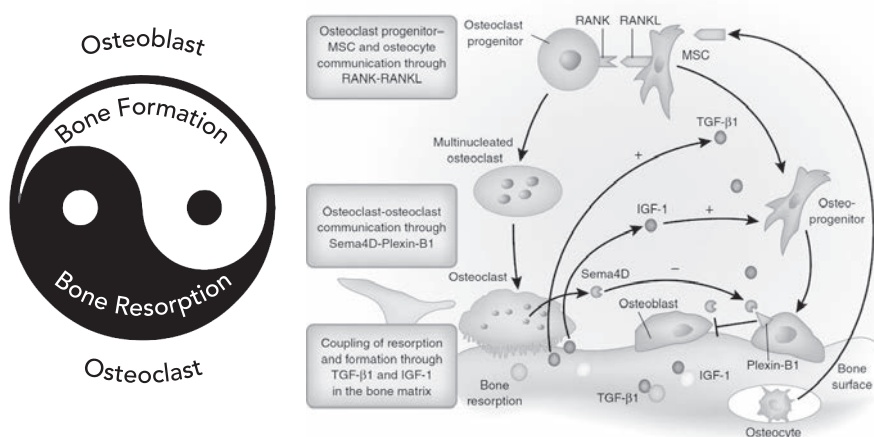


Figure 2. The Yin and Yang of bone homeostasis. Bone formation by osteoblasts and bone resorption by osteoclasts occurs in a tightly balanced process. Both soluble and membrane bound factors allow osteoblasts and osteoclasts to regulate each other's differentiation, maturation, and primary function. Regulatory schematic from Cao X, Nat Med. 2011 Nov 7;17(11):1344-6.

For example, osteoblasts regulate the formation and activity of osteoclasts through both cell-cell and soluble signaling. Specifically, osteoblasts express membrane-bound RANKL (receptor antagonist of NF- κ B receptor ligand) [13] and pre-osteoclasts of the monocyte/macrophage lineage express its membrane bound receptor RANK [14]; when RANK binds its ligand in the presence of macrophage colony stimulating factor (M-CSF), osteoclastogenesis is induced. Osteoclast differentiation is characterized by the fusion of mononuclear monocyte/macrophage precursors to form a multinucleated giant cell, activation of tartrate resistant acid phosphatase (TRAP), and expression of other specialized proteins that allow it to resorb bone. To more precisely control the formation of osteoclasts, osteoblasts also secrete osteoprotegerin (OPG), the endogenous decoy receptor to RANKL, in order to counterbalance osteoclast formation and activity [15]. In concert, osteoclasts regulate the differentiation and function of osteoblasts through cell-cell and soluble signaling as well. For example, Zhao et al. (2006) showed that osteoclasts express membrane-bound ephrinB2 and osteoblasts express its membrane-bound receptor EphB4. When ephrinB2 binds EphB4, bidirectional signaling ensues to attenuate osteoclast activity through the NFATc1 pathway and augment osteoblast differentiation and alkaline phosphatase (ALP) activity [16]. Osteoclasts also secrete soluble signals that induce osteoblast differentiation and bone formation, discussed in more detail later in this chapter. Together, these examples illustrate how the complex balance of bone homeostasis occurs through coupling of osteoblasts and osteoclasts through both cell-cell and soluble signals in order to equilibrate bone formation and bone resorption [12].

During bone formation, osteoblasts secrete bone matrix proteins (collectively, the osteoid) such as collagen I, osteocalcin, and bone sialoprotein that bind calcium (Ca^{2+}) and inorganic phosphate (P_i) ions from the body fluid to form mineralized bone tissue. In this way, bone tissue is essentially a composite of organic bone matrix proteins and inorganic, precipitated CaP mineral. During bone remodeling, osteoclasts devour both bone matrix proteins and bone mineral in a specialized process, which requires osteoclast-specific machinery discussed in more detail later in this thesis. The lamellar characteristic of mature bone, which confers its impressive mechanical strength in multiple directions (anisotropy), is only achieved through the remodeling of woven bone by osteoclasts [17]. Importantly, bone homeostasis also requires an established vascular system to supply the bone tissue with oxygen and nutrients for the heavy metabolic load of bone formation and remodeling [18,19].

Bone autograft: the model material for repairing bony defects

The body is naturally capable of regenerating damaged bone tissue but only to an extent. Beyond a certain “critical size,” a bone defect will not heal on its own and must be surgically repaired using bone grafts to stimulate and support new bone formation in the defect space. An estimated 2.2 million bone grafting procedures occur worldwide per year, including fracture repair, bone tumor resection, orthopaedic prosthetic revision, spine fusion, maxillary sinus lift, and cleft palate repair [20]. Despite the drawbacks of requiring a second surgery and potential risks to the patient, bone autograft is still primarily used in these procedures because it embodies all of the characteristics of an ideal graft material: specifically, it is osteoconductive, resorbable, osteoinductive, osteogenic, and non-immunogenic [21]. The osteoconductivity of autologous bone due to its surface layer of CaP mineral allows native bone to bond to it and grow, providing a template for new bone formation in the defect space. The resorbability of autologous bone is due to its capacity to be remodeled by osteoclasts, allowing for new bone tissue to gradually take the place of the graft with no loss of mechanical integrity. Its non-immunogenicity makes it preferred by surgeons over allograft, which is taken from human donors and always bears the risk of disease transmission. Still, synthetic materials have demonstrated all of these desirable attributes for decades now [22,23].

What sets autograft apart from most synthetic materials and why it is still the gold standard of care is because of its osteogenicity and osteoinductivity. Autograft is osteogenic because it naturally contains osteoblasts and bone marrow cells, which are thought to proliferate and form new bone in the defect space after transplantation. Still, it is unclear how many of these transplanted cells survive in the process and what their role in new bone formation actually is (e.g., stimulatory or direct) [24]. Bone autograft’s osteoinductivity means that it can stimulate new bone formation where no bone was already present (i.e., de novo) through recruitment and differentiation of uncommitted precursor cells, a feature that is particularly useful for repairing critical sized bone defects that are too large for the body to repair on its own.

Bone’s intrinsic osteoinductive capacity was best described by Urist in 1965, when he showed that demineralized bone matrix induced de novo bone in the muscle tissue of rabbits, rats, mice, and guinea pigs [25]. Both foreign body giant cells and “wandering histiocytes” (i.e., tissue macrophages) were almost immediately present at the implantation site and degraded the matrix, suggesting that interactions between the material and the innate immune response were important for the subsequent bone formation. Mechanistically, he speculated that

the cellular “inductor” of de novo bone formation were the tissue macrophages and the “induced” cells that differentiated into bone-forming osteoblasts were the progeny of soft tissue or perivascular precursors. Later, his group identified the origin of these osteoinductive effects: anabolic proteins present in the bone matrix, namely bone morphogenetic proteins (BMPs) [26].

3 CALCIUM PHOSPHATES AS BONE GRAFT SUBSTITUTES

History to the state of the art

To overcome the limitations of bone autograft, current research aims at replicating bone autograft’s desirable attributes in novel synthetic bone graft substitutes. Despite decades in development, synthetic bone graft substitutes still only represent less than 10% of the bone graft market [20]. Bioceramics composed of calcium phosphate – or simply calcium phosphates (CaPs) – are the largest class of synthetic bone graft substitutes and have been used in the clinics since the 1970’s due to their osteoconductive properties. Given their brittle mechanical properties, the clinical applications of CaPs are limited to filling small bone voids or larger defects along with metal screws and plates to provide mechanical support until bone is formed in the defect space [27]. From a commercial standpoint, about half of bone graft substitutes in the U.S. are used in spine fusion procedures, when the surgeon wants to bridge bone between 2 or more vertebral bodies in place of a ruptured or degenerated disc in order to prevent micromotion and pain [28].

The development of the first generation of commercially available CaPs used in the clinics – mainly hydroxyapatite (HA) – focused on osteoconductivity and bioactivity to support bone formation and bond to the existing bone tissue. This aim was achieved mainly through their similar composition to bone mineral [27,29,30] and their capacity to form a mineralized layer of bone-like carbonate apatite on their surface through the dissolution-reprecipitation of Ca^{2+} / P_i ions in the body fluid [31–33]. Later, de Bruijn et al. (1995) showed the importance of material degradation to bone bonding by highlighting that bone matrix was deposited where the surface of HA implants were first degraded [34]; thus, bioactivity and altered microtopography of the degraded/resorbed surface may together determine bone bonding.

Because HA is largely non-resorbable, other CaPs composed of more soluble crystalline phases such as tricalcium phosphate (TCP) or biphasic mixtures of HA and TCP (BCPs) were increasingly researched in order to better integrate them

with the body. In addition to bone bonding, CaP resorbability is an important material attribute in order for the body to eventually replace the material with new bone and restore the original tissue functionality. If a bone graft substitute is not resorbable, the surrounding native bone may become weaker over time because the implant shoulders a disproportionate share of the mechanical load (i.e., stress-shielding) [35].

In order to impart osteoinductive performance to CaPs, BMPs were later added because they bind CaP with high efficiency and remain active to differentiate osteoblasts from precursors at the implantation site [36]. For instance, Oda et al. (1997) showed that BCP loaded with BMP2 formed ectopic bone subcutaneously in rats. Later, Boden et al. (1999) showed that a similar BCP-BMP2 complex could effectively initiate lumbar fusion in non-human primates, thus paving the way for their clinical use [37]. Despite the attractive advantages of adding BMPs to CaPs or other bone graft substitutes, there may be a considerable risk in their use. In 2008, the FDA released a statement warning healthcare practitioners of the dangers of off-label BMP use (e.g., cervical spine fusion) because this could result in excessive bone formation, which could fatally block the airway [38]. In 2014, Medtronic Inc. announced that it would pay \$22 million to settle ~950 lawsuits against its product Infuse® – one of two FDA-approved BMP bone graft substitutes on the market – and set aside an additional \$120-140 million to resolve another 3,000 additional pending claims related to injuries from off-label use [39].

A tissue-engineering approach of combining stem cells with a CaPs attempts to impart osteogenicity to bone graft substitutes [40]. In this strategy, the CaP material acts as an osteoconductive scaffold for the delivery of allogeneic stem cells that have been expanded in vitro. Tissue-engineered bone graft substitutes have had limited success in clinical applications such as repairing fracture non-unions [41] and more success in small spine fusion trials [42], although in various intra-oral defects, bone formation occurred only in 1 out of 10 patients [43]. Two of the biggest challenges to this approach are (1) expanding a renewable source of progenitor cells in vitro to adequately seed the CaP scaffold and significantly improve the clinical outcome, and (2) keeping the seeded cells alive after implantation [44]. To gain regulatory approval for these combination products and access the market, the stem cell expansion method must be proven safe and efficacious in generating minimally altered, non-immunogenic, osteogenic cells using Good Manufacturing Practices (GMP) and Good Tissue Practices (GTP); however, currently there is no gold-standard approach [42]. Regarding implanted stem cell viability in the bone defect, ischemia and hypoxia greatly reduce bone and stem cell viability in vitro [45,46] and are likely a major cause

of why implanted stem cells only occasionally remain viable and form bone in large defects where this approach is most relevant [43]. Thus, tissue-engineered approaches to making bone graft substitutes osteogenic may also require vasculogenic growth factors or blood vessel grafting in order to outperform other existing products like BMPs [44,47]. Another question relates to the biological function of the applied MSCs – for instance, do they actually form new bone tissue directly or indirectly orchestrate the process through cytokine secretion [48]?

To sidestep some of the hurdles facing tissue-engineered bone graft substitutes, there are at least two FDA-approved products – Osteocel Plus® and Trinity Evolution® – that combine bone allograft with allogeneic stem cells originating from the same donor bone. Instead of devitalizing the bone like other allograft processing, these graft materials reportedly undergo complex antibody washing steps to specifically remove platelets and lymphocytes that would cause an immune reaction in the host, but leave the osteogenic, non-immunogenic stem cells intact [49]. Demineralized bone matrix (DBM) from the cortical bone portion of the donor bone is also processed and added back to the final graft material to impart osteoinductivity along with the osteoconductivity and osteogenic cells of the allograft bone [49]. Of course, the limitation of this approach is the acquisition of a constant supply of donor bone and ensuring with high certainty that it is free of disease and pathogens [42]. Moreover, little research has been presented in the literature to clarify what impact allogeneic cells have on the clinical outcome of these combination products since they already contain osteoinductive BMPs in the DBM. Still, this market segment is growing rapidly with a handful of other similar products awaiting regulatory approval [42].

As an alternative to the expensive, complicated, and potentially risky pharmacological and tissue engineering approaches to make CaPs osteoinductive like bone autograft, a small subset of CaPs have been described with intrinsic osteoinductive capacity – i.e., without exogenous growth factors or cells. Despite the fact that these materials have been described and researched for over 20 years, the cellular mechanism is still largely unknown; however, some material properties have been identified as important to the process, which will be discussed later in this chapter [27,50]. Even without a clear cellular mechanism, some groups have already shown that osteoinductive CaPs may provide a promising alternative to merely osteoconductive CaPs, BMPs, or even bone autograft for the repair of large bone defects. For instance, Habibovic et al. (2006) showed that a porous, osteoinductive BCP implant induced extensive bone in the middle of a critical sized sheep ilium defect but a comparable non-inductive BCP only allowed bone conduction around its outer edge [51]. Later,

Yuan et al. (2010) showed that by implanting a more resorbable, osteoinductive TCP in a similar defect, bone formation was significantly better than BMP2 and comparable to bone autograft [52].

Surgeons often require bone graft substitutes that are both osteoinductive and resorbable at similar rates like bone autograft, so that remodeling can occur lockstep with de novo bone formation and there is no loss of bone volume or mechanical rigidity over time. In many instances, they also require materials that can be molded or shaped to fill complex defect shapes and stay at the implantation site without affecting their bone formation or resorption [35].

Before these important challenges are tackled in this thesis, more background is required on two distinct but linked systems that dictate osteoinduction and material resorption: (1) the necessary cell and tissue responses, and (2) the relevant material properties and characteristics that may direct them. Prior to bone formation or material resorption of CaP implants, the host response exerts substantial influence on their function as bone graft substitutes [53], so this is an important point to begin.

The host response

When any biomaterial is implanted in the body, it is immediately surrounded by body fluid, and in milliseconds, the material surface adsorbs serum proteins. In the case of bioactive materials, the material surface begins exchanging ions with the body fluid. In hours, immune cells home to the implant in order to clear the foreign body from the host. At the material surface, these invading cells, mainly neutrophils and monocyte/macrophages, bind to the adsorbed serum proteins, and attempt to break it down through phagocytosis in a process that results in macrophage secretion of inflammatory cytokines. In fact, the inflammatory response of macrophages to HA particles is mediated by the same cellular toll-like receptors (TLRs) that enable macrophage recognition of microbial pathogens [54].

During the inflammatory response, macrophage-material interactions dictate the subsequent tissue response with widely variable outcomes. For instance, depending on their activation state, macrophages can secrete certain cytokines leading to fibrous tissue encapsulation of an implant in the body for its lifetime [55]. In different polarization states, activated macrophages can also direct angiogenesis and wound healing by secreting an entirely different subset of cytokines [56]. For instance, if macrophages are depleted in experimentally induced wounds, healing is severely hindered underscoring their importance in regenerating damaged tissue [57]. Biomaterial topography [58] and chemistry

[59] significantly influence these various macrophage responses in vitro and in vivo although the molecular mechanisms are not completely understood [56,60].

The innate inflammatory reaction may be particularly important to bone graft substitutes in terms of both osteogenesis and osteoclastogenesis because of the interplay between bone and the immune system. This has probably been best shown indirectly by osteoimmunological research into inflammatory signaling during bone fracture repair. For instance, Alexander et al. (2011) and Glass et al. (2011) both showed that without osteal macrophages (OsteoMacs) or macrophage-secreted inflammatory cytokine TNF α , tibial fracture healing in mice was severely limited due to lack of migration and differentiation of osteoblasts [61,62]. Glass et al. went a step further and showed that by adding TNF α to a fracture with an intact macrophage population, fracture healing was accelerated [61]. In addition to osteogenesis, TNF α and other related inflammatory cytokines, such as interleukin-1 (IL-1), IL-6, and prostaglandin E₂ (PGE2) also promote the formation of osteoclasts through the upregulation of RANK and RANKL and downregulation of OPG [63].

With respect to bone graft substitutes, it is possible to influence the innate inflammatory reaction to CaPs by changing their physical and chemical properties [53,55]. Concerning physical geometry, Malard et al. (1999) described how smaller BCP granules, sized 10-20 μm , incited a stronger initial inflammatory response along with superior bony ingrowth and resorption versus larger granules sized 80-100 or 200-400 μm [64]. Concerning chemical composition, Ghanaati et al. (2012) showed that while maintaining macroporosity, microporosity, granule size, and geometry constant, TCP and BCP formed significantly more multinucleated giant cells than HA after 10 days implantation under the skin of rats. At similar time points, TCP and BCP also formed significantly more microvessels than HA, which the authors linked to the early inflammatory response, giant cell formation, and vascular endothelial growth factor (VEGF) expression; still, none of the materials induced de novo bone formation. More research is necessary to explain this relationship, for instance, how material physical and chemical attributes mechanistically influence the inflammatory reaction, and how the inflammatory reaction is potentially linked with osteogenesis. By answering these questions, it may be possible to engineer CaPs to leverage the innate inflammatory response toward enhanced bone formation and material resorption by modulating the interactions of immune cells, such as macrophages, with the material surface.

Cell adhesion and function

The host response to CaPs occurs primarily at the material surface, where ions, proteins, and cells all converge in a complex exchange [10,53]. How is it then that a CaP surface can evoke such different cell and tissue responses resulting in its ultimate success or failure as a bone graft substitute? Just as cells can sense physical and biochemical cues from their microenvironment through adhesion to their ECM substrate, they can also sense cues through adhesion to a biomaterial substrate [10]. Cells bind to surfaces – biological or synthetic – through specialized membrane-bound integrin receptors that recognize specific amino acid motifs in matrix proteins, notably arginine–glycine–aspartic acid (RGD). Because of this, matrix protein adsorption to the material surface, such as fibronectin and vitronectin, is prerequisite for cellular adhesion to the material surface [10].

Both biomaterial chemistry and physical topography have been shown to influence the types and amount of proteins that adsorb to the material surface. For instance, Webster et al. (2001) showed that nanophase alumina adsorbed more vitronectin than did smooth alumina, indicating that the topographical parameter of nanoscale roughness is a determinant factor in matrix protein adsorption [65]. The authors showed that with increased vitronectin adsorption, osteoblast adhesion also increased. In the same year, Webster et al. (2001) showed that osteoclast activation and resorption was also promoted by nanophase alumina, as well as nanophase HA, versus their respective smooth surface controls, which the authors attributed to increased wettability and commensurate matrix protein adhesion [66]. Separately, McNally et al. (2007) reported that of several different matrix proteins, vitronectin is crucial for the fusion of foreign body giant cells from mononuclear macrophage precursors in vitro, one of the key events that characterizes the foreign body response and innate inflammatory reaction [67]. With respect to material chemistry, Keselowsky et al. (2003, 2004) showed that by changing the functional groups of self-assembled monolayers (SAMs) of alkanethiols on gold, fibronectin conformation was modulated and in turn affected how osteoblast-like MC3T3 cell integrins recognized and formed focal adhesions with the surface [68,69]. The authors speculated that the different wettability of the surfaces due to different functional group chemistries was the main material parameter that determined this effect. In view of all these examples, both biomaterial surface chemistry and topography guide the adhesion and differentiation of both bone cells and immune cells in ways that are likely important for synthetic bone graft substitutes.

After matrix proteins have adsorbed the biomaterial surface and cells adhere to

them, cell shape also changes in response to the matrix protein conformation and spatial orientation [70]. In effect, cells change their shape in order to more firmly adhere to the topographical features of their substrate because these features dictate where matrix proteins are absorbed [71]. Kilian et al. (2010) elegantly showed this by micropatterning adhesive islands in various shapes where fibronectin could be adsorbed, but it was unable to adsorb on the non-patterned areas of the substrate. Human mesenchymal stem cells (hMSCs) seeded on the substrate were forced to adhere to the fibronectin ligated to the islands and strikingly conformed their shapes to the pentagon, star, or flower shape of the islands. In this process, the cellular cytoskeleton stretched and bent to achieve the shape, which in turn triggered powerful transcriptional factors in the cell nucleus that determined the cells' phenotypic fate. For instance, conformation to the flower shape promoted differentiation to fat cells (adipogenesis) while the star shape promoted differentiation to osteoblasts [72]. This effect of gene regulation through physical interactions between cells and substrate topography is called mechanotransduction. The mechanical stimulus from actin rearrangement and cytoskeletal tension is transferred to the cell nucleus through various signaling pathways where gene transcription is changed (Figure 3) [73]. Following these principles, it may be possible to control protein adsorption, cell shape, and cell fate by changing the physical geometry of a CaP surface. For instance, it has been reported that changing the micropore size of polycarbonate surfaces can modulate the differentiation of pre-osteoblasts [74], a surface parameter that can also be readily tuned in CaP preparation [9].

Throughout the process of protein adsorption and cell adhesion, CaP surfaces also exchange ions with the body fluid with important implications for the cell and tissue response. As was discussed earlier, this exchange can lead to the precipitation of a layer of carbonate apatite, which may contribute to the bioactivity of the material. Ion exchange and dissolution at the material surface also changes the local ion concentrations available to regulate cell function. For instance, extracellular Ca^{2+} levels influence osteoblasts' adhesion to each other through calcium-dependent cadherins; in turn, cadherins are crucial for endochondral osteogenesis *in vivo* and blocking cadherins stunts osteoblast differentiation *in vitro* [75]. Extracellular Ca^{2+} and P_i levels have also been shown to directly modulate both osteoblastogenesis [76,77] and osteoclastogenesis [78,79] through unique signaling pathways. Both the physical structure and chemical composition of CaPs affects the rate at which they dissolve and reprecipitate ions on their surfaces – for instance, HA is less soluble than TCP and will therefore release less ions through dissolution in physiologic solutions than will TCP [80], and ceramics with more specific surface area (SSA) will tend to release a higher rate of ions [81].

Because the chemical and physical attributes of CaPs can affect protein adsorption, cell adhesion, and ion reactivity all at the same time, separating the biological effects of one material factor from another is challenging. Moreover, changing only one material parameter while maintaining all the others constant is virtually impossible. For instance, by imparting a nanophase surface to alumina, Webster et al. not only changed the surface roughness, a topographical parameter, but also the wettability and likely the surface energy [82], both physicochemical parameters. Additionally, the nanophase surface increased the SSA of the material, a geometric attribute of the material. So protein adhesion may have been increased by one or more material factors that were linked to surface nano/microroughness.

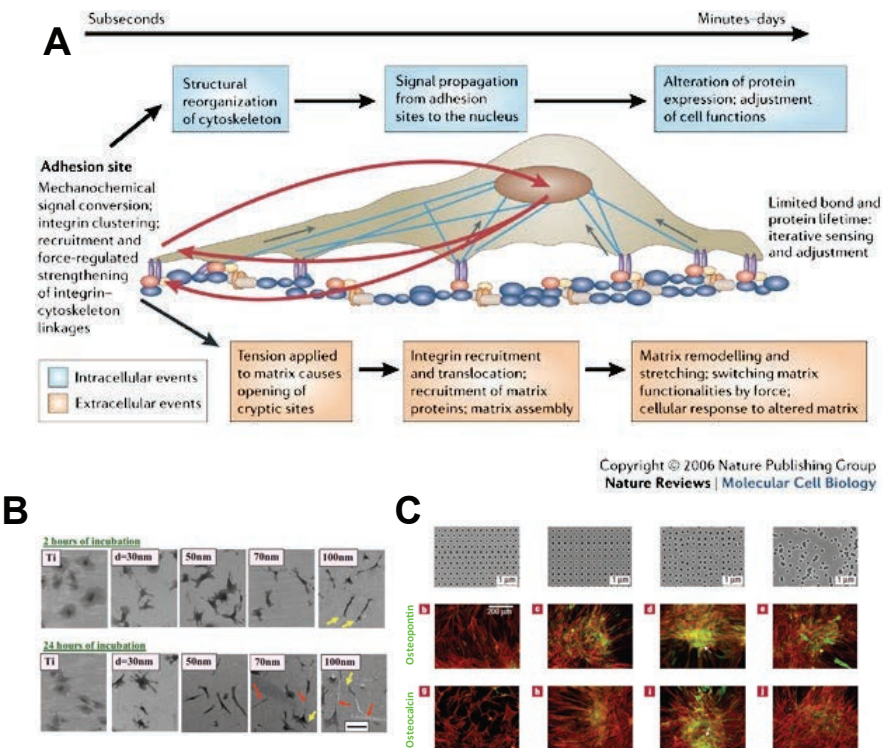


Figure 3. Mechanotransduction. Biomaterial surfaces can alter cell behavior and fate through mechanical signals transmitted to the nucleus (A). For example, cell shape and cell-cell junctions can be changed by the size of substrate surface features (B). Stem cell differentiation into osteoblasts can be modulated by how orderly or randomly surface features are arranged, shown by expression of bone matrix proteins osteopontin and osteocalcin (green stain) (C). Taken from (A) Vogel V, Sheetz M. Nat Rev Mol Cell Biol. 2006 Apr;7(4):265-75; (B) Oh S, et al. Proc Natl Acad Sci U S A. 2009 Feb 17;106(7):2130-5; (C) Dalby MJ, et al. Nat Mater. 2007 Dec;6(12):997-1003.

Biological degradation of calcium phosphates

Having considered the general cell and tissue response to CaP chemical composition and physical structure, these material parameters can be further tuned with the goal of mimicking bone autograft's resorbable properties. CaPs are broken down in the body through a complex, multifactorial process mainly involving passive physicochemical dissolution by the body fluid and active cellular degradation by osteoclasts and macrophages (often termed bioresorption) [83]. Mechanical forces may also disintegrate brittle ceramics over time but because CaPs are known to be mechanically weak and generally only used in non-loadbearing conditions or with load-bearing fixation, this mode of degradation is less relevant than the other modes. Both dissolution in the body fluid and cellular resorption are influenced by the physical structure and chemical composition of CaPs.

Considering first the effects of CaP chemical composition on dissolution and cellular resorption, BCP is a useful example. BCP dissolves more quickly in physiologic solutions the higher the HA/TCP ratio [80,83], and follows similar resorption profiles in bone defects [84,85]. However, studying the cellular resorption profiles *in vitro* is more complex. Intuitively, it would seem that osteoclasts would also be able to resorb BCP with lowest HA content the easiest, due to the way that osteoclastic resorption hinges on acidification of the substrate and subsequent dissolution of the ionic bonds that hold CaP (or bone mineral) together [86]. Indeed, Yamada et al. (1997) showed that osteoclasts cultured on BCP composed of either 25/75 or 75/25 percent HA/TCP ratios resorbed BCP with lower HA most extensively [87]. However, in the same study, TCP with even higher solubility than BCP was hardly resorbed. Later, Detch et al. (2008) reported similar findings of increased osteoclast resorption on HA versus TCP, which the authors speculated may have been due to inhibition of osteoclast resorption by excessive Ca^{2+} levels in the culture medium [88]. In sum, cellular resorption does not always follow the same trends as physicochemical dissolution with respect to CaP chemistry.

The physical structure of CaPs also influences both their dissolution and cellular resorption. As was discussed earlier, increasing the surface roughness or decreasing the surface topographical dimensions of a CaP will necessarily increase its SSA and expose more of the material to the physiologic solution for dissolution. Moreover, surface roughness and (sub)microtopography also change the way osteoclasts differentiate and resorb a mineralized substrate. In the previously discussed study by Webster et al. (2001), osteoclasts hardly resorbed alumina and HA ceramics with grains > 100 nm but proficiently resorbed them

with grains < 100 nm (i.e., nanophase), evidenced by characteristic resorption lacunae. This is particularly intriguing since these materials, at least without a nanophase surface, are characteristically non-resorbable in the body. The authors also noted a ~10 fold increase in tartrate resistant acid phosphatase (TRAP) activity, an enzyme marker of osteoclast differentiation and activation, on the nanophase materials. Costa-Rodrigues et al. (2012) showed that when osteoclasts derived from human peripheral blood mononuclear cells were cultured on HA with low, medium, and high submicroscale surface roughness ($R_a = 0.04 - 0.58 \mu\text{m}$), osteoclast resorption area increased linearly with increasing roughness [89]. Other groups have delved further into the mechanism of how surface topography may modulate osteoclast formation and differentiation – for instance, Makihira et al. (2007) showed that increasing titanium surface roughness ranging from $R_a \sim 0.10 - 1.25 \mu\text{m}$ directly increased RANK expression in RAW264.7 pre-osteoclasts, hence increasing their sensitivity to RANKL [90]. Another mechanistic explanation for how topography influences osteoclast activity and resorption was shown by Geblinger et al. (2010), when they described how surface roughness affects the way that osteoclasts form actin rings, the specialized cytoskeletal structures that allow osteoclasts to form a hermetic sealing zone with its substrate and resorb it. On a similar roughness range as investigated by Costa-Rodriguez and Makihira, Geblinger showed that osteoclast actin rings are small and unstable on a smooth calcite surface ($R_a = 0.12 \mu\text{m}$) but larger and more stable on a rough calcite surface ($R_a = 0.53 \mu\text{m}$).

Moreover, architecture on the macro-scale also plays a role in the way CaPs are degraded and resorbed in the body. Interconnected macropores ($> 100 \mu\text{m}$) increase the surface area available for physicochemical dissolution by the body fluid as well as allow for blood vessel perfusion to deliver a replenishing supply of pre-osteoclasts (monocyte/macrophages). Without isolating the effects of either physicochemical or cellular modes of resorption, von Doernberg et al. (2006) showed that TCP with macropores sized $510 \mu\text{m}$ across was resorbed more readily in the rabbit tibia after 6 weeks than either TCP with 150 or $260 \mu\text{m}$ sized pores [91]. The bulk geometry of CaPs is also important for their dissolution rate – for instance, as a geometric rule, CaP granules with decreasing particle diameter have increasing SSA available for dissolution and will tend to be resorbed by the body faster [64]. Although they are still biocompatible [92], CaP particles smaller than $\sim 10 \mu\text{m}$ will tend to be phagocytosed by macrophages during the foreign body response [55], delineating a lower particle size limit to still be useful as an osteoconductive material.

Tuning the physical structure and surface roughness of CaPs on the (sub)micro-scale, however, is an art unto itself and has been extensively researched in the literature for decades [8,93]. Surface grain and micropore size, microporosity, macropore size, and macroporosity can all be altered by changing the material composition (including trace ions and impurities), reaction kinetics, reaction temperature, mode of Ca-P precipitation, addition of porogens, sintering temperature(s), and sintering time profile to produce the final ceramic product [94,95]. In general, the higher the sintering temperature and longer the hold time, the more crystal grains will fuse and increase in size while simultaneously reducing the microporosity and the SSA [8].

Osteoinduction by calcium phosphates

Osteoconductive, resorbable CaPs have been used in the clinics for decades but mostly lack the main strength of bone autograft: osteoinductivity. Nonetheless, there is a small subset of CaPs and a handful of other biomaterials that have been described in the literature to be able to trigger de novo bone formation to varying extents – both in terms of bone volume and frequency of bone formation in animals (Figure 4). Despite considerable research, the precise material properties necessary to trigger osteoblast differentiation in ectopic locations where no bone exists and BMPs are not concentrated remains undefined. Less clear is the cellular mechanism by which these material factors actually differentiate osteoblasts from uncommitted precursors *in vivo*. However, through an iterative process spanning more than 20 years, some material properties and characteristics have repeatedly been shown to be important for the process of material-induced de novo bone formation and are discussed here. The theoretical basis for why these factors may be important and what cellular functions they are thought to direct will be discussed later in this chapter.

A wide range of CaP chemical compositions have been demonstrated to induce de novo bone formation. For example, certain HAs, various BCP blends, and some TCPs were all shown to be osteoinductive. Some non-CaPs, such as polymers (e.g., poly-HEMA), metallic ceramics (e.g., Al_2O_3 and TiO_2), metals (Ti), and Bioglass have also been shown to occasionally induce de novo bone formation, albeit in less volume than osteoinductive CaPs [50]. Because of this compositional variety, it has been inferred that osteoinductivity likely arises mainly from material architecture – both macrostructural and microstructural – and not so much the chemistry of the material. Still, physicochemical effects may play a role in the form of surface reactivity. For example, in their thorough review, Barradas et al. (2011) pointed out that all of these materials likely form a mineralized layer of carbonate apatite in body fluid, a factor that is theorized to

trigger osteoblast differentiation [50].

On the macro-scale, various groups have described geometric and architectural features such as concavities and interconnected macropores as critical for de novo bone formation (Figure 5). Ripamonti et al. (1999) noted that after dense HA discs machined with macro-concavities (800 and 1,600 μm) were implanted in the baboon muscle for 3 months, ectopic bone only formed in the well-defined concavities and not on the planar surfaces [96]. They then concluded that physical geometry on the macro-scale is the most important consideration for designing osteoinductive CaPs. Macropores have also been described as essential for osteoinduction. For instance, when Yamasaki and Sakai (1992) implanted porous and dense HA granules under the skin of dogs, only the porous granules induced de novo bone formation after 6 months [97]. Kuboki et al. (1998) later confirmed this finding when they combined porous and dense HA particles with BMP2 and implanted them under the skin of rats [98]. In lieu of macropores or well defined concavities, the spacing between microporous CaP granules [99] or channels machined into titanium mesh [100] can also provide a suitable environment for ectopic bone formation.

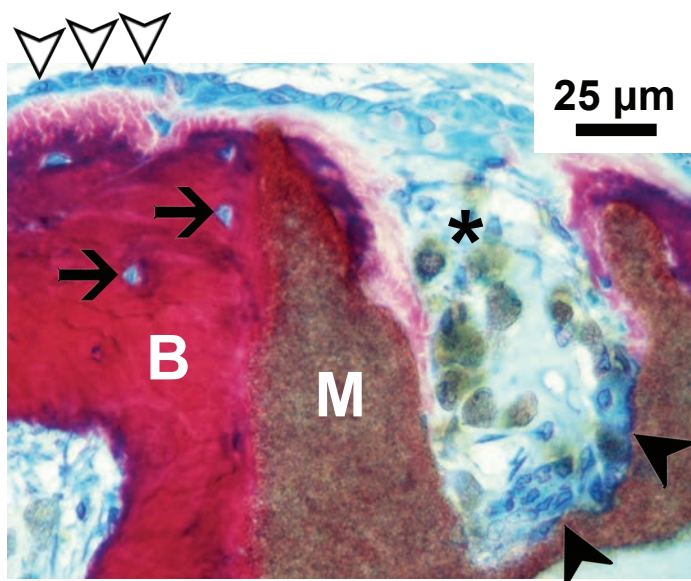


Figure 4. Osteoinductive and resorbable CaP. Microstructured TCP was implanted in the muscle tissue of dogs for 12 weeks and histological sections were stained using basic fuchsin/methylene blue. Mature de novo bone (B, red) containing osteocytes (black arrows) in their lacunae is tightly bonded to the material (M, brown) surface. Cuboidal osteoblasts (white arrowheads) in the pore space form osteoid (pink), the beginnings of bone. Multinucleated osteoclast-like cells (black arrowheads) resorb the material as degraded material particulate (asterisk) is phagocytosed in the pore space.

The groups of Yuan and Habibovic have done the most to show that altering the surface microstructure of CaPs can induce de novo bone formation intramuscularly in dogs, goats, and sheep [51,52,101–104]. As the authors have shown, raising the sintering temperature increases the size of surface grains (through grain fusion) and reduces the microporosity of the material, while maintaining the chemical and macrostructural characteristics constant. In their various studies cited above, microstructured HA, BCP, and TCP sintered at low temperatures, with surface micrograins and micropores sized ~1 µm in diameter, were all shown to be osteoinductive. In contrast, CaPs that were sintered at higher temperatures, with larger grains and little to no microporosity induced little to no bone formation. Interestingly, this effect of imparting small surface structure to a material surface for osteoinductive performance was also shown with titanium. Fujibayashi et al. (2004) and Fukuda et al. (2011) both showed that when a microporous surface structure was applied to macroporous titanium by chemical and thermal treatment, the materials induced de novo bone formation in the muscle of dogs, but without the surface microstructure they were inert [100,105].

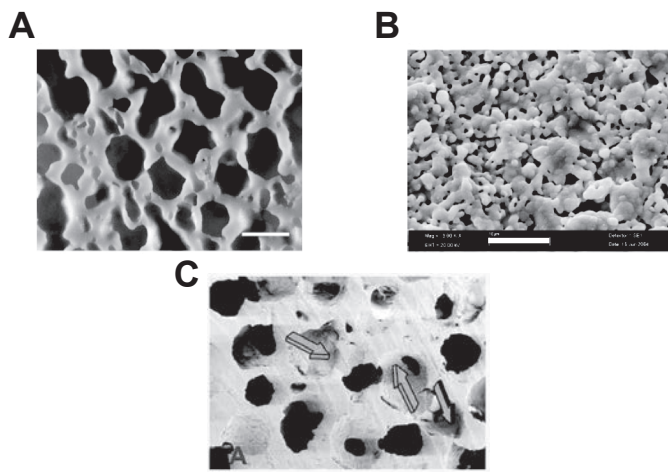


Figure 5. Architectural features reported to influence osteoinductivity by CaPs. Interconnected macropores (A, scale = 1 mm), surface microstructure (B, scale = 10 µm), and surface macroconcavities (C, blue arrows, scale = 200 µm) have all been implicated with osteoinduction by CaPs.

So, of all of these physicochemical and architectural factors is there one singular essential property needed to trigger de novo bone formation? Or do two or more of these factors operate together in necessary synergy? Moreover, what are their ideal specifications? For instance, if surface micrograins are indispensable for osteoinduction, how big should they be to induce the most bone? How fast or slow should Ca²⁺ precipitate or dissolve to most potently differentiate precursor

cells into osteoblasts? Challengingly, many of these material properties are interrelated and nearly impossible to independently change without changing another, as previously described using the example from Webster's nanophase alumina. The same analysis can be applied for osteoinductive CaPs. For instance, imparting a microstructured surface to BCP by sintering at lower temperature will change the surface micrograin and micropore size, and this will in turn alter the surface roughness. These topographical parameters will necessarily change the SSA of the material, and with respect to the physicochemical characteristics, higher surface roughness will likely change the surface free energy and wettability. Smaller grain necks resulting from lower sintering temperature will affect the solubility, not to mention the mechanical stiffness.

Underlying these hypothetical questions is a much more basic question, one whose answer will likely make designing osteoinductive CaPs much more purposeful rather than iterative:

What cascade of biological events occurs immediately after implanting an osteoinductive CaP that eventually leads to de novo bone formation?

It may be that in order to truly narrow down the material factors and specifications essential for osteoinduction, the biological process itself must first be elucidated.

4 THEORIES ON OSTEINDUCTION

To explain the relationship between these important material characteristics and osteoinduction, some theories have been presented in the literature that speculate on their biological function. They can essentially be divided into theories that (1) focus on the physicochemical aspects of osteoinductive materials and how they may stimulate osteoblast differentiation and (2) the architectural features of osteoinductive materials and how they may stimulate inflammation or osteoclastogenesis in order to eventually forming de novo bone. Both families of theories will be discussed and critically evaluated below.

Physicochemical theories on de novo bone formation

Physicochemical theories on osteoinductive CaPs postulate that macrostructural, microstructural, and chemical aspects of osteoinductive CaPs direct de novo bone formation because of their increased ability to form a layer of biological carbonate apatite and adsorb proteins from the body fluid, or because they increase the local concentrations of Ca^{2+} / P_i ions (Figure 6).

Physicochemical Theories on Osteoinduction

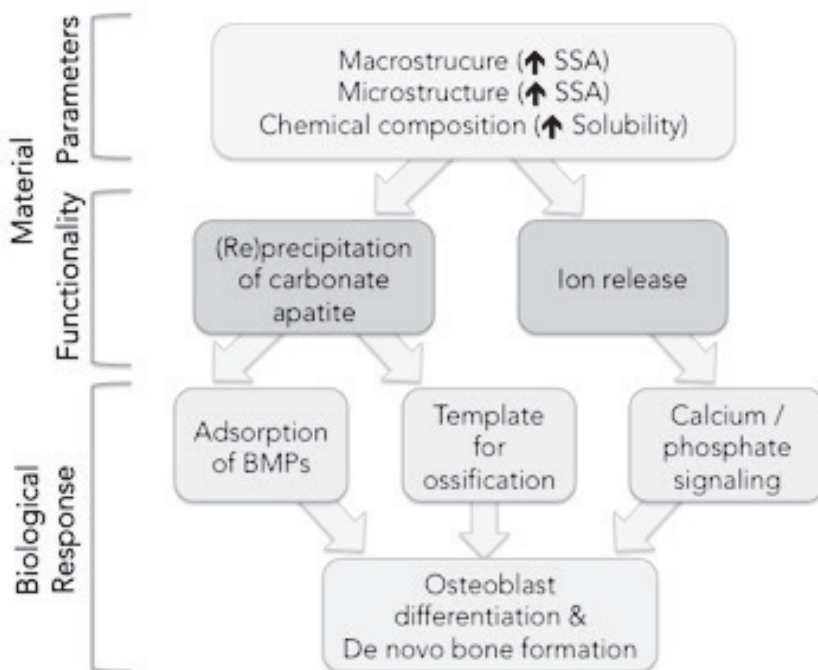


Figure 6. Physicochemical theories on osteoinduction. Material architectural parameters such as macrostructural features (e.g., interconnected macropores, concavities, intergrain space), microstructure (micrograins and micropores), and chemical composition have all been attributed with osteoinductive performance of CaPs. Macrostructural and microstructural parameters both increase specific surface area (SSA), which may increase the formation of a carbonate apatite layer on the material surface as well as ion release. Increasing the solubility of the chemical composition will also increase these functionalities. Formation of a carbonate apatite layer is thought to increase protein adsorption from the body fluid, such as circulating BMPs as well as act as a template for ossification. Release of Ca^{2+} / P_i ions from the material is suggested to initiate osteogenic Ca^{2+} / P_i signaling pathways. Together, these biological responses are thought to result in the differentiation of osteoblasts from uncommitted precursors and de novo bone formation, defining osteoinduction.

Early mechanistic research into the *in vivo* behavior of CaPs and their corresponding bone formation by Daculsi, Legeros and colleagues (1989, 1991) identified the precipitation of a carbonate apatite layer in the body fluid as a potential prerequisite for bone formation [85,106]. De Groot (1998) later elaborated that this layer could act as a collector of circulating BMPs resulting in its proposed osteogenic effects [107]. Habibovic and coworkers (2005) applied these theories to osteoinduction to explain why microstructured BCP stimulated more de novo bone formation in goats than HA with similar microstructure or

BCP with larger surface structure – namely that osteoinductive BCP had (1) higher SSA than BCP with larger structure and (2) higher solubility than HA, both theoretically promoting the formation of a carbonated apatite layer and anabolic protein adsorption [104]. However, no *in vivo* analysis of carbonate apatite formation or adsorption of osteoinductive proteins like BMPs was provided to support this theory.

Rather than precipitation, Barradas and colleagues (2013) speculated that increased Ca^{2+} release from the high SSA of osteoinductive microstructure or more soluble chemical composition may serve to trigger de novo bone formation [108]. Indeed, their group and others have demonstrated that increased concentrations of Ca^{2+} / P_i ions can activate osteogenic signaling pathways in precursor cells *in vitro* [108–111]. However, Yuan et al. (2001) showed that TCP composed of beta but not alpha crystalline phase induced de novo bone formation in dog muscle despite similar microstructure and macrostructure. They speculated the reason for this was that the solubility of alpha TCP was too high to allow for cell proliferation on the implant. Although there is no *in vivo* evidence to show that osteoinductive microstructure triggers de novo bone formation through enhanced Ca^{2+} / P_i release and associated signaling, Barradas et al. (2013) did show that osteoblast markers were upregulated in hMSCs cultured on microstructured (osteoinductive) TCP versus HA with larger surface structure (non-osteoinductive) [108]. Still, whether this effect was due to the differences in microstructure or differences in solubility was not shown. For example, there was no non-microstructured TCP or microstructured HA controls with which to compare this effect, raising the question: If a non-microstructured, non-osteoinductive TCP releases more Ca^{2+} / P_i ions than a microstructured, osteoinductive HA (or non-CaP material such as titanium) how can this theory explain it? TCP and HA in Barradas' study also absorbed similar amounts of Ca^{2+} / P_i ions in serum-free culture medium, because culture medium like body fluid is supersaturated with these ions [108]; therefore, whether MSCs would actually be exposed to higher concentrations of the ions on the surface of TCP versus HA can only be speculated.

Concerning the macrostructural effects on osteoinduction, Ripamonti (1991) hypothesized that the reason why surface concavities invited de novo bone formation but the planar surfaces did not was because they provided a protected shelter for the accumulation and adsorption of BMPs [112]. His group demonstrated this by immunolocalizing both BMP3 and BMP7 (but not BMP2 or 4) at the cell-concavity interface of osteoinductive HA, although the relevance of this is unclear since there was no visible de novo bone in the micrographs where BMPs were localized [96]. Indeed, macrostructural features such as concavities,

macropores, and interparticle gaps may all provide sheltered environments for local increases in proteins and ions. Moreover, they also increase the SSA which may augment the microstructure's capacity to form an apatite layer or release more Ca^{2+} / P_i ions (Figure 6).

Ripamonti also speculated that the geometric shape of a concavity itself provided an intrinsic template for bone formation, which he likened to the concavities that are etched into bone by osteoclasts where osteoblasts then deposit new bone [113]. This theory, though, is difficult to apply to Yuan and de Bruijn's non-macroporous but microporous CaP granules that induced substantial de novo bone formation in the muscle of dogs [99]. Others have suggested that a precipitated layer of carbonate apatite may also provide a direct template for osteogenesis and ossification [9,114].

Cellular theories on osteoinduction

Other less developed theories have been proposed that focus more on the effects of material architecture and geometry on cell and tissue response that may signal osteogenesis rather than the material physicochemistry. One such theory speculates that osteoinductive materials function by stimulating the inflammatory response in ways that induce osteoblast differentiation. Building on the findings of Malard's group that CaP particle geometry near the microscale stimulated the host response and osteogenesis, Le Nihouannen and coworkers linked this effect to osteoinduction by theorizing that microparticles originating from the microporous structure of osteoinductive CaPs may trigger macrophage phagocytosis and an osteogenic inflammatory response [64,115]. To provide an explanation for how this may occur, Fellah and colleagues (2010) cultured macrophages on similar BCP particles implanted by Le Nihouannen and observed that the smallest particles ($< 20 \mu\text{m}$) incited the strongest inflammatory response, measured by secretion of $\text{TNF}\alpha$ and IL-6. To connect this with osteoinduction, the authors then showed that when MC3T3 pre-osteoblasts were cultured with similar levels of cytokines exogenously added to basic culture medium, IL-6 induced upregulation of osteoblast gene markers such as ALP, osteocalcin, and the master osteoblast transcription factor Runx2 [116]. However, it is currently unknown if these cytokines are also triggered by osteoinductive CaPs *in vivo*.

In addition to their sensitivity to particle size, macrophages are also highly sensitive to surface topography and roughness, which could also explain link microstructure, inflammation, and osteoinduction. Still, the role of osteoinductive surface microstructure and roughness on inflammation and corresponding de novo bone formation has not yet been investigated in the literature.

It has also been shown that microstructured CaPs first stimulate osteoclast formation before de novo bone formation, suggesting that osteoclasts may play a role in osteoblast differentiation and osteoinduction [117,118]. Ripamonti et al. (2008) speculated that osteoclastogenesis and resorption precedes osteoinduction through the resorption of instructive concavities as well as the local release of Ca^{2+} due to the resorption process [119]. To investigate this hypothesis, Klar, Ripamonti, and colleagues (2013) showed that when osteoinductive HA was implanted in the muscle of baboons, both verapamil hydrochloride, a calcium channel blocker, or zoledronate, an osteoclast inhibiting bisphosphonate, stunted de novo bone formation [120]. Tanaka et al. (2010) also showed that osteoclast inhibition by alendronate, another bisphosphonate, reduced material resorption and bone formation in an orthotopic location as well [121]. However, neither calcium channel blockers nor bisphosphonates are specific enough to definitely prove the dependence of CaP-directed osteogenesis on osteoclasts.

In addition to releasing osteogenic Ca^{2+} / P_i ions during resorption of CaPs [87], osteoclasts also secrete a variety of anabolic factors (e.g., Wnts, BMPs, sphingosine-1-phosphate) that can both home and differentiate osteoblasts from uncommitted precursors in vitro and in vivo [122–124]. Importantly, Takeshita et al. (2013) recently identified CTHRC1 as the elusive osteoclast-specific coupling factor essential for triggering bone formation after resorption. The authors demonstrated that osteoclast secreted CTHRC1 stimulates osteogenesis of stromal precursors and osteoclast-specific knockout of CTHRC1 results in osteopenia (loss of bone mass). Interestingly, osteoclasts express CTHRC1 during resorption of not only bone but also HA [125]. Currently, osteoclast secretion of inductive proteins has never been evaluated on osteoinductive CaPs.

Intriguingly, these theories on the role of inflammation and osteoclastogenesis in osteoinduction may be linked through principles of osteoimmunology. Osteoclasts differentiate from the same myeloid precursor as macrophages, specifically CD14+ monocytes. Indeed, inflammatory cytokines such as $\text{TNF}\alpha$, IL-1, and IL-6 upregulate stromal cell expression of essential osteoclast differentiating factors RANKL and M-CSF [126,127]. On the other hand, anti-inflammatory cytokines IL-4 and IL-13 inhibit osteoclast formation mainly through the upregulation of OPG, the natural antagonist of RANKL. So, the balance between pro- and anti-inflammatory signaling from macrophage interactions with osteoinductive CaPs may be crucial for osteoclast formation, followed by osteoblast differentiation due to osteoclast-secreted coupling factors or ions.

Natural examples of osteoinduction

In order to understand the biological process of osteoinduction by CaPs, studying how bone formation occurs away from the skeleton in naturally occurring pathologies can provide insight. Heterotopic ossification (HO) is the general term encompassing both acquired and genetic conditions (e.g. fibrodysplasia ossificans progressive, FOP), that give rise to extraskeletal bone formation in the soft tissue [128]. In both disease subsets, trauma or injury to the skeleton or soft tissue is the catalyzing event [128,129]. Arterial calcification is another example of pathologic, extraskeletal bone formation [130]. Whereas HO results in bone formation in skeletal muscle, arterial calcification produces bone-like tissue in the smooth muscle wall of arteries. In fact, histological sections of calcified arteries are indistinguishable from those of trabecular bone with regard to cell and tissue morphology, complete with osteoclasts, osteoblasts, and even bone marrow [131].

Mounting evidence shows that macrophage-secreted factors – both inflammatory and osteogenic – play a central role in the ectopic bone formation of each of these pathologies. For instance, when macrophages were selectively depleted in a mouse model of HO, osteogenesis was significantly blocked [129]. This effect was attributed to the elimination of macrophage-secreted BMPs at the injury site. In arterial calcification, macrophage-secreted TNF α was identified as the potential activator because it can trigger osteoblast differentiation through the Wnt and protein Kinase A pathways [130,131]. In support of this link, administration of TNF α antibody infliximab proved to be an effective treatment for arterial calcification in mice [130]. Concerning the “induced” cells that differentiate into osteoblasts and form the ectopic bone, these studies also suggest the involvement of a stromal or vascular stem cell population (i.e. pericytes) that can (trans)differentiate into osteoblasts given the appropriate inflammatory signals [128,130].

5 AIM OF THIS THESIS

Given the current knowledge in the field of CaP bone graft substitutes, the overarching goal of this research is to lay a biological foundation for understanding their osteoinductive and resorbable performance. In essence, this work seeks to answer the question, “What CaP material parameters evoke what cellular responses necessary for CaP osteoinduction and resorption?” By answering this question, new insight will be gained to propel the design of better CaPs.

We hypothesize that the inflammatory reaction and subsequent osteoclastogenesis play a central role in translating osteoinductive surface microstructure into de novo bone formation.

To investigate this hypothesis, several broad aims will be addressed in this thesis:

- More clearly understand the cell-material interactions that give rise to osteoinduction by CaPs, particularly from the standpoint of inflammation and osteoclastogenesis. Is there a link between inflammation, osteoclastogenesis, and osteoinduction?
- Identify the material properties necessary to trigger osteoinduction – e.g., microstructure, material chemistry, macrostructure (macropores, concavities). Of these, is microstructure solely essential for osteoinduction?
- How does surface microstructure specifically affect osteoclast formation in vitro and in vivo? Does it serve to stimulate osteoclast-secreted anabolic factors? Can it modulate osteoclast resorption?
- Are osteoclasts necessary for osteoinduction? What happens if osteoclasts and their precursors are depleted? Does the innate inflammatory reaction play a role in this process?

The first experimental chapter of this book (Chapter 2) will undertake a practical challenge of designing a moldable, shapeable osteoinductive CaP-based material useful for surgical applications. In this study, different polymeric carriers will be combined with CaP and implanted in both ectopic and orthotopic locations to evaluate if the osteoinductive and osteoconductive capacity of microstructured CaP can be preserved despite temporarily obstructing its surface microstructure from the biological environment. The time required to dissolve the carriers and the amount of bone formation in vivo will be correlated in an effort to understand if the early implantation period, characterized by the innate inflammatory reaction, is important for osteoinduction.

The second experimental chapter of this book (Chapter 3) will evaluate if surface microstructure of CaP without macrostructural features can trigger de novo bone formation and what effects microstructure has on osteoclastogenesis. In other words, is microstructure the only essential CaP parameter to trigger osteoclastogenesis and ectopic bone formation? To study this, planar microstructured CaP discs without macropores or concavities will be implanted in an ectopic model of osteoinduction. Moreover, the influence of surface chemistry will be compared to surface microstructure by coating discs with a thin layer of titanium. Multinucleated osteoclast-like cell formation will be characterized

and correlated with de novo bone formation in vivo and the effects of surface microstructure and chemistry on osteoclast formation will be investigated in vitro.

The third experimental chapter of this book (Chapter 4) will isolate the effects of surface microstructure on osteoclastogenesis in mediating both osteoinduction and resorption of TCP. Here to now, the effects of CaP microstructure on osteoclastogenesis and resorption have not been clearly addressed, nor is it known if osteoclasts secrete anabolic factors in response to microstructured CaP surfaces. The presence of multinucleated osteoclast-like cells will be correlated with material resorption and bone formation in vivo and the effects of microstructure on osteoclast formation and secretion of anabolic factors will be studied in vitro using the same model developed in Chapter 3.

The fourth experimental chapter of this book (Chapter 5) will consider the effects of selectively depleting osteoclasts and macrophages in vivo to understand if they are essential for osteoinduction. CaP cubes that only differ in their surface microstructure will be implanted in subcutaneous pockets of mice and liposome-encapsulated clodronate will be locally injected to deplete phagocytic osteoclasts and macrophages. By depleting invading macrophages, the role of inflammation in generating osteoclasts and directing de novo formation in response to CaP microstructure will be investigated. Furthermore, osteoclasts will be immunohistologically distinguished from foreign body giant cells and compared between the CaPs with different surface microstructure for the first time.

The fifth and final experimental chapter of this book (Chapter 6) will explore how CaP microstructure specifically modulates osteoclast formation resorption in vitro – from both a biochemical and molecular basis – and if their multinucleated relatives, foreign body giant cells, can also resorb CaP. To investigate these topics, a new in vitro model for generating both osteoclasts and foreign body giant cells from same population of human peripheral blood monocytes will be introduced. The capacity of surface microstructure to regulate osteoclastogenesis in vitro will be linked with the previous in vivo findings of Chapters 4 and 5 in order to validate the model.

R E F E R E N C E S

- [1] Ratner BD, Bryant SJ. Biomaterials: where we have been and where we are going. *Annu Rev Biomed Eng* 2004;6:41–75.
- [2] Hench LL, Polak JM. Third-generation biomedical materials. *Science* 2002;295:1014–7.
- [3] Bongio M, van den Beucken JJJP, Leeuwenburgh SCG, Jansen JA. Development of bone substitute materials: from “biocompatible” to “instructive.” *J Mater Chem* 2010;20:8747.
- [4] Anderson JM. The future of biomedical materials. *J Mater Sci Mater Med* 2006;17:1025–8.
- [5] Midwood KS, Williams LV, Schwarzbauer JE. Tissue repair and the dynamics of the extracellular matrix. *Int J Biochem Cell Biol* 2004;36:1031–7.
- [6] Uygun BE, Soto-Gutierrez A, Yagi H, Izamis M-L, Guzzardi MA, Shulman C, et al. Organ reengineering through development of a transplantable recellularized liver graft using decellularized liver matrix. *Nat Med* 2010;16:814–20.
- [7] Shin H, Jo S, Mikos AG. Biomimetic materials for tissue engineering. *Biomaterials* 2003;24:4353–64.
- [8] Dorozhkin S V. Calcium Orthophosphates as Bioceramics: State of the Art. *J Funct Biomater* 2010;1:22–107.
- [9] LeGeros RZ. Calcium phosphate-based osteoinductive materials. *Chem Rev* 2008;108:4742–53.
- [10] Stevens MM, George JH. Exploring and engineering the cell surface interface. *Science* 2005;310:1135–8.
- [11] Sims NA, Gooi JH. Bone remodeling: Multiple cellular interactions required for coupling of bone formation and resorption. *Semin Cell Dev Biol* 2008;19:444–51.
- [12] Nakahama K-I. Cellular communications in bone homeostasis and repair. *Cell Mol Life Sci* 2010;67:4001–9.
- [13] Yasuda H, Shima N, Nakagawa N, Yamaguchi K, Kinoshita M, Mochizuki S, et al. Osteoclast differentiation factor is a ligand for osteoprotegerin/osteoclastogenesis-inhibitory factor and is identical to TRANCE/RANKL. *Proc Natl Acad Sci U S A* 1998;95:3597–602.
- [14] Hsu H, Lacey DL, Dunstan CR, Solovyev I, Colombero A, Timms E, et al. Tumor necrosis factor receptor family member RANK mediates osteoclast differentiation and activation induced by osteoprotegerin ligand. *Proc Natl Acad Sci U S A* 1999;96:3540–5.
- [15] Simonet WS, Lacey DL, Dunstan CR, Kelley M, Chang MS, Lüthy R, et al. Osteoprotegerin: a novel secreted protein involved in the regulation of bone density. *Cell* 1997;89:309–19.
- [16] Zhao C, Irie N, Takada Y, Shimoda K, Miyamoto T, Nishiwaki T, et al. Bidirectional ephrinB2-EphB4 signaling controls bone homeostasis. *Cell Metab* 2006;4:111–21.
- [17] Schindeler A, McDonald MM, Bokko P, Little DG. Bone remodeling during fracture repair: The cellular picture. *Semin Cell Dev Biol* 2008;19:459–66.
- [18] Gerber HP, Vu TH, Ryan AM, Kowalski J, Werb Z, Ferrara N. VEGF couples hypertrophic cartilage remodeling, ossification and angiogenesis during endochondral bone formation. *Nat Med* 1999;5:623–8.
- [19] Carano RA., Filvaroff EH. Angiogenesis and bone repair. *Drug Discov Today* 2003;8:980–9.
- [20] Bucholz RW. Nonallograft osteoconductive bone graft substitutes. *Clin Orthop Relat Res* 2002;44–52.
- [21] Goulet JA, Senunas LE, DeSilva GL, Greenfield ML. Autogenous iliac crest bone graft. Complications and functional assessment. *Clin Orthop Relat Res* 1997:76–81.
- [22] Misch CE, Dietsh F. Bone-grafting materials in implant dentistry. *Implant Dent* 1993;2:158–67.
- [23] LeGeros RZ. Properties of osteoconductive biomaterials: calcium phosphates. *Clin Orthop Relat Res* 2002:81–98.
- [24] Kruyt MC, Delawi D, Habibovic P, Oner FC, van Blitterswijk CA, Dhert WJA. Relevance of bone graft viability in a goat transverse process model. *J Orthop Res* 2009;27:1055–9.
- [25] Urist MR. Bone: formation by autoinduction. *Science* 1965;150:893–9.
- [26] Urist MR, Strates BS. Bone Morphogenetic Protein. *J Dent Res* 1971;50:1392–406.
- [27] Dorozhkin S. Medical Application of Calcium Orthophosphate Bioceramics. *BIO* 2011;1:1–51.

- [28] Greenwald AS, Boden SD, Barrack RL, Bostrom MPG, Goldberg VM, Yaszemski MJ, et al. The evolving role of bone-graft substitutes. *Am. Acad. Orthop. Surg. 77th Annu. Meet.*, vol. 83, New Orleans, Louisiana: 2010, p. 98–103.
- [29] Jarcho M. Calcium phosphate ceramics as hard tissue prosthetics. *Clin Orthop Relat Res* 1981;259:78.
- [30] Denissen HW, de Groot K. Immediate dental root implants from synthetic dense calcium hydroxylapatite. *J Prosthet Dent* 1979;42:551–6.
- [31] Kokubo T, Takadama H. How useful is SBF in predicting in vivo bone bioactivity? *Biomaterials* 2006;27:2907–15.
- [32] Kokubo T. Bioactive glass ceramics: properties and applications. *Biomaterials* 1991;12:155–63.
- [33] Osborn JF, Newesely H. The material science of calcium phosphate ceramics. *Biomaterials* 1980;1:108.
- [34] De Brujin JD, van Blitterswijk CA, Davies JE. Initial bone matrix formation at the hydroxyapatite interface in vivo. *J Biomed Mater Res* 1995;29:89–99.
- [35] Bohner M, Galea L, Doebelein N. Calcium phosphate bone graft substitutes: failures and hopes. *J Eur Ceram Soc* 2012;32:2663–71.
- [36] Yuan H, Zou P, Yang Z, Zhang X, De Brujin JD, De Groot K. Bone morphogenetic protein and ceramic-induced osteogenesis. *J Mater Sci Mater Med* 1998;9:717–21.
- [37] Boden SD, Martin GJ, Morone MA, Ugbo JL, Moskowitz PA. Posterolateral lumbar intertransverse process spine arthrodesis with recombinant human bone morphogenetic protein 2/hydroxyapatite-tricalcium phosphate after laminectomy in the nonhuman primate. *Spine (Phila Pa 1976)* 1999;24:1179–85.
- [38] United States Food and Drug Administration [Internet]. Public health notification: life-threatening complications associated with recombinant human bone morphogenetic protein in cervical spine fusion; 1 July, 2008 [cited 3 July, 2014]. Available from: <http://www.fda.gov/medicaldevices/safety/alertsandnotices/publichealthnotifications/ucm062000.htm>.
- [39] Medtronic Inc [Internet]. Press release: Medtronic agrees to settle certain INFUSE® bone graft product liability; 6 May, 2014 [cited 3 July, 2014]. Available from: <http://newsroom.medtronic.com/phoenix.zhtml?c=251324&p=irol-newsArticle&id=1927406>.
- [40] Burg KJ, Porter S, Kellam JF. Biomaterial developments for bone tissue engineering. *Biomaterials* 2000;21:2347–59.
- [41] Petite H, Viateau V, Bensaïd W, Meunier A, de Pollak C, Bourguignon M, et al. Tissue-engineered bone regeneration. *Nat Biotechnol* 2000;18:959–63.
- [42] Wei C, Lin AB, Hung S. Mesenchymal stem cells in regenerative medicine for musculoskeletal diseases: bench, bedside, and industry. *Cell Transplant* 2014;23:505–12.
- [43] Meijer GJ, de Brujin JD, Koole R, van Blitterswijk CA. Cell-based bone tissue engineering. *PLoS Med* 2007;4:e9.
- [44] Logeart-Avramoglou D, Anagnostou F, Bizios R, Petite H. Engineering bone: challenges and obstacles. *J Cell Mol Med* 2005;9:72–84.
- [45] Potier E, Ferreira E, Meunier A, Sedel L, Logeart-Avramoglou D, Petite H. Prolonged hypoxia concomitant with serum deprivation induces massive human mesenchymal stem cell death. *Tissue Eng* 2007;13:1325–31.
- [46] James J, Steijn-Myagkaya GL. Death of osteocytes. *Electron microscopy after in vitro ischaemia. J Bone Joint Surg Br* 1986;68:620–4.
- [47] Rose FRAJ, Orefeo ROC. Bone tissue engineering: hope vs hype. *Biochem Biophys Res Commun* 2002;292:1–7.
- [48] Granero-Molto F, Weis JA, Longobardi L, Spagnoli A. Role of mesenchymal stem cells in regenerative medicine: application to bone and cartilage repair. *Expert Opin Biol Ther* 2008;8:255–68.
- [49] Li S, L'Heureux N, Elisseeff J, editors. *Stem cell and tissue engineering*. 1st ed. Hackensack, NJ: World Scientific; 2011.
- [50] Barradas AMC, Yuan H, van Blitterswijk CA, Habibovic P. Osteoinductive biomaterials: current knowledge of properties, experimental models and biological mechanisms. *Eur Cell Mater* 2011;21:407–29.
- [51] Habibovic P, Yuan H, van den Doel M, Sees TM, van Blitterswijk CA, de Groot K. Relevance of

C H A P T E R 1

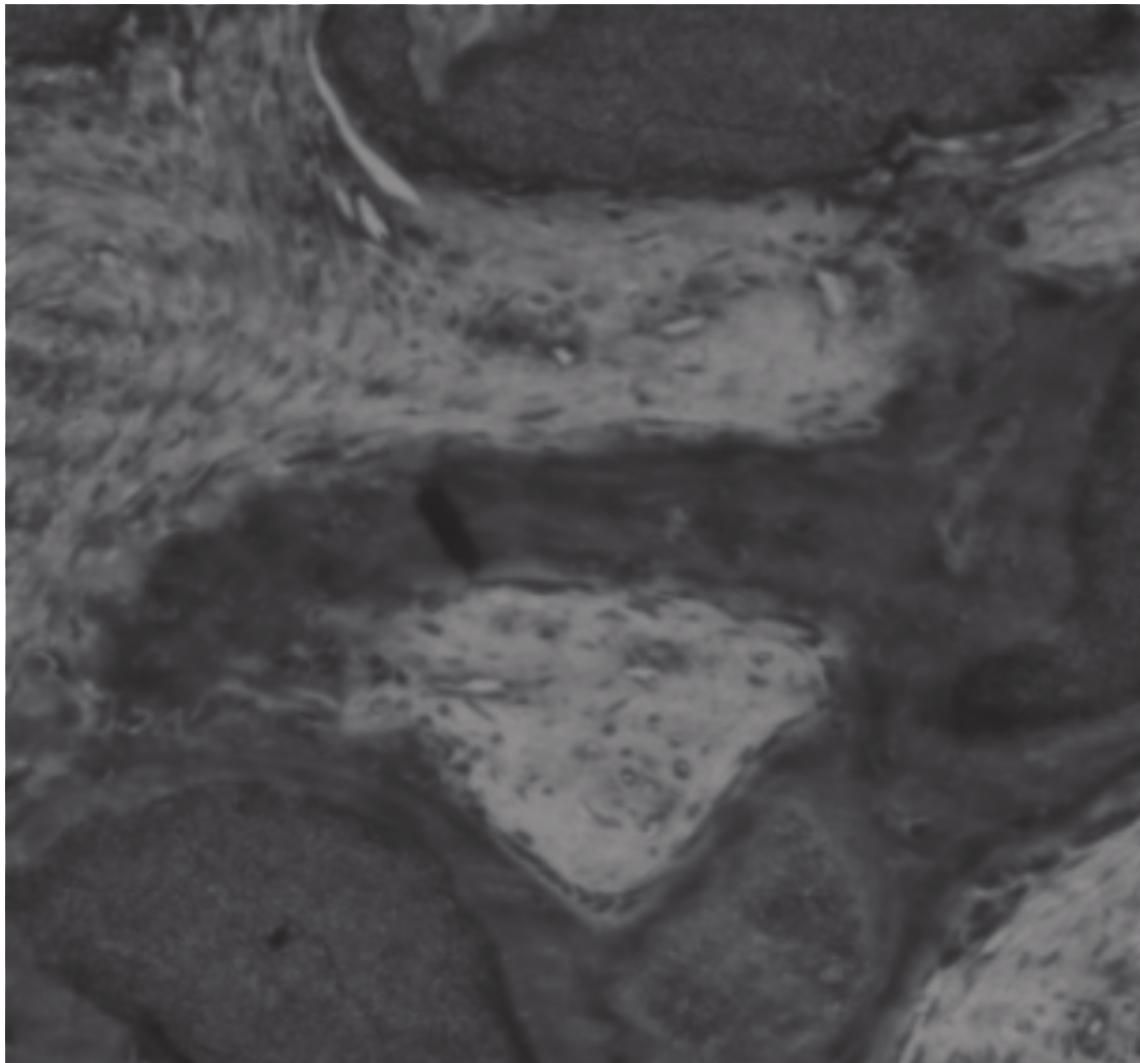
- osteoinductive biomaterials in critical-sized orthotopic defect. *J Orthop Res* 2006;24:867–76.
- [52] Yuan H, Fernandes H, Habibovic P, de Boer J, Barradas AMC, de Ruiter A, et al. Osteoinductive ceramics as a synthetic alternative to autologous bone grafting. *Proc Natl Acad Sci U S A* 2010;107:13614–9.
- [53] Velard F, Braux J, Amedee J, Laquerriere P. Inflammatory cell response to calcium phosphate biomaterial particles: an overview. *Acta Biomater* 2013;9:4956–63.
- [54] Grandjean-Laquerriere A, Tabary O, Jacquot J, Richard D, Frayssinet P, Guenounou M, et al. Involvement of toll-like receptor 4 in the inflammatory reaction induced by hydroxyapatite particles. *Biomaterials* 2007;28:400–4.
- [55] Anderson J, Rodriguez A, Chang D. Foreign body reaction to biomaterials. *Semin Immunol* 2008;20:86–100.
- [56] Mosser DM, Edwards JP. Exploring the full spectrum of macrophage activation. *Nat Rev Immunol* 2008;8:958–69.
- [57] Leibovich SJ, Ross R. The role of the macrophage in wound repair. A study with hydrocortisone and antimacrophage serum. *Am J Pathol* 1975;78:71–100.
- [58] Chen S, Jones JA, Xu Y, Low H-Y, Anderson JM, Leong KW. Characterization of topographical effects on macrophage behavior in a foreign body response model. *Biomaterials* 2010;31:3479–91.
- [59] Jones JA, Chang DT, Meyerson H, Colton E, Kwon IK, Matsuda T, et al. Proteomic analysis and quantification of cytokines and chemokines from biomaterial surface-adherent macrophages and foreign body giant cells. *J Biomed Mater Res A* 2007;83:585–96.
- [60] Xia Z, Triffitt JT. A review on macrophage responses to biomaterials. *Biomed Mater* 2006;1:R1–9.
- [61] Glass GE, Chan JK, Freidin A, Feldmann M, Horwood NJ, Nanchahal J. TNF-alpha promotes fracture repair by augmenting the recruitment and differentiation of muscle-derived stromal cells. *Proc Natl Acad Sci U S A* 2011;108:1585–90.
- [62] Alexander KA, Chang MK, Maylin ER, Kohler T, Müller R, Wu AC, et al. Osteal macrophages promote in vivo intramembranous bone healing in a mouse tibial injury model. *J Bone Miner Res* 2011;26:1517–32.
- [63] Liu X-H, Kirschenbaum A, Yao S, Levine AC. Interactive effect of interleukin-6 and prostaglandin E2 on osteoclastogenesis via the OPG/RANKL/RANK system. *Ann N Y Acad Sci* 2006;1068:225–33.
- [64] Malard O, Bouler JM, Guicheux J, Heymann D, Pilet P, Coquard C, et al. Influence of biphasic calcium phosphate granulometry on bone ingrowth, ceramic resorption, and inflammatory reactions: preliminary in vitro and in vivo study. *J Biomed Mater Res* 1999;46:103–11.
- [65] Webster TJ, Schadler LS, Siegel RW, Bizios R. Mechanisms of enhanced osteoblast adhesion on nanophase alumina involve vitronectin. *Tissue Eng* 2001;7:291–301.
- [66] Webster TJ, Ergun C, Doremus RH, Siegel RW, Bizios R. Enhanced osteoclast-like cell functions on nanophase ceramics. *Biomaterials* 2001;22:1327–33.
- [67] McNally AK, Jones JA, Macewan SR, Colton E, Anderson JM. Vitronectin is a critical protein adhesion substrate for IL-4-induced foreign body giant cell formation. *J Biomed Mater Res A* 2008;86:535–43.
- [68] Keselowsky BG, Collard DM, García AJ. Surface chemistry modulates fibronectin conformation and directs integrin binding and specificity to control cell adhesion. *J Biomed Mater Res A* 2003;66:247–59.
- [69] Keselowsky BG, Collard DM, García AJ. Surface chemistry modulates focal adhesion composition and signaling through changes in integrin binding. *Biomaterials* 2004;25:5947–54.
- [70] Guilak F, Cohen DM, Estes BT, Gimble JM, Liedtke W, Chen CS. Control of stem cell fate by physical interactions with the extracellular matrix. *Cell Stem Cell* 2009;5:17–26.
- [71] Curtis A, Wilkinson C. Topographical control of cells. *Biomaterials* 1997;18:1573–83.
- [72] Kilian KA, Bugarija B, Lahn BT, Mrksich M. Geometric cues for directing the differentiation of mesenchymal stem cells. *Proc Natl Acad Sci U S A* 2010;107:4872–7.
- [73] McNamara LE, McMurray RJ, Biggs MJP, Kantawong F, Oreffo ROC, Dalby MJ. Nanotopographical control of stem cell differentiation. *J Tissue Eng* 2010;2010:120623.
- [74] Lee SJ, Choi JS, Park KS, Khang G, Lee YM, Lee HB. Response of MG63 osteoblast-like

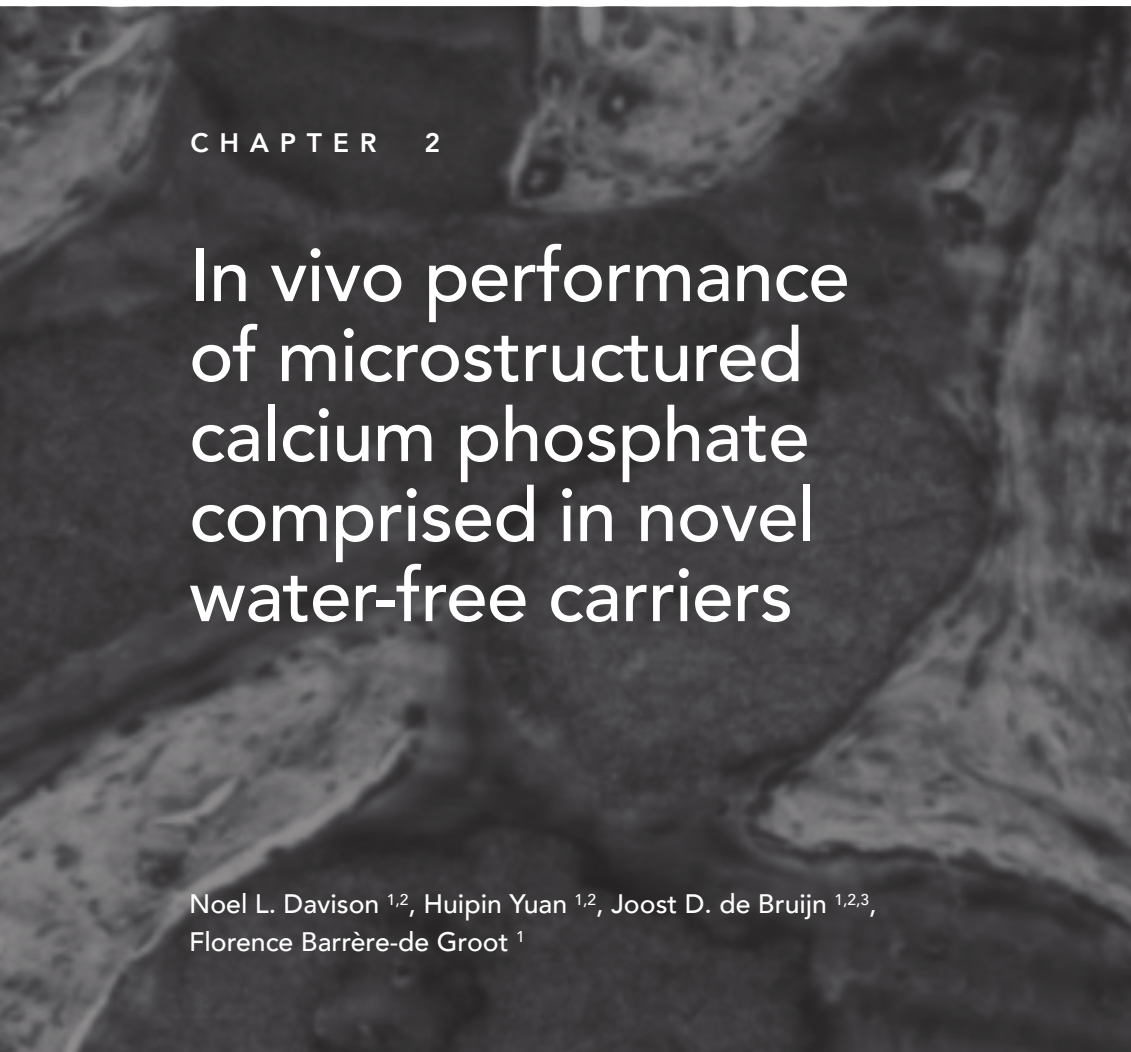
- cells onto polycarbonate membrane surfaces with different micropore sizes. *Biomaterials* 2004;25:4699–707.
- [75] Guntur AR, Rosen CJ, Naski MC. N-cadherin adherens junctions mediate osteogenesis through PI3K signaling. *Bone* 2012;50:54–62.
- [76] Dvorak MM, Siddiqua A, Ward DT, Carter DH, Dallas SL, Nemeth EF, et al. Physiological changes in extracellular calcium concentration directly control osteoblast function in the absence of calcitropic hormones. *Proc Natl Acad Sci U S A* 2004;101:5140–5.
- [77] Beck GR. Inorganic phosphate as a signaling molecule in osteoblast differentiation. *J Cell Biochem* 2003;90:234–43.
- [78] Miyauchi A, Hruska KA, Greenfield EM, Duncan R, Alvarez J, Barattolo R, et al. Osteoclast cytosolic calcium, regulated by voltage-gated calcium channels and extracellular calcium, controls podosome assembly and bone resorption. *J Cell Biol* 1990;111:2543–52.
- [79] Mozar A, Haren N, Chasseraud M, Louvet L, Mazière C, Wattel A, et al. High extracellular inorganic phosphate concentration inhibits RANK-RANKL signaling in osteoclast-like cells. *J Cell Physiol* 2008;215:47–54.
- [80] Ducheyne P, Radin S, King L. The effect of calcium phosphate ceramic composition and structure on *in vitro* behavior. I. Dissolution. *J Biomed Mater Res* 1993;27:25–34.
- [81] Ducheyne P, Radin S, Heughebaert M, Heughebaert JC. Calcium phosphate ceramic coatings on porous titanium: effect of structure and composition on electrophoretic deposition, vacuum sintering and *in vitro* dissolution. *Biomaterials* 1990;11:244–54.
- [82] Anselme K. Osteoblast adhesion on biomaterials. *Biomaterials* 2000;21:667–81.
- [83] LeGeros RZ. Biodegradation and bioresorption of calcium phosphate ceramics. *Clin Mater* 1993;14:65–88.
- [84] Jensen SS, Bornstein MM, Dard M, Bosshardt DD, Buser D. Comparative study of biphasic calcium phosphates with different HA/TCP ratios in mandibular bone defects. A long-term histomorphometric study in minipigs. *J Biomed Mater Res B Appl Biomater* 2009;90:171–81.
- [85] Daculsi G, LeGeros RZ, Nery E, Lynch K, Kerebel B. Transformation of biphasic calcium phosphate ceramics *in vivo*: ultrastructural and physicochemical characterization. *J Biomed Mater Res* 1989;23:883–94.
- [86] Rousselle A, Heymann D. Osteoclastic Acidification Pathways During Bone Resorption 2002;30:533–40.
- [87] Yamada S, Heymann D, Bouler JM, Daculsi G. Osteoclastic resorption of calcium phosphate ceramics with different hydroxyapatite/beta-tricalcium phosphate ratios. *Biomaterials* 1997;18:1037–41.
- [88] Detsch R, Mayr H, Ziegler G. Formation of osteoclast-like cells on HA and TCP ceramics. *Acta Biomater* 2008;4:139–48.
- [89] Costa-Rodrigues J, Fernandes A, Lopes MA, Fernandes MH. Hydroxyapatite surface roughness: complex modulation of the osteoclastogenesis of human precursor cells. *Acta Biomater* 2012;8:1137–45.
- [90] Makihira S, Mine Y, Kosaka E, Nikawa H. Titanium surface roughness accelerates RANKL-dependent differentiation in the osteoclast precursor cell line, RAW264. 7. *Dent Mater J* 2007;26:739–45.
- [91] Von Doernberg M-C, von Rechenberg B, Bohner M, Grünenfelder S, van Lenthe GH, Müller R, et al. In vivo behavior of calcium phosphate scaffolds with four different pore sizes. *Biomaterials* 2006;27:5186–98.
- [92] Epple M, Ganeshan K, Heumann R, Klesing J, Kovtun A, Neumann S, et al. Application of calcium phosphate nanoparticles in biomedicine. *J Mater Chem* 2010;20:18.
- [93] De Groot K. Effect of porosity and physicochemical properties on the stability, resorption, and strength of calcium phosphate ceramics. *Ann NY Acad Sci* 1988;523:227–33.
- [94] Webster T. Enhanced functions of osteoblasts on nanophase ceramics. *Biomaterials* 2000;21:1803–10.
- [95] LeGeros RZ, Lin S, Rohanzadeh R, Mijares D, LeGeros JP. Biphasic calcium phosphate bioceramics: preparation, properties and applications. *J Mater Sci Mater Med* 2003;14:201–9.
- [96] Ripamonti U, Crooks J, Kirkbride AN. Sintered porous hydroxyapatites with intrinsic osteoinductive activity: geometric induction of bone formation. *South African J Sci* 1999;335–

C H A P T E R 1

- 43.
- [97] Yamasaki H, Sakai H. Osteogenic response to porous hydroxyapatite ceramics under the skin of dogs. *Biomaterials* 1992;13:308–12.
- [98] Kuboki Y, Takita H, Kobayashi D, Tsuruga E, Inoue M, Murata M, et al. BMP-induced osteogenesis on the surface of hydroxyapatite with geometrically feasible and nonfeasible structures: topology of osteogenesis. *J Biomed Mater Res* 1998;39:190–9.
- [99] Yuan H, de Bruijn JD. Osteoinductive calcium phosphates. U.S. Patent 7,942,934, 2009.
- [100] Fukuda A, Takemoto M, Saito T, Fujibayashi S, Neo M, Pattanayak DK, et al. Osteoinduction of porous Ti implants with a channel structure fabricated by selective laser melting. *Acta Biomater* 2011;7:2327–36.
- [101] Yuan H, Yang Z, Li Y, Zhang X, De Bruijn JD, De Groot K. Osteoinduction by calcium phosphate biomaterials. *J Mater Sci Mater Med* 1998;9:723–6.
- [102] Yuan H, Van Den Doel M, Li S, Van Blitterswijk CA, De Groot K, De Bruijn JD. A comparison of the osteoinductive potential of two calcium phosphate ceramics implanted intramuscularly in goats. *J Mater Sci Mater Med* 2002;13:1271–5.
- [103] Habibovic P, Sees TM, van den Doel MA, van Blitterswijk CA, de Groot K. Osteoinduction by biomaterials—physicochemical and structural influences. *J Biomed Mater Res A* 2006;77:747–62.
- [104] Habibovic P, Yuan H, van der Valk CM, Meijer G, van Blitterswijk CA, de Groot K. 3D microenvironment as essential element for osteoinduction by biomaterials. *Biomaterials* 2005;26:3555–75.
- [105] Fujibayashi S, Neo M, Kim H-M, Kokubo T, Nakamura T. Osteoinduction of porous bioactive titanium metal. *Biomaterials* 2004;25:443–50.
- [106] Daculsi G, LeGeros RZ, Heughebaert M, Barbier I. Formation of carbonate-apatite crystals after implantation of calcium phosphate ceramics. *Calcif Tissue Int* 1990;46:20–7.
- [107] de Groot K. Carriers That Concentrate Native Bone Morphogenetic Protein in Vivo. *Tissue Eng* 1998;4:337–41.
- [108] Barradas AMC, Monticone V, Hulsman M, Danoux C, Fernandes H, Tahmasebi Birgani Z, et al. Molecular mechanisms of biomaterial-driven osteogenic differentiation in human mesenchymal stromal cells. *Integr Biol (Camb)* 2013;5:920–31.
- [109] Barradas AMC, Fernandes HAM, Groen N, Chai YC, Schroten J, van de Peppel J, et al. A calcium-induced signaling cascade leading to osteogenic differentiation of human bone marrow-derived mesenchymal stromal cells. *Biomaterials* 2012;33:3205–15.
- [110] Chai YC, Roberts SJ, Desmet E, Kerckhofs G, van Gastel N, Geris L, et al. Mechanisms of ectopic bone formation by human osteoprogenitor cells on CaP biomaterial carriers. *Biomaterials* 2012;33:3127–42.
- [111] Eyckmans J, Roberts SJ, Bolander J, Schroten J, Chen CS, Luyten FP. Mapping calcium phosphate activated gene networks as a strategy for targeted osteoinduction of human progenitors. *Biomaterials* 2013;34:4612–21.
- [112] Ripamonti U. The morphogenesis of bone in replicas of porous hydroxyapatite obtained from conversion of calcium carbonate exoskeletons of coral. *J Bone Joint Surg Am* 1991;73:692–703.
- [113] Ripamonti U. Soluble, insoluble and geometric signals sculpt the architecture of mineralized tissues. *J Cell Mol Med* 2004;8:169–80.
- [114] Daculsi G, Layrolle P. Osteoinductive Properties of Micro Macroporous Biphasic Calcium Phosphate Bioceramics. *Key Eng Mater* 2004;254–256:1005–8.
- [115] Le Nihouannen D, Daculsi G, Saffarzadeh A, Gauthier O, Delplace S, Pilet P, et al. Ectopic bone formation by microporous calcium phosphate ceramic particles in sheep muscles. *Bone* 2005;36:1086–93.
- [116] Fellah BH, Delorme B, Sohier J, Magne D, Hardouin P, Layrolle P. Macrophage and osteoblast responses to biphasic calcium phosphate microparticles. *J Biomed Mater Res A* 2010;93:1588–95.
- [117] Kondo N, Ogose A, Tokunaga K, Umezawa H, Arai K, Kudo N, et al. Osteoinduction with highly purified beta-tricalcium phosphate in dog dorsal muscles and the proliferation of osteoclasts before heterotopic bone formation. *Biomaterials* 2006;27:4419–27.
- [118] Akiyama N, Takemoto M, Fujibayashi S, Neo M, Hirano M, Nakamura T. Difference between

- dogs and rats with regard to osteoclast-like cells in calcium-deficient hydroxyapatite-induced osteoinduction. *J Biomed Mater Res A* 2011;96:402–12.
- [119] Ripamonti U, Richter PW, Nilen RWN, Renton L. The induction of bone formation by smart biphasic hydroxyapatite tricalcium phosphate biomimetic matrices in the non-human primate Papio ursinus. *J Cell Mol Med* 2008;12:2609–21.
- [120] Klar RM, Duarte R, Dix-Peek T, Dickens C, Ferretti C, Ripamonti U. Calcium ions and osteoclastogenesis initiate the induction of bone formation by coral-derived macroporous constructs. *J Cell Mol Med* 2013;17:1444–57.
- [121] Tanaka T, Saito M, Chazono M, Kumagae Y, Kikuchi T, Kitasato S, et al. Effects of alendronate on bone formation and osteoclastic resorption after implantation of beta-tricalcium phosphate. *J Biomed Mater Res A* 2010;93:469–74.
- [122] McCullough KA, Waits CA, Garimella R, Tague SE, Sipe JB, Anderson HC. Immunohistochemical localization of bone morphogenetic proteins (BMPs) 2, 4, 6, and 7 during induced heterotopic bone formation. *J Orthop Res* 2007;25:465–72.
- [123] Pederson L, Ruan M, Westendorf JJ, Khosla S, Oursler MJ. Regulation of bone formation by osteoclasts involves Wnt/BMP signaling and the chemokine sphingosine-1-phosphate. *Proc Natl Acad Sci U S A* 2008;105:20764–9.
- [124] Karsdal MA, Neutzsky-Wulff AV, Dziegiele MH, Christiansen C, Henriksen K. Osteoclasts secrete non-bone derived signals that induce bone formation. *Biochem Biophys Res Commun* 2008;366:483–8.
- [125] Takeshita S, Fumoto T, Matsuoka K, Park K, Aburatani H, Kato S, et al. Osteoclast-secreted CTHRC1 in the coupling of bone resorption to formation. *J Clin Invest* 2013;123:3914–24.
- [126] Nakashima T, Takayanagi H. Osteoimmunology: crosstalk between the immune and bone systems. *J Clin Immunol* 2009;29:555–67.
- [127] Baud'huin M, Lamoureux F, Duplomb L, Rédini F, Heymann D. RANKL, RANK, osteoprotegerin: key partners of osteoimmunology and vascular diseases. *Cell Mol Life Sci* 2007;64:2334–50.
- [128] Shore EM, Kaplan FS. Role of altered signal transduction in heterotopic ossification and fibrodysplasia ossificans progressiva. *Curr Osteoporos Rep* 2011;9:83–8.
- [129] Kan L, Liu Y, McGuire TL, Berger DMP, Awatramani RB, Dymecki SM, et al. Dysregulation of local stem/progenitor cells as a common cellular mechanism for heterotopic ossification. *Stem Cells* 2009;27:150–6.
- [130] Sage AP, Tintut Y, Demer LL. Regulatory mechanisms in vascular calcification. *Nat Rev Cardiol* 2010;7:528–36.
- [131] Thompson B, Towler DA. Arterial calcification and bone physiology: role of the bone-vascular axis. *Nat Rev Endocrinol* 2012;8:529–43.





CHAPTER 2

In vivo performance of microstructured calcium phosphate comprised in novel water-free carriers

Noel L. Davison ^{1,2}, Huipin Yuan ^{1,2}, Joost D. de Bruijn ^{1,2,3},
Florence Barrère-de Groot ¹

- 1 Xpand Biotechnology BV, Bilthoven, Netherlands
2 MIRA Institute for Biomedical Technology and Technical Medicine,
University of Twente, Enschede, Netherlands
3 School of Engineering and Materials Science (SEMS), Queen Mary
University of London, London, United Kingdom

A B S T R A C T

Osteoinductive calcium phosphate (CaP) ceramics can be combined with polymeric carriers to make shapeable bone substitutes as an alternative to autologous bone. Carriers containing water may degrade the ceramics' surface microstructure, which is crucial to bone formation, so water-free alternatives are necessary for prolonged storage. In this study, 5 novel tricalcium phosphate (TCP) formulations were designed from water-free polymeric binders and osteoinductive TCP granules of different particle sizes (500-1000 μm for moldable putty forms, and 150-500 μm for flowable paste forms). The performance of these novel TCP formulations was studied and compared to control TCP granules alone (both 150-500 and 500-1000 μm). In vitro, the 5 TCP formulations were characterized by their carrier dissolution time and TCP mineralization kinetic profile in simulated body fluid (SBF). In vivo, formulations were implanted in the dorsal muscle and unicortical femoral defect ($\varnothing=5$ mm) of dogs for 12 weeks. The two TCP control groups produced equivalent amounts of bone and allowed surface mineralization in vitro by day 7. TCP formulations based on carboxymethyl cellulose-glycerol (CMCG) and Polyoxy 15-hydroxystearate-Pluronic® F127 (HSF) allowed the in vitro surface mineralization of TCP by day 7 and produced the most ectopic bone and orthotopic bone bridging. Ectopic bone formation by these formulations was equivalent to the TCP controls by week 12; however, fluorescent labeling indicated that bone formation occurred between weeks 6 and 9 in the formulations, which was up to 3 weeks later than the control. The TCP formulation based on a xanthan gum-glycerol carrier exhibited fast carrier dissolution (1 hour) and TCP mineralization (day 7) in vitro but inflammation and little ectopic bone formation (4.9%). This carrier chemistry was, therefore, found to disrupt early cellular response related to osteoinduction of microstructured TCP. These results demonstrate the in vivo performance of novel water-free carriers that allow the preservation of the chemistry, microstructure, and function of osteoinductive CaP ceramics.

1 INTRODUCTION

The clinical use of synthetic bone graft substitutes steadily grows due to improved material performance and an aging population that requires more bone grafting procedures annually [1, 2]. These substitutes are used as an alternative to autograft tissue, which is in limited supply and can engender donor site pain, morbidity, and infection [3, 4]. Currently, bone graft substitutes such as calcium phosphate (CaP) ceramic can be applied as bone void fillers and are used to treat a variety of cranio-maxillofacial [5], foot and ankle [6], long bone [7], and vertebral bony defects [8].

The bone repair potential of CaP ceramic was first documented by Albee and Morrison in 1920, when they applied injectable tricalcium phosphate to repair 1/4" radial defects in rabbits [9]. More widespread development and use came later in the 1970s [10], ranging from periodontal to orthopedic applications [11, 12]. In the early 1990s, the intrinsic capability of some CaP ceramics to form bone in non-osseous (ectopic) sites without the addition of committed osteoblasts, stem cells, or growth factors – defined as osteoinduction – was described, confirmed, and characterized by various authors [13, 14]. The precise mechanism of osteoinduction by biomaterials is unknown, but current understanding emphasizes the importance of micro- and nanostructure of the ceramic surface for bone formation [15]. The clinical utility of osteoinductive CaP ceramics has been demonstrated in critical sized bone defects, showing that these materials are better orthotopic bone void fillers than those that are merely osteoconductive. Osteoconductive materials guide bone formation given the presence of committed osteoblasts but do not induce its formation through the differentiation of stromal precursors [16, 17].

In many clinical applications the preferred handling properties of a bone graft substitute are cohesive moldability or injectability in order to fill complex volumetric defects as in mandibular alveolar ridge reconstruction [18] or span between bony surfaces as in spine fusion [19]. For this purpose, CaP cements have been developed as alternative to the classical granular or block forms [20-22] but inherent drawbacks include unstable flowability which is dependent on the setting time [23], a lack of micro- and macroporosity useful for vascularity and tissue ingrowth [24], and slow resorption [22]. A newer alternative consists of mixing granular CaP particles with a polymeric binder (also "carrier") material with stable and appropriate rheological properties for graft cohesion and shape conformance to the defect. However, this approach introduces an additional component, the binder, to the bone graft formulation, which must be carefully selected. In general, the polymeric binder should be biocompatible and should

not interfere with the bone repair capacity of the CaP particles comprised therein. Specifically, the carrier should not inhibit direct bone formation and bone bonding onto the ceramic, ceramic granule retention, or optimal packing of the granules into the bony defect [25]. Related to these parameters, there is the risk of excessively increasing the carrier content or decreasing CaP particle size to optimize handling characteristics of the bone graft formulation at the expense of its performance [26].

Previously, Barbieri et al. (2011) screened different carriers in combination with 1-2 mm osteoinductive CaP particles *in vivo* and established the influence of the *in vitro* carrier dissolution profile on the osteoinductive potential of the CaP. Briefly, carriers dissolving rapidly, i.e. in less than 48 h, did not alter the osteoinductive potential of the CaP granules, while carriers dissolving slower significantly inhibited osteoinduction [25]. This indicated that the availability of the ceramic micro- and nanostructured surface to the surrounding tissue in the first hours following implantation is of primary importance. The carriers, like other compositions reported in literature, were water-based [27, 28]. A limitation of water-based formulations is that CaP ceramics will eventually degrade during prolonged storage [29], even for biphasic calcium phosphates containing mostly non-resorbable hydroxyapatite [27]. As a consequence, the CaP surface and chemistry will be altered, which is detrimental to the initial characteristics of osteoinductive ceramics. Therefore, the long-term preservation of micro- and nanostructured ceramics prior to surgical application could be achieved by storage in non-aqueous carriers.

From this perspective, the aim of this work was to design clinically relevant water-free carriers with a range of chemistries and dissolution profiles, offering a range of handling properties from moldable to flowable after optimized combination with CaP granules of different size distribution and minimum carrier content. Functionally, the carrier were intended to preserve the intrinsic osteoinductive potential the constituent tricalcium phosphate granules comprised therein and allow the retention of CaP granules into a bony defect. It was hypothesized that to achieve this, the timely availability of the ceramic surface to the surrounding physiologic environment was of primary importance. Pertaining to this, potential correlations between *in vitro*, orthotopic, and intramuscular performance were explored in relation to different physical and chemical characteristics of these formulations.

2 MATERIALS AND METHODS

2.1 Preparation of osteoinductive tricalcium phosphate (TCP)

Micro- and nanostructured β -tricalcium phosphate (TCP) (composition > 99% β -tricalcium phosphate) ceramic particles were made by wet precipitation of apatite powder (Ca/P ratio=1.5), followed by green body H_2O_2 foaming and sintering at 1050 °C, as previously described [30]. This material was known to possess osteoinductive potential as previously demonstrated [17]. Two TCP granule fractions were separated by sieving (Retsch) into 150-500 and 500-1000 μm size ranges, and finally cleaned with ethanol, acetone and deionized water.

2.2 Preparation of water-free carriers

Water-free carriers were designed using a variety of natural and synthetic materials that were selected on the basis of their documented biocompatibility as well as their water solubility, thus influencing their physiological dissolution kinetics (Table 1). Their design was specifically oriented toward clinical relevance, and therefore emphasis was placed on the qualitative rheological characteristics of the formulations – particularly cohesion when combined with ceramic particles and adhesion to wet bone.

Table 1. Material components of water-free carriers.

Material (abbreviation)	Form	Supplier
Glycerol, UltraPure®	Liquid	Sigma Aldrich
Poly(ethylene glycol) M_w =400 (PEG 400)	Liquid	Merck
Carboxymethyl cellulose, M_w =50,000, CeKol® (CMC ₁)	Powder	CPKelco
Dextran, M_w = 40,000	Powder	Pharmacosmos
Poly(ethylene glycol) M_w =4,000 (PEG 4,000)	Powder	Fluka
Pluronic® F 127	Powder	BASF
Polyoxyl 15 hydroxystearate, Solutol® HS 15 (HS15)	Powder	BASF
Sodium carboxymethyl cellulose, Blanose® 7H4XF PH (CMC ₂)	Powder	Hercules-Aqualon
Starch, soluble	Powder	Sigma Aldrich
Xanthan, XGF FNHV	Powder	Jungbunzlauer

For each carrier composition, all components were mixed using a digital stirrer (Ika) equipped with helical arm, under applied heat controlled by a hot plate at specified temperatures (Table 1). Carriers were then allowed to cool to room temperature (RT) naturally and stored at RT in closed container. The pH of the carriers was measured at RT using a digital probe, after complete dissolution under gentle magnetic stirring in deionized water (0.5 g in 10 cc, respectively) (Table 1).

2.3 Preparation of TCP formulations

Each TCP formulation was prepared by combining TCP particles with one water-free carrier by manually mixing with a spatula until visually homogenous. Carriers intended to be flowable pastes were technically found to be best combined with smaller TCP particles (150-500 µm) at equal volumetric ratios (1:1) while those meant to be moldable putties were combined with larger TCP particles (500-1000 µm) at volumetric ratios of 2:3 for optimal handling characteristics (Table 2). For both flowable pastes and moldable putty formulations, the volumetric ratio of carrier to ceramic particles was designed to be low so as to minimize volume loss due to carrier dissolution after implantation.

Table 2. Bone void filler formulations.

Ceramic Formulations	Carrier composition	Preparation Temp (°C)	pH	TCP size range (µm)	Carrier:TCP ratio (V/V)	Form
XDS	2.5% Xanthan, 60% Dextran, 10% Starch (w/v) in Glycerol	98	6.4	500-1000	2:3	Putty
CMCPEG	15% CMC ₂ , 25% PEG 4000 (w/v) in PEG 400, glycerol (1:1 v/v)	98	6.9	500-1000	2:3	Putty
XG	1% Xanthan (w/v) in Glycerol	85	6.3	150-500	1:1	Paste
HSF	58% HS15, 42% Pluronic E127 (w/w)	70	6.3	150-500	1:1	Paste
CMCG	5% CMC ₁ in Glycerol (w/w)	95	7.1	150-500	1:1	Paste

2.4 X-ray diffraction (XRD) and scanning electron microscopy (SEM)

Tricalcium phosphate chemistry and microstructure was confirmed using X-ray diffraction (XRD) (Rigaku Miniflex II) and scanning electron microscopy (Jeol JSM-5600) before and after combination with water-free carriers including e-beam sterilization (25 kGy, Isotron) and 208 days storage at 50 °C equating to 4 years aging at RT according to ASTM F1980 [31]. After accelerated aging, TCP formulations were immersed in water until complete carrier dissolution. The TCP particles were thereafter rinsed thoroughly with deionized water and dried at 60 °C. For XRD, TCP particles were uniformly ground using pellet and pestle, evenly applied to a glass holder slide, then scanned from $2\Theta=25-45^\circ$ with a step size of 0.01° and a rate of $1^\circ/\text{min}$. For SEM, TCP particles were sputter coated with gold (Jeol JFC 1300) for 60-90 s prior to microscopy. Tricalcium phosphate particles that were not mixed with a carrier served as controls for both tests.

2.5 In vitro dissolution and mineralization assays on TCP formulations

Carrier dissolution kinetics of the ceramic putties and pastes were evaluated by individually incubating the formulations (0.5 cc) in phosphate buffered saline (15 cc) in glass jars without shaking at 37 °C. Samples were judged to have dissolved when TCP particles were completely and freely dispersed at the bottom of the vessel, as previously described [25].

Availability of the TCP surface at the micro- and nanoscale was modeled by in vitro mineralization using the methods described by Kokubo [32]. Briefly, simulated body fluid (SBF) having the same ion concentration of blood serum was prepared under laminar flow to prevent contamination. Ceramic paste and putty samples (0.5 cc) were placed in glass jars containing 100 cc of SBF and incubated at 37 °C for up to 14 days, with refreshment on days 4, 7, and 10. Disassociated TCP particles were periodically retrieved, rinsed 3 times with deionized water, dried at RT, sputter coated with gold, and evaluated with SEM. For quantification, 10 particles were selected at random on which at least 3 locations were visually inspected for mineralization. Tricalcium phosphate particles alone were treated the same way and served as control.

2.6 In vivo study: ectopic and orthotopic implantation models

Tricalcium phosphate paste and putty samples were electron beam sterilized (25 kGy, Isotron) and implanted in both femoral (orthotopic) defects and incised

dorsal muscle (ectopic) pockets of healthy male dogs (1-4 years, 11-15 kg). All surgeries were conducted under general anesthesia by abdominal injection of sodium pentobarbital (30 mg/kg body weight) with the permission of the local animal ethics committee. Following the surgeries, animals were given penicillin (40 mg/kg) by intramuscular injection for 3 consecutive days to prevent infection.

Ectopic implantation

Longitudinal incisions through the skin exposed the paraspinal muscles on both sides of the spine of dogs (Table 3). Muscle pockets were created along these incision lines by blunt dissection, spaced 2-3 cm apart to ensure sample isolation. Paste and putty samples (1 cc) were inserted into each pocket. Muscle and skin incisions were closed layer by layer with non-resorbable sutures for identification at harvest. Both 150-500 and 500-1000 μm range TCP particles alone (denoted TCP 150-500 and TCP 500-1000, respectively) were implanted as controls.

To monitor ectopic bone formation over time, calcein (5 mg/mL), xylenol orange (50 mg/mL), and oxytetracycline (10 mg/mL) (all Sigma-Aldrich) fluorescent markers were dissolved in physiologic saline, filter sterilized, and administered intravenously (25 mL/animal) at 3, 6, and 9 weeks, respectively.

Orthotopic implantation

Round, unicortical femoral defects ($\varnothing = 5$ mm) were made using a trephine drill under copious irrigation with physiological saline. Four defects were created on one femur per animal and spaced ~2 cm apart to ensure sample isolation and bone rigidity. Paste and putty samples were randomly assigned to animal subjects and implanted once per animal by manual insertion (Table 3). Tissue incisions were closed layer by layer using nonresorbable sutures.

Table 3. Summary of implanted samples.

Formulation	Test subjects	
	Femoral defect	Intramuscular
XDS	6	8
CMCPEG	6	8
XG	5	8
HSF	5	8
CMCG	5	8
TCP 150-500	0	8
TCP 500-1000	0	8

Sample harvest and histological processing

At the end of 12 weeks, animals were sacrificed by abdominal injection of sodium pentobarbital (60 mg/kg) and samples were immediately harvested with their surrounding tissue. Tissue explants were fixed in cold phosphate buffered formalin solution for 72 h. The samples were rinsed, trimmed of excess soft tissue, dehydrated in an increasing series of ethanol solutions (70, 80, 90, 95, and 100% x 2), and embedded in methyl methacrylate (MMA) (LTI Nederland). Histological sections (~30 µm) of the un-decalcified samples were made using a diamond blade microtome (Leica SP1600). The sections were stained with 1% methylene blue and 0.3% basic fuchsin solutions for histological analysis or left unstained for fluorescent microscopy.

2.7 Histology and histomorphometry

Stained histological sections were scanned using a slide scanner (Dimage Scan Elite 5400II, Konica Minolta) for gross evaluation and histomorphometric analysis, as well as at higher magnification using a light microscope (Nikon Eclipse E200). Unstained sections were imaged on a fluorescent microscope (Olympus BX51, camera: Olympus DP70) equipped with a tri-band filter for DAPI-TRITC-FITC.

Histomorphometry was performed using photo analysis software (Adobe Photoshop Elements 4.0) by selecting a region of interest (ROI) encompassing the whole sample and pseudo-coloring pixels of bone tissue (B) and TCP material (M) within the ROI. The area percentage of bone formed (Bp%) was then calculated by the following equation:

$$\text{Bp\%} = \frac{\text{B}}{\text{(ROI-M)}} \times 100.$$

2.8 Statistical analysis

One-way repeated measures ANOVA of histomorphometric Bp% results, followed by Holm-Sidak post-hoc pair-wise comparison of all groups including controls, was conducted using SigmaPlot 12 software (Systat Software Inc). A P-value < 0.05 was considered statistically significant.

3 RESULTS

3.1 pH of water-free carriers

The pH of the dissolved water-free carriers were all near neutral, ranging from 6.3 to 7.1 (Table 2).

3.2 Conservation of TCP chemistry and microstructure in water-free carriers

X-ray diffraction analysis of the synthesized TCP ceramic particles confirmed nearly pure β -TCP phase ($2\Theta = 31^\circ$) with trace amounts of hydroxyapatite (< 5%) [33], which was unchanged by combination with water-free carriers. The TCP microstructure was visually inspected by SEM and showed complete conservation of the grain size, micropore size, and inter-grain boundaries as compared to the control, through 208 days at 50 °C (i.e., 4 years accelerated aging). For comparison, the surface microstructure of TCP stored in pure deionized water was significantly altered by the formation of mineralized crystals between 1 and 2 years accelerated aging (Figure 1).

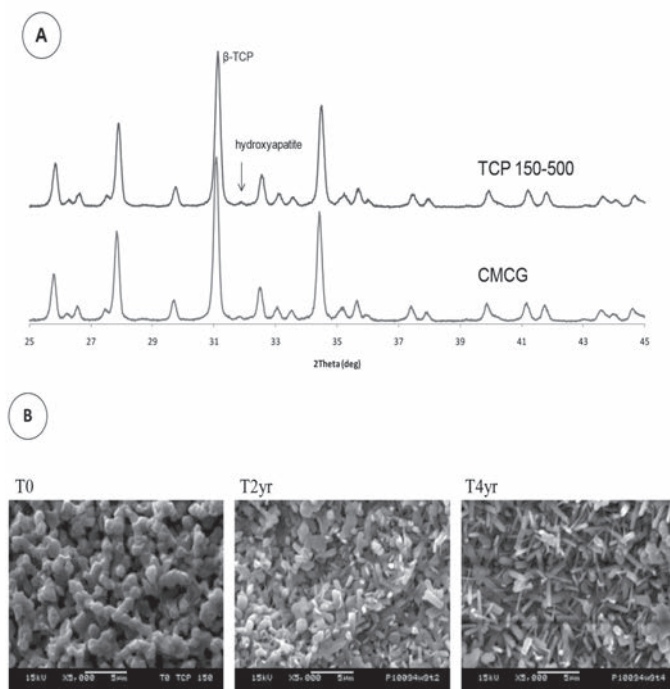


Figure 1. TCP chemistry and microstructure by XRD and SEM. (A) XRD spectra show nearly pure β -TCP and trace hydroxyapatite (<1%) peaks of CaP ceramic particles before (TCP 150-500) and after combination in water-free carrier CMCG. (B) Surface microstructure of TCP contained in pure deionized water was altered by the formation of mineralized crystals after 2 and 4 years accelerated aging.

3.3 In vitro dissolution and mineralization of TCP formulations

The carrier component of all TCP formulations dissolved in PBS at 37°C between 2 and 8 hours except for CMCPEG which required longer than 48 hours (Table

4). Surface mineralization of TCP in SBF was observed at day 7 for paste formulations XG, HSF, and CMCG, which was the same as control TCP 150-500 and 500-1000 μm particles alone. Mineralization of putty formulations XDS and CMCPEG required more time and was observed by day 10 (Table 4). The extent of mineralization (particles out of 10 that exhibited mineralization) varied by time point and formulation (Figure 2).

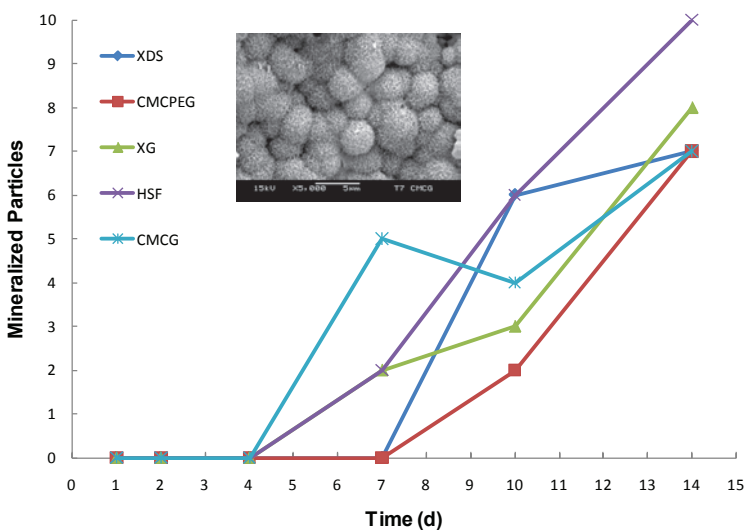


Figure 2. Surface mineralization kinetics. Bone void fillers were immersed in simulated body fluid (SBF) and monitored for mineralization using scanning electron microscopy (SEM) (inset: mineralization of CMCG at day 7). Ten particles were inspected at random and mineralized particles were tallied. The surface of TCP combined in low mass carriers XG, HSF and CMCG mineralized by day 7 versus day 10 for high mass carriers XDS and CMCPEG.

Table 4. In vitro characterization and ectopic bone formation.

Formulation	Carrier Dissolution (hours)	Surface Mineralization in SBF (days)	Ectopic bone formation (%)
XDS	8	10	0.7 \pm 0.7
CMCPEG	> 48	10	4.3 \pm 7.6
XG	1	7	4.9 \pm 4.4
HSF	8	7	12.7 \pm 13.4
CMCG	4	7	21.3 \pm 13.0
TCP 500-1000	--	7	21.3 \pm 14.5
TCP 150-500	--	7	17.9 \pm 8.8

3.4 Histology and histomorphometry

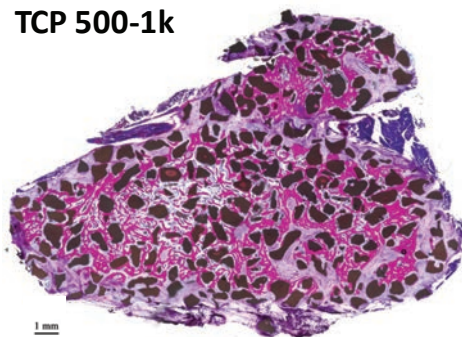
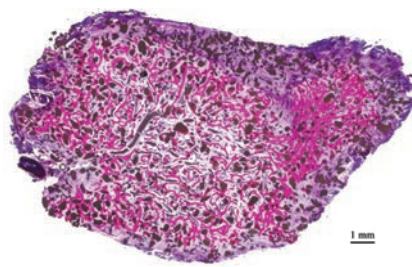
Ectopic implantation

After 12 weeks implantation, the ceramic pastes and putties performed differently with respect to bone formation, fibrous tissue formation, and inflammation (Figures 3 and 4). The percent area of ectopic bone formation (Bp%) within the implant was calculated by histomorphometry and averaged across test subjects (Table 4, Figure 5). Both TCP 150-500 and 500-1000 µm size range particles without carrier were implanted as control and induced statistically equivalent ($P > 0.05$) amounts of bone: Bp% = 17.9 ± 8.8 and 21.3 ± 14.5 , respectively. XDS implants formed little bone formation (Bp% = 0.7 ± 0.7), dense fibrous tissue encapsulating the TCP particles, and a moderate inflammatory response evident by many mononuclear cells in the interstitial space. CMCPEG induced more bone (Bp% = 4.3 ± 7.6) and fibrous tissue, although the fibrous tissue tended to be less dense and present between particles rather than directly in contact with them. Moderate inflammation was also evident by multinucleated giant cells that were present near TCP fragmentation and resorption. XG was only recovered in 6 out of 8 muscle pockets, in which there was $4.9 \pm 4.4\%$ bone formation. Loose fibrous tissue and significant inflammation typified the inter-particle space. Multinucleated cells were observed in close proximity to fragmented TCP particles and also between intact particles. HSF produced bone to a comparable extent as TCP 150-500 µm alone (Bp% = 12.7 ± 13.4 , $P > 0.05$) and loose connective tissue similar to the bone marrow observed in the femoral defects. Low amounts of loose fibrous tissue and inflammation were observed. Likewise, CMCG performed comparably to TCP particles alone in terms of bone formation (Bp% = 21.3 ± 13.0) and also promoted little fibrous tissue formation or inflammation except where TCP particle fragmentation and resorption occurred.

Xylenol orange fluorescence (red) was observed mainly in bone formed by TCP 150-500 and 500-1000 µm implants, without carrier, indicating this bone formed between 3 and 6 weeks. Oxytetracycline (yellow) was the predominant fluorophore observed in bone-forming ceramic pastes and putties, most notably CMCG and HSF, indicating bone mostly formed between 6 and 9 weeks (Figure 6). Little fluorescence was observed in samples that did not appreciably produce bone (Bp < 5%), suggesting that this bone formed after 9 weeks.

Orthotopic implantation

After 12 weeks implantation, the formulations performed differently with respect to TCP particle retention and bone bridging (i.e.: contiguous bone formation across the walls of the defect) in the femoral defect (Table 5). Of the XDS implants,

TCP 500-1k**TCP 150-500**

2

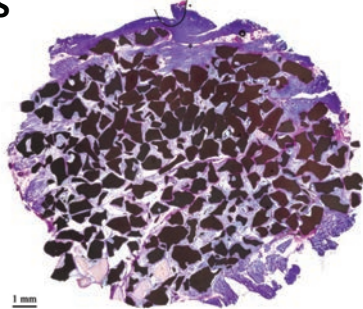
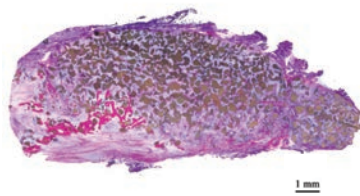
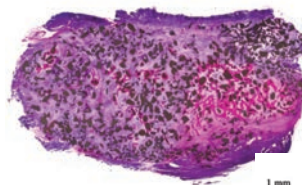
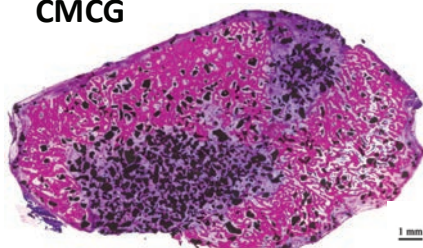
XDS**XG****HSF****CMCPEG****CMCG**

Figure 3. Histological overview of formulations implanted in canine dorsal muscle at 12 weeks. Bone formation (red/dark pink) of high carrier mass formulations (XDS and CMCPEG) did not occur to the extent of low carrier mass formulations (XG, HSF, and CMCG) but was instead typified by fibrous tissue (purple/blue). Bone marrow (white) can be seen in TCP controls and to a lesser extent CMCG.

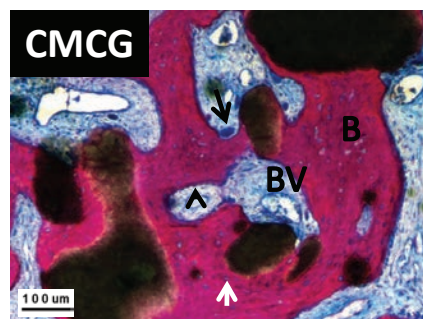
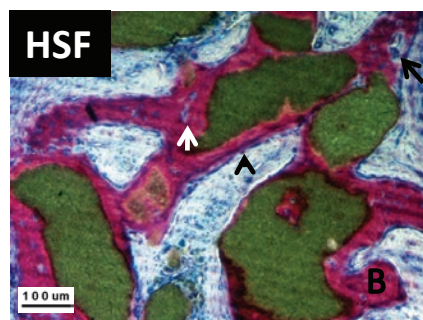
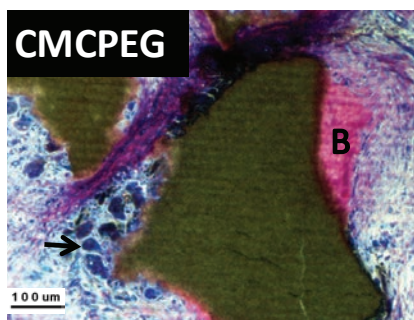
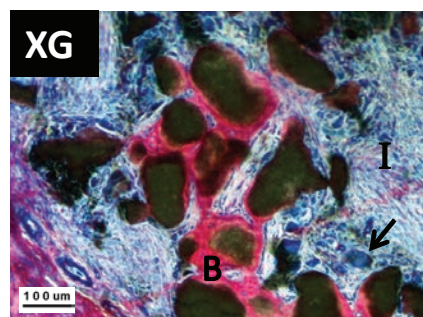
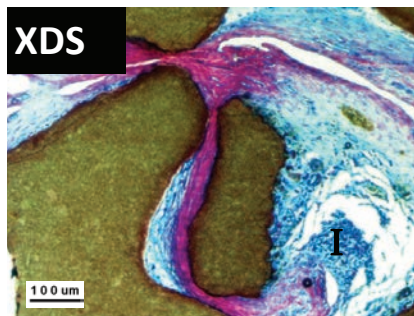
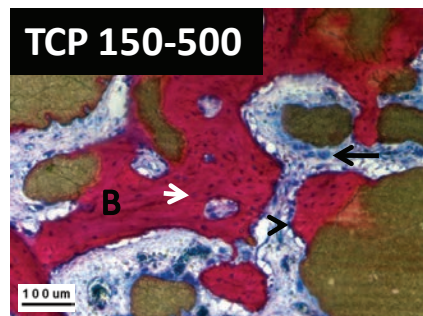
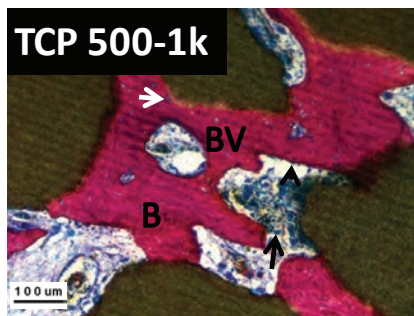


Figure 4, opposite. Ectopic bone formation in canine dorsal muscle at 12 weeks (10x magnification). Formed bone (red/pink) (B) surrounds particles (Brown) in low mass formulations XG, HSF, and CMCG. Inflammation (I) is evident in XDS, CMCPEG, and XG, whereas blood vessels (BV) are seen throughout the implant CMCG and TCP controls (TCP 150-500 and TCP 500-1k). Osteoblasts (black arrow heads) and osteocytes (white arrow heads) are present in bone tissue. Multinucleated cells (black arrows) can be identified in contact with formed bone and degraded TCP, suggesting remodeling.

Ectopic Bone Formation

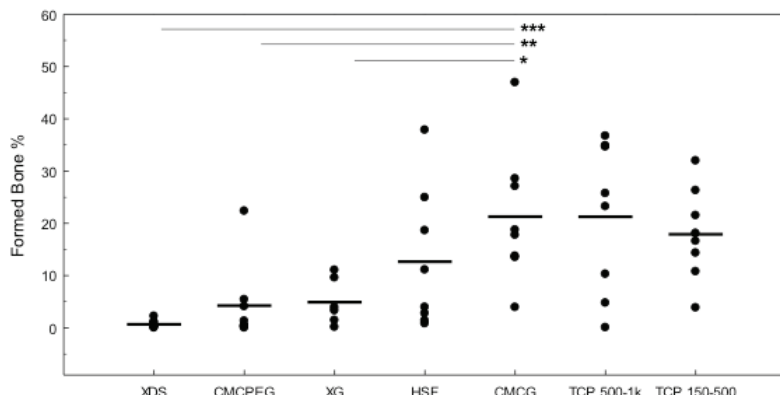
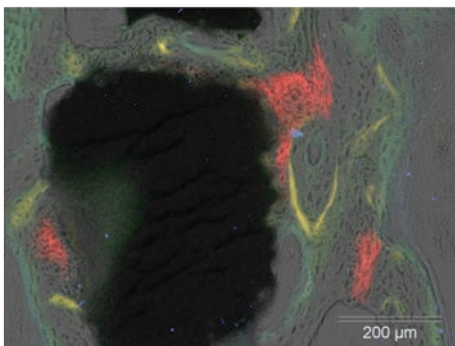


Figure 5. Ectopic bone formation calculated by histomorphometry. Points represent individual samples and horizontal lines denote the mean. Point spread highlights the nature of subject variability. CMCG and HSF were statistically equivalent to the TCP 150-500 control. * P<0.05, ** P<0.01, *** P<0.001.

TCP 150-500



CMCG

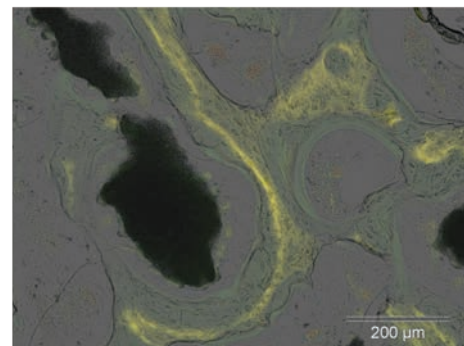


Figure 6. Ectopic bone formation time course. Fluorescent injection of xylene orange (red) at 6 weeks and oxytetracycline (yellow) at 9 weeks indicates that TCP particles without carrier (left) formed bone between 6 and 9 weeks versus CMCG (right), which formed bone after 9 weeks. The percentage of formed bone was equivalent between these groups at 12 weeks.

TCP particle retention was observed in 2 out of 6 defects, and of those occurrences bone bridging did not occur. Substantial fibrous tissue encapsulation of the TCP particles and inflammation was evident in both cases. CMCPEG demonstrated TCP particle retention in all 6 defects implanted; however, bone bridging was only apparent in 2. Fibrous tissue and inflammation were present in 3 of the defects, which also did not present bone bridging. XG was implanted in 5 defects and no particles were retained in any; however, bone bridging occurred in all 5 cases because this defect was not critical-sized. HSF demonstrated particle retention in 5 out of 5 defects, and 4 were bridged by bone. Little inflammation or fibrous tissue was observed. Last, CMCG demonstrated particle retention in 5 out of 5 defects treated and bone bridging in all (Figure 7).

Table 5. Orthotopic Implant Performance Summary.

	XDS	CMCPEG	XG	HSF	CMCG
TCP retainment	2/6	6/6	0/5	5/5	5/5
Bone bridging	0/6	2/6	5/5	4/5	5/5

4 DISCUSSION

Tricalcium phosphate granules of different size distribution exhibited similar osteoinductive capacity, while the TCP pastes and putties with a range of dissolution and mineralization profiles demonstrated different bone forming performance in both orthotopic and ectopic sites. The formulations were all composed of the same bioactive ceramic material, TCP, with identical microstructure favorable for osteoinduction [17], which was unaltered by combination with any of the water-free carriers as shown by XRD and SEM. The significance of this is emphasized when compared to similar aqueous carriers studied by our group and by others, which changed the surface microstructure of the ceramic after prolonged storage likely due to hydrolysis [27].

The in vitro results presented here, particularly time for onset of mineralization, generally related well to both orthotopic and ectopic bone forming potential of the developed formulations. For instance, formulations that formed as much ectopic bone as the control and presented greater than 80% bridging incidence also demonstrated TCP surface mineralization as early as the control. Conversely, formulations that presented TCP surface mineralization later than the control particles alone did not present appreciable ectopic bone formation or orthotopic bone bridging. One possible reason for this is evident in the dense fibrous tissue

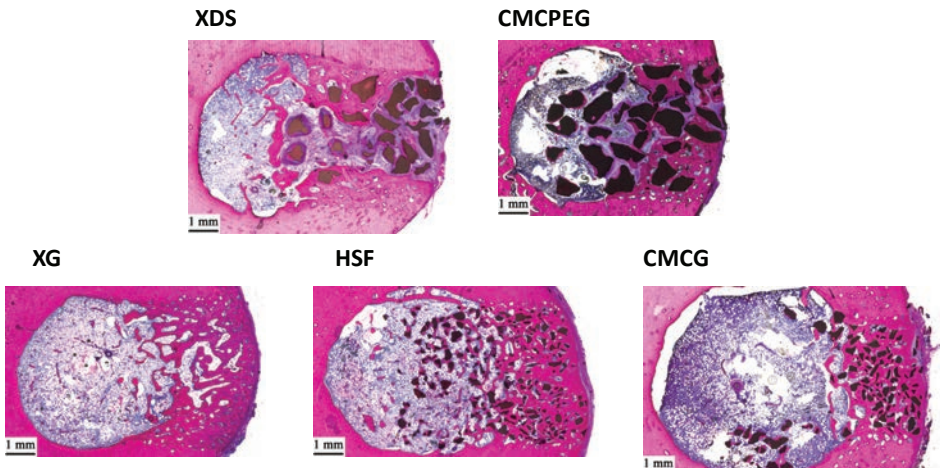


Figure 7. Orthotopic bone formation in canine femoral defect at 12 weeks. Histological staining (Methylene Blue, Basic Fuchsin) shows TCP particles (brown, Black) were retained in the defects except for XG. High carrier mass formulations (XDS and CMCPEG) were typified by inter-particle fibrous tissue (purple), which obstructed bone (pink) bridging contrary to low carrier mass formulations (HSF and CMCG) which demonstrated high rates of bone bridging.

present in putty formulations XDS and CMCPEG, suggesting that these higher mass carriers were not cleared away fast enough to allow for bone formation on the surface of the TCP particles. This data implies that the time required for a carrier to dissolve, allowing for the availability of the constituent TCP micro- and nanostructure, can affect its bone forming capacity.

The exception to this trend was XG, which demonstrated TCP mineralization as early as TCP alone but presented strong inflammation and limited bone formation. Little fibrous tissue was observed, suggesting the bulk mass of the carrier dissolved or was degraded quickly enough to prevent fibrous encapsulation of the particles; however, pronounced leukocyte density around the particles suggests that the immunogenicity of XG may have obstructed the osteoinductive potential of the TCP instead of its physical properties. Concerning these immunogenic properties, it has been shown in murine models that xanthan gum, which is a microbial fermented polysaccharide and thickening agent in XG, can activate polyclonal antibody generation as potently as lipopolysaccharide [34], although others have shown it to illicit only a weak foreign body response subcutaneously in rats at 12 weeks [35]. When incorporated into a TCP containing CaP cement and implanted in femoral condyle defects of rabbits, Flautre et al. (2003) claimed the addition of xanthan gum to be 'detrimental' to the biological response of the cement although new bone formation was not adversely affected [36]. Taken

together with the fact that XG binder dissolved quickly and the TCP particles mineralized as early as TCP control in vitro, it is possible that early, local cellular response to dissolving XG carrier was detrimental to long-term bone formation.

In vitro carrier dissolution time, which relates to the time required for body fluid to infiltrate the implant and introduce cells and biomolecules to the active particle surface, provided insight into a clinically relevant time frame for a ceramic paste or putty to remain intact. This was particularly evident for the extremes, XG and CMCPEG. In the femoral defect, the absence of XG particles in all implanted sites suggested that the carrier dissolved too quickly for a blood clot to form around the implant and hold the TCP particles in place. Conversely, the TCP particles of CMCPEG bound in a carrier component which required more than 48 hours to dissolve were surrounded by fibrous tissue which likely obstructed bone formation in both the muscle and bone defect. This point confirms the work of Barbieri et al. (2011) who suggest that the optimal dissolution time of a carrier containing osteoinductive CaP should not exceed 48 hours, based on findings that a non-degradable polyvinyl alcohol carrier prevented any bone formation from otherwise osteoinductive ceramic particles [25]. Although not substantial, CMCPEG did form some ectopic bone, which could be attributed to its highly hydrophilic nature. In physiologic solutions, CMC swells to form a hydrogel that could absorb critical nutrients and growth factors. Moreover, other groups have shown that CMC implanted in rabbit calvarial defects increased orthotopic bone formation without any additional factors [37, 38], which was attributed to its hydrophilicity [38]. These properties may explain the significantly better performance of CMCG in terms of TCP retention and bone bridging in the femoral defect despite comparable binder dissolution and mineralization kinetics.

The performance of the ceramic pastes and putties in both in vivo models seemed to be linked: TCP formulations that formed appreciable amounts of bone ectopically also presented high bone bridging incidence rates where granules were retained. This aspect of these models serves to confirm previous work suggesting that an osteoinductive material will tend to perform better in a bony defect than one that is not inductive [16, 39]. For example, ceramic pastes HSF and CMCG, which formed comparable amounts of ectopic bone as the control also exhibited high bone bridging incidence, whereas putties XDS and CMCPEG neither produced appreciable ectopic bone nor high bone bridging. Although different size particles were required to make pastes or putties with clinically relevant handling properties, the ectopic bone formation of both control TCP size ranges were statistically equivalent, ruling this out as a factor. Bohner and Baroud (2005) previously described that reduction of particle size and increase

of particle to carrier ratio is important for optimal injectability [26], similar to why smaller particles were used for flowable paste formulations here.

On a broader level, fluorescent data of ectopic implants revealed that the addition of a carrier to TCP may alter the bone forming kinetics of the particles alone. CMCG was presented as an example because it formed statistically equivalent amounts of bone as TCP alone, but in a later time range. It seems then that the addition of a carrier to TCP may have delayed bone formation although the effect was equilibrated by week 12 versus the control. One potential explanation for this is bone remodeling. Osteoclast-like multinucleated cells appeared to be more prevalent in sites where bone formation was high, especially in close proximity to sites of TCP fragmentation and newly formed bone. In the case of TCP alone, it is possible that bone formation reached maturity and was then remodeled by week 12, maintaining an amount that was eventually reached by CMCG and HSF. Indeed, bone marrow was more evident in control TCP particle implants, indicative of mature bone, than in the CMCG or HSF implants.

Our in vitro results suggest that a water-free carrier containing a bioactive ceramic should not slow the onset of mineralization versus the ceramic alone under the test conditions presented if the functionality of the ceramic is to be conserved (e.g., CMCG and HSF). Clearly, more carrier materials should be evaluated to confirm this trend, but for the formulations studied here, the availability of TCP surface delivered in a carrier was related to its bone forming potential is. However, it is apparent that the in vitro assays alone do not provide fully correlated insight into ectopic bone forming potential of ceramic formulations – particularly in the case of XG.

This point emphasizes the need for the mechanistic understanding of osteoinduction by CaP ceramics. As of yet, there is no consensus on cell populations or systems able to evaluate osteoinductive biomaterial, rendering the understanding of the binder effect incomplete. From our current understanding, a range of physicochemical parameters seem to play a role in osteoinduction such as high Ca^{2+} dissolution kinetic and protein adsorption capacity [17, 40], carbonated apatite layer precipitation [41], interconnected porosity for cellular invasion [42], and most importantly nano/micro-scale surface structure [15]. Additionally, certain cell populations seem to play a crucial role preceding de novo bone formation such as osteoclast remodeling [40, 43, 44] and macrophage secretion of anabolic factors (i.e., bone morphogenetic proteins) in response to osteoinductive CaP ceramics [45, 46].

Therefore, given the current hypotheses and observations in the present study, further investigations into osteoinductive TCP formulations could provide more

insight, namely (i) calcium release and multiple protein adsorption studies at the ceramic interface [15, 17, 41], and (ii) cellular models to characterize the initial cell populations colonizing these biomaterials, for example the development of a leukocyte/stromal pre-osteoblast co-culture system [47, 48].

5 CONCLUSION

The design of rapidly dissolving water-free carriers allows for the preparation of shapeable osteoinductive formulations with extended shelf life versus aqueous carriers. Water-free carriers were shown to be capable of preserving the microstructure and chemistry of microstructured TCP and in select cases did not limit the bone forming performance of TCP. In particular, the flowable osteoinductive paste CMCG demonstrated 100% granule retention and bone bridging in a bone defect and ample ectopic bone formation equivalent to TCP alone.

This study also suggests that the early cellular response to carrier chemistry can supersede fast dissolution kinetics alone and has prolonged limiting effects on bone formation by osteoinductive CaP. It is then likely that this early biological response must be critical in determining the osteoinductivity of implanted microstructured CaP ceramics, which should be more closely examined if the mechanism of action is to be understood.

A C K N O W L E D G E M E N T S

The authors gratefully acknowledge the support of the TeRM Smart Mix Program of the Netherlands Ministry of Economic Affairs and the Netherlands Ministry of Education, Culture and Science. This research forms part of the Project P2.04 BONE-IP of the research program of the Biomedical Materials institute, co-funded by the Dutch Ministry of Economic Affairs, Agriculture and Innovation. This work is also supported by funding under the Seventh Research Framework Program of the European Union, through the project REBORNE under the grant agreement No. 241879. Special thanks are due to Marieke Meijer (Xpand Biotechnology), Davide Barbieri (Xpand Biotechnology) and Mattie van Rijen (Dept. of Orthopaedics, UMC Utrecht) for technical expertise and useful discussion.

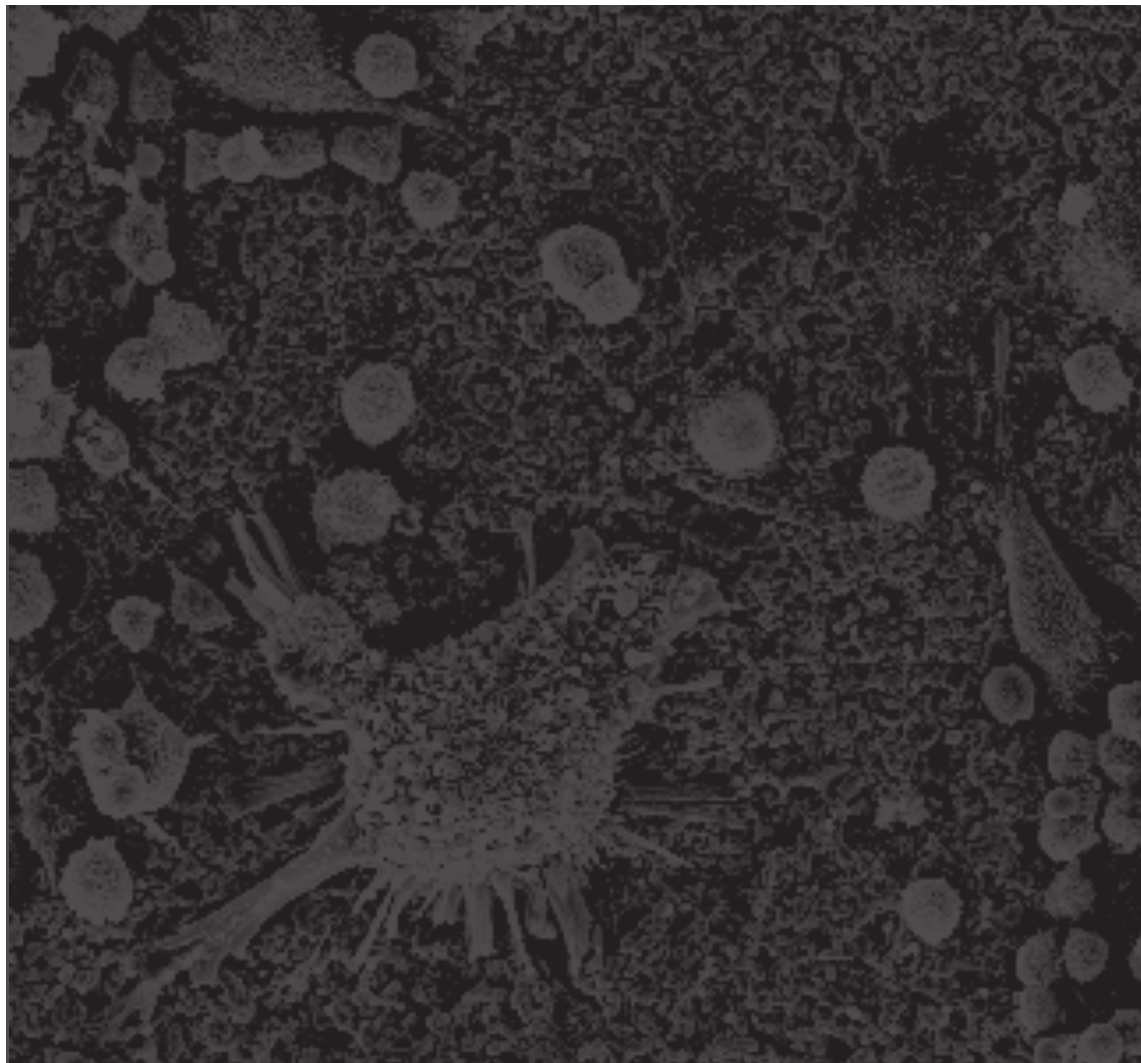
R E F E R E N C E S

- [1] Buchholz RW. Nonallograft osteoconductive bone graft substitutes. *Clin Orthop Relat Res.* 2002 Feb;(395):44-52.
- [2] Anscomb A. *Orthopedic Biomaterials*, The World Market New York: Kalorama Information 2011.
- [3] Tiedeman JJ, Garvin KL, Kile TA, Connolly JF. The role of a composite, demineralized bone matrix and bone marrow in the treatment of osseous defects. *Orthopedics.* 1995 Dec;18(12):1153-8.
- [4] Summers BN, Eisenstein SM. Donor site pain from the ilium. A complication of lumbar spine fusion. *J Bone Joint Surg Br.* 1989 Aug;71(4):677-80.
- [5] Nkenke E, Stelzle F. Clinical outcomes of sinus floor augmentation for implant placement using autogenous bone or bone substitutes: a systematic review. *Clin Oral Implants Res.* 2009 Sep;20 Suppl 4:124-33.
- [6] Cook EA, Cook JJ. Bone graft substitutes and allografts for reconstruction of the foot and ankle. *Clin Podiatr Med Surg.* 2009 Oct;26(4):589-605.
- [7] Tamai N, Myoui A, Kudawara I, Ueda T, Yoshikawa H. Novel fully interconnected porous hydroxyapatite ceramic in surgical treatment of benign bone tumor. *J Orthop Sci.* 2010 Jul;15(4):560-8.
- [8] Miyazaki M, Tsumura H, Wang JC, Alanay A. An update on bone substitutes for spinal fusion. *Eur Spine J.* 2009 Jun;18(6):783-99.
- [9] Albee FH. Studies in Bone Growth: Triple Calcium Phosphate as a Stimulus to Osteogenesis. *Ann Surg.* 1920 Jan;71(1):32-9.
- [10] Bohner M. Calcium orthophosphates in medicine: from ceramics to calcium phosphate cements. *Injury.* 2000 Dec;31 Suppl 4:37-47.
- [11] Levin MP, Getter L, Cutright DE, Bhaskar SN. Biodegradable ceramic in periodontal defects. *Oral Surg Oral Med Oral Pathol.* 1974 Sep;38(3):344-51.
- [12] Bhaskar SN, Brady JM, Getter L, Grower MF, Driskell T. Biodegradable ceramic implants in bone. Electron and light microscopic analysis. *Oral Surg Oral Med Oral Pathol.* 1971 Aug;32(2):336-46.
- [13] Yamasaki H, Sakai H. Osteogenic response to porous hydroxyapatite ceramics under the skin of dogs. *Biomaterials.* 1992;13(5):308-12.
- [14] Ripamonti U. The morphogenesis of bone in replicas of porous hydroxyapatite obtained from conversion of calcium carbonate exoskeletons of coral. *J Bone Joint Surg Am.* 1991 Jun;73(5):692-703.
- [15] Habibovic P, Yuan H, van der Valk CM, Meijer G, van Blitterswijk CA, de Groot K. 3D microenvironment as essential element for osteoinduction by biomaterials. *Biomaterials.* 2005 Jun;26(17):3565-75.
- [16] Habibovic P, Yuan H, van den Doel M, Sees TM, van Blitterswijk CA, de Groot K. Relevance of osteoinductive biomaterials in critical-sized orthotopic defect. *J Orthop Res.* 2006 May;24(5):867-76.
- [17] Yuan H, Fernandes H, Habibovic P, de Boer J, Barradas AM, de Ruiter A, et al. Osteoinductive ceramics as a synthetic alternative to autologous bone grafting. *Proc Natl Acad Sci U S A.* 2010 Aug 3;107(31):13614-9.
- [18] Sato I, Akizuki T, Oda S, Tsuchioka H, Hayashi C, Takasaki AA, et al. Histological evaluation of alveolar ridge augmentation using injectable calcium phosphate bone cement in dogs. *J Oral Rehabil.* 2009 Oct;36(10):762-9.
- [19] Kwon B, Jenis LG. Carrier materials for spinal fusion. *Spine J.* 2005 Nov-Dec;5(6 Suppl):224S-30S.
- [20] Ginebra MP, Fernandez E, Boltong MG, Bermudez O, Planell JA, Driessens FC. Compliance of an apatitic calcium phosphate cement with the short-term clinical requirements in bone surgery, orthopaedics and dentistry. *Clin Mater.* 1994;17(2):99-104.
- [21] Mirtchi AA, Lemaitre J, Terao N. Calcium phosphate cements: study of the beta-tricalcium phosphate--monocalcium phosphate system. *Biomaterials.* 1989 Sep;10(7):475-80.
- [22] Comuzzi L, Ooms E, Jansen JA. Injectable calcium phosphate cement as a filler for bone

C H A P T E R 2

- defects around oral implants: an experimental study in goats. *Clin Oral Implants Res.* 2002 Jun;13(3):304-11.
- [23] Roemhildt ML, Wagner SD, McGee TD. Characterization of a novel calcium phosphate composite bone cement: flow, setting, and aging properties. *J Mater Sci Mater Med.* 2006 Nov;17(11):1127-32.
- [24] Felix Lanao RP, Leeuwenburgh SC, Wolke JG, Jansen JA. Bone response to fast-degrading, injectable calcium phosphate cements containing PLGA microparticles. *Biomaterials.* 2011 Aug 24.
- [25] Barbieri D, Yuan H, de Groot F, Walsh WR, de Brujin JD. Influence of different polymeric gels on the ectopic bone forming ability of an osteoinductive biphasic calcium phosphate ceramic. *Acta Biomater.* 2011 May;7(5):2007-14.
- [26] Bohner M, Baroud G. Injectability of calcium phosphate pastes. *Biomaterials.* 2005 May;26(13):1553-63.
- [27] Daculsi G, Rohanizadeh R, Weiss P, Bouler JM. Crystal polymer interaction with new injectable bone substitute; SEM and HR TEM study. *J Biomed Mater Res.* 2000 Apr;50(1):1-7.
- [28] Bohner M. Design of ceramic-based cements and putties for bone graft substitution. *Eur Cell Mater.* 2010;20:1-12.
- [29] LeGeros RZ. Biodegradation and bioresorption of calcium phosphate ceramics. *Clin Mater.* 1993;14(1):65-88.
- [30] Yuan H, De Brujin JD, Li Y, Feng J, Yang Z, De Groot K, et al. Bone formation induced by calcium phosphate ceramics in soft tissue of dogs: a comparative study between porous alpha-TCP and beta-TCP. *J Mater Sci Mater Med.* 2001 Jan;12(1):7-13.
- [31] ASTM standard F1980, "Standard Guide for Accelerated Aging of Sterile Barrier Systems for Medical Devices." West Conshohocken, PA: ASTM International; 2007.
- [32] Kokubo T, Takadama H. How useful is SBF in predicting in vivo bone bioactivity? *Biomaterials.* 2006 May;27(15):2907-15.
- [33] Elliott JC. Structure and Chemistry of the Apatites and Other Calcium Orthophosphates. Amsterdam: Elsevier; 1994.
- [34] Ishizaka S, Sugawara I, Hasuma T, Morisawa S, Moller G. Immune responses to xanthan gum. I. The characteristics of lymphocyte activation by xanthan gum. *Eur J Immunol.* 1983 Mar;13(3):225-31.
- [35] Chellat F, Tabrizian M, Dumitriu S, Chornet E, Magny P, Rivard CH, et al. In vitro and in vivo biocompatibility of chitosan-xanthan polyionic complex. *J Biomed Mater Res.* 2000 Jul;51(1):107-16.
- [36] Flautre B, Lemaitre J, Maynou C, Van Landuyt P, Hardouin P. Influence of polymeric additives on the biological properties of brushite cements: an experimental study in rabbit. *J Biomed Mater Res A.* 2003 Aug 1;66(2):214-23.
- [37] Duggirala SS, Rodgers JB, DeLuca PP. The evaluation of lyophilized polymer matrices for administering recombinant human bone morphogenetic protein-2. *Pharm Dev Technol.* 1996 Jul;1(2):165-74.
- [38] Rodgers JB, Vasconez HC, Wells MD, DeLuca PP, Faugere MC, Fink BF, et al. Two lyophilized polymer matrix recombinant human bone morphogenetic protein-2 carriers in rabbit calvarial defects. *J Craniofac Surg.* 1998 Mar;9(2):147-53.
- [39] Habibovic P, Juhl MV, Clyens S, Martinetti R, Dolcini L, Theilgaard N, et al. Comparison of two carbonated apatite ceramics in vivo. *Acta Biomater.* 2010 Jun;6(6):2219-26.
- [40] Ripamonti U, Richter PW, Nilen RW, Renton L. The induction of bone formation by smart biphasic hydroxyapatite tricalcium phosphate biomimetic matrices in the non-human primate Papio ursinus. *J Cell Mol Med.* 2008 Dec;12(6B):2609-21.
- [41] Barradas AM, Yuan H, van Blitterswijk CA, Habibovic P. Osteoinductive biomaterials: current knowledge of properties, experimental models and biological mechanisms. *Eur Cell Mater.* 2011;21:407-29; discussion 29.
- [42] Fujibayashi S, Neo M, Kim HM, Kokubo T, Nakamura T. Osteoinduction of porous bioactive titanium metal. *Biomaterials.* 2004 Feb;25(3):443-50.
- [43] Kondo N, Ogose A, Tokunaga K, Umezawa H, Arai K, Kudo N, et al. Osteoinduction with highly purified beta-tricalcium phosphate in dog dorsal muscles and the proliferation of osteoclasts before heterotopic bone formation. *Biomaterials.* 2006 Sep;27(25):4419-27.

- [44] Eggli PS, Muller W, Schenk RK. Porous hydroxyapatite and tricalcium phosphate cylinders with two different pore size ranges implanted in the cancellous bone of rabbits. A comparative histomorphometric and histologic study of bony ingrowth and implant substitution. *Clin Orthop Relat Res.* 1988 Jul;(232):127-38.
- [45] Fellah BH, Delorme B, Sohier J, Magne D, Hardouin P, Layrolle P. Macrophage and osteoblast responses to biphasic calcium phosphate microparticles. *J Biomed Mater Res A.* 2010 Jun 15;93(4):1588-95.
- [46] Champagne CM, Takebe J, Offenbacher S, Cooper LF. Macrophage cell lines produce osteoinductive signals that include bone morphogenetic protein-2. *Bone.* 2002 Jan;30(1):26-31.
- [47] Heinemann C, Heinemann S, Worch H, Hanke T. Development of an osteoblast/osteoclast co-culture derived by human bone marrow stromal cells and human monocytes for biomaterials testing. *Eur Cell Mater.* 2011;21:80-93.
- [48] Papadimitropoulos A, Scherberich A, Guven S, Theilgaard N, Crooijmans HJ, Santini F, et al. A 3D in vitro bone organ model using human progenitor cells. *Eur Cell Mater.* 2011;21:445-58; discussion 58.



CHAPTER 3

Influence of surface microstructure and chemistry on osteoinduction and osteoclastogenesis by biphasic calcium phosphate discs

Noel L. Davison^{1,2}, Jinyi Su², Huipin Yuan^{1,2,3}, Jeroen J. J. P. van den Beucken⁴, Joost D. de Bruijn^{1,2,5}, Florence Barrère-de Groot²

- 1 MIRA Institute for Biomedical Technology and Technical Medicine, University of Twente, Enschede, Netherlands
- 2 Xpand Biotechnology BV, Bilthoven, Netherlands
- 3 College of Physical Science and Technology, Sichuan University, Chengdu, Sichuan, P.R. China
- 4 Department of Biomaterials, Radboud University Medical Center, Nijmegen, The Netherlands
- 5 School of Engineering and Materials Science (SEMS), Queen Mary University of London, London, United Kingdom

SUBMITTED TO EUROPEAN CELLS & MATERIALS

A B S T R A C T

It has been reported that surface microstructure dimensionality can influence the osteoinductivity of calcium phosphates (CaPs). It has also been shown that osteoclast formation may be linked to osteoinduction through interactions with this surface structure. We hypothesized that CaP surface structure dimensions of $\leq 1 \mu\text{m}$ may drive osteoinduction and osteoclast formation irrespective of macrostructure (e.g., concavities, interconnected macropores, interparticle space) or surface chemistry in vitro and in vivo. To test this, biphasic calcium phosphate (BCP, 80% hydroxyapatite / 20% tricalcium phosphate) was prepared with surface structure dimensions of $\sim 1 \mu\text{m}$ or $\sim 2\text{-}4 \mu\text{m}$ (BCP1150 and BCP1300, respectively) in the form of planar discs without macropores and concavities. BCP1150 was also sputter coated with titanium (BCP1150Ti) to change its surface chemistry but not alter its surface structure or chemical reactivity. After 12 weeks implantation, BCP1150 and BCP1150Ti induced ectopic bone in the muscle of 4/5 and 3/5 dogs, respectively, but BCP1300 formed no ectopic bone. Large, densely organized multinucleated osteoclast-like cells colonized BCP1150 but were smaller and less fused on BCP1150Ti; in contrast to both, few multinucleated cells formed on BCP1300. In vitro, RAW264.7 cells cultured in the presence of RANKL proliferated and differentiated into fused, TRAP positive osteoclasts on BCP1150 and BCP1150Ti, but cell proliferation, survival, and TRAP activity were significantly inhibited on BCP1300. Together, these results suggest that surface microstructure of CaPs is the preeminent material factor necessary for osteoinduction potentially based on a link between surface microstructure and osteoclast formation.

1 INTRODUCTION

Cells interact with biomaterial surfaces in specific ways that can modulate their attachment, growth, and survival [1,2]. Although topographical control of cell behavior is not a new field of research [3,4], recent studies have shed light on how cell-surface interactions can direct cell differentiation which may be useful for biomaterial-guided tissue regeneration strategies [5].

Certain biomaterials, such as microstructured calcium phosphates (CaPs), can induce de novo bone formation without exogenous stem cells or growth factors, thus making them particularly attractive for use as bone graft substitutes [6]. When bone formation is induced by osteoinductive CaP, the newly formed bone is tightly bonded to the material surface suggesting that cell-surface interactions are largely driving this response. Although the material parameters necessary to induce de novo bone formation are unclear, osteoinductive materials developed by different groups seem to share similar surface structure, specifically surface topographical features on a (sub)micron-scale size range. For instance, Yuan et al. (1998, 1999) showed that hydroxyapatite (HA) with surface microstructure was osteoinductive in the dorsal muscle of dogs, while chemically and macroscopically similar HA with a dense surface was not [7,8]. Additionally, Yuan et al. (1998), Habibovic et al. (2005), and Le Nihouannen et al. (2005) all demonstrated that microstructured biphasic calcium phosphate (BCP), containing both HA and tricalcium phosphate (TCP), was osteoinductive [8–10]; however, BCP sintered at a higher temperature resulting in little microstructure was not osteoinductive [11]. Proving that osteoinduction can also be achieved by non-CaP materials as well, Fujibayashi et al. (2004) and later Fukuda et al. (2011) both reported that when surface nano/microstructure was conferred to a titanium surface by thermal and chemical treatment, the material induced bone formation in the dorsal muscle of dogs, but no bone was formed by the untreated material with a smooth surface despite similar macroporosity and geometry [12,13]. These studies show that despite different material chemistry and macro-scale geometry, the surface architecture may be the prevailing material characteristic necessary for their osteoinductive capacity.

Stemming from the lack of clarity into what precisely makes a material osteoinductive, various theories attempt to explain how surface microstructure may biologically drive osteogenic differentiation of progenitor cells and consequently induce de novo bone formation. One explanation is that cell differentiation can be induced by the mechanical signals transmitted to the nucleus through attachment to microstructured topography, i.e. mechanotransduction [14]. Both osteoblasts and osteoclasts are sensitive to surface topography, in

particular surface nano-/micro-roughness [15,16], micropore size [17], and even how orderly or randomly the topographical features are spatially arranged [18]. Another prevailing theory proposes that the biological importance of surface microstructure results from increased surface reactivity arising from a larger specific surface area. For instance, by increasing the surface area available for re-precipitation of apatite crystals in the body, more osteogenic growth factors, such as bone morphogenetic proteins (BMPs), with strong binding affinity to CaP would be able to adsorb to the surface [9,19–21]. Additionally, higher surface area of soluble CaPs potentiates the release of calcium and phosphate ions, which have shown to directly stimulate osteogenic differentiation of mesenchymal stromal cells *in vitro* [22–24]. Considering these two major theories on how microstructure may direct osteoinduction, it is difficult to investigate them independently because both physical topography and surface reactivity are intrinsically linked to the surface architecture [21]. Thus, it is unknown if physical topography or surface reactivity plays a prevailing role in osteoinduction.

Still, surface microstructure is only one material parameter of several that have been implicated with osteoinduction. Macro-scale features such as interconnected macropores, implant particle size, and surface concavities have all been previously described to be “essential” and “requisite” for osteoinduction [9,25–27]. Similar to surface microstructure, it is straightforward to assume that macropores and concavities are important for bone formation because they also increase the surface area available for ion exchange and protein adsorption. Additionally, interconnected macropores allow blood vessel perfusion and bony ingrowth [21]. However, surveying the complete literature of osteoinductive materials recently reviewed by Barradas et al. (2011), none were devoid of macropores or surface concavities that arise thereof, probably due to the fact that dense (or only microporous) materials are not ideal bone graft substitutes because they restrict bony ingrowth [28]. Consequently, it remains unclear whether macropores and concavities are in fact essential to initiate de novo bone formation or if microstructure alone is sufficient.

Histologically, osteoinduction by CaPs is characterized by the presence of bone forming osteoblasts, bone-regulating osteocytes in their bony lacunae, and multinucleated osteoclasts resorbing the material and newly formed bone (shown in Chapter 2). Of these cell types, it has been speculated that osteoclasts may be prerequisite for de novo bone formation by TCP [29,30], hydroxyapatite/calcium carbonate [31,32], as well as one of the most researched osteoinductive CaPs, microstructured BCP [33]. To further investigate this relationship, we developed an *in vitro* model of osteoclastogenesis by culturing RAW264.7 macrophages on planar CaP discs in the presence of osteoclast differentiating

factor RANKL (receptor activator of NF- κ B ligand). Whether this *in vitro* model of osteoclastogenesis is relevant to the *in vivo* performance of prominent osteoinductive CaPs such as microstructured BCP is currently unknown.

Given the present knowledge, we hypothesized that surface structure is the preeminent material factor responsible for the formation of both osteoclast-like cells and de novo bone. To evaluate this, two BCPs with different surface structure were prepared in the form of planar discs, thus eliminating the effects of interconnected macropores or concavities. To evaluate whether or not surface chemistry also contributes to osteoinductivity, BCP was also surface coated with titanium. Disc-shaped constructs were implanted in the dorsal muscle of dogs, the classical model for evaluating osteoinduction, and the formation of de novo formed ectopic bone and multinucleated osteoclast-like cells were histologically analyzed. The effects of surface structure and chemistry on osteoclast formation were further evaluated by developing and *in vitro* osteoclastogenesis model to assay osteoclast survival, activity, and morphology.

2 MATERIALS AND METHODS

2.1 Preparation and characterization of BCP

BCP powder composed of 80% HA/ 20% β -TCP was prepared by wet precipitation as described elsewhere [25]. The powder was foamed with diluted H₂O₂ (0.1%) (Merck) at 60 °C to produce microporous green bodies and then dried. The dry green bodies were subsequently sintered at 1150 °C or 1300 °C for 8 hours to achieve surface micro-grains and pores (BCP1150) or larger fused grains and few micropores (BCP1300). Ceramic discs (\varnothing 9 x 1 mm) were machined from the ceramic bodies using a lathe and a diamond saw microtome (Leica SP1600). Discs were ultrasonically cleaned in successive baths of acetone, ethanol, and deionized water for 15 minutes, and then dried at 60 °C.

To obtain a different surface chemistry while preserving the surface microstructure, BCP1150 discs were sputter coated with titanium (BCP1150Ti) using a radiofrequency magnetron unit (Edwards ESM 100) as previously described [34]. Both sides of the discs were coated for 15 minutes at 200 W, resulting in a visually complete layer of titanium roughly 50 nm thick. The elemental composition and distribution of the titanium coating was verified using electron dispersive spectroscopy (EDS), as previously described [35]. Briefly, samples were affixed to metal stubs and scanned by a scanning electron microscope (Philips XL30) equipped with an energy dispersive spectrometer (EDAX; AMETEK, USA). The

distribution of elements of interest (Ca, P, and Ti) was analyzed and visually displayed. The associated error for all the EDS analyses was calculated to be less than 10%.

Crystal chemistry of the materials was analyzed by X-ray diffraction (Rigaku Miniflex II) scanning the range $2\theta = 25\text{--}45^\circ$ (step size = 0.01° , rate = 1° min^{-1}) as previously described in Chapter 2. Surface topography of the materials was characterized by scanning electron microscopy (SEM) (JEOL JSM-5600) after sputter coating with gold for 90 seconds (JEOL JFC 1300). Surface grain and pore size were analyzed by manually measuring the vertical distance across the features ($n > 50$) in scanning electron micrographs (magnification: 5000x) taken at $n = 3$ random locations using Image J software (NIH, USA).

The surface reactivity of the discs was analyzed in simulated physiologic solution (SPS) (50 mM HEPES, 140 mM NaCl, and 0.4 mM NaN₃ for sterility; all from Sigma Aldrich) at pH3 and pH7. Discs ($n = 3$) were incubated in SPS (8 mL) in a tissue culture multiwell plate incubated at 37 °C, 5% CO₂ for 7 days with gentle shaking. The solution was sampled and refreshed with the same amount (100 µL) after 10 minutes, 1, 2, 4 hours, 1, 4, and 7 days. Calcium and phosphate released into the solution were quantified using QuantiChrom (BioAssay System, USA) and PhoshoWorks (AAT BioQuest, USA) colorimetric assay kits, respectively, following the manufacturers' instructions. Absorbance was detected using a Zenyth 3100 multimode spectrophotometer.

2.2 ***In vivo study of osteoinduction by BCP constructs***

Implantation of sandwich constructs

BCP constructs were implanted in the dorsal muscle of dogs to test their capacity to form ectopic bone. BCP constructs were made by gluing (Cyanoacrylate "superglue", Pertex) two discs together with two strips of nylon wire ($\sim \text{Ø}0.7 \text{ mm}$) in between to create a central gap (Figure 3a). "Sandwich" shaped constructs were sterilized by gamma irradiation ($> 25 \text{ kGy}$) prior to implantation.

All surgery was conducted at the Animal Center of Sichuan University in conformance with the institutional animal ethics committee's guidelines. Sterile BCP constructs were implanted in the dorsal muscle of healthy male mongrel dogs ($n = 5$ dogs, 1–4 years, 10–15 kg) for 12 weeks. Animals were first given general anesthesia by abdominal injection of sodium pentobarbital (30 mg kg^{-1} body weight) and constructs were implanted into paraspinal muscle pockets created by scalpel incision and blunt dissection. One construct of each material was implanted in each dog resulting in 3 constructs implanted per animal. Skin

incisions were closed layer by layer with non-resorbable sutures for identification at harvest. Following surgery, the animals were given daily intramuscular injections of buprenorphine (0.1 mg per animal) for 2 days and penicillin (40 mg kg^{-1}) for 3 days to relieve pain and prevent infection. Animals were allowed to undertake full activity and received a normal diet immediately after surgery.

Sample harvest and histological processing

At the end of 12 weeks, the animals were sacrificed by abdominal injection of sodium pentobarbital (60 mg kg^{-1}) and samples were immediately harvested and fixed in cold phosphate-buffered formalin solution, dehydrated in graded ethanol series, and embedded in methyl methacrylate (MMA) (LTI, Netherlands) at room temperature.

Histological sections ($\sim 30 \mu\text{m}$) of the undecalcified samples were made using a Leica SP1600 microtome and stained en bloc with 1% methylene blue and 0.3% basic fuchsin solutions for histological analysis.

Stained histological sections were scanned using a Dimage Scan Elite 5400II slide scanner (Konica Minolta) for gross evaluation. Bone formation was analyzed at 20x magnification using a light microscope (Nikon Eclipse E200). More than 10 sections per sample spanning more than half the construct were analyzed for de novo bone formation by 2 investigators (ND & JS), and the number of samples positive for bone formation per the total number of samples implanted (i.e., bone incidence rate) was recorded.

2.3 *In vitro studies*

Culture of RAW264.7 osteoclasts and C2C12 myoblasts on BCP discs

To model osteoclastogenesis in vitro, murine RAW264.7 macrophages (ECACC, Wiltshire, UK) were cultured on BCP discs for up to 5 days in the presence of osteoclast differentiation factor RANKL as described previously [36]. RAW264.7 cells were first expanded in tissue culture flasks with basic medium composed of alpha MEM (Lonza), supplemented with 10% HyClone FetalClone I serum (Thermo Scientific) and 1% penicillin-streptomycin (Life Technologies). At $\sim 75\%$ confluence, cells were scraped loose from the tissue culture flasks, resuspended in basic medium supplemented with RANKL (40 ng mL^{-1} , Peprotech, UK), and seeded on BCP discs ($2 \times 10^4 \text{ cells cm}^{-2}$) contained in 48-well culture plates (Greiner Bio-One). All discs were heat sterilized in a dry chamber at 200°C for 2 hours prior to cell culture.

RAW264.7 cells were culture for 5 days with medium refreshment (basic medium + RANKL) after 1 day. In this culture model, cells begin to fuse and differentiate into osteoclasts by day 3, continue fusing through day 4-5, and undergo apoptosis by day 6-7 [36,37]. Therefore, biochemical assays focused on day 3-5 as the relevant period of osteoclastogenesis. Osteoclast culture experiments were repeated to confirm the results of the various assays described below.

C2C12 myoblasts were also cultured on BCP discs for comparison. C2C12 cells were similarly expanded in basic medium, trypsinized at confluence, and cultured on BCP discs (seeding density = 2×10^4 cells cm $^{-2}$) for 5 days. All cells were cultured in a humidified incubator maintained at 37 °C and 5% CO $_2$.

Cell viability, proliferation, and DNA content

The AlamarBlue (AB) fluorescent assay (Life Technologies) was used to measure cell viability and proliferation [38] on BCP. AB measures the reductive activity inside living cells, and is commonly used in the literature as a more sensitive alternative to formazan-based cell viability assays such as MTT and XTT [39,40]. At various culture time points, cells were incubated with culture medium containing 5% AB reagent for 2 hours in culture conditions and then media samples were collected in a 96-well plate for fluorescent detection (excitation = 530 nm, emission = 590 nm) using a Zenyth Multimode plate reader. Cell proliferation can be measured by assaying cell viability over time [38]. For this assay, the same procedure was followed except that AB-containing culture medium was removed and refreshed with normal culture medium, and then continuously cultured until the next time point. For viability and proliferation assays, n = 3 culture replicates were measured.

DNA content was measured in the cell lysate using a CyQuant DNA detection kit (Life Technologies). After 3, 4, and 5 days culture on discs, adherent cells were rinsed in PBS and then freeze-thawed in CyQuant cell lysis buffer as recommend by the manufacturer. Cell lysate was thoroughly homogenized and sampled from n = 3 replicate discs for measurement using the kit. A Zenyth 3100 Multimode plate reader was used to detect the fluorescent signal of the assay.

Tartrate resistant acid phosphatase (TRAP) activity

Tartrate resistant acid phosphatase (TRAP), an enzyme marker of osteoclast differentiation and activation [41], was measured in RAW264.7 cells cultured on discs after 3, 4, and 5 days by both biochemical activity and cytochemical staining.

TRAP activity in the cell lysate from n = 3 culture replicates was quantified by

conversion of *p*-nitrophenylphosphate to *p*-nitrophenol (pNP) in sodium acetate buffer (pH 5.8) containing potassium sodium tartrate (10 mM) as reported by Ljusberg et al. (1999). Cell lysate was obtained by first rinsing disc-adherent cells with PBS and then freeze-thawing in cell lysis buffer (0.1 M sodium acetate, 0.1% Triton X-100, pH 5.8). Optical absorbance of the assay reaction was measured using a Zenthy multimode spectrophotometer. Absorbance was converted to mM pNP using a standard curve of pNP (Sigma) and normalized to viable cell signal from AlamarBlue.

TRAP was also visualized on $n = 2$ disc replicates using a commercial staining kit (Leukocyte Acid Phosphatase Kit, Sigma). Prior to staining, cells were briefly rinsed in PBS and fixed in acetone methanol solution per the manufacturer's instructions. Images were captured using a Nikon SMZ800 stereomicroscope equipped with a Nikon camera.

SEM of osteoclast morphology

Osteoclast morphology was analyzed by SEM. Cells cultured on discs ($n = 2$) were fixed in 2.5% gluteraldehyde, dehydrated in a graded ethanol series, and finally dried in HMDS (Alfa Aesar). Dehydrated cells were then sputter coated with gold for enhanced imaging resolution. Osteoclast size was quantified in scanning electron micrographs (400x magnification) by calculating the mean surface area of cells at 3 random locations of replicate discs ($n = 2$) using automated threshold, edge detection, and particle analysis functions in ImageJ software (NIH, USA). Only cells $> 400 \mu\text{m}^2$ were included in the analysis to exclude mononuclear cells.

2.4 Statistics

Statistical comparisons were performed using One-way ANOVA and Tukey's post hoc tests; P values < 0.05 were considered significant. All statistical analyses were conducted in GraphPad Prism 6.0.

3 RESULTS

3.1 BCP characterization

BCP with different surface microstructure was prepared by changing the sintering temperatures, shown by SEM (Figure 1a). BCP1150 contained grains and pores sized $\leq 1 \mu\text{m}$ in diameter but BCP1300 contained larger, fused grains ($\sim 3 \mu\text{m}$) and larger but fewer micropores ($\sim 2 \mu\text{m}$) (Figure 1b). Because no macropore porogens were introduced during synthesis, neither material

contained macropores or substantial concavities. BCP1150 was sputter coated with titanium, which preserved the original surface microstructure as shown by SEM and grain/pore size analysis (Figure 1a,b). The crystal chemistry of the materials was confirmed by XRD to be BCP containing 80-85% HA and 15-20% TCP (Figure 1c). Coating BCP1150 with titanium did not substantially alter the XRD spectra.

The surface reactivity of the materials was analyzed by measuring calcium and phosphate ion release in SPS at pH7 and pH3 (Figure 1d). At neutral pH, all

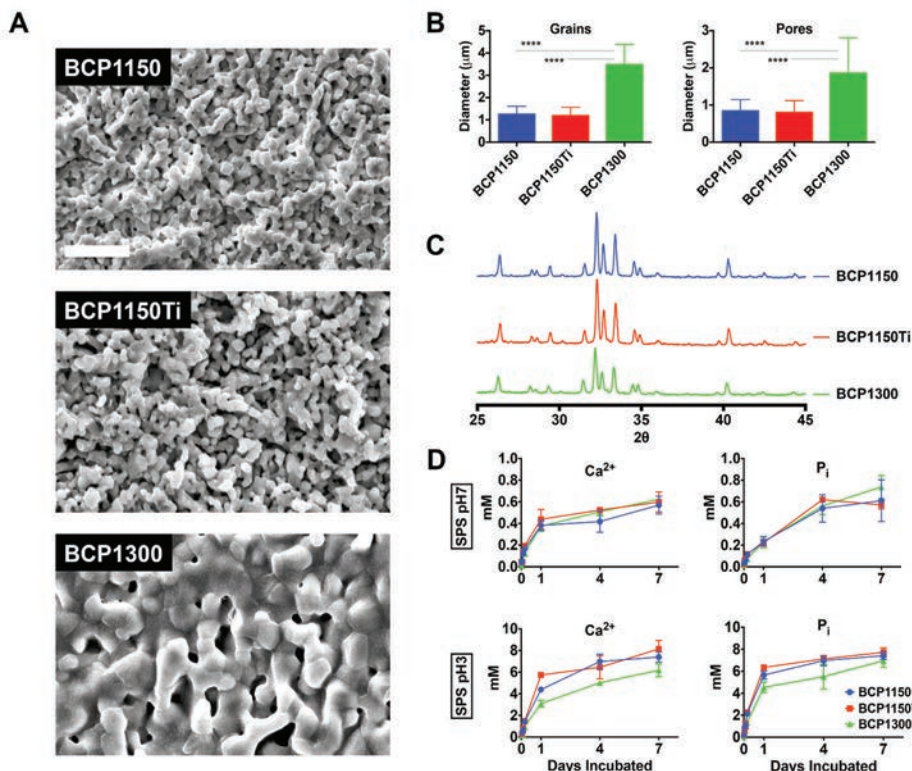


Figure 1. Physicochemical characterization of BCP. Scanning electron micrographs show the difference in surface microstructure between BCP1150 and BCP1300 and the similarity between BCP1150 and BCP1150Ti with titanium coating (scale = 10 μm) (A). Surface grain and pore size $\leq 1 \mu\text{m}$ of BCP1150 were unchanged by titanium coating; however, grains and pores of BCP1300 were significantly larger (B). (C) All three materials have equivalent BCP spectra by XRD. (D) Chemical reactivity in simulated physiologic solution (SPS) show that ion release of all three materials is equivalent at pH7 but slightly faster for BCP1150 with and without titanium coating than BCP1300 at pH3. Data represents the mean \pm S.D. of $n = 3$ replicate discs; **** $P < 0.0001$.

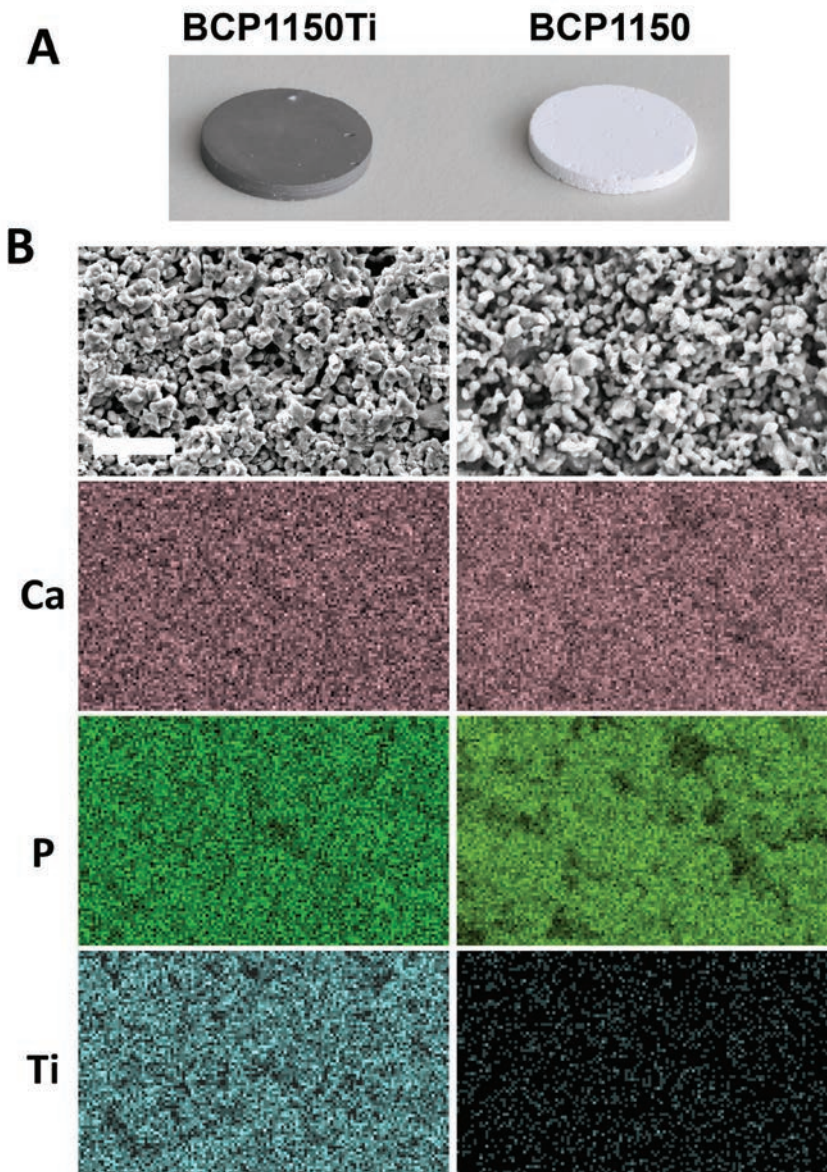


Figure 2. Elemental analysis of BCP1150Ti by electron dispersive spectroscopy (EDS). (A) Overview images of BCP1150 and BCP1150Ti show that discs were appreciably devoid of concavities or macropores and that titanium coating uniformly covered the disc surfaces. (B) Elemental diffraction spectroscopy (EDS) analysis (2000x magnification) shows titanium (Ti) on the surface of BCP1150Ti (left column) is evenly distributed and porous similar to the underlying substratum composed of calcium (Ca) and phosphorus (P). In comparison, BCP1150 (right column) only showed background noise (30x scale = 500 µm; 2000x scale = 10 µm).

three materials released similar amounts of ions over time, but at acidic pH, ion release from BCP1150 and BCP1150Ti was higher than BCP1300 resulting from the increased surface area of the microstructure. There was no change in ion release by BCP1150 with or without the titanium coating showing that the coating did not change the surface reactivity of the material (Figure 1d).

Sputter coating BCP1150 with titanium resulted in a visually homogenous layer on all sides of the discs (Figure 2a). The titanium layer was analyzed by EDS (Figure 2b), which showed the presence and homogeneous distribution of titanium coating on the surface. In summary, sputter coating BCP1150 with titanium resulted in a material with identical surface structure and chemical reactivity but different surface chemistry.

3.2 *In vivo* results

BCP sandwich constructs were implanted into the dorsal muscle of dogs for 12 weeks to study the effects of surface microstructure and chemistry on osteoinduction. A gap between the BCP discs was created using nylon wire spacers to allow tissue in-growth and bone formation (Figure 3a). However, soft tissue formation in the space between the discs and around the nylon wires tended to be weak for all materials compared to tissue formation on the outer edges of the constructs (Figure 3b).

The incidence of de novo bone formation was quantified by thorough analysis of histological sections. De novo bone formation was observed in 4 out of 5 BCP1150 constructs, 3 out of 5 BCP1150Ti constructs, and 0 out of 5 BCP1300 constructs (Table 1). For BCP1150 and BCP1150Ti, bone was predominantly formed on the outer surfaces of the constructs (Figure 3c) rather than on the inner surfaces of the central gap. Although stretches of bone were not thicker than ~50 µm and generally spanned less than several hundred microns long, cuboidal osteoblasts were seen forming new bone and osteocytes were present in bone lacunae (Figure 3c). Bone area was not quantified by histomorphometry due to the small amounts present.

Multinucleated osteoclast-like cells extensively covered the surface of BCP1150 but were smaller and less organized on BCP1150Ti (Figure 3c,d). For both materials, osteoclast-like cells adhered to the material adjacent to de novo formed bone. In contrast to BCP1150 with and without a titanium coating, BCP1300 was largely encapsulated by fibrous tissue and contained scarce multinucleated osteoclast-like cells (Figure 3c,d).

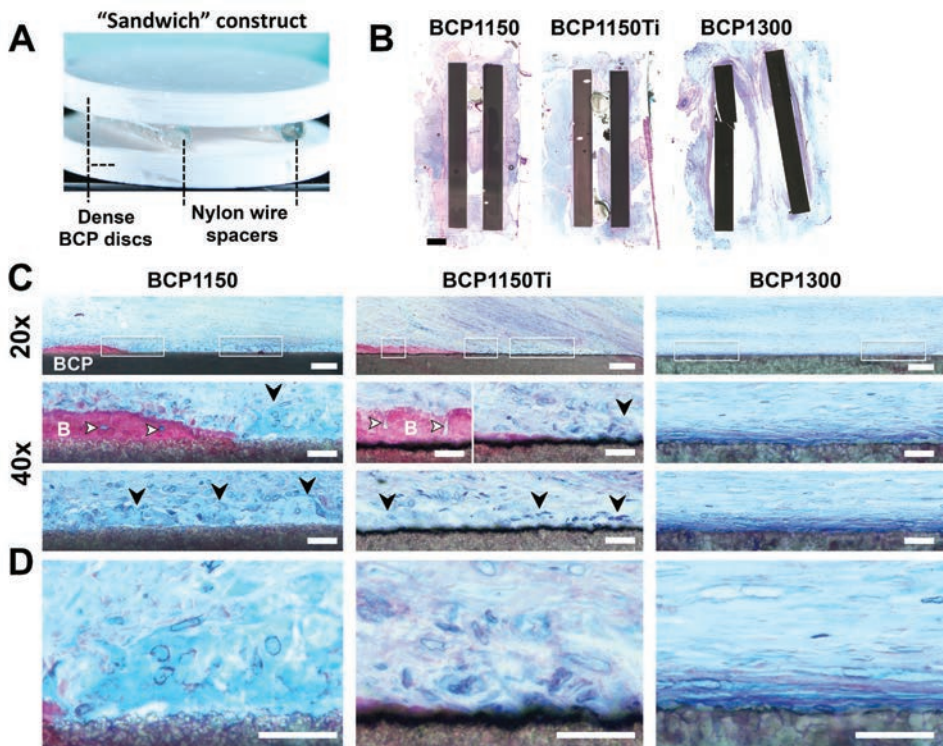


Figure 3. Intramuscular implantation of BCP sandwich constructs. BCP sandwich constructs were made by gluing together two BCP discs with a central gap in between them created by nylon wire spacers (A). Constructs were implanted in the dorsal muscle of dogs for 12 weeks and histological sections were stained for bone using methylene blue and basic fuchsin. Overview images of cross-sections taken through the middle of explants show soft tissue (pink, purple, blue) formation around the BCP constructs (brown, black) with limited tissue infiltration in the gap between the discs. Note: few macropores or concavities are present in the discs (scale = 1 mm) (B). At 20x magnification of the outer surface of the constructs, a thin layer of ectopic bone (pink) is evident on BCP1150 and BCP1150Ti but only fibrous tissue (dark blue, purple) is seen on BCP1300 (scale = 100 μ m). At 40x magnification (top row), osteocytes (white arrows) reside in characteristic bone (B) lacunae. Multinucleated osteoclast-like cells (black arrows) border ectopic bone on BCP1150 and BCP1150Ti. However, these cells appear smaller, less fused, and less organized on BCP1150Ti than on BCP1150 (40x, bottom row). The titanium layer on BCP1150Ti remained intact throughout the implantation (black strip on the surface of the disc) (scale = 25 μ m). The difference in multinucleated cell formation on BCP1150 versus BCP1150Ti can be seen in detail micrographs, in contrast to the dense fibrous tissue on BCP1300 (D) (scale = 25 μ m).

Table 1. Incidence rate of specimens containing de novo bone formation.

BCP1150	BCP1150Ti	BCP1300
4/5	3/5	0/5

3.3 *In vitro* results

Cell viability and proliferation

To further investigate the effects of BCP surface structure and chemistry on osteoclast-like cell formation, RAW264.7 macrophages were cultured on BCP discs and differentiated into osteoclast-like cells in the presence of RANKL. At day 3, 4 and 5, DNA content from cells cultured on BCP1150 was ~3-5 times greater than on BCP1300 (day 3: $P < 0.0001$; day 4: $P = 0.0001$; day 5: $P = 0.004$) (Figure 4a). DNA content from cells cultured on BCP1150Ti was also significantly greater than on BCP1300 ($P < 0.01$), at levels similar to BCP1150 at day 4 and 5 (Figure 4a). These data indicated that the difference in titanium coating had little effect on cell growth; however, the difference in microstructure had a pronounced effect. After 5 days of culture, cell viability was ~2x higher on both BCP1150 and BCP1150Ti than on BCP1300 (both $P < 0.0001$) (Figure 4b). Further, cell viability was higher for BCP1150Ti than for BCP1150 ($P = 0.002$) (Figure 4b).

RAW264.7 cell proliferation was analyzed on BCP1150 and BCP1300 by measuring cell viability over time normalized to the viability at the time of seeding (d0) (Figure 4c). BCP1150Ti was not included in this analysis, focusing only on the effects of surface structure, not surface chemistry. At day 1, cell viability was similar on the materials suggesting that initial cell attachment was equivalent. By day 3, RAW264.7 cell proliferation was significantly greater for BCP1150, resulting in ~2x greater viability than on BCP1300 ($P = 0.001$). The same difference in cell viability was maintained through day 4 ($P = 0.004$) and day 5 ($P = 0.005$), indicating that BCP1150 stimulated significantly more proliferation of RAW264.7 cells than BCP1300 over the entire culture period. In fact, RAW264.7 cells cultured on BCP1300 did not proliferate between 1 and 5 days culture (Figure 4c). To evaluate if interactions with BCP1300 inhibited the proliferation of other cell types, C2C12 myoblasts were also cultured on the materials but in contrast, these cells proliferated in typical logarithmic fashion on BCP1300 and to a greater extent than on BCP1150 by day 4 and 5 ($P = 0.003$ and $P = 0.001$, respectively) (Figure 4d).

In sum, BCP1150 promoted significantly higher cell growth and viability of RAW264.7 (pre-)osteoclasts than BCP1300 in a process that was not adversely affected by titanium coating; however, this response was not universal to other cell types such as C2C12 myoblasts.

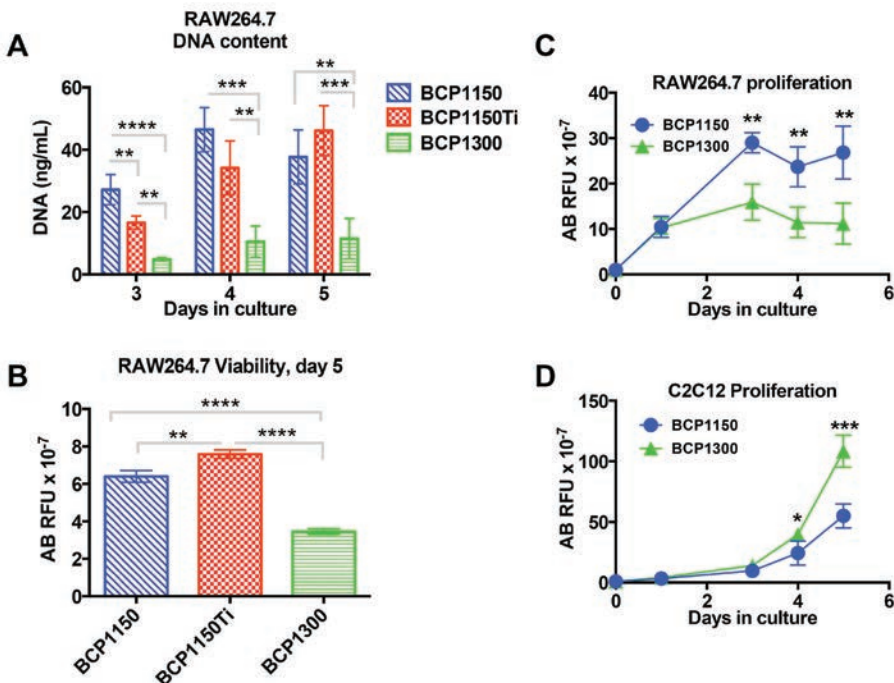


Figure 4. Cell viability and proliferation on BCP in vitro. RAW264.7 cells were cultured on BCP discs in the presence of RANKL for 5 days to stimulate osteoclast formation. DNA content in the lysate from cells cultured on BCP1150 was significantly higher than on BCP1300 at day 3, 4, and 5. DNA content was different between BCP1150 and BCP1150Ti at day 3 and 4; however, they were equivalent by day 5 (A). At day 5, osteoclast viability was also significantly higher on BCP1150 and BCP1150Ti than on BCP1300, as measured by AlamarBlue (AB) metabolic indicator (AB RFU = AB relative fluorescent units) (B). Comparing the effects of only surface microstructure, RAW264.7 cells were again cultured in the presence of RANKL on BCP1150 and BCP1300 and cell viability was measured over time indicating cell proliferation. After 1 day, viability was equivalent between BCP1150 and BCP1300, but by days 3, 4, and 5 cells had proliferated on BCP1150 but not on BCP1300 (C). In contrast, C2C12 myoblasts proliferated more on BCP1300 than on BCP1150 (D). Data represents the mean \pm S.D. of n = 3 replicate discs; * P < 0.05, ** P < 0.01, *** P < 0.001, **** P < 0.0001.

TRAP activity

TRAP enzyme activity in the RAW264.7 cells was assayed both biochemically in the cell lysate and cytochemically by staining. Biochemical TRAP activity in the lysate of cells cultured on BCP1150 was significantly higher than that of BCP1300 at day 3 (~4x, P < 0.0001), day 4 (~3x, P < 0.0001), and day 5 (~2x, P = 0.008) (Figure 5a). Cells cultured on BCP1150Ti also expressed significantly more TRAP activity than BCP1300 at day 3 (~2x, P = 0.023) and day 4 (~2.5x, P=0.002), although at day 5 there was no statistical difference (P = 0.194). Cellular TRAP activity was different between BCP1150 and BCP1150Ti at day 3 (~1.8x, P

=0.004); however, by day 4 and 5, there was no statistical difference ($P = 0.144$ and 0.102 , respectively).

To visually confirm the biochemical results, cells were stained for TRAP at the same time points (Figure 5b). Visualization of TRAP staining on BCP1150Ti was not possible because of the dark color of the coating. A clear difference in osteoclast fusion and TRAP activity between BCP1150 and BCP1300 was observed (Figure 5b): cells were substantially larger and more intensely stained on BCP1150 at all time points. On BCP1150, numerous cell-cell junctions were observed between densely distributed cells; in contrast, on BCP1300, cell junctions were sparse likely owing to less cells present (Figure 5b), in confirmation of the cell viability and DNA assays (Figure 4).

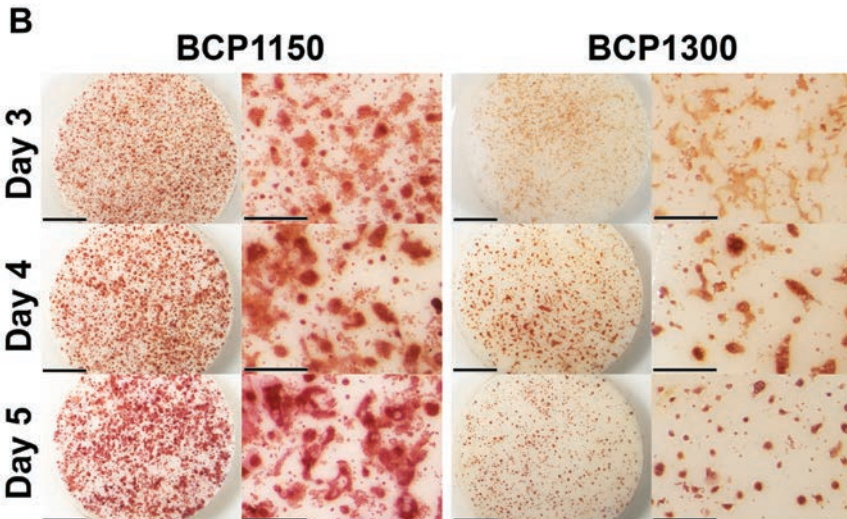
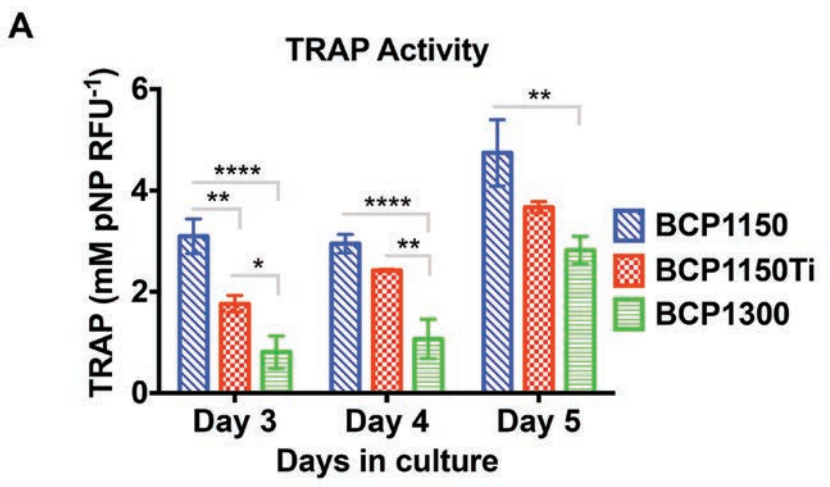


Figure 5, opposite. Tartrate resistant acid phosphatase (TRAP) activity of RAW264.7 osteoclasts cultured on BCP. Biochemical TRAP activity in the cell lysate was significantly higher on BCP1150 than BCP1300 throughout the culture period, as well as BCP1150Ti at day 3 (A). By cytochemical staining, osteoclasts formed on BCP1150 are consistently larger, denser, and more intensely stained than on BCP1300, in agreement with the biochemical assay (overview scale = 2 mm; detail scale = 500 μ m). Visualization of TRAP staining was not possible on BCP1150Ti discs due to their dark color. Biochemical TRAP activity (mM pNP normalized to viable cells, AB RFU) represents the mean \pm S.D. of n = 3 replicate discs; * P < 0.05, ** P < 0.01, *** P < 0.001, **** P < 0.0001.

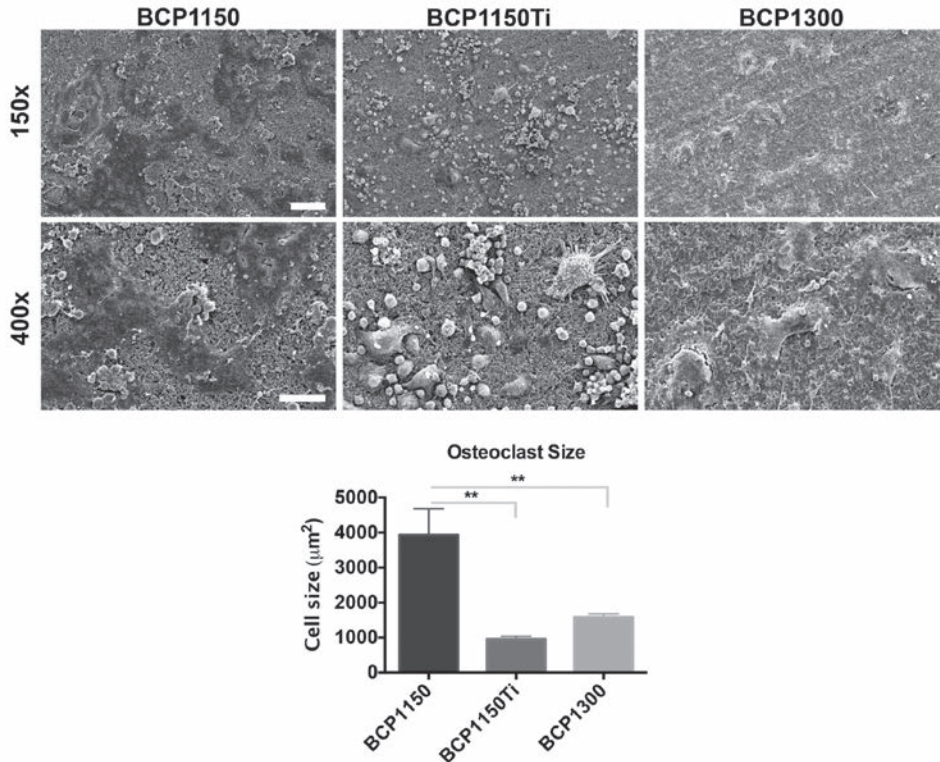


Figure 6. Scanning electron microscopy (SEM) of osteoclasts formed on BCP. SEM micrographs captured at day 5 show massive networks of fused osteoclasts on BCP1150 (large dark cells) whereas cells were significantly smaller and less fused on BCP1150Ti and BCP1300 (150x scale = 100 μ m; 400x scale = 50 μ m). Osteoclast size data represents the mean \pm S.D. of n = 2 replicate discs; ** P < 0.01.

Osteoclast morphology and size

Osteoclast morphology and size were analyzed by SEM at day 5, corresponding with the peak of TRAP activity and cell fusion visualized by TRAP staining (Figure 6). On BCP1150, fused cells were massive ($\sim 4,000 \mu\text{m}^2$) and tightly attached to the BCP surface in an extensive cell network. Single cells were generally found in clusters with partially fused cell membranes. In contrast, fused cells on BCP1150Ti were $\sim 75\%$ smaller ($\sim 1,000 \mu\text{m}^2$, $P = 0.002$) and appeared rounder and less spread out on the surface. On BCP1300, fused cells were also smaller than on BCP1150 ($\sim 1,500 \mu\text{m}^2$, $P = 0.008$), and often appeared to be apoptotic or necrotic with deteriorating cell membranes. Less cells were present on BCP1300 than BCP1150 and BCP1150Ti, in agreement with the cell viability and DNA assays.

4 DISCUSSION

Over the years, the importance of surface microstructure on the osteoinductive potential of microstructured CaPs – and in particular BCP – has been well characterized by different research groups; however, the material parameters necessary for osteoinduction remain unclear. For instance, macroporosity and concavities have also both been described as “essential.”[9,26,27] Indeed, in all of relevant literature describing osteoinduction, implants have been macroporous to allow for bony ingrowth and blood vessel perfusion [28], so whether surface microstructure is solely sufficient to trigger de novo bone formation has not been addressed. By synthesizing two chemically equivalent BCPs in the form of planar discs differing only in the size scale of their surface features, macropores and concavities were virtually eliminated; thus, the effect of surface structure on osteoinduction was more clearly isolated. Specifically, BCP1150 contained surface grains and pores sized $\leq 1 \mu\text{m}$ (submicron-scale) while BCP1300, sintered at a higher temperature, contained larger grains and larger but fewer pores. By introducing a submicrostructured BCP coated with titanium as a control, the effects of surface chemistry on osteoinduction were investigated. Titanium was chosen on account of its documented potential as an osteoinductive metal as well as high biocompatibility. In order to preserve the microstructure of BCP1150, only a thin layer of titanium was applied. Rather than being fully sealed, the line-of-sight sputter deposition of titanium also preserved the chemical reactivity of BCP1150 and was still intact after implantation (Figure 7).

In a classical intramuscular model for evaluating osteoinduction, the materials with submicron-scale surface structure – BCP1150 and BCP1150Ti – induced

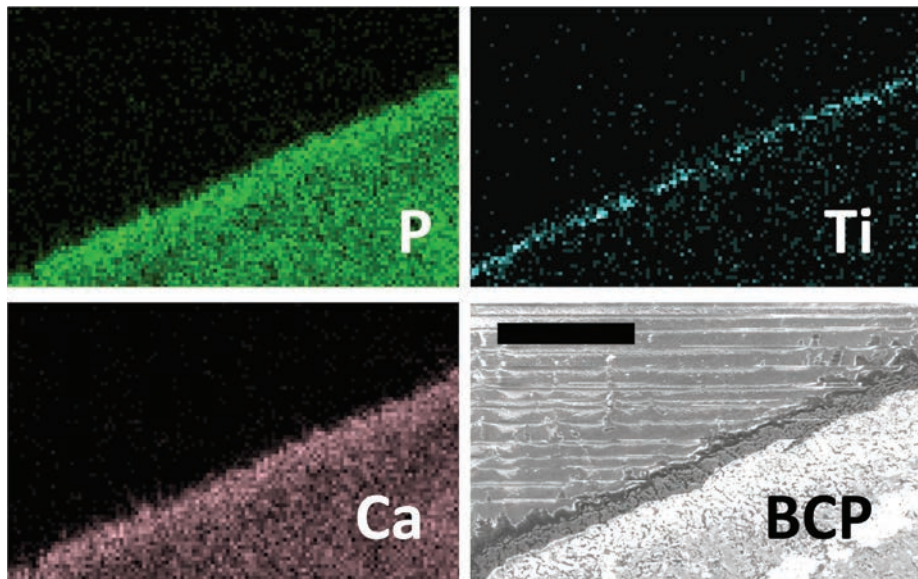


Figure 7. Elemental analysis of BCP1150Ti construct explant. After 12 weeks intramuscular implantation, a thin layer of titanium is still present on the edge of the BCP115Ti construct disc. Scale = 50 μm .

ectopic bone formation in 3-4 out of 5 dogs. In contrast, BCP1300 with micron-scale surface features and few micropores did not induce de novo bone formation, despite having similar chemical reactivity to the osteoinductive materials. These results suggest that macropores and concavities are not essential for osteoinductive capacity and surface chemistry may be a flexible material parameter as long as osteoinductive surface structure is maintained.

Because all three materials shared similar chemical reactivity, the prevailing theory that microstructure directs osteoinduction due to increased release of osteogenic Ca^{2+} and P_i ions cannot fully explain the observed differences in the incidence of bone formation [21–23,42]. Rather, these results suggest that physical interactions of cells with submicron-scale surface structure are essential in triggering de novo bone formation. Although not evaluated here, (sub) microstructured BCP has previously been shown to adsorb more proteins than less microporous BCP [6]. Thus, increased protein absorption could play a role in promoting cell-surface adhesion and physical interactions.

Still, the amount of bone formation in the planar constructs used in the present study was small in comparison to similar microstructured BCP with macroporous structure [6,11]. It may be that macropores and concavities promote and enhance bone deposition by providing a shielded environment for bone matrix protein

and condensation and ion precipitation. By incorporating a central gap between the disc constructs, bone was expected to form within this protected space, yet tissue infiltration into this gap was limited possibly due to the glue holding the constructs together. Instead, thin layers of ectopic bone formed predominantly on the outside surface of the BCP1150 and BCP1150Ti constructs.

Notably, multinucleated osteoclast-like cells accompanied de novo bone formation by the submicrostructured BCPs, closely bordering stretches of bone in tight adherence to BCP1150 and BCP1150Ti. In contrast, mainly fibrous tissue and scarce multinucleated cells covered the surface of BCP1300, suggesting that BCP surface structure affects the formation of these cells. The *in vivo* results also suggest that surface chemistry plays a role in osteoclast-like cell morphology and organization because multinucleated cells appeared smaller and sparser on BCP1150Ti than BCP1150. Considering the osteoclast-like cell and bone formation of BCP1150 versus BCP1300, these results were in agreement with those reported in the literature that osteoinductive CaPs not only induce de novo bone formation but also stimulate the formation of multinucleated cells in a related process [29,33,43].

To further investigate these *in vivo* findings, RAW264.7 pre-osteoclasts were cultured on the surface of the BCP discs in the presence of osteoclast differentiating factor RANKL, based on a well defined *in vitro* osteoclast model [36,44]. Similar to the *in vivo* results, osteoclast-like cell survival was significantly promoted by submicron-scale BCP1150 and BCP1150Ti surfaces versus BCP1300. In stark contrast, pre-osteoclast proliferation was stunted by BCP1300 and osteoclast survival was attenuated. However, C2C12 myoblasts proliferated strongly on BCP1300, which may explain why few multinucleated cells but abundant soft tissue was present on this surface *in vivo*. In this way, surface topography may differentially affect how osteoclasts and their precursors are able to proliferate and survive on a material surface.

In agreement with the *in vivo* findings, BCP1150 stimulated the *in vitro* formation of large, fused osteoclasts that were 2-4 times larger than those formed on BCP1300 or BCP1150Ti, respectively. These results suggest that both surface chemistry and microstructure affect osteoclast-like cell fusion. Indeed, several other research groups have described how osteoclast formation and function is highly dependent on the structure and chemical composition of the substrate to which they adhere [45–48] in a process that could be due to differences in proteins adsorption to the substrate [49].

In addition to promoting osteoclast survival, submicrostructured BCP1150 and BCP1150Ti also increased TRAP activation, an enzyme marker of osteoclast

differentiation, relative to BCP1300. Although many markers of osteoclast differentiation exist [50], TRAP activity is most frequently assayed in the literature and may be related to the bone resorption process [51]. Despite differences in osteoclast fusion, osteoclast survival and TRAP activation was similar between both osteoinductive materials (i.e. BCP1150 and BCP1150Ti). In contrast, BCP1300 strongly inhibited osteoclast survival and TRAP activity and did not induce bone formation.

Taken together, the *in vivo* and *in vitro* findings presented here show that submicron-scale BCP surface structure promotes multinucleated osteoclast-like cell formation *in vivo* and *in vitro* concurrent with de novo bone formation, versus non-inductive micron-scale structure, which stunts osteoclastogenesis. These findings add to the growing theory that osteoclast formation may be a critical directive step for osteoinductive capacity by materials [10,29,32].

How exactly osteoclastogenesis may stimulate osteoblast differentiation can currently only be speculated. Other groups have importantly shown that osteoclastogenesis precedes ectopic bone formation by osteoinductive CaPs [29,30,33] and their inhibition by various drug delivery approaches blocks or reduces bone formation [31,32,52]. An explanation for this connection is that osteoclasts naturally direct osteoblast differentiation of mesenchymal precursors through the secretion of osteogenic bone-coupling factors, e.g. Wnts, BMPs, S1P, and CTHRC1 [53,54]. The importance of surface structure in this process may be that osteoclasts require a specific substrate to promote their proliferation, differentiation, and survival in ectopic locations.

Because surface (sub)microstructure may be the only essential material parameter necessary for osteoinduction and osteoclast formation may be important for this process, it would be useful to investigate osteoclastogenesis and de novo bone formation of other materials with tunable surface structures. If for example, microstructured HA and titanium also promoted osteoclastogenesis and ectopic bone in contrast to their non-microstructured controls, a broader link between osteoclast formation and de novo bone formation would be further substantiated. Furthermore, by blocking osteoclastogenesis in these studies, the importance of osteoclast formation to de novo bone formation could be more generally elucidated. In the future, pending further biological insight, it may even be possible to use simplified *in vitro* models, such as osteoclastogenesis, as predictive models of osteoinduction.

5 CONCLUSION

BCP with surface microstructure sized $\leq 1 \mu\text{m}$, coated or not with a nanometer thin layer of titanium, induced the formation of small amounts of de novo bone in the muscle of dogs despite being devoid of macropores or concavities; however, BCP with larger surface structure did not. Both *in vivo* and *in vitro*, the BCP submicron-scale surface structure promoted the differentiation and survival of osteoclast-like cells, which may be connected with its osteoinductive capacity.

A C K N O W L E D G E M E N T S

The authors gratefully acknowledge the support of the TeRM Smart Mix Program of the Netherlands Ministry of Economic Affairs and the Netherlands Ministry of Education, Culture and Science. This research forms part of the Project P2.04 BONE-IP of the research program of the Biomedical Materials Institute, co-funded by the Dutch Ministry of Economic Affairs. This work was also supported by funding under the Seventh Research Framework Program of the European Union, through the project REBORNE under Grant agreement no. 241879. Special thanks are due to Dr. Zeinab Tahmasebi Birgani (MIRA) for her technical expertise with EDS.

R E F E R E N C E S

- [1] García AJ. Get a grip: integrins in cell-biomaterial interactions. *Biomaterials* 2005;26:7525–9.
- [2] Stevens MM, George JH. Exploring and engineering the cell surface interface. *Science* 2005;310:1135–8.
- [3] Curtis A, Wilkinson C. Topographical control of cells. *Biomaterials* 1997;18:1573–83.
- [4] Ito Y. Surface micropatterning to regulate cell functions. *Biomaterials* 1999;20:2333–42.
- [5] Lutolf MP, Gilbert PM, Blau HM. Designing materials to direct stem-cell fate. *Nature* 2009;462:433–41.
- [6] Yuan H, Fernandes H, Habibovic P, de Boer J, Barradas AMC, de Ruiter A, et al. Osteoinductive ceramics as a synthetic alternative to autologous bone grafting. *Proc Natl Acad Sci U S A* 2010;107:13614–9.
- [7] Yuan H, Kurashina K, de Brujin JD, Li Y, de Groot K, Zhang X. A preliminary study on osteoinduction of two kinds of calcium phosphate ceramics. *Biomaterials* 1999;20:1799–806.
- [8] Yuan H, Yang Z, Li Y, Zhang X, De Brujin JD, De Groot K. Osteoinduction by calcium phosphate biomaterials. *J Mater Sci Mater Med* 1998;9:723–6.
- [9] Habibovic P, Yuan H, van der Valk CM, Meijer G, van Blitterswijk CA, de Groot K. 3D microenvironment as essential element for osteoinduction by biomaterials. *Biomaterials* 2005;26:3565–75.

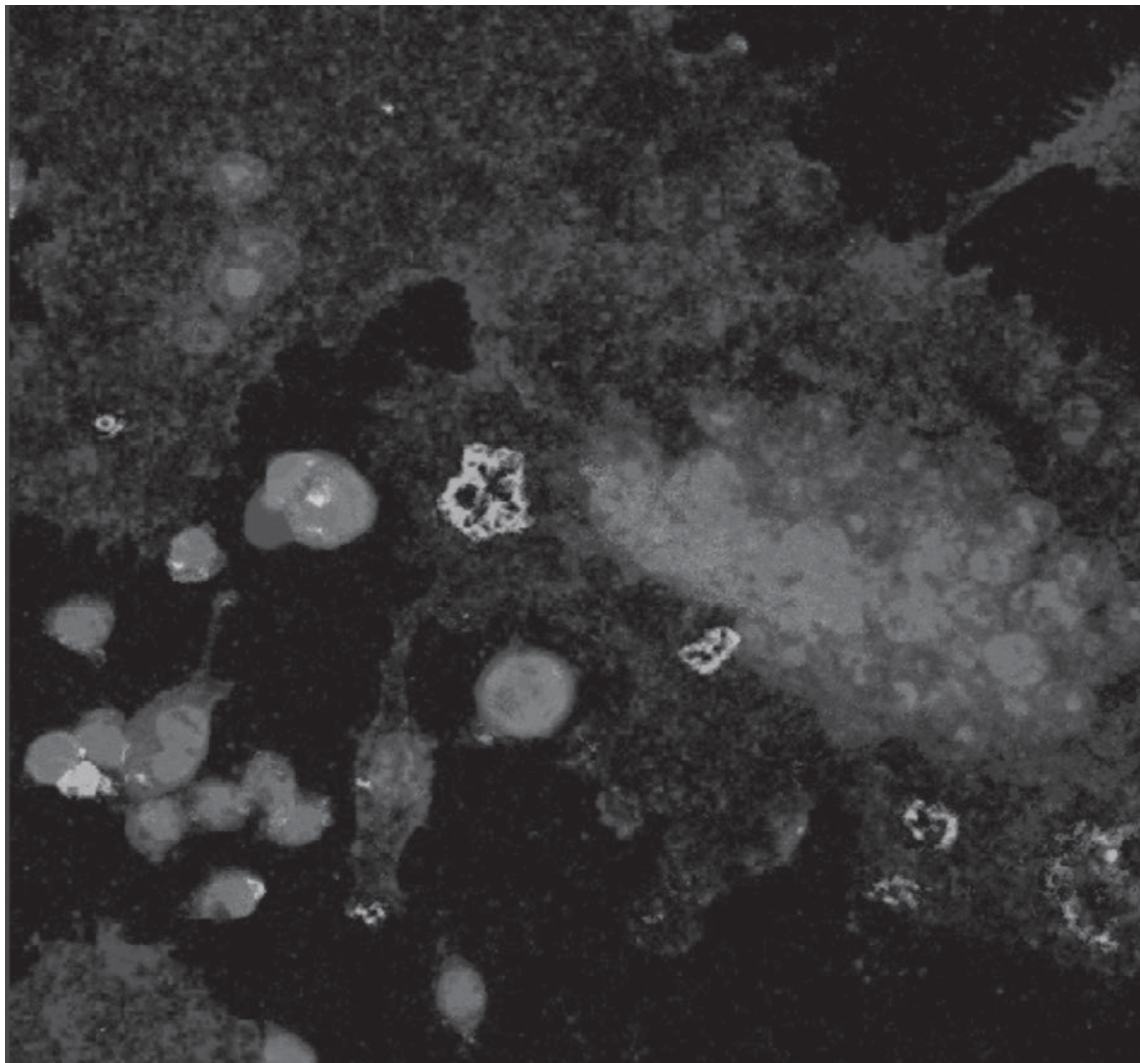
INFLUENCE OF SURFACE MICROSTRUCTURE AND CHEMISTRY ON OSTEOINDUCTION

- [10] Le Nihouannen D, Daculsi G, Saffarzadeh A, Gauthier O, Delplace S, Pilet P, et al. Ectopic bone formation by microporous calcium phosphate ceramic particles in sheep muscles. *Bone* 2005;36:1086–93.
- [11] Habibovic P, Yuan H, van den Doel M, Sees TM, van Blitterswijk CA, de Groot K. Relevance of osteoinductive biomaterials in critical-sized orthotopic defect. *J Orthop Res* 2006;24:867–76.
- [12] Fukuda A, Takemoto M, Saito T, Fujibayashi S, Neo M, Pattanayak DK, et al. Osteoinduction of porous Ti implants with a channel structure fabricated by selective laser melting. *Acta Biomater* 2011;7:2327–36.
- [13] Fujibayashi S, Neo M, Kim H-M, Kokubo T, Nakamura T. Osteoinduction of porous bioactive titanium metal. *Biomaterials* 2004;25:443–50.
- [14] Guilak F, Cohen DM, Estes BT, Gimble JM, Liedtke W, Chen CS. Control of stem cell fate by physical interactions with the extracellular matrix. *Cell Stem Cell* 2009;5:17–26.
- [15] Gittens RA, McLachlan T, Olivares-Navarrete R, Cai Y, Berner S, Tannenbaum R, et al. The effects of combined micron-/submicron-scale surface roughness and nanoscale features on cell proliferation and differentiation. *Biomaterials* 2011;32:3395–403.
- [16] Costa-Rodrigues J, Fernandes A, Lopes MA, Fernandes MH. Hydroxyapatite surface roughness: complex modulation of the osteoclastogenesis of human precursor cells. *Acta Biomater* 2012;8:1137–45.
- [17] Lee SJ, Choi JS, Park KS, Khang G, Lee YM, Lee HB. Response of MG63 osteoblast-like cells onto polycarbonate membrane surfaces with different micropore sizes. *Biomaterials* 2004;25:4699–707.
- [18] Dalby MJ, Gadegaard N, Tare R, Andar A, Riehle MO, Herzyk P, et al. The control of human mesenchymal cell differentiation using nanoscale symmetry and disorder. *Nat Mater* 2007;6:997–1003.
- [19] Allen LT, Tosetto M, Miller IS, O'Connor DP, Penney SC, Lynch I, et al. Surface-induced changes in protein adsorption and implications for cellular phenotypic responses to surface interaction. *Biomaterials* 2006;27:3096–108.
- [20] Ducheyne P, Qiu Q. Bioactive ceramics: the effect of surface reactivity on bone formation and bone cell function. *Biomaterials* 1999;20:2287–303.
- [21] Habibovic P, Sees TM, van den Doel MA, van Blitterswijk CA, de Groot K. Osteoinduction by biomaterials--physicochemical and structural influences. *J Biomed Mater Res A* 2006;77:747–62.
- [22] Barradas AMC, Monticone V, Hulsman M, Danoux C, Fernandes H, Tahmasebi Birgani Z, et al. Molecular mechanisms of biomaterial-driven osteogenic differentiation in human mesenchymal stromal cells. *Integr Biol (Camb)* 2013;5:920–31.
- [23] Syed-Picard FN, Jayaraman T, Lam RSK, Beniash E, Sfeir C. Osteoinductivity of calcium phosphate mediated by connexin 43. *Biomaterials* 2013;34:3763–74.
- [24] Beck GR, Zerler B, Moran E. Phosphate is a specific signal for induction of osteopontin gene expression. *Proc Natl Acad Sci U S A* 2000;97:8352–7.
- [25] Yuan H, Van Den Doel M, Li S, Van Blitterswijk CA, De Groot K, De Bruijn JD. A comparison of the osteoinductive potential of two calcium phosphate ceramics implanted intramuscularly in goats. *J Mater Sci Mater Med* 2002;13:1271–5.
- [26] Habibovic P, Li J, van der Valk CM, Meijer G, Layrolle P, van Blitterswijk CA, et al. Biological performance of uncoated and octacalcium phosphate-coated Ti6Al4V. *Biomaterials* 2005;26:23–36.
- [27] Magan A, Ripamonti U. Geometry of porous hydroxyapatite implants influences osteogenesis in baboons (*Papio ursinus*). *J Craniofac Surg* 1996;7:71–8.
- [28] Barradas AMC, Yuan H, van Blitterswijk CA, Habibovic P. Osteoinductive biomaterials: current knowledge of properties, experimental models and biological mechanisms. *Eur Cell Mater* 2011;21:407–29.
- [29] Kondo N, Ogose A, Tokunaga K, Umezawa H, Arai K, Kudo N, et al. Osteoinduction with highly purified beta-tricalcium phosphate in dog dorsal muscles and the proliferation of osteoclasts before heterotopic bone formation. *Biomaterials* 2006;27:4419–27.
- [30] Kondo N, Ogose A, Tokunaga K, Ito T, Arai K, Kudo N, et al. Bone formation and resorption of highly purified beta-tricalcium phosphate in the rat femoral condyle. *Biomaterials* 2005;26:5600–8.

C H A P T E R 3

- [31] Ripamonti U, Klar RM, Renton LF, Ferretti C. Synergistic induction of bone formation by hOP-1, hTGF-beta3 and inhibition by zoledronate in macroporous coral-derived hydroxyapatites. *Biomaterials* 2010;31:6400–10.
- [32] Klar RM, Duarte R, Dix-Peek T, Dickens C, Ferretti C, Ripamonti U. Calcium ions and osteoclastogenesis initiate the induction of bone formation by coral-derived macroporous constructs. *J Cell Mol Med* 2013;17:1444–57.
- [33] Ripamonti U, Richter PW, Nilen RWN, Renton L. The induction of bone formation by smart biphasic hydroxyapatite tricalcium phosphate biomimetic matrices in the non-human primate Papio ursinus. *J Cell Mol Med* 2008;12:2609–21.
- [34] Wolke JG, de Groot K, Jansen JA. In vivo dissolution behavior of various RF magnetron sputtered Ca-P coatings. *J Biomed Mater Res* 1998;39:524–30.
- [35] Bongio M, van den Beucken JJJ, Nejadnik MR, Tahmasebi Birgani Z, Habibovic P, Kinard LA, et al. Subcutaneous tissue response and osteogenic performance of calcium phosphate nanoparticle-enriched hydrogels in the tibial medullary cavity of guinea pigs. *Acta Biomater* 2013;9:5464–74.
- [36] Collin-Osdoby P, Yu X, Zheng H, Osdoby P. RANKL-mediated osteoclast formation from murine RAW 264.7 cells. *Methods Mol Med* 2003;80:153–66.
- [37] Takahashi N, Udagawa N, Kobayashi Y, Suda T. Generation of osteoclasts in vitro, and assay of osteoclast activity. *Methods Mol Med* 2007;135:285–301.
- [38] Nakayama GR, Caton MC, Nova MP, Parandoosh Z. Assessment of the Alamar Blue assay for cellular growth and viability in vitro. *J Immunol Methods* 1997;204:205–8.
- [39] Ahmed SA, Gogal RM, Walsh JE. A new rapid and simple non-radioactive assay to monitor and determine the proliferation of lymphocytes: an alternative to [³H]thymidine incorporation assay. *J Immunol Methods* 1994;170:211–24.
- [40] Gloeckner H, Jonuleit T, Lemke HD. Monitoring of cell viability and cell growth in a hollow-fiber bioreactor by use of the dye Alamar Blue. *J Immunol Methods* 2001;252:131–8.
- [41] Halleen JM, Alatalo SL, Janckila AJ, Woitge HW, Seibel MJ, Väänänen HK. Serum tartrate-resistant acid phosphatase 5b is a specific and sensitive marker of bone resorption. *Clin Chem* 2001;47:597–600.
- [42] Barradas AMC, Fernandes HAM, Groen N, Chai YC, Schrooten J, van de Peppel J, et al. A calcium-induced signaling cascade leading to osteogenic differentiation of human bone marrow-derived mesenchymal stromal cells. *Biomaterials* 2012;33:3205–15.
- [43] Akiyama N, Takemoto M, Fujibayashi S, Neo M, Hirano M, Nakamura T. Difference between dogs and rats with regard to osteoclast-like cells in calcium-deficient hydroxyapatite-induced osteoinduction. *J Biomed Mater Res A* 2011;96:402–12.
- [44] Miyazaki T, Miyauchi S, Anada T, Imaizumi H, Suzuki O. Evaluation of osteoclastic resorption activity using calcium phosphate coating combined with labeled polyanion. *Anal Biochem* 2011;410:7–12.
- [45] Geblinger D, Addadi L, Geiger B. Nano-topography sensing by osteoclasts. *J Cell Sci* 2010;123:1814–1814.
- [46] Geblinger D, Zink C, Spencer ND, Addadi L, Geiger B. Effects of surface microtopography on the assembly of the osteoclast resorption apparatus. *J R Soc Interface* 2012;9:1599–608.
- [47] Brinkmann J, Hefti T, Schlottig F, Spencer ND, Hall H. Response of osteoclasts to titanium surfaces with increasing surface roughness: an in vitro study. *Biointerfaces* 2012;7:34.
- [48] Xia Z, Grover LM, Huang Y, Adamopoulos IE, Gbureck U, Triffitt JT, et al. In vitro biodegradation of three brushite calcium phosphate cements by a macrophage cell-line. *Biomaterials* 2006;27:4557–65.
- [49] Fuller K, Ross JL, Szewczyk KA, Moss R, Chambers TJ. Bone is not essential for osteoclast activation. *PLoS One* 2010;5(9): e128.
- [50] Everts V, de Vries TJ, Helfrich MH. Osteoclast heterogeneity: lessons from osteopetrosis and inflammatory conditions. *Biochim Biophys Acta* 2009;1792:757–65.
- [51] Ljusberg J, Ek-Rylander B, Andersson G. Tartrate-resistant purple acid phosphatase is synthesized as a latent proenzyme and activated by cysteine proteinases. *Biochem J* 1999;343 Pt 1:63–9.
- [52] Tanaka T, Saito M, Chazono M, Kumagae Y, Kikuchi T, Kitasato S, et al. Effects of alendronate on bone formation and osteoclastic resorption after implantation of beta-tricalcium

- phosphate. *J Biomed Mater Res A* 2010;93:469–74.
- [53] Pederson L, Ruan M, Westendorf JJ, Khosla S, Oursler MJ. Regulation of bone formation by osteoclasts involves Wnt/BMP signaling and the chemokine sphingosine-1-phosphate. *Proc Natl Acad Sci U S A* 2008;105:20764–9.
- [54] Takeshita S, Fumoto T, Matsuoka K, Park K, Aburatani H, Kato S, et al. Osteoclast-secreted CTHRC1 in the coupling of bone resorption to formation. *J Clin Invest* 2013;123:3914–24.



CHAPTER 4

Submicron-scale surface architecture of tricalcium phosphate directs osteogenesis in vitro and in vivo

Noel L. Davison^{1, 2}, Xiaoman Luo^{1, 2}, Ton Schoenmaker³,
Vincent Everts³, Huipin Yuan^{1, 2}, Florence Barrère-de Groot²,
Joost D. de Bruijn^{1, 2, 4}

- 1 MIRA Institute for Biomedical Technology and Technical Medicine, University of Twente, 7522 NB Enschede, Netherlands
- 2 Xpand Biotechnology BV, 3723 MB Bilthoven, Netherlands
- 3 Departments of Oral Cell Biology and Periodontology, Academic Centre for Dentistry Amsterdam (ACTA), University of Amsterdam and VU University Amsterdam, Research Institute MOVE, 1081 BT Amsterdam, Netherlands
- 4 School of Engineering and Materials Science (SEMS), Queen Mary University of London, E1 4NS London, United Kingdom

A B S T R A C T

A current challenge of synthetic bone graft substitute design is to induce bone formation at a similar rate to its biological resorption, matching bone's intrinsic osteoinductivity and capacity for remodeling. We hypothesize that both osteoinduction and resorption can be achieved by altering surface microstructure of beta-tricalcium phosphate (TCP). To test this, two TCP ceramics are engineered with equivalent chemistry and macrostructure but with either submicron- or micron-scale surface architecture. In vitro, submicron-scale surface architecture differentiates larger, more active osteoclasts – a cell type shown to be important for both TCP resorption and osteogenesis – and enhances their secretion of osteogenic factors to induce osteoblast differentiation of human mesenchymal stem cells. In an intramuscular model, submicrostructured TCP forms 20% bone in the free space, is resorbed by 24%, and is densely populated by multinucleated osteoclast-like cells after 12 weeks; however, TCP with micron-scale surface architecture forms no bone, is essentially not resorbed, and contains scarce osteoclast-like cells. Thus, a novel submicron-structured TCP induces substantial bone formation and is resorbed at an equivalent rate, potentially through the control of osteoclast-like cells.

1 INTRODUCTION

A novel approach to regenerative biomaterial design is to engineer instructive physiologic signals to stimulate tissue repair. In the case of synthetic materials used for repairing bone tissue, some of the most widely used clinically are calcium phosphates (CaPs), which are well tolerated by the body due to their chemical homology to native bone mineral [1]. CaPs provide a particularly flexible platform for material design because the physicochemical and topographical characteristics can be tuned by modifying their synthesis parameters [2–4]. Of these materials, a small subset can stimulate the formation of bone even in heterotopic, non-bony locations without exogenous cells or growth factors [5,6]. Such osteoinductive CaPs have been shown to be superior to non-inductive (e.g., merely osteoconductive) materials for repairing critical size bony defects that exceed the natural repair capacity of the bone organ [7,8].

The purposeful design of osteoinductive CaPs is an elusive challenge for materials science because the material parameters necessary to instruct osteogenesis are still critically undefined. In an iterative approach spanning more than 20 years, macrostructural elements such as three-dimensional architecture [9,10], surface concavities [11], and interconnected pore structure [12,13] were all shown to enhance bone formation by CaP. Other materials such as Bioglass [14] and titanium [12,15] have also been shown in some scattered studies to induce small amounts of ectopic bone formation. The surface microstructure of osteoinductive biomaterials has been suggested to have a directive effect on ectopic bone formation in intramuscular models [7,8,15–17]. For instance, bioactivity may occur at the material surface where ions and proteins are absorbed from the blood. It is speculated that augmenting the specific surface area by changing the surface architecture, e.g. increasing micropore volume, may increase reprecipitation/release of Ca^{2+} and absorption of bone morphogenetic proteins (BMPs), both of which can stimulate the osteogenic differentiation of stem cells [8,9].

Beyond physicochemical effects, osteoinductive surface architecture may also confer powerful cell-fate regulating signals directly to adherent cells through cell-substrate interactions via mechanotransduction. For example, osteoblast genes in human mesenchymal stem cells (hMSC) are upregulated following culture on osteoinductive CaP surfaces in osteogenic conditions [8], presumably due to the topographical cues transduced by cell adhesion molecules. Similar effects have been described on polymer substrates with submicron- and nano-scale surface features even without osteogenic additives, suggesting that instructive surface architecture can induce osteogenesis irrespective of surface chemistry when it is engineered on a certain size scale and topographical arrangement [18].

Another important aspect of material design for bone regeneration is the resorbability of the implant. Because bone itself is a continuously remodeled material, resulting from the tightly coupled interplay between specialized bone-resorbing osteoclasts and bone-secreting osteoblasts [19], a synthetic bone substitute that can also be physiologically remodeled or resorbed would provide a more biomimetic scaffold for bony ingrowth, deposition, and long term homeostasis. If a material is non-resorbable, there is a risk that the mechanical loading will be distributed unequally due to stress shielding of the implant, weakening the less loaded surrounding bone over time. Consequently, because β -tricalcium phosphate (TCP) ceramics have been shown to be highly resorbable both clinically and in vitro, they are often preferred versus hydroxyapatites, which are mostly non-resorbable [20]. The proposed mechanisms of CaP resorption are diverse and include passive dissolution, hydrolysis, and cell-mediated dissolution. For instance, it is speculated that osteoclasts play a principal role in the cellular resorption and this can be evaluated by characteristic osteoclastic resorption pits in vitro [21,22]. Because of the multifactorial nature of the physiologic phenomenon, the only true test to evaluate material resorbability is to evaluate the bulk loss of material in vivo [1]. Still, understanding the dominant mechanism of resorption would prove useful for the design of better TCP.

Though the cellular events leading to de novo bone formation by CaPs are largely unknown, it has been demonstrated in several studies that osteoclasts may play an important role. For instance the formation of osteoclasts has been found to precede de novo bone formation by osteoinductive TCP in the dorsal muscle of dogs by four weeks [23]. Moreover, studies by Ripamonti et al. (2010) and Tanaka et al. (2010) published in the same year showed that administering osteoclast-inhibiting bisphosphonate reduced the bone formation of two different osteoinductive ceramics (hydroxypapitate/calcium carbonate and TCP) in both heterotopic and orthotopic sites [24,25]. One potential explanation for these findings is that osteoclasts express and secrete osteogenic factors such as BMPs [26,27] and that surface architecture – in particular surface roughness – can profoundly influence their development and function [28,29].

Although CaPs provide a flexible platform for designing material chemistry and architecture, the fine control of one variable at a time while maintaining the other properties static continues to be a challenge for materials science. Indeed, altering surface architecture, i.e. surface micropore and grain size, consequently changes other surface properties that stem from it, including specific surface area, surface reactivity and physical topography; as such, these factors are inextricably linked. Nevertheless, whether there is an instructive size scale of surface architecture necessary to trigger both bone induction coupled with an equivalent amount of

material resorption remains unknown. The aim of this work was thus to tune the surface microstructure while keeping the material chemistry and macrostructure constant with the end goal of designing a resorbable CaP with instructive surface features to stimulate osteogenesis. We hypothesized that the scale of surface features plays a determinant role in this outcome because cellular behavior has been shown to be powerfully influenced at the material surface interface [30]. To test this, two TCP with either micron-scale or submicron-scale surface features and equivalent chemistries were carefully synthesized and their physico-chemical properties were characterized. The effect of different scale surface architecture on osteoclast formation and activity – in particular secreted osteogenic signals – was evaluated in vitro and the bone inductive capacity and resorbability of the materials was evaluated in vivo.

2 MATERIALS AND METHODS

2.1 Preparation and characterization of TCP with micron- and submicron-scale surface architecture

TCP powders were synthesized by mixing calcium hydroxide and phosphoric acid (both from Fluka) at a Ca/P ratio of 1.50. TCP powders with small (TCPs) or big grains (TCPb) in the final ceramics were prepared by controlling the reaction rates. The powders were foamed with diluted H_2O_2 (1%) (Merck) at 60 °C to get macro/microporous green bodies; meanwhile the powders were mixed with diluted H_2O_2 (0.1%) and kept dried at room temperature to get microporous green bodies. The dry green bodies (both macro/micro and microporous ones) were subsequently sintered at 1050 °C or 1100 °C for 8 hours to achieve small and big grains for TCPs and TCPb, all respectively.

Macro/microporous cylinders ($\varnothing 7 \times 10$ mm) and microporous discs ($\varnothing 9 \times 1$ mm) were machined from the ceramic bodies using a lathe and a diamond-coated saw microtome (Leica SP1600) and ultrasonically cleaned, and heat sterilized at 160 °C for 2 hours. Macro/microporous cylinders were used for animal implantation to allow for quantification of bone formation and implant resorption, whereas microporous discs were used for in vitro experiments to avoid effects of three-dimensional macrostructure, i.e. variability of cell seeding, cell infiltration into the material, incomplete cell lysis, and limitations visualizing cells by microscopy. Crystal chemistry of the materials was analyzed by X-ray diffraction (Rigaku Miniflex II) scanning the range $2\theta = 25\text{--}45^\circ$ (step size = 0.01°, rate = 1° min⁻¹) and confirmed to be TCP as previously described in Chapter 2.

Surface topography of the materials was characterized using scanning electron microscopy (SEM) (JEOL JSM-5600) after sputter coating them with gold for 90 seconds (JEOL JFC 1300). At least 50 grains and pores were measured across their vertical diameter using ImageJ software (NIH, USA). Porosity and total pore area were determined by mercury intrusion testing (Table 1) (Micromeritics, USA). For surface profile characterization including calculation of surface roughness parameters, SEM stereomicrographs of the same location were captured at two different tilt angles (2500x, $\pm 5^\circ$) and then digitally reconstructed into three-dimensional surfaces for automated profile analysis using MeX v5.1 software (Alicona Imaging, Austria).

Surface reactivity of the materials was evaluated during incubation in complete cell culture medium (described below) at 37 °C and 5% CO₂ for up to 14 days to mimic a physiologic environment. Medium (1 mL) incubated with TCP discs was collected and refreshed at several time points (3, 7, 10, and 14 days) and assayed for Ca²⁺ and inorganic phosphate (P) concentrations using QuantiChrom (BioAssay Systems, USA) and PhoshoWorks (AAT BioQuest, USA) colorimetric biochemical kits, respectively. Medium incubated without TCP served as control to calculate the mass of ions absorbed by the materials. At each time point, ion concentrations measured in medium incubated with TCP were subtracted from those measured in the control medium, yielding the ion mass absorbed by TCP. Cumulative absorption was computed by summing the ion absorption at all previous time points in a compounding fashion. The media from n = 3 TCP disc replicates was measured at each time point.

2.2 In vivo study

Intramuscular implantation

All surgery was conducted at the Animal Center of Sichuan University in conformance with the institutional animal ethics committee's guidelines. Sterile TCP macro/microporous cylinders were implanted in the dorsal muscle of healthy male mongrel dogs (n = 8, 1–4 years, 10–15 kg) for 12 weeks. Animals were first given general anesthesia by abdominal injection of sodium pentobarbital (30 mg kg⁻¹ body weight) and cylinders were implanted into paraspinal muscle pockets created by scalpel incision and blunt dissection. Skin incisions were closed layer by layer with non-resorbable sutures for identification at harvest. Following surgery, the animals were given daily intramuscular injections of buprenorphine (0.1 mg per animal) for 2 days and penicillin (40 mg kg⁻¹) for 3 days to relieve pain and prevent infection. Animals were allowed to undertake full activity and received a normal diet immediately after surgery.

Sample harvest and histological processing

At the end of 12 weeks the animals were sacrificed by abdominal injection of sodium pentobarbital (60 mg kg^{-1}) and samples were immediately harvested and fixed in cold phosphate-buffered formalin solution, dehydrated in graded ethanol series, and embedded in methyl methacrylate (MMA) (LTI, Netherlands) at room temperature.

Histological sections ($\sim 30\text{ }\mu\text{m}$) of the undecalcified samples were made using a Leica SP1600 microtome, stained en bloc with 1% methylene blue and 0.3% basic fuchsin solutions for histological analysis and histomorphometry.

Histology and histomorphometry

Stained histological sections were scanned using a Dimage Scan Elite 5400II slide scanner (Konica Minolta) for gross evaluation and histomorphometric analysis, as well as at higher magnifications using a light microscope (Nikon Eclipse E200).

Histomorphometry of bone formation and TCP resorption in the stained sections was performed by pseudo-coloring pixels representing formed bone (B) and remaining material (M) in a region of interest (ROI) using photo analysis software (Adobe Photoshop Elements 4.0). The percent area of bone formed (B%) in the available space was then calculated by the equation:

$$\text{B\%}=\text{B}/(\text{ROI-M})\times 100.$$

The percent area of material resorbed (M%) was calculated by subtracting the pixel area of remaining material, M, from the mean pixel area of similarly embedded, sectioned, and pseudo-colored TCP cylinders ($n = 3$) that had not been implanted (Mo):

$$\text{M\%}=(\text{Mo-M})/\text{Mo}\times 100.$$

2.3 In vitro studies

RAW264.7 monocyte/macrophage culture on TCP discs

Murine monocyte/macrophage cell line RAW264.7 (ECACC, Wiltshire, UK) was expanded in basic medium composed of alpha MEM (Lonza), supplemented with 10% HyClone FetalClone I serum (Thermo Scientific) and 1% penicillin-streptomycin (Life Technologies). Near-confluent cells were detached by scraping and seeded on TCP discs ($2 \times 10^4\text{ cells cm}^{-2}$) in non-tissue culture treated 48-well plates (Greiner Bio-One) containing basic medium supplemented with RANKL (40 ng mL^{-1} , Peprotech, UK) to induce osteoclast formation. TCP discs incubated

in basic medium +/- RANKL without cells served as acellular controls. After 5 days of culture, conditioned medium was collected from n = 5 replicate discs, centrifuged to remove cellular debris, and frozen.

Human mesenchymal stem cell culture in conditioned media

Human mesenchymal stem cells (hMSC) were isolated from bone marrow biopsies obtained from the femoral head of 3 patients (68-80 years) undergoing total hip replacement surgery (Albert Schweitzer Hospital, Dordrecht, The Netherlands, approved under Medical Ethical Committee trial number 2011.07) by density gradient isolation of the buffy coat. Adherent cells were expanded in flasks containing growth medium: basic medium supplemented with L-glutamine (2 mM) (GlutaMAX I, Fisher Scientific), L-ascorbic acid 2-phosphate (0.2 mM) (Sigma), and basic fibroblast growth factor (1 ng mL⁻¹) (Serotech, UK); non-adherent cells were removed in subsequent media refreshments. Twice-passaged hMSC were trypsinized and seeded in 96-well plates containing basic medium (1×10^4 cells cm⁻²). After one day, hMSC were supplemented with conditioned medium (50 µL) and refreshed with the same amount every other day for 7 days total. All culture was maintained at 37 °C, 100% humidity, and 5% CO₂. Four replicates were cultured per condition, per hMSC donor.

TRAP staining

The presence of the osteoclast enzyme tartrate resistant acid phosphatase (TRAP) was detected using a commercial staining kit (Leukocyte Acid Phosphatase Kit, Sigma). Staining was visualized using a Nikon SMZ800 stereomicroscope equipped with a Nikon camera. Two replicate discs were stained and analyzed per condition.

Biochemical activity

For biochemical assays on the cell lysate, cells were lysed in a commercial lysis buffer (Promega). TRAP activity was quantified in the cell lysate of RANKL-stimulated RAW264.7 by conversion of p-nitrophenylphosphate to p-nitrophenol (NP) in sodium acetate buffer (pH 5.8) containing potassium sodium tartrate (10 mM) as reported by Ljusberg et al. (1999) [61]. Alkaline phosphatase (ALP) activity was measured in the hMSC lysate using the AttoPhos Alkaline Phosphatase Fluorescent Substrate kit (Promega). Relative ALP was normalized to the basal ALP level measured in the negative control: hMSC cultured in basic medium; hMSC cultured with osteogenic supplements dexamethasone (10 nM) and L-ascorbic 2-phosphate (0.2 mM) served as the positive control reference. Both TRAP and ALP were normalized to DNA content in the same lysate using a CyQuant DNA detection kit (Life Technologies). A Zenyth 3100 Multimode plate

reader was used to detect optical density and fluorescent signal of the assays. Four replicate discs were analyzed per condition.

Fluorescent confocal microscopy of osteoclast formation

Osteoclast fusion and actin ring formation were analyzed using fluorescent confocal microscopy. Osteoclast-cultured discs were rinsed with PBS, fixed in 4% formaldehyde for 48 hours, blocked with 20% normal goat serum, then sequentially incubated with rat anti-mouse monoclonal primary antibody CD44 targeting the osteoclast plasma membrane (1:100 dilution) (Cedarlane, USA), goat anti-rat Alexa467-conjugated secondary antibody (1:400) (Invitrogen), Alexa488-conjugated phalloidin targeting F-actin (1:400) (Invitrogen), and propidium iodide (1:1000) (Sigma) to stain nuclei, as previously described [62]. Fluorescence was visualized using a Leica TCS-SP2 laser scanning confocal microscope (Leica, Germany) and image stacks were generated by scanning from the apical to basal surface of the cell and overlaid. Two replicate discs were stained and analyzed.

4

SEM of osteoclast morphology

Osteoclast morphology was evaluated using SEM (JEOL JSM-5600). RANKL-treated RAW264.7 were fixed in 2.5% gluteraldehyde, dehydrated in a graded ethanol series and finally dried in HMDS (Alfa Cesar). Dehydrated cells were then sputter coated with gold for enhanced imaging resolution. Osteoclast size was quantified in SEM micrographs ($\times 100$) by calculating the mean surface area of cells at 3 random locations per disc using automated threshold, edge detection, and particle analysis functions in ImageJ software, as previously described [63]. Only cells whose area was $> 200 \mu\text{m}^2$ were included in the analysis to safely exclude mononuclear cells. Three replicate discs were analyzed per condition.

2.4 Statistics

Statistical comparisons were performed using One-way ANOVA and Tukey's post hoc tests; $P < 0.05$ was considered significant. Grain and pore size frequency distributions were fit by non-linear regression analysis using Log(Gaussian) model for non-normal distributions. All statistical analyses were conducted in Graphpad Prism 6.0.

3 RESULTS

3.1 Characterization of micro- and submicrostructured TCP

Analysis of SEM micrographs (Figure 1.a,b) and 3D-reconstructed stereomicrographs (Figure 1.c,d) clearly confirmed the synthesis of two microstructurally different TCP (Figure 1.a,b). The surface profile of TCPs followed a quasi-regular sinusoidal pattern, with peaks and valleys spanning a submicron scale range, versus that of TCPb which spanned a micron-scale range (Figure 1.g). These differences were quantified in terms of average (R_a) and root-mean-square (R_{RMS}) roughness parameters: 126 ± 3 nm and 158 ± 3 nm, respectively for TCPs, versus 1.287 ± 0.011 μm and 1.597 ± 0.011 μm , respectively for TCPb (Table 1). Quantification of the grains and pores in SEM micrographs showed that both features were on average < 1 μm for TCPs and > 1 peak to valley height roughness parameters: 126 ± 3 nm and 158 ± 3 nm, respectively for TCPs, versus 1.287 ± 0.011 μm and 1.597 ± 0.011 μm , respectively for TCPb (Table 1). Quantification of the grains and pores in SEM micrographs resulted in submicron-scale surface structure and TCPb resulted in micron-scale surface structure (Figure 1.e,f).

Though total porosity of TCPs and TCPb was similar (~46-50% for microporous discs; ~69-72% for macro/microporous cylinders), total pore area was roughly 2 times greater for TCPs than TCPb, owing to smaller pores but equal overall porosity (Table 2).

Table 1. Surface characterization and roughness profile of TCP.

	TCPs	TCPb
Average grain diameter (μm)	0.95 ± 0.27	3.66 ± 1.05
Average pore diameter (μm)	0.63 ± 0.33	1.78 ± 0.85
Average roughness, R_a (μm)	0.126 ± 0.003	1.287 ± 0.011
Root-mean-square roughness, R_{RMS} (μm)	0.158 ± 0.003	1.597 ± 0.011

Table 2. Porosity by mercury intrusion testing.

	Microporous Discs		Macro/Microporous Cylinders	
	TCPs	TCPb	TCPs	TCPb
Total pore area (m^2/g)	1.424	0.521	1.477	0.769
Total Porosity (%)	46.3	49.8	69.6	72.0

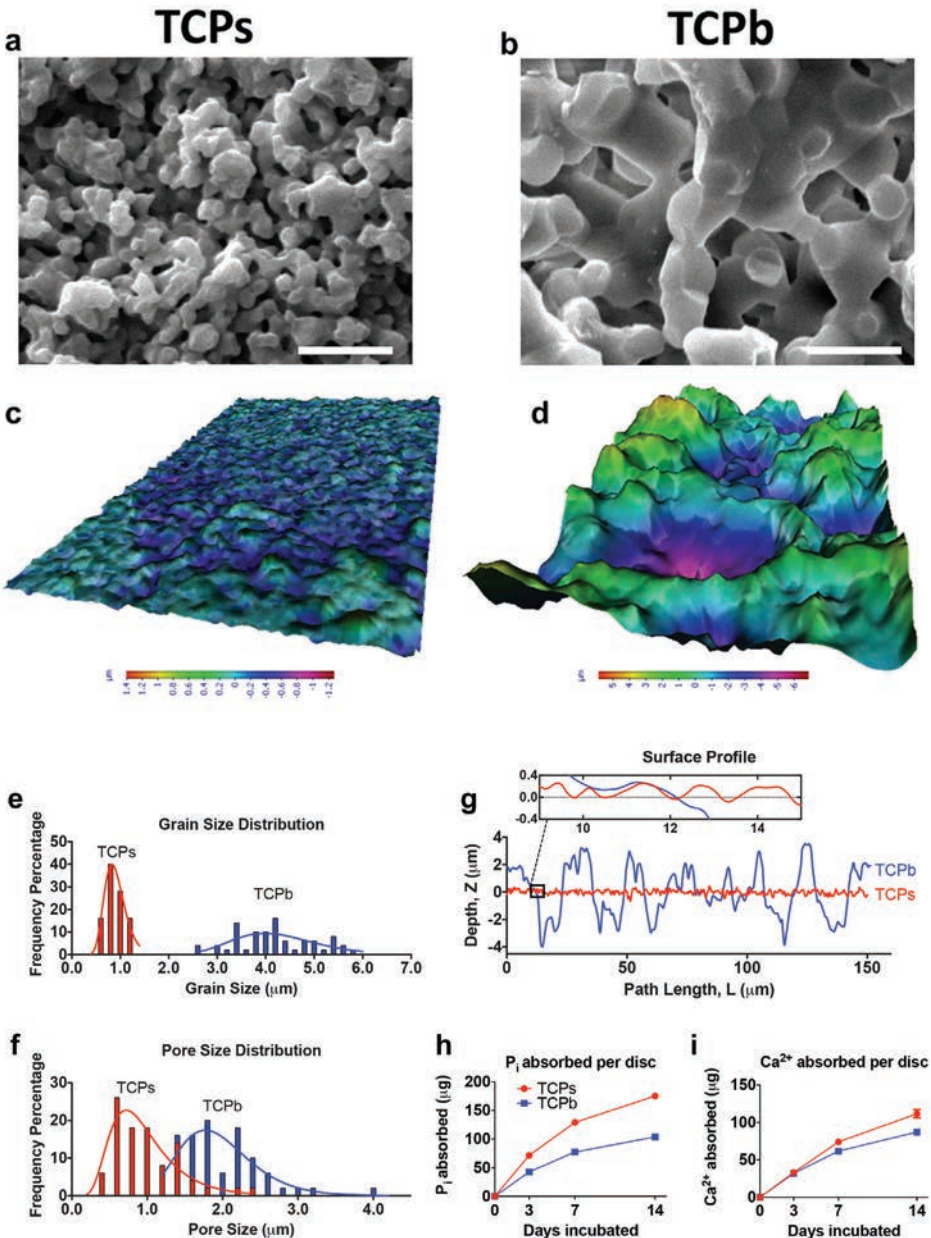


Figure 1. Characterization of TCP physico-chemistry. (a, b) SEM micrographs depict different surface microstructure of microporous TCPs and TCPb (scale bars = 5 μm). (c, d) 3D surface reconstruction, (g) corresponding surface profiles, (e, f) and grain/pore size distribution emphasize the submicron-scale versus micron-scale architecture of TCPs and TCPb, respectively. Surface reactivity of TCPs and TCPb discs as measured by cumulative (h) P_i and (i) Ca^{2+} absorption during incubation in serum-containing medium (mean \pm s.d. of $n = 3$ discs).

To test the surface reactivity in physiologic conditions, the materials were incubated for up to 14 days in cell culture medium containing serum to simulate blood plasma. $\text{Ca}^{2+}/\text{P}_i$ concentrations in the medium decreased over time, indicating that these ions were continuously absorbed by the materials and not released; however, ion absorption of the materials was substantially different throughout the incubation period presumably due to differences in specific surface area, a consequence of different surface architecture (Figure 1.h,i).

3.2 Effects of submicron-scale TCP surface architecture on osteoclast formation and activity in vitro

Submicron-scale surface structure promotes larger, more multinucleated osteoclasts

It was speculated that differences in surface microstructure modulate the formation of osteoclasts pertinent to osteogenesis by TCP. To test this, the murine monocyte/macrophage RAW264.7 cells were cultured on TCP discs in the presence of RANKL (Receptor Activator of NF- κ b Ligand) to stimulate the differentiation of osteoclasts. Because these discs lacked macroporosity, surface micropore size restricted cells only to surface interactions and not material infiltration. SEM micrographs confirmed that mononuclear macrophages fused to form multinucleated osteoclast-like cells on the surface of both materials by day 3. However, at this time, osteoclast fusion on TCPb appeared to be less complete than on TCPs across disc replicates, illustrated by fragile gaps in the cell membranes between fusing cells (Figure 2) not observed on TCPs despite identical sample preparation.

After 4 days culture, distinct differences could be seen in terms of osteoclast size, morphology, and integration with the material surface (Figure 3). Prominent filopodia stretched out between osteoclasts, connecting them in a highly networked cell population on TCPs (Figure 3.a,b). At higher magnifications, cell membranes were tightly integrated with the material, and the apical sides were decorated by microvilli (Figure 3.c). Conversely, osteoclasts formed on TCPb (Figure 3.d,e) were far less connected by less frequent filopodia, and appeared rounder and less integrated with the surface at higher magnifications (Figure 3.f).

Osteoclast size was quantified in SEM micrographs captured after 4 days of culture, which coincided with the peak of osteoclast fusion and TRAP activity, described in detail below. Osteoclasts formed on TCPs were on average more than twice as large those formed on TCPb ($P = 0.023$) (Figure 3.g) in some cases encompassing $> 1,000 \mu\text{m}^2$. By day 5, osteoclasts were observed to be less actively fusing and appeared in some cases apoptotic (not shown), indicating

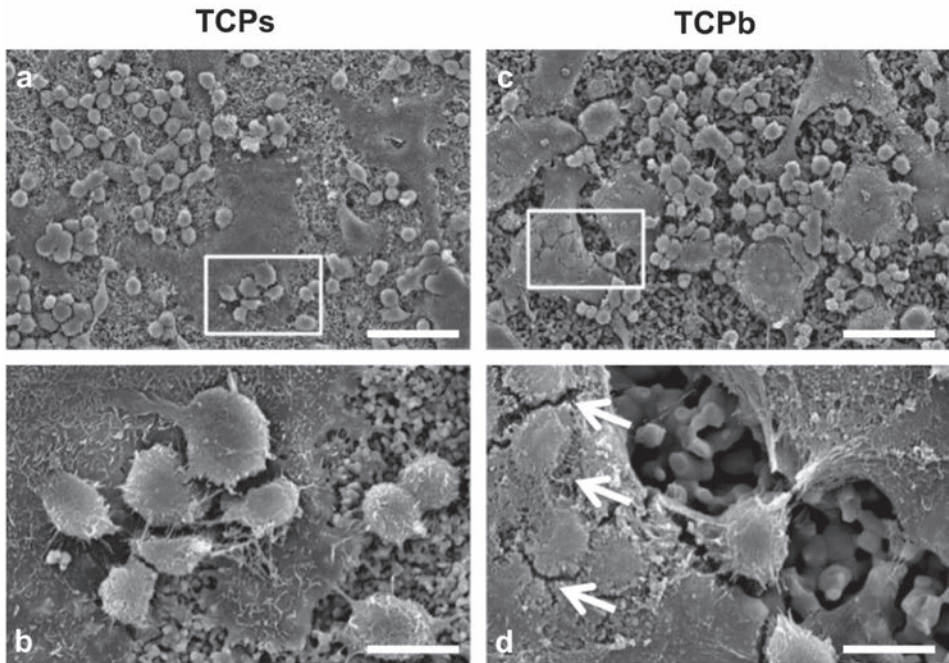


Figure 2. SEM micrographs of osteoclast formation on (a, b) TCPs and (c, d) TCPb after 3 days of culture. Incomplete cell fusion on TCPb was implicated by fragile cell membrane gaps (arrows), compared to complete membrane closure and active fusion on TCPs. Scale bars: a,c = 50 μ m; b,d = 10 μ m.

that 4 days culture was the peak of osteoclast formation in this culture system.

Cell membrane and nuclei staining visualized by fluorescent confocal microscopy confirmed the trends observed in SEM: osteoclasts formed on TCPs were clearly larger, owing to more fusion and multinucleation (Figure 4). Membrane staining in particular confirmed the presence of massive networks of fused osteoclasts on TCPs (Figure 4.a), in contrast to isolated, smaller osteoclasts formed on TCPb (Figure 4.c), which were also multinucleated but to a far lesser extent. Actin rings visualized by F-actin staining were of similar size and number on both materials (Figure 4.b,d), suggesting that these cytoskeletal rearrangements indicative of mature osteoclasts proceeded without dependence on the scale of surface structure tested here.

Submicron-scale surface architecture promotes osteoclast TRAP activity

Surface microstructure was also found to affect osteoclast differentiation and activation indicated by TRAP activity (Figure 5). On submicrostructured TCPs, TRAP per DNA in the cell lysate of disc-adherent osteoclasts peaked after 4

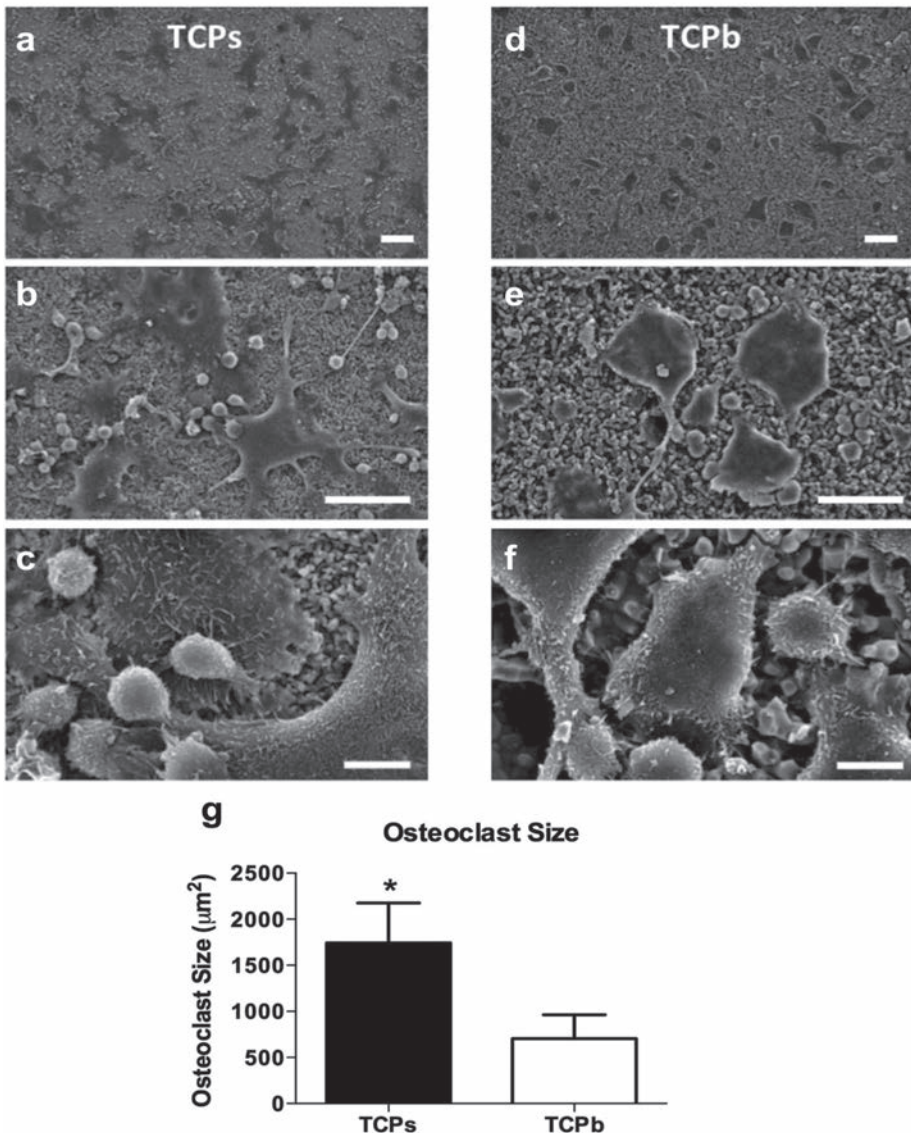


Figure 3. SEM micrographs of osteoclast formation on (a-c) TCPs and (d-f) TCPb after 4 days culture. At low magnification, osteoclasts formed on (a) TCPs are larger ($> 150 \mu\text{m}$) than those formed on (d) TCPb (scale bars = 100 μm). Prominent cellular filopodia connected adjacent cells and attached to the surface on (b) TCPs versus (e) TCPb (scale bars = 50 μm). At high magnification, (c) osteoclasts appeared tightly bound to TCPs, with spread cell membranes decorated with microvilli actively fusing with small ($< 10 \mu\text{m}$) mononuclear cells; (f) OC on TCPb appeared rounded with less frequent fusion (scale bars = 10 μm). (g) Osteoclast size after 4 days culture calculated using ImageJ software (mean \pm s.d. of $n = 3$ discs; * $P < 0.05$).

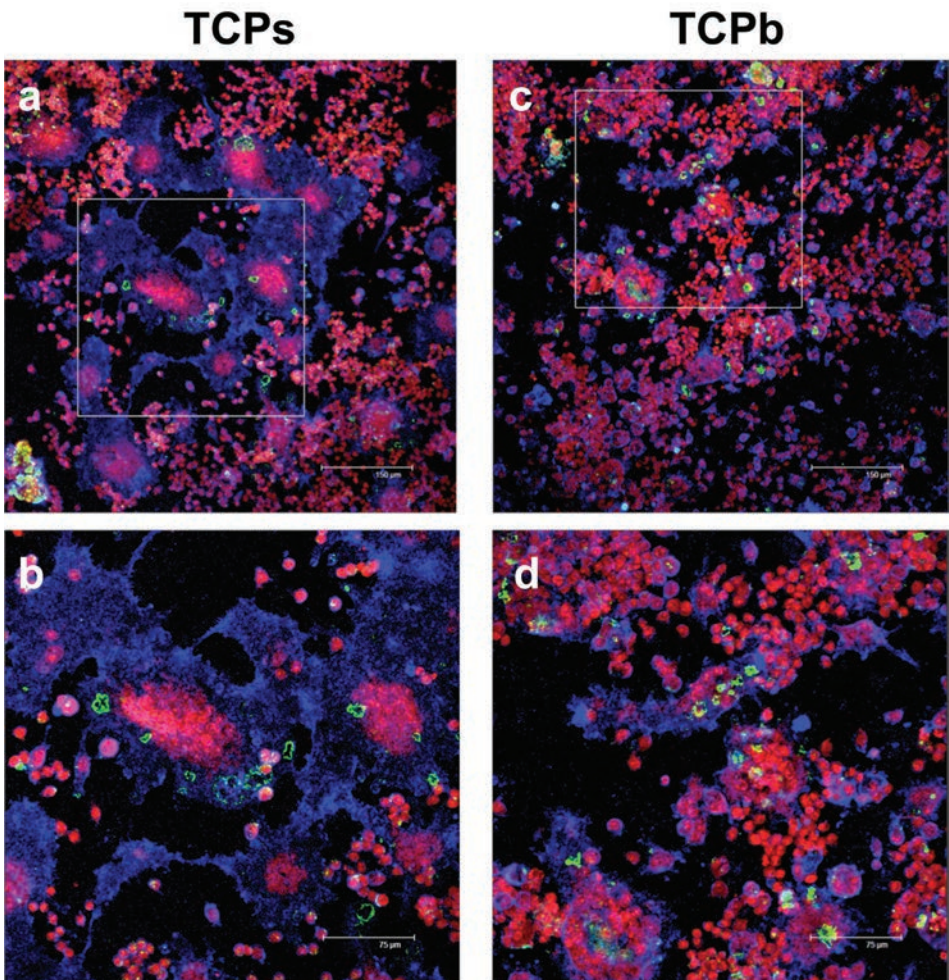


Figure 4. Confocal fluorescent microscopy of osteoclasts formed on (a-b) TCPs and (c-d) TCPb after 4 days culture. In low zoom images, (a) osteoclasts on TCPs were extensively interconnected by large cell membranes (CD44, blue) with highly multinucleated centers (propidium iodide, red) versus those on (c) TCPb, which were less multinucleated and less interconnected by smaller cell membranes (scale bars = 150 μm). At higher magnification (b, d), actin rings (phalloidin, green) were formed by cells on both materials (scale bars = 75 μm).

days culture, which was ~25% higher than on TCPb ($P = 0.001$) – in contrast, TRAP activity did not increase from 3 to 5 days of culture on TCPb (Figure 5.a). TRAP staining consistently confirmed these results with intense TRAP positive staining on TCPs versus low TRAP activity on TCPb (Figure 5.c-f). Considering cell proliferation, DNA content similarly plateaued by day 4 on both materials due to osteoclast differentiation (Figure 5.b). Thus, different surface microstructure affected the TRAP activity but not cell proliferation.

Submicron-scale surface architecture amplifies osteoclast-secreted osteogenic signals

Conditioned medium from osteoclast cultures on TCP discs with RANKL was administered to hMSC cultured in basic medium, and ALP activity in the hMSC cell lysate was measured as an indicator of osteoblast differentiation. After one week of culture, hMSC ALP activity (Figure 6) was 50% higher than in hMSC treated with conditioned medium from osteoclasts formed on TCPb ($P = 0.002$) or the positive hMSC control cultured in osteogenic medium ($P = 0.001$).

To compare the effects of osteoclast versus macrophage secreted osteogenic factors on osteoblast differentiation, conditioned medium from unstimulated RAW264.7 macrophages (i.e., no RANKL) was also administered to hMSC. Following culture on TCPs, osteoclast-secreted factors induced ~3 times more hMSC ALP than did macrophage-secreted factors ($P < 0.001$). Still, macrophage-secreted factors from culture on TCPs still induced significantly more hMSC ALP activity than hMSC cultured in basic medium, which was not the case for macrophage conditioned medium from culture on TCPb.

To confirm that these effects were cell mediated and not due to the soluble chemistry of the materials or RANKL in the medium, hMSC were treated with culture medium supplemented with or without RANKL for one week, which had been similarly incubated with TCP but without RAW264.7, i.e., acellular conditioned medium. These treatments did not appreciably change hMSC ALP levels ($P > 0.99$), confirming that the observed ALP-inductive effects were mediated by RAW264.7 and not TCP or RANKL alone (Figure 6).

3.3 Effects of submicron-scale surface architecture on bone formation and resorption in vivo

Histological analysis (Figure 7.a-g) and histomorphometry (Figure 7.h,i) of intramuscular TCP implants harvested at 12 weeks demonstrated the binary effects of submicron- versus micron-scale surface architecture on bone formation: TCPs induced $20 \pm 8\%$ area bone formation in the free implant space whereas TCPb

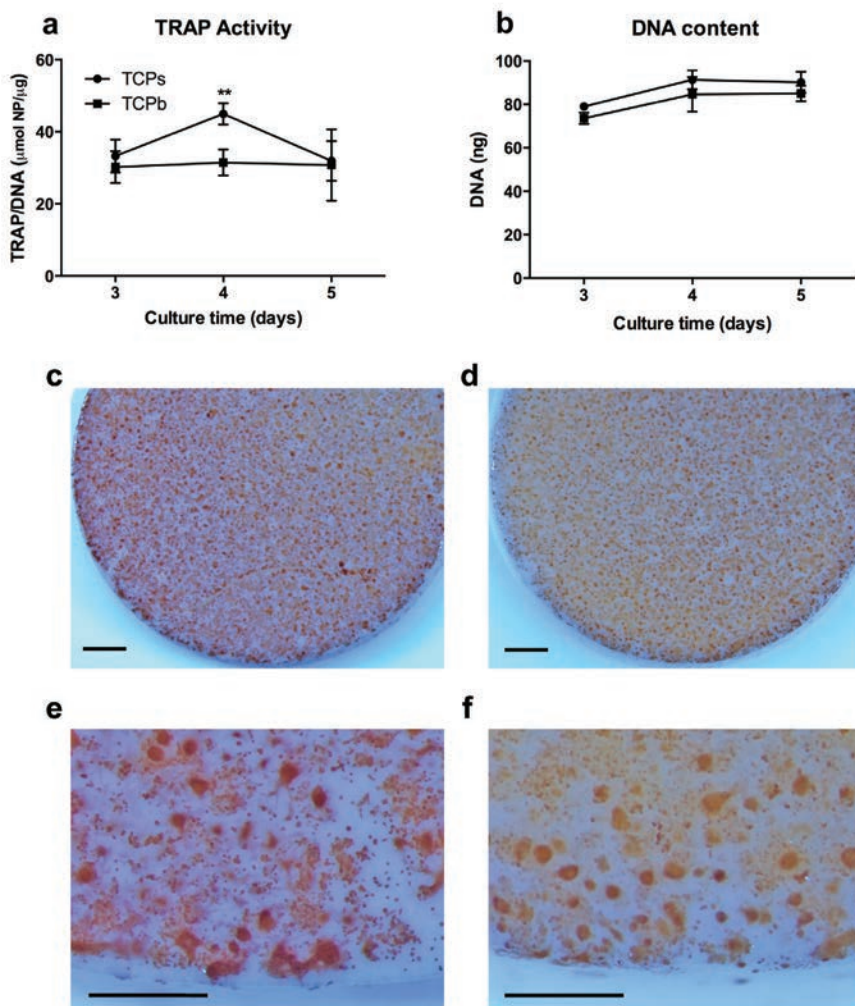


Figure 5. Osteoclast TRAP activity on TCP discs. (a) TRAP activity per DNA in the cell lysate peaked after 4 days culture on submicrostructured TCPs but remained flat on microstructured TCPb (mean \pm s.d. of $n = 5$ discs. ** $P \leq 0.01$). (b) DNA content was equivalent between materials at the same time points. Representative TRAP staining of cells cultured on (c, d) TCPs and (e, f) TCPb after 4 days clearly showed this difference, with most intense staining near the edge of the discs.

formed no bone in any of the 8 test subjects (Figure 7.h). Percent area material resorption by histomorphometry was also profoundly different: resorption of TCPs was $24 \pm 5\%$ but TCPb was almost entirely unresorbed ($0.3 \pm 0.1\%$) (Figure 7.i). Consistent throughout the TCPs samples, cuboidal osteoblasts were observed forming new bone and osteocytes resided in the lacunae of mature lamellar and woven bone. Multinucleated cells morphologically resembling osteoclasts were regularly found resorbing the material, densely populating the surface that was not already occupied by new bone (Figure 7.g). These osteoclast-like cells were occasionally found on the bone but to a much lesser extent than on the material. TRAP staining to substantiate that these cells were osteoclasts was not possible due to the high curing temperature of the embedding procedure resulting in inactivation of the enzyme. In striking contrast, virtually no multinucleated cells were present in any of the histological sections of TCPb though loose connective tissue ingrowth was apparently unhindered.

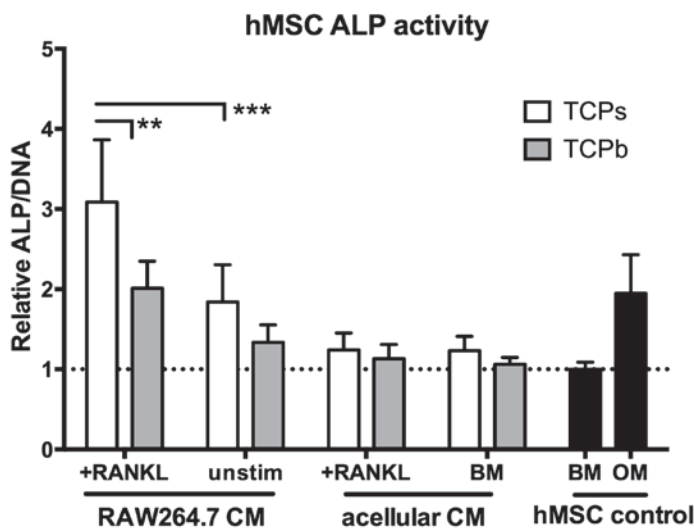


Figure 6. Biochemical ALP/DNA activity in hMSC lysate after treatment with conditioned medium (CM) for 7 days on tissue culture plastic. CM was collected from RAW264.7 cultured for 5 days on TCP discs stimulated with or without RANKL (unstimulated) to form osteoclasts or macrophages, respectively. CM collected from TCP discs without cells incubated in basic medium (BM) with or without RANKL served as acellular CM controls. hMSC cultured in BM or osteogenic medium (OM) without CM served as hMSC controls. Values represent the mean \pm s.d. of $n = 4$ independent cultures of one representative hMSC donor normalized to hMSC cultured in BM. ** $P \leq 0.01$, *** $P \leq 0.001$.

4 DISCUSSION

It is the longstanding goal of biomaterial design for bone tissue repair to engineer materials that more closely simulate autologous bone. Here, we focused on replicating the aspects of bone's capacity to be remodeled and stimulate formation of new bone – i.e., material resorbability coupled with osteoinductivity. Surveying the sparse but diverse array of materials that have been shown to induce ectopic bone formation, which stands as the gold standard demonstration of osteoinductivity, Barradas et al. (2011) suggest that surface microstructure may play a determining role in stimulating osteogenesis [5]. But, as the authors point out, because most prior work lacks surface profile characterization, there is no consensus on if a particular size range of surface features, such as grains and pores, can induce bone formation [5]. Therefore, we began with the hypothesis that in order to make a material osteoinductive, the scale of surface architecture on the order of ~ 1 μm may be crucial. Concerning the material resorbability, TCP provides an ideal platform, as it is commonly known to be the most resorbable of synthetic CaPs used in the clinic.

4

After careful control of the synthesis technique, as we have previously described in detail [10,31], TCP with either submicron- or micron-scale pores, grains, and roughness was successfully synthesized while maintaining material chemistry and macroporosity. The surface profiles of the materials reflected sinusoidal undulations resulting from reciprocating pores and grains, whose amplitudes spanned a submicron or micron scale range (Figure 1). In evaluating the intrinsic capacity of the materials to direct cell behavior and induce bone formation *in vitro* and *in vivo*, the osteogenic effects of these surface architectural differences proved to be disparate and striking. *In vitro*, submicron-scale surface structure promoted osteoclast-like cell activity, fusion, and secretion of factors that amplified osteogenic differentiation of hMSC versus micron-scale topography (Figures 2-6). *In vivo*, TCPs possessing submicron grains, pores, and roughness promoted extensive osteoclast-like cell colonization and considerable ectopic bone formation (Figure 7), comparable to the bone area of normal trabecular bone [32]. In stark contrast, TCPb with micron-scale surface structure contained few osteoclast-like cells and formed no bone. Because of this, the scale of surface architecture was found to determine the osteogenic potential of TCP.

Unexpectedly, submicron surface structure determined the resorbability of the materials, also in a dichotomous manner. By histology, multinucleated osteoclast-like cells could be seen actively resorbing TCPs, whereas no such activity could be seen for TCPb. Surprisingly, TCPb with micron-scale structure was left virtually unresorbed, despite its composition of β -tricalcium phosphate, shown

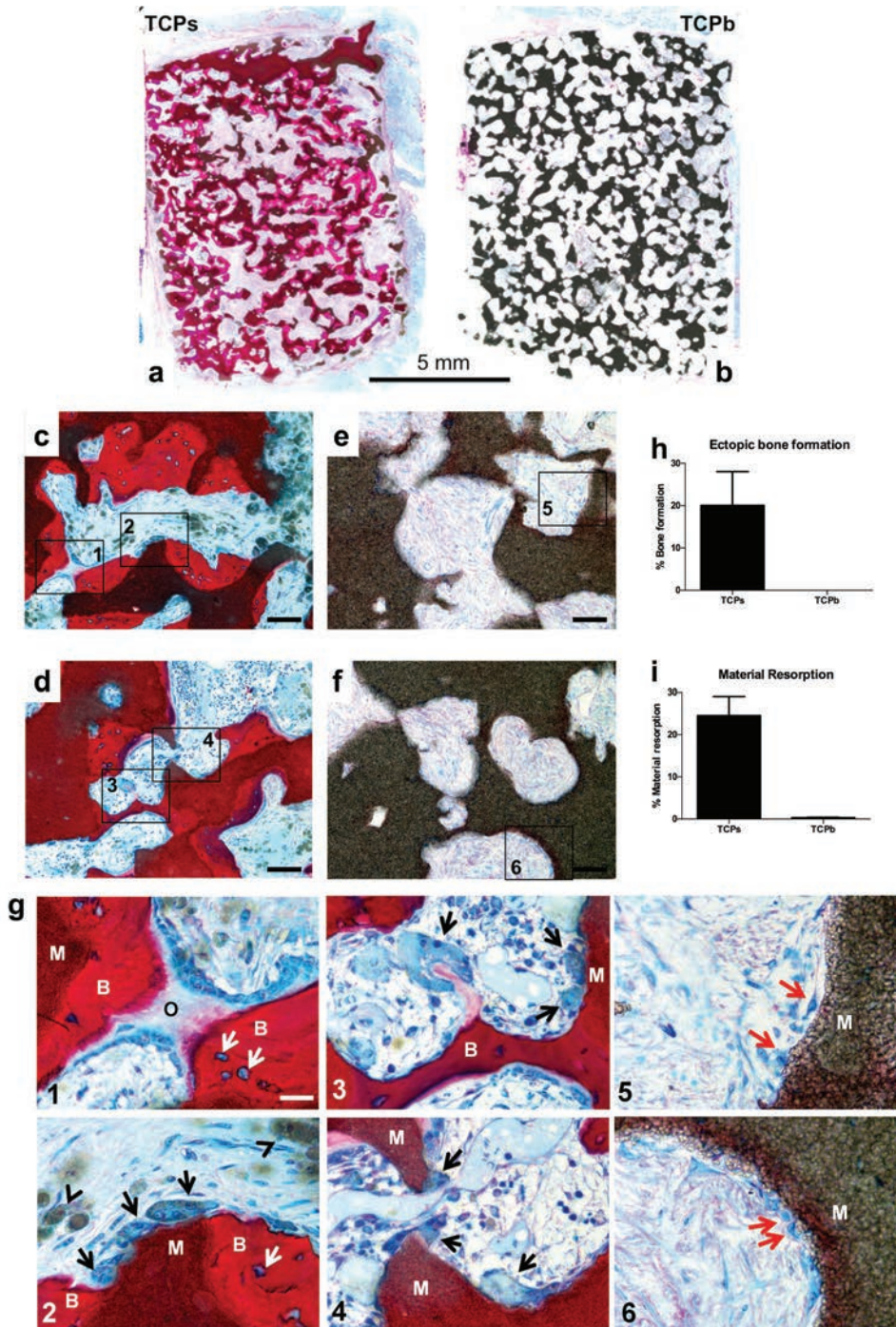


Figure 7. Representative histological sections of macro/microporous TCP cylinders implanted in the dorsal muscle of dogs for 12 weeks. Basic fuchsin/methylene blue

staining for bone (red). (a,b) Gross comparison shows ectopic bone formation by (a) TCPs and not by (b) TCPb. (c,d) Bone coverage and material fragmentation of TCPs, (e, f) No bone, no material particulate, and little tissue response in TCPb (scale bars = 100 µm). (g) Detail insets: 1-4 = TCPs, 5-6 = TCPb (scale bar = 25 µm). Note: cuboidal osteoblasts form osteoid (O) bridging mature bone (B); osteocytes (white arrows) in characteristic lacunae (1,2); multinucleated osteoclast-like cells (OCLC) (black arrows) resorbing microconcavities on TCPs material (M) between stretches of bone (2-4); phagocytosed material particulate inside OCLC (arrow heads, 2); mononuclear cells (red arrows) on TCPb surrounded by loose connective tissue (5,6). (h) Ectopic bone formation and (i) material resorption calculated by histomorphometry (mean ± s.d. of n = 8 dogs).

to readily resorb in vivo [20]. Prior work on the mechanism of TCP resorption in vivo presents conflicting interpretations, with some groups reporting that the process is principally mediated by cellular degradation [33], and other groups hypothesizing the process is mainly due to the passive dissolution by interstitial fluids [34]. In another case, TCP implanted in a non-loading cranial defect was not resorbed even after 6 months [35]. Taking into account the surface reactivity of the materials in vitro, in particular the tendency of both materials to continuously absorb rather than release Ca²⁺/P_i in physiologic (supersaturated) solution even with medium refreshment, we speculate that these materials may be primarily resorbed in vivo by cellular degradation versus passive physiologic dissolution which is supported by the clear contrast of the presence of multinuclear cells and disparate resorption values. Importantly, this finding presents the possibility that surface architecture – specifically, smaller grains and pores – may promote CaP resorption through the differential formation of multinucleated osteoclast-like cells in addition to increasing the specific surface area available for dissolution.

In support of this inference that the scale of surface architecture may directly influence cell behavior with direct relevance to bone formation and material resorption, we found that submicron architecture modulated osteoclast differentiation, form, and function – importantly, the secretion of osteogenic signals. These findings add to the growing understanding that surface microstructure and roughness greatly influence the formation and function of osteoclasts [29,36–38]. Toward a potential molecular mechanism for these surface-induced effects, Makihira et al. (2007) found that submicron rough titanium upregulated osteoclast gene expression in RAW264.7 macrophages, which they attributed to elevated RANK expression, the membrane-bound receptor of RANKL [39]. Because surface structure determines resultant material properties such as surface reactivity and topographical profile (Figure 1), it is impossible to isolate a single factor in the cellular control by these materials. A comparison of osteoclastogenesis on unreactive materials with various surface structures might help to elucidate the effects of topography versus surface reactivity, a strategy that we are currently researching. Indeed, topographical

cues as well as differences in surface reactivity of TCP tested here may have affected osteoclast behavior synergistically. For example, extracellular Ca^{2+} concentration [40], surface roughness [41], and surface feature scale [37] have all been shown to greatly affect osteoclast morphology and function.

Despite other reports of osteoclast resorption of various CaPs and specifically TCP, characteristic osteoclast resorption pits could not be found by SEM in this study [21,22,42–44]. Osteoclast resorption occurs exclusively in the sealing zone bounded by cytoskeletal actin rings [45]. Here, the size of the observed actin rings overlapped the size range of surface pores and grains, so it is possible that the micro-rough surface profile may have obscured any potential resorption. If appreciable resorption did occur, elevated $\text{Ca}^{2+}/\text{P}_i$ ions in the medium might be expected, though this also was not the case (data not shown). Confoundingly, elevation of $\text{Ca}^{2+}/\text{P}_i$ would likely be masked by the high affinity of TCP to rapidly absorb these ions in a supersaturated solution (Figure 1.f). Last, it is possible that appreciable resorption of sintered ceramics may require longer culture time (e.g., 28 days rather than 5 days) [44] and larger actin rings formed by primary osteoclasts, both potential limitations of the RAW264.7 cell line in this culture model.

Still, the submicron-scale architecture of TCPs promoted osteoclast-mediated factors potent enough to induce osteoblast differentiation of hMSC without osteogenic medium supplements, confirmed in multiple donors. Given neither clear evidence of osteoclast resorption nor depleted $\text{Ca}^{2+}/\text{P}_i$ in the conditioned medium, we speculate that the osteogenic effects were due to osteoclast-secreted trophic factors in response to the submicrostructured surface topography. In a broader biological context, it is pertinent to note that non-resorbing osteoclasts have been identified as a source of osteogenic factors *in vivo* [46–48], emphasizing that resorption is not necessary for osteogenic signaling [49], potentially an interesting link for non-resorbable, osteoinductive materials such as microstructured titanium. Concerning the interspecies potency of the osteogenic factors demonstrated here, Pederson et al. (2008) first reported that RAW264.7 osteoclast-like cells secrete soluble sphingosine 1 phosphate (S1P) and BMP6, which can differentiate hMSC into mineralizing osteoblasts [27]. Various other osteoclast-expressed osteogenic factors such as PDGF-BB [48], Wnt10b [27], other BMPs [26], and the recently identified coupling factor CTHRC1 [50] may have also played a role.

Here, monocyte/macrophages cultured without RANKL on TCPs but not TCPb also induced significant hMSC ALP activity versus the negative control (Figure 6, $P < 0.05$), suggesting that these cells can also impact osteogenesis directly

in response to osteoinductive surface structure, as others have previously suggested [51]. In vitro, inflammatory macrophages secrete osteogenic factors such as oncostatin M (OSM) [52,53] and may also express BMPs [54–56]. In vivo, Omar et al. (2011) showed that a titanium screw coated with lipopolysaccharide (LPS) to stimulate classical activation of macrophages resulted in higher bone contact when in orthotopic sites [57] though it is unknown what impact classically activated macrophages may have on bone formation in ectopic sites.

The broad physiologic effects of surface architectural scale observed here deserve further investigation as more biomimetic materials are engineered to repair and regenerate native bone. For instance, by tuning synthesis methods to achieve pore and grain architecture on the nano-scale, the resulting osteogenic effects can only be speculated. At the root of this, it is unclear if one or more resulting effects of small surface architecture – such as smaller physical topography, smaller surface roughness, higher specific surface area, or surface reactivity – may play a singularly directive role in the ectopic bone formation and material resorption observed here. Additionally, surface architecture may also impact other biological processes important for bone formation such as vasculogenesis and stem cell recruitment. Interestingly, many of the same osteogenic factors that are expressed by osteoclasts and their monocyte/macrophage precursors have also been shown to chemotactically home pre-osteoblasts (OSM, PDGF, CTHRC1) and stimulate blood vessel formation (TNF- α) [48,50,58]. For instance, invading macrophages signaled by the foreign body response may preferentially secrete cytokines important for both blood vessel formation and stem cell recruitment (e.g., pericytes) [59], followed by osteoblast/osteoclast differentiation [60] – all in response to surface architecture. In this way, the biological insight derived from engineering new osteogenic material surface architectures could inspire the design of other biomaterial implants where the foreign body reaction plays a key role.

5 CONCLUSION

A novel TCP ceramic composed of submicron-scale grains, pores, and surface roughness was found to potently induce ectopic bone formation, coupled with a similar rate of resorption, mimicking bone's own osteoinductivity and capacity to be remodeled. Whereas an equivalent TCP ceramic with micron-scale topographical features was unable to induce bone formation or to be resorbed, a more specific range of surface architecture for stimulating osteogenesis and material remodeling was identified. As a potential link, submicron-scale, surface structure of TCP promoted the differentiation and activity of osteoclasts resulting

in the osteogenic differentiation of mesenchymal stem cells without osteogenic additives.

A C K N O W L E D G E M E N T S

The authors gratefully acknowledge the support of the TeRM Smart Mix Program of the Netherlands Ministry of Economic Affairs and the Netherlands Ministry of Education, Culture and Science. This research forms part of the Project P2.04 BONE-IP of the research program of the Biomedical Materials Institute, co-funded by the Dutch Ministry of Economic Affairs. This project has also received funding from the European Union's Seventh Program for research, technological development, and demonstration under grant agreement number 241879. Special thanks are due to Davide Barbieri, Jinyi Su, Ruud Das, Rens Roosloot (Xpand Biotechnology) and Lorenzo Moroni (MIRA, University of Twente) for their technical expertise and useful discussion.

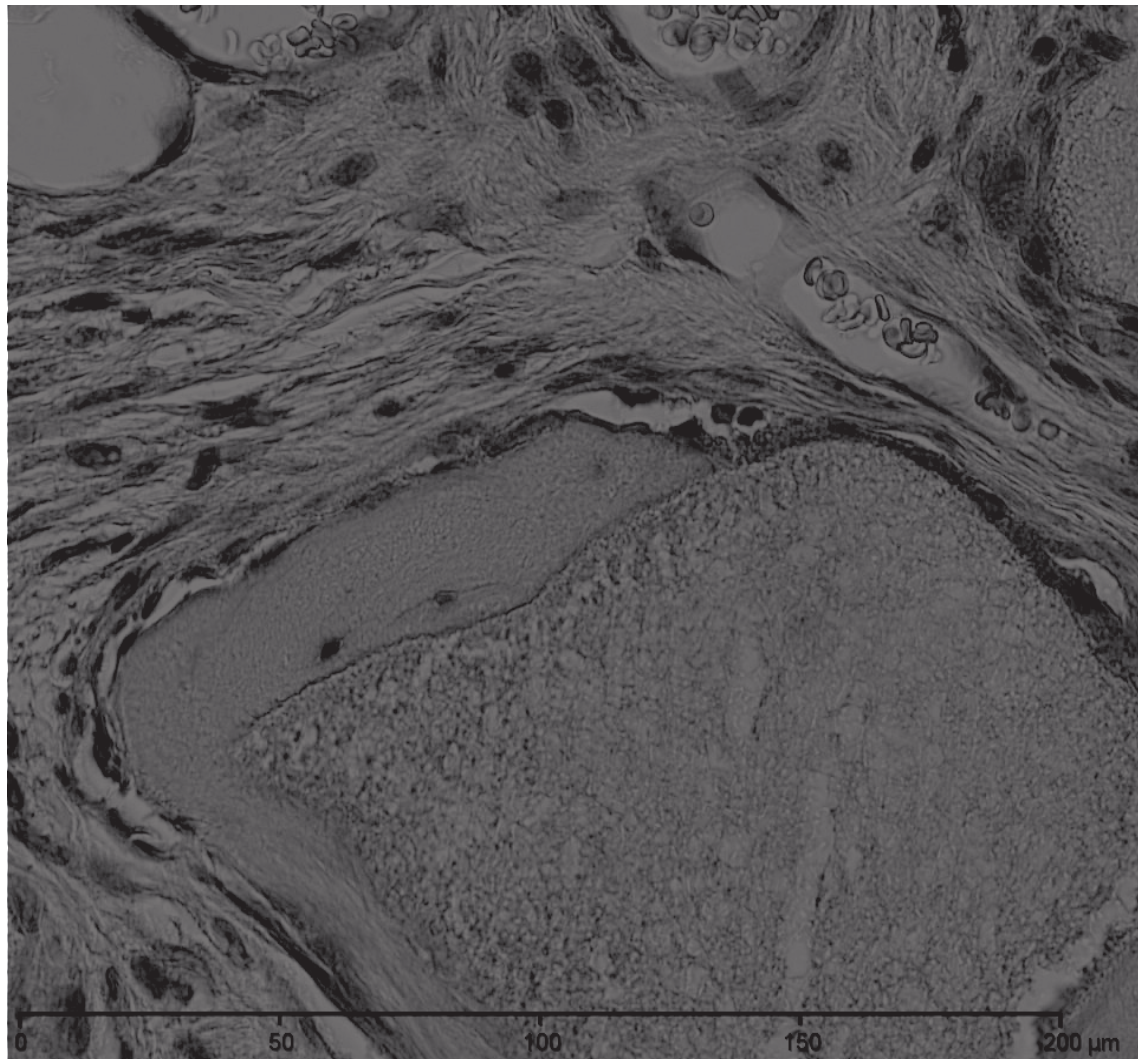
R E F E R E N C E S

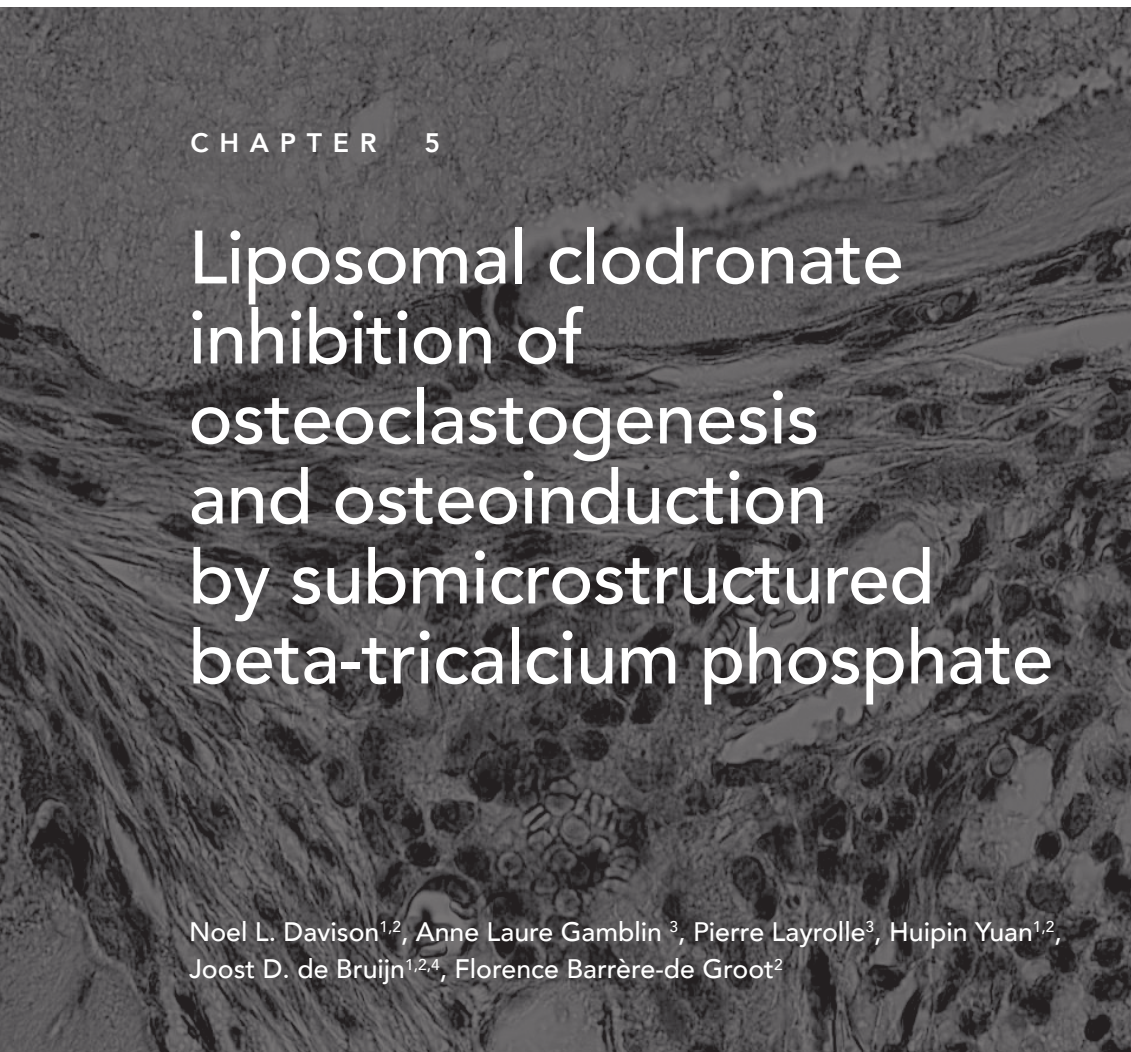
- [1] Bohner M, Galea L, Doebelin N. Calcium phosphate bone graft substitutes: failures and hopes. *J Eur Ceram Soc* 2012;32:2663–71.
- [2] Dorozhkin SV. Calcium Orthophosphates as Bioceramics: State of the Art. *J Funct Biomater* 2010;1:22–107.
- [3] Famery R, Richard N, Boch P. Preparation of α - and β -tricalcium phosphate ceramics, with and without magnesium addition. *Ceram Int* 1994;20:327–36.
- [4] Osborn JF, Newesely H. The material science of calcium phosphate ceramics. *Biomaterials* 1980;1:108.
- [5] Barradas AMC, Yuan H, van Blitterswijk CA, Habibovic P. Osteoinductive biomaterials: current knowledge of properties, experimental models and biological mechanisms. *Eur Cell Mater* 2011;21:407–29.
- [6] LeGeros RZ. Calcium phosphate-based osteoinductive materials. *Chem Rev* 2008;108:4742–53.
- [7] Habibovic P, Yuan H, van den Doel M, Sees TM, van Blitterswijk CA, de Groot K. Relevance of osteoinductive biomaterials in critical-sized orthotopic defect. *J Orthop Res* 2006;24:867–76.
- [8] Yuan H, Fernandes H, Habibovic P, de Boer J, Barradas AMC, de Ruiter A, et al. Osteoinductive ceramics as a synthetic alternative to autologous bone grafting. *Proc Natl Acad Sci U S A* 2010;107:13614–9.
- [9] Habibovic P, Yuan H, van der Valk CM, Meijer G, van Blitterswijk CA, de Groot K. 3D microenvironment as essential element for osteoinduction by biomaterials. *Biomaterials* 2005;26:3565–75.
- [10] Yuan H, De Bruijn JD, Li Y, Feng J, Yang Z, De Groot K, et al. Bone formation induced by

- calcium phosphate ceramics in soft tissue of dogs: a comparative study between porous alpha-TCP and beta-TCP. *J Mater Sci Mater Med* 2001;12:7–13.
- [11] Ripamonti U, Richter PW, Nilen RWN, Renton L. The induction of bone formation by smart biphasic hydroxyapatite tricalcium phosphate biomimetic matrices in the non-human primate Papio ursinus. *J Cell Mol Med* 2008;12:2609–21.
- [12] Fukuda A, Takemoto M, Saito T, Fujibayashi S, Neo M, Pattanayak DK, et al. Osteoinduction of porous Ti implants with a channel structure fabricated by selective laser melting. *Acta Biomater* 2011;7:2327–36.
- [13] Yuan H, Kurashina K, de Bruijn JD, Li Y, de Groot K, Zhang X. A preliminary study on osteoinduction of two kinds of calcium phosphate ceramics. *Biomaterials* 1999;20:1799–806.
- [14] Yuan H, de Bruijn JD, Zhang X, van Blitterswijk CA, de Groot K. Bone induction by porous glass ceramic made from Bioglass (45S5). *J Biomed Mater Res* 2001;58:270–6.
- [15] Fujibayashi S, Neo M, Kim H-M, Kokubo T, Nakamura T. Osteoinduction of porous bioactive titanium metal. *Biomaterials* 2004;25:443–50.
- [16] Le Nihouannen D, Daculsi G, Saffarzadeh A, Gauthier O, Delplace S, Pilet P, et al. Ectopic bone formation by microporous calcium phosphate ceramic particles in sheep muscles. *Bone* 2005;36:1086–93.
- [17] Yamasaki H, Sakai H. Osteogenic response to porous hydroxyapatite ceramics under the skin of dogs. *Biomaterials* 1992;13:308–12.
- [18] Dalby MJ, Gadegaard N, Tare R, Andar A, Riehle MO, Herzyk P, et al. The control of human mesenchymal cell differentiation using nanoscale symmetry and disorder. *Nat Mater* 2007;6:997–1003.
- [19] Sims NA, Gooi JH. Bone remodeling: Multiple cellular interactions required for coupling of bone formation and resorption. *Semin Cell Dev Biol* 2008;19:444–51.
- [20] Blokhuis TJ, Termaat MF, den Boer FC, Patka P, Bakker FC, Haarman HJ. Properties of calcium phosphate ceramics in relation to their in vivo behavior. *J Trauma* 2000;48:179–86.
- [21] Monchau F, Lefèvre A, Descamps M, Belquin-myrdycz A, Laffargue P, Hildebrand HF. In vitro studies of human and rat osteoclast activity on hydroxyapatite, beta-tricalcium phosphate, calcium carbonate. *Biomol Eng* 2002;19:143–52.
- [22] Yamada S, Heymann D, Bouler JM, Daculsi G. Osteoclastic resorption of biphasic calcium phosphate ceramic in vitro. *J Biomed Mater Res* 1997;37:346–52.
- [23] Kondo N, Ogose A, Tokunaga K, Umez H, Arai K, Kudo N, et al. Osteoinduction with highly purified beta-tricalcium phosphate in dog dorsal muscles and the proliferation of osteoclasts before heterotopic bone formation. *Biomaterials* 2006;27:4419–27.
- [24] Ripamonti U, Klar RM, Renton LF, Ferretti C. Synergistic induction of bone formation by hOP-1, hTGF-beta3 and inhibition by zoledronate in macroporous coral-derived hydroxyapatites. *Biomaterials* 2010;31:6400–10.
- [25] Tanaka T, Saito M, Chazono M, Kumagae Y, Kikuchi T, Kitasato S, et al. Effects of alendronate on bone formation and osteoclastic resorption after implantation of beta-tricalcium phosphate. *J Biomed Mater Res A* 2010;93:469–74.
- [26] McCullough KA, Waits CA, Garimella R, Tague SE, Sipe JB, Anderson HC. Immunohistochemical localization of bone morphogenetic proteins (BMPs) 2, 4, 6, and 7 during induced heterotopic bone formation. *J Orthop Res* 2007;25:465–72.
- [27] Pederson L, Ruan M, Westendorf JJ, Khosla S, Oursler MJ. Regulation of bone formation by osteoclasts involves Wnt/BMP signaling and the chemokine sphingosine-1-phosphate. *Proc Natl Acad Sci U S A* 2008;105:20764–9.
- [28] Costa-Rodrigues J, Fernandes A, Lopes MA, Fernandes MH. Hydroxyapatite surface roughness: complex modulation of the osteoclastogenesis of human precursor cells. *Acta Biomater* 2012;8:1137–45.
- [29] Marchisio M, Di Carmine M, Pagone R, Piattelli A, Mischia S. Implant surface roughness influences osteoclast proliferation and differentiation. *J Biomed Mater Res B Appl Biomater* 2005;75:251–6.
- [30] Stevens MM, George JH. Exploring and engineering the cell surface interface. *Science* 2005;310:1135–8.
- [31] Yuan H, Van Den Doel M, Li S, Van Blitterswijk CA, De Groot K, De Bruijn JD. A comparison of the osteoinductive potential of two calcium phosphate ceramics implanted intramuscularly

- in goats. *J Mater Sci Mater Med* 2002;13:1271–5.
- [32] Sato K, Wakamatsu E, Sato T, Honma T, Kotake H, Byers P. Histomorphometric study of trabecular channels in normal iliac bone. *Calcif Tissue Int* 1986;39:2–7.
- [33] Egglie PS, Müller W, Schenk RK. Porous hydroxyapatite and tricalcium phosphate cylinders with two different pore size ranges implanted in the cancellous bone of rabbits. A comparative histomorphometric and histologic study of bony ingrowth and implant substitution. *Clin Orthop Relat Res* 1988;127–38.
- [34] Lu J, Descamps M, Dejou J, Kouki G, Hardouin P, Lemaître J, et al. The biodegradation mechanism of calcium phosphate biomaterials in bone. *J Biomed Mater Res* 2002;63:408–12.
- [35] Handschel J, Wiesmann HP, Stratmann U, Kleinheinz J, Meyer U, Joos U. TCP is hardly resorbed and not osteoconductive in a non-loading calvarial model. *Biomaterials* 2002;23:1689–95.
- [36] Geblinger D, Zink C, Spencer ND, Addadi L, Geiger B. Effects of surface microtopography on the assembly of the osteoclast resorption apparatus. *J R Soc Interface* 2012;9:1599–608.
- [37] Geblinger D, Addadi L, Geiger B. Nano-topography sensing by osteoclasts. *J Cell Sci* 2010;123:1814–1814.
- [38] Zou W, Teitelbaum SL. Integrins, growth factors, and the osteoclast cytoskeleton. *Ann N Y Acad Sci* 2010;1192:27–31.
- [39] Makihira S, Mine Y, Kosaka E, Nikawa H. Titanium surface roughness accelerates RANKL-dependent differentiation in the osteoclast precursor cell line, RAW264. 7. *Dent Mater J* 2007;26:739–45.
- [40] Miyauchi A, Hruska KA, Greenfield EM, Duncan R, Alvarez J, Barattolo R, et al. Osteoclast cytosolic calcium, regulated by voltage-gated calcium channels and extracellular calcium, controls podosome assembly and bone resorption. *J Cell Biol* 1990;111:2543–52.
- [41] Brinkmann J, Hefti T, Schlottig F, Spencer ND, Hall H. Response of osteoclasts to titanium surfaces with increasing surface roughness: an in vitro study. *Biointerphases* 2012;7:34.
- [42] Wenisch S, Stahl J-P, Horas U, Heiss C, Kilian O, Trinkaus K, et al. In vivo mechanisms of hydroxyapatite ceramic degradation by osteoclasts: fine structural microscopy. *J Biomed Mater Res A* 2003;67:713–8.
- [43] Winkler T, Hoenig E, Gildenhaar R, Berger G, Fritsch D, Janssen R, et al. Volumetric analysis of osteoclastic bioresorption of calcium phosphate ceramics with different solubilities. *Acta Biomater* 2010;6:4127–35.
- [44] Xia Z, Grover LM, Huang Y, Adamopoulos IE, Gbureck U, Triffitt JT, et al. In vitro biodegradation of three brushite calcium phosphate cements by a macrophage cell-line. *Biomaterials* 2006;27:4557–65.
- [45] Teitelbaum SL. The osteoclast and its unique cytoskeleton. *Ann N Y Acad Sci* 2011;1240:14–7.
- [46] Karsdal MA, Neutzsky-Wulff AV, Dziegiele MH, Christiansen C, Henriksen K. Osteoclasts secrete non-bone derived signals that induce bone formation. *Biochem Biophys Res Commun* 2008;366:483–8.
- [47] Karsdal MA, Martin TJ, Bollerslev J, Christiansen C, Henriksen K. Are nonresorbing osteoclasts sources of bone anabolic activity? *J Bone Miner Res* 2007;22:487–94.
- [48] Kreja L, Brenner RE, Tautzenberger A, Liedert A, Friemert B, Ehrnhaller C, et al. Non-resorbing osteoclasts induce migration and osteogenic differentiation of mesenchymal stem cells. *J Cell Biochem* 2010;109:347–55.
- [49] Fuller K, Ross JL, Szewczyk KA, Moss R, Chambers TJ. Bone is not essential for osteoclast activation. *PLoS One* 2010;5(9): e128.
- [50] Takeshita S, Fumoto T, Matsuoka K, Park K, Aburatani H, Kato S, et al. Osteoclast-secreted CTHRC1 in the coupling of bone resorption to formation. *J Clin Invest* 2013;123:3914–24.
- [51] Fellah BH, Josselin N, Chappard D, Weiss P, Layrolle P. Inflammatory reaction in rats muscle after implantation of biphasic calcium phosphate micro particles. *J Mater Sci Mater Med* 2007;18:287–94.
- [52] Guihard P, Danger Y, Brounais B, David E, Brion R, Delecrin J, et al. Induction of osteogenesis in mesenchymal stem cells by activated monocytes/macrophages depends on oncostatin m signaling. *Stem Cells* 2012;30:762–72.
- [53] Nicolaïdou V, Wong MM, Redpath AN, Ersek A, Baban DF, Williams LM, et al. Monocytes

- induce STAT3 activation in human mesenchymal stem cells to promote osteoblast formation. *PLoS One* 2012;7(7): e398:e39871.
- [54] Takebe J, Champagne CM, Offenbacher S, Ishibashi K, Cooper LF. Titanium surface topography alters cell shape and modulates bone morphogenetic protein 2 expression in the J774A.1 macrophage cell line. *J Biomed Mater Res A* 2003;64:207–16.
- [55] Champagne CM, Takebe J, Offenbacher S, Cooper LF. Macrophage cell lines produce osteoinductive signals that include bone morphogenetic protein-2. *Bone* 2002;30:26–31.
- [56] Honda Y, Anada T, Kamakura S, Nakamura M, Sugawara S, Suzuki O. Elevated extracellular calcium stimulates secretion of bone morphogenetic protein 2 by a macrophage cell line. *Biochem Biophys Res Commun* 2006;345:1155–60.
- [57] Omar OM, Granéli C, Ekström K, Karlsson C, Johansson A, Lausmaa J, et al. The stimulation of an osteogenic response by classical monocyte activation. *Biomaterials* 2011;32:8190–204.
- [58] Glass GE, Chan JK, Freidin A, Feldmann M, Horwood NJ, Nanchahal J. TNF-alpha promotes fracture repair by augmenting the recruitment and differentiation of muscle-derived stromal cells. *Proc Natl Acad Sci U S A* 2011;108:1585–90.
- [59] Bergers G, Song S. The role of pericytes in blood-vessel formation and maintenance. *Neuro Oncol* 2005;7:452–64.
- [60] Fellah BH, Delorme B, Sohier J, Magne D, Hardouin P, Layrolle P. Macrophage and osteoblast responses to biphasic calcium phosphate microparticles. *J Biomed Mater Res A* 2010;93:1588–95.
- [61] Ljusberg J, Ek-Rylander B, Andersson G. Tartrate-resistant purple acid phosphatase is synthesized as a latent proenzyme and activated by cysteine proteinases. *Biochem J* 1999;343 Pt 1:63–9.
- [62] Jansen IDC, Vermeer JAF, Bloemen V, Stap J, Everts V. Osteoclast fusion and fission. *Calcif Tissue Int* 2012;90:515–22.
- [63] Dalby MJ, Riehle MO, Sutherland DS, Agheli H, Curtis ASG. Changes in fibroblast morphology in response to nano-columns produced by colloidal lithography. *Biomaterials* 2004;25:5415–22.





CHAPTER 5

Liposomal clodronate inhibition of osteoclastogenesis and osteoinduction by submicrostructured beta-tricalcium phosphate

Noel L. Davison^{1,2}, Anne Laure Gamblin³, Pierre Layrolle³, Huipin Yuan^{1,2}, Joost D. de Bruijn^{1,2,4}, Florence Barrère-de Groot²

- 1 MIRA Institute of Biomedical Technology and Technical Medicine, University of Twente, The Netherlands;
- 2 Xpand Biotechnology B.V., The Netherlands;
- 3 INSERM UMR 957 Department of Pathophysiology of Bone Resorption, University of Nantes, France;
- 4 School of Engineering and Materials Science (SEMS), Queen Mary University of London, United Kingdom

A B S T R A C T

Bone graft substitutes such as calcium phosphates are subject to the innate inflammatory reaction, which may bear important consequences for bone regeneration. We speculate that the surface architecture of osteoinductive β -tricalcium phosphate (TCP) stimulates the differentiation of invading monocyte/macrophages into osteoclasts, and that these cells may be essential to ectopic bone formation. To test this, porous TCP cubes with either submicron-scale surface architecture known to induce ectopic bone formation (TCPs, positive control) or micron-scale, non-osteoinductive surface architecture (TCPb, negative control) were subcutaneously implanted on the backs of FVB strain mice for 12 weeks. Additional TCPs samples received local, weekly injections of liposome-encapsulated clodronate (TCPs+LipClod) to deplete invading monocyte/macrophages. TCPs induced osteoclast formation, evident by positive tartrate resistant acid phosphatase (TRAP) cytochemical staining and negative macrophage membrane marker F4/80 immunostaining. No TRAP positive cells were found in TCPb or TCPs+LipClod, only F4/80 positive macrophages and foreign body giant cells. TCPs stimulated subcutaneous bone formation in all implants, while no bone could be found in TCPb or TCPs+LipClod. In agreement, expression of bone and osteoclast gene markers was upregulated in TCPs versus both TCPb and TCPs+LipClod, which were equivalent. In summary, submicron-scale surface structure of TCP induced osteoclastogenesis and ectopic bone formation in a process that is blocked by monocyte/macrophage depletion.

1 INTRODUCTION

Following the evolving insight into biomaterial design [1], particular emphasis has been devoted to understanding how physical properties of calcium phosphates (CaP) may influence their bone forming performance. For instance, implant geometry [2], 3D surface concavities [3,4], and interconnected porous structure [5] have all been shown to influence bone formation. Most recently, material surface architecture on the submicron- and micron-scale has been shown to be particularly important to the osteoinductivity of a small subset of CaP through an unknown biological mechanism [6,7]. It is at this CaP-tissue interface where proteins and ions are absorbed and exchanged, as a function of the material surface reactivity and physico-chemistry [8]. On a cellular level, it is at this interface where invading monocyte/macrophages interact with the material surface, mediating inflammation and tissue repair during the host response to a foreign body [9]. Accordingly, specific interactions with the host response may be essential for the functional performance of bone graft substitutes to even further stimulate bone tissue regeneration in bony defects.

Though material properties can be adjusted to mitigate the innate inflammatory reaction, inflammation is at least to some extent unavoidable after implanting CaP due to the normal host response to a foreign body [10]. It has been speculated that in the case of osteoinductive CaP, invading tissue macrophages signaled by the innate inflammatory reaction may play a role in osteogenesis because of their dense and persistent presence surrounding an osteoinductive implant [11,12]. On the other hand, an adverse host response can also obstruct bone formation: in our previous work, chronic inflammation due to the addition of a polymeric carrier completely abrogated ectopic bone formation by osteoinductive betacalcium phosphate (TCP) although the carrier dissolved relatively quickly (Chapter 2). Indeed, macrophages, the principal cell responsible for clearing a foreign body by phagocytosis, have been shown to express a distinct family of cytokines depending on their activation state in response to material properties such as surface chemistry, topography, and bioactivity [13,14].

During the innate inflammatory reaction, invading macrophages secrete cytokines that can also spur the fusion and specialization of bone-resorbing osteoclasts from their monocyte/macrophage precursors. Pro-inflammatory cytokines such as TNF α , IL-1, and IL-6 activate T-cell expression of soluble RANKL (receptor activator of NF- κ B ligand) the essential osteoclast differentiation factor, as well as upregulate its membrane-bound receptor RANK on the surface of osteoclast precursors, thus inducing osteoclastogenesis [15–18]. On the other hand, other secreted cytokines such as IL-4 and IL-13 stimulate stromal cell expression of

OPG (osteoprotegerin), the natural decoy receptor to RANKL, thus antagonizing osteoclast differentiation [19]. In this way, inflammation and osteoclastogenesis may be linked and dependent on the precise cytokine cascade and a biomaterial substrate supporting pre-osteoclast fusion and differentiation. Osteoclasts have also been implicated with the functionality of osteoinductive CaP, with reports that osteoclasts form prior to ectopic bone formation [20] and that their inhibition may stunt osteoinduction [21,22].

As it pertains to osteogenesis, macrophage-mediated inflammation has been associated with pathological heterotopic ossification (HO) that results in marrow-containing bone neogenesis in the muscle tissue triggered by injury. However, when liposome-encapsulated bisphosphonate was locally administered to selectively deplete tissue macrophages in a transgenic mouse model of HO, osteogenesis was significantly blocked. This effect was attributed to the elimination of macrophage-secreted BMP4 at the injury site [23]. In an experimental mouse model of osteoarthritis, macrophage depletion by liposomal bisphosphonate resulted in the reduction of osteophytes (heterotopic bony nodules), which was attributed to reduced macrophage expression of osteogenic TGF β , BMP2, and BMP4. And as it pertains to the natural regenerative capacity of bone, when macrophages were depleted using liposomal clodronate (a bisphosphonate) in a long bone fracture model, bone formation in the fracture callus was fully inhibited [24], shown elsewhere to be likely mediated by macrophage-expressed TNF- α and IL-6 [25]. These studies and others like them emphasize the apparent importance of macrophages and phagocyte relatives to both aberrant and reparative bone formation.

Considering cell-material interactions, both bone cells and macrophages have been shown to be highly sensitive to surface architecture of CaP. In our previous research investigating two TCP ceramics with different sized surface features, both ectopic bone formation and the presence of actively resorbing osteoclast-like multinucleated cells were strongly promoted on submicron-scale TCP surface features. On the other hand, no ectopic bone and scarce non-resorbing multinucleated cells were found on the TCP implants with micron-scale surface features (Chapter 4).

Following on these findings, we asked whether these multinucleated cells were differentiated osteoclasts or merely fused macrophages, i.e. foreign body giant cells. Because their presence and resorative activity appeared to be linked to osteoinduction, we hypothesized that they may play a directive role in ectopic bone formation by forming differently on the two different topographies during the host response. To investigate these questions, we implanted the same two

TCP ceramics with equivalent chemistry but different surface structure – serving as positive and negative controls – in a recently validated mouse model of subcutaneous osteoinduction [26] and analyzed the ectopic bone formation and the phenotype of formed multinucleated cells using (immuno-)histological and gene expression analysis. To address the role that these multinucleated cells play in osteoinduction, we applied liposome-encapsulated clodronate (LipClod) to selectively deplete invading phagocytic monocyte/macrophages [27] – the mononuclear precursors of both osteoclasts and foreign body giant cells – and then evaluated ectopic bone formation.

2 MATERIALS AND METHODS

2.1 Preparation and characterization of porous TCP cubes

TCP powders were synthesized as previously described in Chapter 4. Briefly, calcium hydroxide and phosphoric acid (both from Fluka) were mixed at a Ca/P ratio of 1.50. TCP powders with small (TCPs) or big grains (TCPb) in the final ceramics were prepared by controlling the reaction rates. The powders were foamed with diluted H_2O_2 (1%) (Merck) at 60 °C then dried at room temperature to get porous green bodies. The dry green bodies were subsequently sintered at 1050 °C or 1100 °C for 8 hours to achieve small and big grains for TCPs and TCPb, all respectively.

Porous cubes (4 x 4 x 4 mm) were machined from the ceramic bodies using a wet saw and then ultrasonically cleaned in successive baths of acetone, ethanol, and distilled water, and dried. Prior to implantation, TCP cubes were heat sterilized at 160 °C for 2 hours. Crystal chemistry of the materials was analyzed by X-ray diffraction (Rigaku Miniflex II) scanning the range $2\theta = 25\text{--}45^\circ$ (step size = 0.01°, rate = 1° min⁻¹) and confirmed to be β -TCP as previously described in Chapter 4.

The TCP ceramics were characterized to confirm that they were composed of different surface (micro)structure but similar macrostructure as previously reported in Chapter 4. Surface microstructure was characterized by scanning electron microscopy (SEM) (JEOL JSM-5600) after sputter coating with gold for 90 seconds (JEOL JFC 1300) and > 50 surface grains and micropores were measured in the using Image J image analysis software (NIH, USA). To measure the surface profile (i.e., surface roughness), SEM stereo-micrographs of the same location taken at two different tilt angles (2500x, ±5°) were digitally reconstructed into three-dimensional surfaces for automated profile analysis using MeX v5.1 software (Alicona Imaging, Austria). Additionally, porosity and total pore area

were determined by mercury intrusion testing (Table 1) (Micromeritics, USA).

In summary, the synthesis of TCPs and TCPb resulted in submicron-scale and micron-scale surface grains, micropores, and roughness, respectively. The ceramics possessed similar total porosity but different total pore area owing to the smaller surface features of TCPs.

Table 1. Physical characterization of TCP.

Physical parameters	TCPs	TCPb
Average grain diameter (μm)	0.95 ± 0.27	3.66 ± 1.05
Average pore diameter (μm)	0.63 ± 0.33	1.78 ± 0.85
Average roughness, R_a (μm)	0.126 ± 0.003	1.287 ± 0.011
Root-mean-square roughness, R_{RMS} (μm)	0.158 ± 0.003	1.597 ± 0.011
Porosity (%)	69.6	72.0
Total pore area (m^2/g)	1.477	0.769

2.2 Subcutaneous implantation in FVB mice

Ethical approval for animal experimentation was obtained from the local ethical committee (CREEA). The animals were housed in certified premises at the Experimental Therapeutic Unit at the Faculty of Medicine, University of Nantes, France. Animals were stabled in cages with food and water ad libidum with artificial day/night cycle of 12 hours and regulated temperature of $20 \pm 1^\circ\text{C}$.

Five-week-old male FVB strain mice ($n = 14$) were received from Charles River Laboratory (France) and allowed to equilibrate to their new surroundings for one week. Prior to surgery, the mice were placed under general anesthesia using isoflurane gas (2.5% in air, 2.5 L/min, Forene). Analgesic (Buprenorphine 60 $\mu\text{L}/\text{kg}$, Buprécare, MedVet) was subcutaneously injected at the time of surgery and 1 day later. Backs of animals were shaved and disinfected with sterile gauzes soaked with iodine solution and covered with a surgical sheet. Subcutaneous dorsal pockets were created using a scalpel and blunt nosed forceps, each allowing for the insertion of a single TCP cube. Two subcutaneous pockets were created on the left side of the back, in which TCPs positive control and TCPb negative control samples were inserted. An additional TCPs cube receiving liposomal clodronate treatment was implanted in one pocket on the right side of the back in order to avoid potential contamination of the injected liposomes into the pockets containing the controls. Skin incisions were tightly closed with

degradable sutures (Vicryl 4-0, Ethicon).

Immediately following surgery, sterile liposomal clodronate (100 µL) (Clodronate Liposomes Foundation, The Netherlands) was injected into one pocket containing TCPs per animal. The same volume of sterile saline was injected into the pockets containing the TCPs positive control and TCPb negative control. This same injection regimen was repeated once a week and then animals were sacrificed after 12 weeks by inhalation of an overdose of carbon dioxide gas. The terminal time point was selected based on previous work establishing the FVB mouse model of osteoinduction by Barradas et al [26].

At this time, one long incision through the skin was made down the back and carefully separated from the muscle using a scalpel. TCP implants were carefully cut away from the soft tissue and skin and placed in vials containing either 4% formaldehyde for histological analysis or in RNase/DNAse free tubes containing 1 mL TRI® Reagent (Sigma-Aldrich) for RNA isolation and qPCR. Histological replicates were stored at 4 °C for and qPCR replicates were frozen at -80 °C for further processing.

2.3 Histological processing and imaging

TCP explants from 9 mice were processed for histological analysis. This sample size was based on the recent work of Barradas et al (2012) in developing the FVB mouse model of osteoinduction [26]. Explants were placed in cassettes and then decalcified in 4.13% EDTA/0.2% paraformaldehyde in PBS (pH 7.4) at 50 °C using an automated microwave decalcifying apparatus (KOS Histostation, Milestone Med. Corp. MI, U.S.A). Samples were periodically checked with x-ray to ensure complete and consistent decalcification, which required up to 17 days. After complete decalcification, samples were then rinsed with tap water and dehydrated in ascending series of ethanol baths: 80, 95, 100%, and finally in butanol for 30 min (Automated dehydration station, Microm Microtech, France). Samples were then impregnated in liquid paraffin at 56 °C (Histowax) and embedded at -16 °C. Embedded explants were completely sectioned at 4-7 locations spaced ~500 µm using a standard microtome (Leica RM2250) set at 5 µm thickness. Following the various stains described below, coverslips were mounted with Pertex and slides were digitally scanned at up to 40x magnification (NanoZoomer 2.0RS, Hamamatsu Corp. Japan) and analyzed with virtual microscope software (NDP View, Hamamatsu Corp).

2.4 Masson's trichrome staining for bone formation

Sections were stained by Masson's trichrome technique by using an automated coloration station (Microm, Microtech). This staining combined hematoxylin for cell nuclei in blue/black, fuchsin for cytoplasm, muscle and erythrocytes in red, and bright green for collagen and allowed the visualization general tissue response and new bone formation. Cover slips were mounted with Pertex and digitally scanned as previously described. After creating digital scans of each stained section using the NanoZoomer, the presence of bone in each histological sample was carefully determined by two researchers in at least 5 different sections taken at different levels throughout the sample. Each randomly selected section was visually scanned, from top to bottom in its entirety, at 20x magnification in NDP view software. Bone stands out as vividly stained dark green with characteristic osteocyte lacunae.

2.5 Immunohistochemical staining of macrophage marker F4/80 and osteoblast transcription factor Osterix

Immunohistochemical staining of murine macrophage membrane marker F4/80 and osteoblast transcription factor Osterix served to identify macrophages and osteoblasts in serial histological sections. Sections were first deparaffinized in Ottix histological solvent (3 x 5 min), rehydrated in a graded ethanol series (100%, 3 x 5 min; 95%, 1 x 5 min; 80%, 1 x 5 min), and then rinsed in distilled water (3 x 5 min). To retrieve antigens, sections were incubated in citrate buffer, pH 6, at 95 °C for 10 min. Sections were then incubated with 3% H₂O₂ for 15 min to inactivate endogenous peroxidase, rinsed with TBS-Tween 0.05% pH 7.6, blocked with 5% normal goat serum in 1% BSA in TBS-0.05% Tween pH 7.6 at room temperature for 30 min, then incubated at 4 °C overnight with primary antibodies (AbCAM) targeting F4/80 (rabbit anti-mouse monoclonal, 1:100) and sp7/Osterix (rabbit polyclonal, 1:800) diluted in blocking buffer. Sections were again rinsed with TBS-Tween then incubated with secondary goat anti-rabbit antibody (Dako) diluted 1:200 in blocking buffer for 30 min at RT, rinsed with TBS-tween, incubated with streptavidin-linked HRP (Dako) for 30 min at RT, and finally visualized with DAB chromogen (Dako) with Mayer's hematoxylin counterstain. Cover slips were mounted with Pertex and digitally scanned as previously described.

2.6 Cytochemical staining of osteoclast enzyme marker TRAP

Cytochemical staining of osteoclast enzyme tartrate resistant acid phosphatase (TRAP) was used as a marker to identify osteoclasts in histological sections.

TRAP staining was performed using a commercial staining kit (Acid Phosphatase Leukocyte Staining Kit, Sigma) following the manufacturer's instructions. Briefly, staining solution was prepared with Fast Red TR salt (3.9 mM), naphthol AS-TR phosphate disodium salt (2.3 mM), N-N dimethylformamide (68 µM), and L(+)-tartaric acid (100 mM) all diluted in sodium acetate buffer (0.1 M, pH 5.2). Deparaffinized sections were incubated in the solution for 90 min at 37 °C and then counterstained with Mayer's hematoxylin. TRAP positive stained cells appeared red.

2.7 Gene expression by qPCR

TCP explants from 5 mice were processed for gene expression analysis by qPCR. Frozen samples were thawed and thoroughly pulverized in TRI® Reagent (Sigma-Aldrich) using a motorized pestle homogenizer. Samples were centrifuged to remove TCP particles, and the RNA in the supernatant was precipitated in chloroform following the manufacturer's instructions. Total RNA concentration and purity was measured using a Nanodrop machine. Reverse transcription of cDNA was performed using a ThermoScript First-Strand kit (Invitrogen).

Quantitative PCR (qPCR) was performed on a BioRad CFX 96 System. The PCR reactions were performed with 20 ng cDNA in a total volume of 10 µL containing iQ SYBR Green Supermix (Biorad) and forward and reverse primers (300 nM). After an initial activation step for 30 seconds at 98 °C, 40 cycles were run of a two-step PCR consisting of a denaturation step at 95 °C for 15 seconds and annealing and extension step at 60 °C for 30 seconds. Subsequently the PCR products were subjected to melting curve analysis to test if any unspecific PCR products were generated. Each sample was tested in duplicate.

Quantitative PCR primers were designed using Primer-BLAST (www.ncbi.nlm.nih.gov) spanning at least 1 intron to avoid amplification of genomic DNA (Table 2). Expression of housekeeping genes HPRT and cyc1 was not affected by the experimental conditions and were thus used for endogenous normalization of the gene targets. Relative fold expression of the normalized gene targets was calculated versus expression levels in the negative control, TCPb (equal to 1).

2.8 Statistics

Statistical comparisons of gene target expression were performed using One-way ANOVA and Tukey's post hoc tests in GraphPad Prism 6.0 software. P values < 0.05 were considered significant.

Table 2. qPCR primer sequences.

Gene Target	Sequence (5' -> 3')	Product size (bp)	Accession ID
HPRT	tccctcctcagaccgcttt	90	NM_013556.2
	cctggttcatcatcgctaats		
Cyc1	tgtgctcacacggaggaagaa	72	NM_025567.1
	catcatcattaggggcatcc		
RANKL	tcctgtactttcgagcgcag	337	NM_011613.3
	ttatgggaaccggatgggatg		
BSP	cggcgatagttccgaagagga	76	NM_008318.1
	cccctcagaatcttcattgttt		
TRAP	cgtctctgcacagattgcat	75	NM_001102405.1
	aagcgcaaacggtagtaagg		
CR	ccttccagaggagaagaaacc	95	NM_007588.2
	ggagattccgcctttcac		
OC	agactccggcgctacatt	86	NM_001032298.2
	caaggcagggttaagctcaca		
RANK	tgcagctttccatgacactg	103	NM_009399.3
	cagccactactaccacagagatg		
OPG	atgaacaagtggctgtgctg	106	NM_008764.3
	cagttctgggtataatgcaa		
Runx2	ccacaaggacagagtcagattaca	92	NM_001145920.2
	tggctcagataggaggggta		
F4/80	tcctccttgccctggacact	100	NM_010130.4
	gccttgaagggtcagcaacc		
NFATc1	catgcgagccatcatcga	130	NM_001164112.1
	tggatgtgaactcggaaagac		

3 RESULTS

3.1 Ectopic bone formation and tissue response

TCPs and TCPb porous cubes were implanted in subcutaneous pockets on the backs of mice and resulting ectopic bone formation was evaluated both by histological and whole-sample gene expression analysis. During implantation

some replicates were lost: 2 TCPs control samples, 2 TCPb control samples, and 6 TCPs samples treated with LipClod. Given that substantially more samples were lost from the LipClod treatment group versus either control group, it is likely that LipClod depletion of macrophages prevented proper wound healing as extensively described in the literature [28]. At the end of 12 weeks, samples were recovered from 9 mice for histological analysis ($n = 7$ TCPs control, $n = 8$ TCPb control, and $n = 5$ TCPs + LipClod sample replicates) and 5 mice for gene expression analysis ($n = 5$ TCPs control, $n = 4$ TCPb control, and $n = 3$ TCPs + LipClod sample replicates).

After careful scrutiny of multiple random levels of each harvested sample, ectopic bone tissue could be identified in all of the TCPs explants (7 out of 7) and in none of the TCPb explants (0 out of 8), thus validating these materials as positive and negative controls in this model of osteoinduction. No bone was found in TCPs implants treated locally with LipClod (0 out of 5) to deplete the invading phagocytes (Table 3).

Table 3. Incidence rate of ectopic bone formation by histological analysis.

TCPs	TCPs + LipClod	TCPb
7/7	0/5	0/8

In TCPs, bone formation was little compared to the total implant area and it varied substantially between mice; however, cuboidal osteoblasts, osteocytes in characteristic lacunae, and multinucleated osteoclast-like cells could all be identified. Moreover, a difference in the tissue response was observed in that the pore structure of TCPs was generally occupied by darkly stained highly condensed collagen fibrils whereas that of TCPb appeared to be lighter stained loose connective tissue. In TCPs samples treated with LipClod, sparse connective tissue in the pore structure appeared disorganized and did not stain the same dark, vivid green as the dense collagen observed in TCPs control (Figure 1).

Expression of mature bone markers bone sialoprotein (BSP) and osteocalcin (OC) was significantly upregulated in TCPs versus the negative control TCPb (~350 fold, $P = 0.0002$; 3.6 fold, $P = 0.039$; respectively); however, expression levels in TCPs treated with LipClod were unchanged versus TCPb ($P = 0.999$ and 0.931, respectively), substantiating the histological analysis that LipClod treatment blocked bone formation by TCPs (Figure 1).

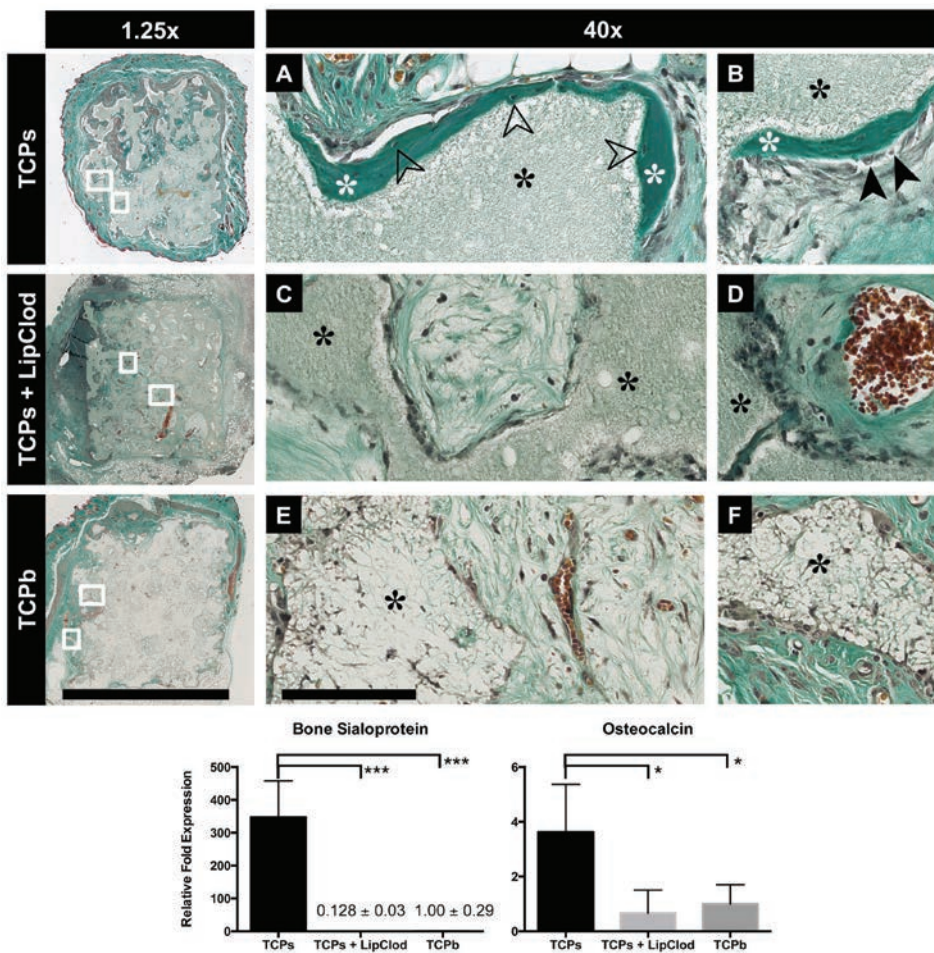


Figure 1. Ectopic bone formation by TCPs and blockade by phagocyte depletion. (Top) Representative sections stained with Masson's Trichrome from decalcified TCP (black stars) cubes subcutaneously implanted in mice for 12 weeks. Ectopic bone formation (white stars) was only found in TCPs (A, B), shown by dark green collagen staining. Osteocytes in lacunae (A, open arrows) and cuboidal osteoblasts (B, black arrows) can be seen in and on the mature bone matrix. Local liposomal clodronate injections blocked bone formation in TCPs (TCPs + LipClod) (C, D). Connective tissue in the pore space was generally less condensed (C, light green) though blood vessels were still formed (D, orange stained erythrocytes). TCPb (E, F) formed no bone although the pore structure was vascularized (E, orange erythrocytes) and cells had colonized the material surface (F, grey staining). 1.25x scale bar = 4 mm; 40x scale bar = 100 µm. (Bottom) Gene expression of mature bone markers bone sialoprotein and osteocalcin were upregulated in TCPs versus TCPs + LipClod and TCPb, while expression levels between TCPs + LipClod and non-inductive TCPb were equivalent. * P < 0.05, *** P < 0.001.

3.2 Identification of TRAP positive, F4/80 negative osteoclasts on TCP

Enzymatic staining for osteoclast marker TRAP served to identify osteoclasts in the implants. Because mature osteoclasts are F4/80 negative [29–31], we compared TRAP and F4/80 staining of the same multinucleated cells in serial sections in order to unambiguously differentiate between multinucleated osteoclasts and fused macrophage foreign body giant cells.

In TCPs, TRAP positive multinucleated cells were located primarily between stretches of ectopic bone attached to the material surface. In serial sections, these same cells were confirmed to be F4/80 negative, establishing their identity as differentiated osteoclasts rather than fused macrophages. Not all TRAP positive osteoclasts were located next to bone suggesting that the presence of bone may not be necessary for their formation. Moreover, not all multinucleated cells in TCPs were TRAP positive indicating the heterogeneity of multinucleated cells throughout the explant. In contrast, TRAP positive cells – either mononucleated or multinucleated – could not be found in neither TCPb nor in TCPs treated with LipClod. The multinucleated cells colonizing these implants were uniformly F4/80 positive (Figure 2).

In support of the finding that TCPs promoted osteoclastogenesis while TCPb did not, osteoclast gene markers TRAP, calcitonin receptor (CR), and osteoclast transcription factor NFATc1 were analyzed and indeed, these markers were significantly upregulated in TCPs (fold differences = ~2, 200, and 3; P = 0.027, 0.021, and 0.031, all respectively). In contrast, LipClod treatment left them unchanged versus TCPb (P = 0.342, 0.999, and 0.493, respectively). In an effort to explain these results, expression of the critical osteoclast-signaling axis RANK-RANKL-OPG was analyzed, showing that RANK expression was sharply downregulated in TCPs + LipClod versus TCPs control (22 fold, P = 0.0099), likely due to the selective eradication of phagocytic monocyte/macrophage osteoclast precursors. However, the expression of RANKL or OPG was statistically equivalent between TCPs with and without LipClod treatment (P = 0.152 and 0.103, respectively). Thus, the reason for osteoclast depletion may have been more due to loss of RANK-expressing monocyte/macrophage osteoclast precursors rather than alteration of the balance between RANKL and its antagonist OPG (Figure 2).

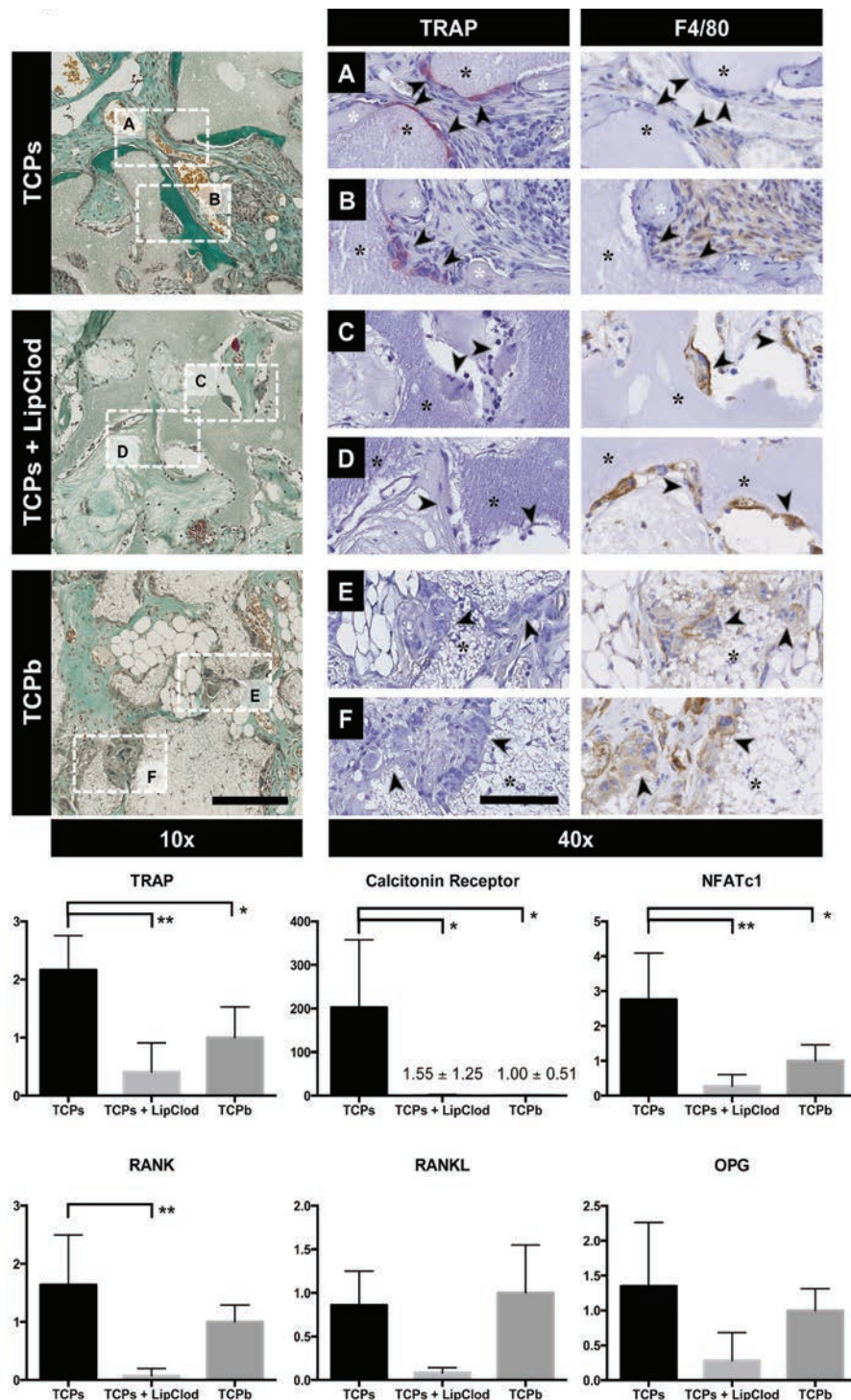


Figure 2, opposite. Osteoclastogenesis by TCPs and depletion by Liposomal Clodronate. (Top) Representative overview images (10x) stained with Masson's Trichrome show ectopic bone formation in TCPs (dark green) and not in TCPs treated with Liposomal Clodronate (LipClod) or non-inductive TCPb. (A, B) 40x insets of serial sections stained for osteoclast marker tartrate resistant acid phosphatase (TRAP) and macrophage membrane marker F4/80 show TRAP positive (red) F4/80 negative osteoclasts colonizing the material (black stars) between stretches of ectopic bone (white stars). No TRAP positive cells could be found in TCPs treated with Liposomal Clodronate (LipClod) (C, D) or the non-inductive TCPb (E, F). Multinucleated cells (black arrows) in these explants were uniformly F4/80 positive (brown) fused macrophages. 10x scale bar = 200 μ m; 40x scale bar = 100 μ m. (Bottom) Gene expression of osteoclast markers TRAP, calcitonin receptor, and NFATc1 were significantly upregulated in TCPs versus TCPs + LipClod or TCPb. Expression of RANK was downregulated in TCPs + LipClod versus TCPs, indicative of pre-osteoclast depletion. Expression levels of RANKL and its decoy receptor OPG varied between groups but were statistically equivalent. * P < 0.05, ** P < 0.01.

3.3 Macrophage colonization and depletion

Macrophage-specific membrane marker F4/80 was visualized using immunohistochemistry in order to evaluate the efficacy of LipClod treatment in depleting phagocytic macrophages and foreign body giant cells characteristic of the foreign body reaction. Indeed, LipClod treatment effectively depleted F4/80 positive cells particularly at the outer surfaces of the implant accompanied by large numbers of negatively stained mononuclear cells and cell fragments indicative of LipClod-initiated apoptosis. In contrast, the outer edge of TCPs control was prominently lined with a dense layer of F4/80 positive macrophages (Figure 3).

Despite the clear efficacy of macrophage depletion at the edge of the TCPs implants, positively stained macrophages were still prevalent in the inner pore structure, similar to the untreated TCPs control. There in particular, F4/80 positive multinucleated cells colonized the surface of TCPs regardless of LipClod treatment (Figure 3).

Positively stained macrophages were also present in TCPb, but appeared substantially less organized than TCPs control. In particular, F4/80 positive macrophages did not densely line the outer edge of TCPb as on TCPs control. In the pore structure, however, F4/80 positive multinucleated cells were observed similar to TCPs with and without LipClod treatment (Figure 3).

In agreement with the positive F4/80 immunohistochemistry throughout all groups, there was no statistical difference in F4/80 gene expression between any of the groups. F4/80 expression in TCPs treated with LipClod was lower on average than TCPs control, but expression levels were statistically equivalent ($P = 0.579$), possibly due to the incomplete macrophage depletion observed in the

histology. F4/80 expression was equivalent between TCPs and TCPb controls ($P = 0.986$), despite histological differences in staining intensity and organization (Figure 3).

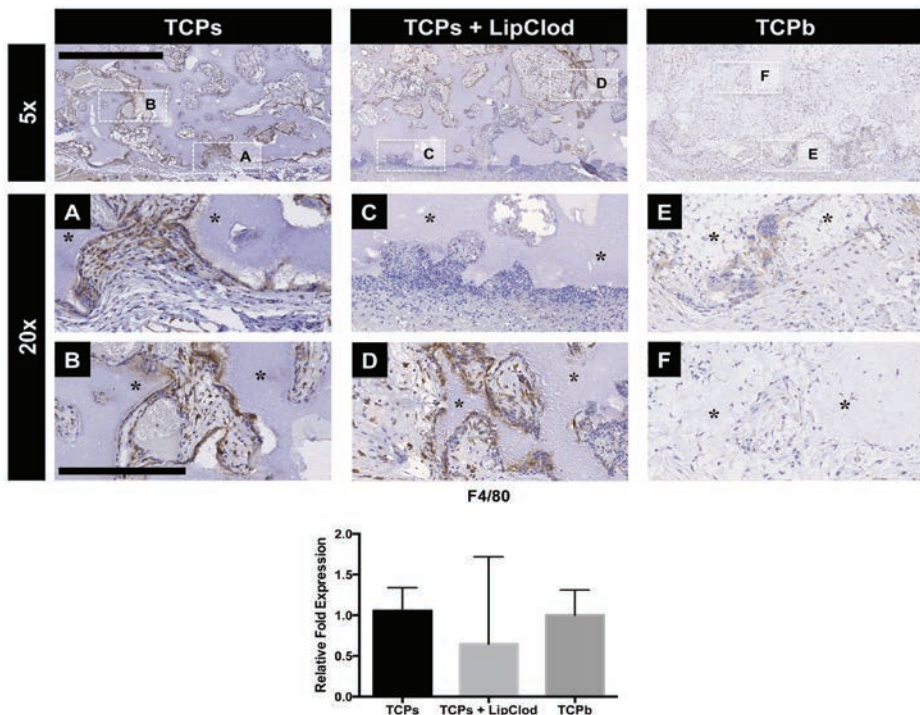


Figure 3. Macrophage colonization of TCP and depletion by Liposomal Clodronate. (Top) Representative sections of TCP (black stars) immunohistochemically stained for macrophage membrane marker F4/80. F4/80 positive macrophages (brown) densely lined the (A) outer surface and (B) inner pore structure of TCPs, resembling osteal macrophages. Weekly liposomal Clodronate injections (TCPs + LipClod) effectively depleted F4/80 positivity at the (C) outer surface of TCPs with evident cell fragments indicative of apoptosis due to the treatment; however F4/80 positive macrophages still colonized the (D) inner pore structure. Positively stained macrophages less densely colonized the (E) outer surface and (F) inner pore structure of TCPb (TCP marked by black stars). 5x scale bar = 1 mm; 20x scale bar = 300 μ m. (Bottom) Gene expression of F4/80 was equivalent between all groups.

3.4 Osteoblast differentiation inhibited by phagocyte depletion

To evaluate if LipClod treatment affected osteoblast differentiation associated with osteoinduction by TCPs, immunohistochemical staining of Osterix confirmed the presence of osteoblast-like cells in TCPs treated with LipClod, though less frequent than in TCPs without treatment. Moreover, whereas Osterix

positive cuboidal osteoblasts were mainly located on or next to ectopic bone in the TCPs control, they were located in loose connective tissue contained in the pore structure of TCPs + LipClod (Figure 4). These histological results were substantiated by significantly lower expression of osteoblast transcription factor Runx2 versus TCPs (6 fold, $P = 0.029$) and equivalent expression to TCPb ($P = 0.741$). Despite no Osterix positive cells evident in TCPb (not shown), expression of Runx2 was statistically equivalent between TCPs and TCPb controls (2.8 fold, $P = 0.053$), potentially due to high variability between samples (Figure 4).

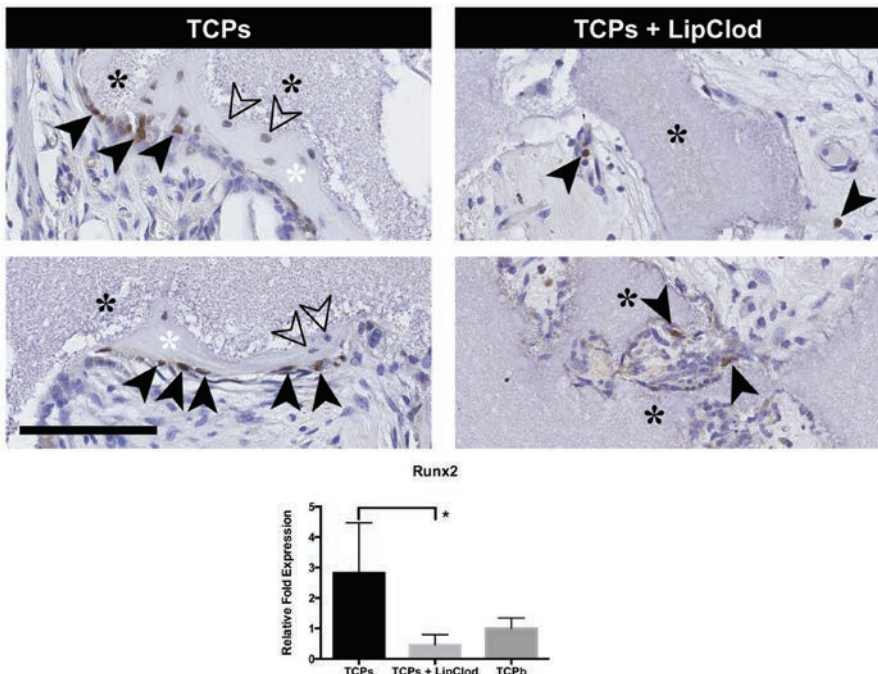


Figure 4. Osteoblast differentiation by TCPs is inhibited by phagocyte depletion. (Top) Immunohistochemical staining of osteoblast marker Osterix in (left) Osterix positive cells (black arrows) were found colonizing the surface of TCPs (black stars) as well as bone tissue (white stars) containing osteocytes in lacunae (open arrows). (Right) Positively stained cells were also found in TCPs treated with Liposomal Clodronate (TCPs + LipClod) but to a lesser extent, both in the (top) inter-pore space and (bottom) in contact with the TCP surface, despite no bone formation. (Bottom) Gene expression of Runx2 was downregulated in TCPs + LipClod versus TCPs without treatment, which was at an equivalent level as non-inductive TCPb. * $P < 0.05$.

4 DISCUSSION

By identifying multinucleated cells that were positively stained for osteoclastic enzyme TRAP but negatively stained for macrophage membrane marker F4/80

and vice versa, the distinct presence of both osteoclasts and foreign body giant cells were found on the surface of osteoinductive submicrostructured TCPs in subcutaneous implants. Although giant cells widely populated the surface of non-osteoinductive microstructured TCPb, no such TRAP positive multinucleated cells could be found. Osteoclast markers were significantly downregulated on TCPb, suggesting that osteoclastogenesis is not common to all CaP but is preferentially directed by osteoinductive surface architecture. This finding could provide an explanation for the widely varied and conflicting reports on the identity of multinucleated cells surrounding different CaP in various implantation models [32–35]: all CaP are not created equal; one material with a particular surface architecture may promote osteoclastogenesis while another composed of the same chemistry and macrostructure may not. In support of this finding, our previous work demonstrated that TCPs promotes the formation and activity of osteoclasts *in vitro*, emphasizing the directive role of surface submicron surface structure on osteoclastogenesis (Chapter 4). It is interesting to consider that while biomaterials comprising a wide range of material chemistries and structures trigger giant cell formation during the foreign body response [10], an osteoinductive CaP material directs the formation of the three major bone cells in a heterotopic location: osteoclasts (multinucleated, F4/80 negative, TRAP positive, residing on the material surface; Figure 2), osteoblasts (cuboidal, strongly Osterix positive, residing on the bone surface; Figure 4), and osteocytes (weakly Osterix positive, residing in bone lacunae; Figure 4).

In addition to this result, LipClod treatment impeded both bone formation and osteoclastogenesis, substantiated by equivalent bone and osteoclast markers to the negative non-osteoinductive control. Our hypothesis that specific interactions of osteoinductive TCP with the host response may determine ectopic bone formation is therefore confirmed. LipClod treatment was shown to potently deplete F4/80 positive macrophages around the perimeter of the implants as intended. However, F4/80 positive mono- and multinucleated cells could still be found in the internal pore structure of the implants. It is possible that the liposomes were unable to substantially penetrate the inner pore structure thereby allowing macrophages migrating from the internal vasculature to survive and proliferate. Nonetheless, LipClod treatment evidently disrupted the invading phagocyte activity enough to prevent ectopic bone and Osteoclast formation.

LipClod is extensively used in the literature to study the role of macrophages in various disorders where inflammation and wound healing play a key role. The function and efficacy of LipClod depletion of phagocytes, particularly macrophages, has been thoroughly researched for over 20 years and is a

strategy that has been used in more than 800 peer reviewed citations, attesting to its wide breadth of applications as a research tool [36]. Mechanistically, when a clodronate-encapsulated liposome is phagocytosed, the liposome is opened by intracellular lysozyme and the drug is released in the cytoplasm where it is metabolized into a toxic ATP analog resulting in both apoptosis and necrosis [37,38]. The specificity of LipClod in its ability to deplete only “professional” phagocytes arises from the liposomes’ fast clearance time, the short half-life, non-toxicity of free clodronate, and the inability of the liposomes to passively infiltrate the cell membrane [27]. Following subcutaneous injection of large (~> 0.1 micron) multilamellar liposomes, such as those used here, liposomes are confined to the injection site either to degrade over time or be phagocytosed by tissue macrophages [39]. Hence in this experimental model, the risk of cross contamination of LipClod treatment was minimal.

Expounding on the idea that the host response to an osteoinductive implant may determines its osteogenic capacity, we hypothesized that the lack of multinucleated cells such as osteoclasts and foreign body giant cells stemming from the host response would impede ectopic bone formation. This was supported by our previous observations in which the presence and resorptive activity of these cells on implanted TCP was correlated with osteoinductivity. LipClod treatment was selected to deplete these cells because it targets their mutual monocyte/macrophage phagocyte precursors as well as osteoclasts themselves. Although giant cells were still present in the internal pore structure of the treated implants, no TRAP positive multinucleated cells could be found in the treatment samples and osteoclast gene markers were significantly downregulated, indicating that osteoclastogenesis or osteoclast survival was reduced. It is unclear if osteoclasts simply were unable to differentiate due to depleted levels monocyte-macrophage precursors or whether osteoclasts formed but then were directly depleted in the same mechanism as macrophages – through phagocytosis of LipClod – as reported in the literature [40,41]. A time course study might be useful in illuminating this question. In either case, ectopic bone formation was impeded in the absence of depleted TRAP positive osteoclasts, although F4/80 positive mononuclear macrophages and multinucleated giant cells were still present.

The question remains how phagocytes such as osteoclasts or macrophages mediate ectopic bone formation. Previous results from our group showed that when osteoclasts and to a lesser extent macrophages are cultured on osteoinductive TCP, they secrete soluble factors that potently induce alkaline phosphatase enzyme activity in human mesenchymal stem cells without osteogenic additives (Chapter 4). Other groups have described the secretion of anabolic bone factors by both osteoclasts and macrophages extensively as

well. Most recently, osteoclast-specific deletion of CTHRC1, a much sought after soluble bone coupling factor, was shown to result in osteopenia in mice emphasizing the importance of osteoclast-secreted anabolic factors on normal bone homeostasis [42]. Additionally, osteoclasts have been reported to secrete various other osteoblast differentiating factors such as bone morphogenetic proteins (BMPs), sphingosine 1-phosphate (S1P), and Wnt10b [43–45].

It has been suggested that macrophage-mediated inflammation may play a role in osteoinduction by CaP though until now no experiments were conducted to specifically target this cell type, nor have they shown a clear link between CaP-incited inflammation and osteoinduction [11,12]. Inflammatory macrophages have also been demonstrated to secrete osteogenic factors such as oncostatin M (OSM) [46,47] and may also express BMPs [48–50]. The results here substantiate the importance of macrophages in osteoinduction, although it is unclear if they act directly on the differentiation and bone secretion of osteoblasts or whether they mediate other cellular processes necessary for osteoinduction such as differentiating into bone-promotive osteoclasts or secreting vasculogenic factors to increase blood flow and a supply of stem cells necessary for osteogenesis [25].

LipClod treatment also affected the expression of early osteoblast markers Osterix and Runx2 in TCP compared to the control, in conjunction with no bone formation and equivalent bone marker levels to non-inductive TCPb. One possible explanation for this is that macrophages and osteoclasts secrete chemotactic signals such as TNF- α , OSM, PDGF [45], and S1P [44] that attract pre-osteoblasts. Another explanation follows the potency of macrophage- and osteoclast-secreted anabolic factors to differentiate stem cells directly as previously described. Thus, the role of these cells in osteoinduction may be to first home mesenchymal stem cells to the implant site and then differentiate them into osteoblasts by secreting anabolic trophic factors. Still, it is possible that osteoblasts phagocytosed the liposomes directly since they have been observed to internalize wear debris from prosthetics [51]. It has been reported that osteoblast markers are upregulated in mesenchymal stem cells cultured on similarly osteoinductive TCP [7,52], so the direct interaction of stem cells with an osteoinductive material may also aid osteoblast formation. However, Osterix positive cells were observed without bone formation suggesting that the activation of early osteoblast transcription factors may not guarantee bone matrix secretion of mature osteoblasts without a normally functioning phagocyte population.

Although the precise material parameters necessary for material-directed osteoinduction remain unknown, the results presented here reinforce the

importance of the scale of surface structure and add to the growing understanding that the physical form of a biomaterial surface can invoke profoundly different tissue responses [53–56]. Here, the influence of surface architecture was again emphasized in the disparate nature of bone formation and bone marker expression between two TCP that differ in the scale of their surface features. By recapitulating the same bone incidence rate of these TCP as previously described in a canine intramuscular model (Chapter 4), the FVB mouse model of subcutaneous osteoinduction recently reported by Barradas et al. (2012) was further validated [26]. Moreover, the application of weekly LipClod injections to locally deplete invading macrophages at an implant surface also presents a useful strategy to evaluate the importance of the host response to different material surfaces. Indeed, the sensitivity of monocyte/macrophage-lineage cells to substrate topography alludes to an intriguing way of controlling the foreign body response by modulating the scale of surface architecture.

5 CONCLUSION

TCP with submicron-scale surface architecture was found to generate TRAP positive, F4/80 negative osteoclasts along with consistent ectopic bone formation in subcutaneous pockets of mice but TCP with micron-scale surface architecture did not. LipClod treatment, resulting in the complete depletion of osteoclasts but not (fused) macrophages was found to block ectopic bone formation. Thus, the scale of TCP surface architecture may be essential to ectopic bone formation by directing the host response and subsequent osteoclastogenesis.

A C K N O W L E D G E M E N T S

The authors gratefully acknowledge the support of the TeRM Smart Mix Program of the Netherlands Ministry of Economic Affairs and the Netherlands Ministry of Education, Culture and Science. This research forms part of the Project P2.04 BONE-IP of the research program of the Biomedical Materials Institute, co-funded by the Dutch Ministry of Economic Affairs. This project has also received funding from the European Union's Seventh Program for research, technological development, and demonstration under grant agreement number 241879. Special thanks are due to Dr. Ana Barradas (MIRA, University of Twente) for her invaluable advice concerning the FVB mouse model, and Jinyi Su (Xpand Biotechnology), Martine Berreur, and Jerome Amiaud (both INSERM UMR957) for their help and technical expertise.

R E F E R E N C E S

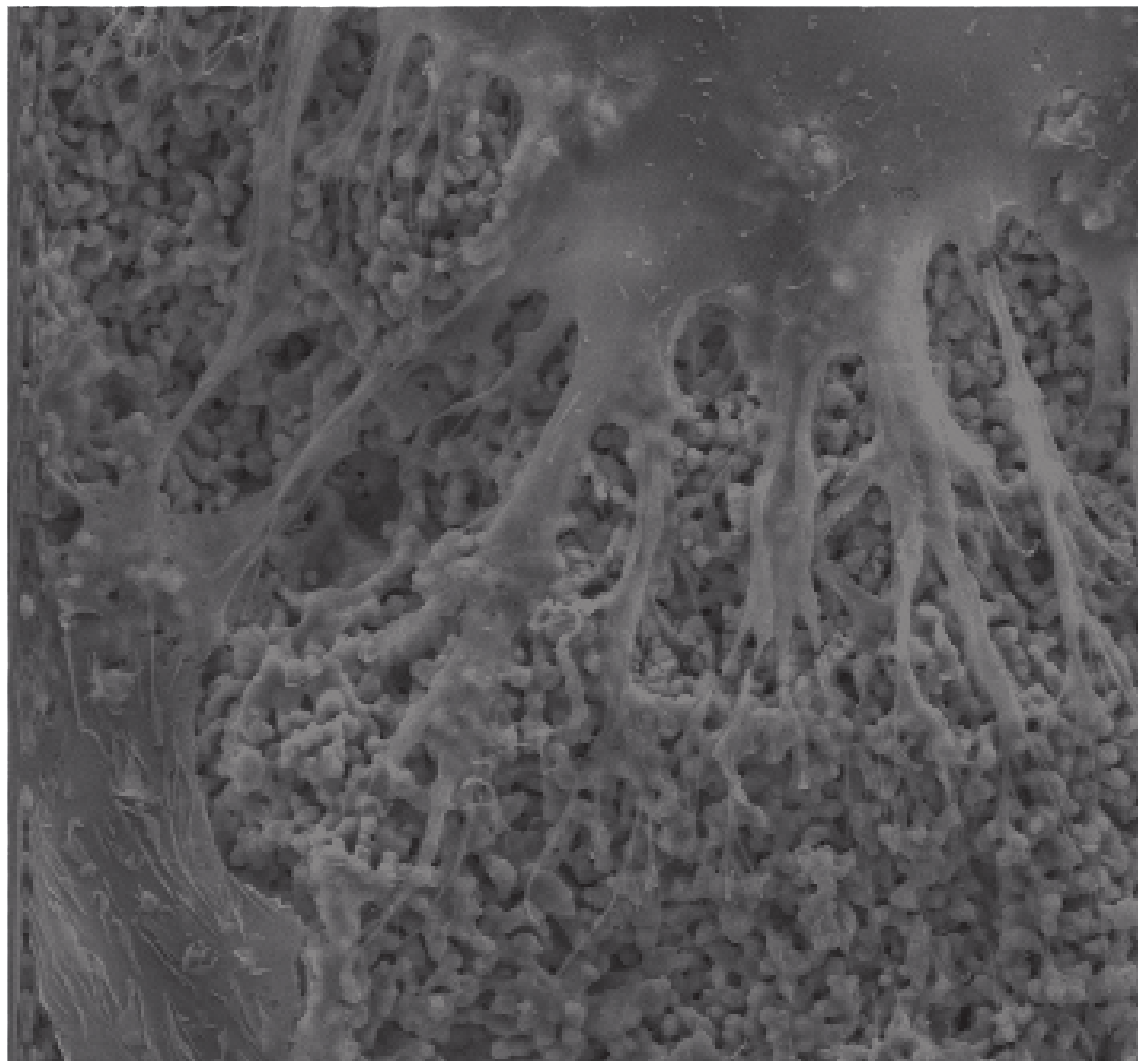
- [1] Mitragotri S, Lahann J. Physical approaches to biomaterial design. *Nat Mater* 2009;8:15–23.
- [2] Magan A, Ripamonti U. Geometry of porous hydroxyapatite implants influences osteogenesis in baboons (*Papio ursinus*). *J Craniofac Surg* 1996;7:71–8.
- [3] Ripamonti U, Richter PW, Nilen RW, Renton L. The induction of bone formation by smart biphasic hydroxyapatite tricalcium phosphate biomimetic matrices in the non-human primate *Papio ursinus*. *J Cell Mol Med* 2008;12:2609–21.
- [4] Habibovic P, Yuan H, van der Valk CM, Meijer G, van Blitterswijk CA, de Groot K. 3D microenvironment as essential element for osteoinduction by biomaterials. *Biomaterials* 2005;26:3565–75.
- [5] Yuan H, De Bruijn JD, Li Y, Feng J, Yang Z, De Groot K, et al. Bone formation induced by calcium phosphate ceramics in soft tissue of dogs: a comparative study between porous alpha-TCP and beta-TCP. *J Mater Sci Mater Med* 2001;12:7–13.
- [6] Habibovic P, Yuan H, van den Doel M, Sees TM, van Blitterswijk CA, de Groot K. Relevance of osteoinductive biomaterials in critical-sized orthotopic defect. *J Orthop Res* 2006;24:867–76.
- [7] Yuan H, Fernandes H, Habibovic P, de Boer J, Barradas AMC, de Ruiter A, et al. Osteoinductive ceramics as a synthetic alternative to autologous bone grafting. *Proc Natl Acad Sci U S A* 2010;107:13614–9.
- [8] Stevens MM, George JH. Exploring and engineering the cell surface interface. *Science* 2005;310:1135–8.
- [9] Eriksson C, Nygren H, Ohlson K. Implantation of hydrophilic and hydrophobic titanium discs in rat tibia: cellular reactions on the surfaces during the first 3 weeks in bone. *Biomaterials* 2004;25:4759–66.
- [10] Anderson J, Rodriguez A, Chang D. Foreign body reaction to biomaterials. *Semin Immunol* 2008;20:86–100.
- [11] Fellah BH, Josselin N, Chappard D, Weiss P, Layrolle P. Inflammatory reaction in rats muscle after implantation of biphasic calcium phosphate micro particles. *J Mater Sci Mater Med* 2007;18:287–94.
- [12] Fellah BH, Delorme B, Sohier J, Magne D, Hardouin P, Layrolle P. Macrophage and osteoblast responses to biphasic calcium phosphate microparticles. *J Biomed Mater Res A* 2010;93:1588–95.
- [13] Mosser DM, Edwards JP. Exploring the full spectrum of macrophage activation. *Nat Rev Immunol* 2008;8:958–69.
- [14] Jones JA, Chang DT, Meyerson H, Colton E, Kwon IK, Matsuda T, et al. Proteomic analysis and quantification of cytokines and chemokines from biomaterial surface-adherent macrophages and foreign body giant cells. *J Biomed Mater Res A* 2007;83:585–96.
- [15] Takayanagi H. Osteoimmunology: shared mechanisms and crosstalk between the immune and bone systems. *Nat Rev Immunol* 2007;7:292–304.
- [16] Sima C, Glogauer M. Macrophage subsets and osteoimmunology: tuning of the immunological recognition and effector systems that maintain alveolar bone. *Periodontol 2000* 2013;63:80–101.
- [17] Steeve KT, Marc P, Sandrine T, Dominique H, Yannick F. IL-6, RANKL, TNF-alpha/IL-1: interrelations in bone resorption pathophysiology. *Cytokine Growth Factor Rev* 2004;15:49–60.
- [18] Theoleyre S, Wittrant Y, Tat SK, Fortun Y, Redini F, Heymann D. The molecular triad OPG/RANK/RANKL: involvement in the orchestration of pathophysiological bone remodeling. *Cytokine Growth Factor Rev* 2004;15:457–75.
- [19] Stein NC, Kreutzmann C, Zimmermann S-P, Niebergall U, Hellmeyer L, Goettsch C, et al. Interleukin-4 and interleukin-13 stimulate the osteoclast inhibitor osteoprotegerin by human endothelial cells through the STAT6 pathway. *J Bone Miner Res* 2008;23:750–8.
- [20] Kondo N, Ogose A, Tokunaga K, Umez H, Arai K, Kudo N, et al. Osteoinduction with highly purified beta-tricalcium phosphate in dog dorsal muscles and the proliferation of osteoclasts before heterotopic bone formation. *Biomaterials* 2006;27:4419–27.
- [21] Tanaka T, Saito M, Chazono M, Kumagae Y, Kikuchi T, Kitasato S, et al. Effects of alendronate on bone formation and osteoclastic resorption after implantation of beta-tricalcium

INHIBITION OF OSTEOCLASTOGENESIS AND OSTEOINDUCTION

- phosphate. *J Biomed Mater Res A* 2010;93:469–74.
- [22] Ripamonti U, Klar RM, Renton LF, Ferretti C. Synergistic induction of bone formation by hOP-1, hTGF-beta3 and inhibition by zoledronate in macroporous coral-derived hydroxyapatites. *Biomaterials* 2010;31:6400–10.
- [23] Kan L, Liu Y, McGuire TL, Berger DMP, Awatramani RB, Dymecki SM, et al. Dysregulation of local stem/progenitor cells as a common cellular mechanism for heterotopic ossification. *Stem Cells* 2009;27:150–6.
- [24] Alexander KA, Chang MK, Maylin ER, Kohler T, Müller R, Wu AC, et al. Osteal macrophages promote in vivo intramembranous bone healing in a mouse tibial injury model. *J Bone Miner Res* 2011;26:1517–32.
- [25] Glass GE, Chan JK, Freidin A, Feldmann M, Horwood NJ, Nanchahal J. TNF-alpha promotes fracture repair by augmenting the recruitment and differentiation of muscle-derived stromal cells. *Proc Natl Acad Sci U S A* 2011;108:1585–90.
- [26] Barradas AMC, Yuan H, van der Stok J, Le Quang B, Fernandes H, Chaterjea A, et al. The influence of genetic factors on the osteoinductive potential of calcium phosphate ceramics in mice. *Biomaterials* 2012;33:5696–705.
- [27] Van Rooijen N, van Kesteren-Hendrikx E. "In vivo" depletion of macrophages by liposome-mediated "suicide". *Methods Enzymol* 2003;373:3–16.
- [28] Martin P. Wound healing--aiming for perfect skin regeneration. *Science* 1997;276:75–81.
- [29] Takahashi N, Udagawa N, Tanaka S, Murakami H, Owan I, Tamura T, et al. Postmitotic osteoclast precursors are mononuclear cells which express macrophage-associated phenotypes. *Dev Biol* 1994;163:212–21.
- [30] Hume DA, Loutit JF, Gordon S. The mononuclear phagocyte system of the mouse defined by immunohistochemical localization of antigen F4/80: macrophages of bone and associated connective tissue. *J Cell Sci* 1984;66:189–94.
- [31] Boyle W, Simonet W, Lacey D. Osteoclast differentiation and activation. *Nature* 2003;423:337–42.
- [32] Wenisch S, Stahl J-P, Horas U, Heiss C, Kilian O, Trinkaus K, et al. In vivo mechanisms of hydroxyapatite ceramic degradation by osteoclasts: fine structural microscopy. *J Biomed Mater Res A* 2003;67:713–8.
- [33] Dersot JM, Colombier ML, Lafont J, Baroukh B, Septier D, Saffar JL. Multinucleated giant cells elicited around hydroxyapatite particles implanted in craniotomy defects are not osteoclasts. *Anat Rec* 1995;242:166–76.
- [34] Baslé MF, Chappard D, Grizon F, Filmon R, Delecrin J, Daculsi G, et al. Osteoclastic resorption of Ca-P biomaterials implanted in rabbit bone. *Calcif Tissue Int* 1993;53:348–56.
- [35] Eggli PS, Müller W, Schenk RK. Porous hydroxyapatite and tricalcium phosphate cylinders with two different pore size ranges implanted in the cancellous bone of rabbits. A comparative histomorphometric and histologic study of bony ingrowth and implant substitution. *Clin Orthop Relat Res* 1988;127–38.
- [36] Van Rooijen N. The liposome-mediated macrophage "suicide" technique. *J Immunol Methods* 1989;124:1–6.
- [37] Lehenkari PP, Kellinsalmi M, Näpänkangas JP, Ylitalo K V, Mönkkönen J, Rogers MJ, et al. Further insight into mechanism of action of clodronate: inhibition of mitochondrial ADP/ATP translocase by a nonhydrolyzable, adenine-containing metabolite. *Mol Pharmacol* 2002;61:1255–62.
- [38] Frith JC, Mönkkönen J, Blackburn GM, Russell RG, Rogers MJ. Clodronate and liposome-encapsulated clodronate are metabolized to a toxic ATP analog, adenosine 5'-(beta, gamma-dichloromethylene) triphosphate, by mammalian cells in vitro. *J Bone Miner Res* 1997;12:1358–67.
- [39] Oussoren C, Storm G. Liposomes to target the lymphatics by subcutaneous administration. *Adv Drug Deliv Rev* 2001;50:143–56.
- [40] Wang W, Ferguson DJ, Quinn JM, Simpson AH, Athanasou NA. Osteoclasts are capable of particle phagocytosis and bone resorption. *J Pathol* 1997;182:92–8.
- [41] Frith JC, Mönkkönen J, Auriola S, Mönkkönen H, Rogers MJ. The molecular mechanism of action of the antiresorptive and antiinflammatory drug clodronate: evidence for the formation in vivo of a metabolite that inhibits bone resorption and causes osteoclast and macrophage

C H A P T E R 5

- apoptosis. *Arthritis Rheum* 2001;44:2201–10.
- [42] Takeshita S, Fumoto T, Matsuoka K, Park K, Aburatani H, Kato S, et al. Osteoclast-secreted CTHRC1 in the coupling of bone resorption to formation. *J Clin Invest* 2013;123:3914–24.
- [43] McCullough KA, Waits CA, Garimella R, Tague SE, Sipe JB, Anderson HC. Immunohistochemical localization of bone morphogenetic proteins (BMPs) 2, 4, 6, and 7 during induced heterotopic bone formation. *J Orthop Res* 2007;25:465–72.
- [44] Pederson L, Ruan M, Westendorf JJ, Khosla S, Oursler MJ. Regulation of bone formation by osteoclasts involves Wnt/BMP signaling and the chemokine sphingosine-1-phosphate. *Proc Natl Acad Sci U S A* 2008;105:20764–9.
- [45] Kreja L, Brenner RE, Tautzenberger A, Liedert A, Friemert B, Ehrnhaller C, et al. Non-resorbing osteoclasts induce migration and osteogenic differentiation of mesenchymal stem cells. *J Cell Biochem* 2010;109:347–55.
- [46] Guihard P, Danger Y, Brounais B, David E, Brion R, Delecrin J, et al. Induction of osteogenesis in mesenchymal stem cells by activated monocytes/macrophages depends on oncostatin m signaling. *Stem Cells* 2012;30:762–72.
- [47] Nicolaidou V, Wong MM, Redpath AN, Ersek A, Baban DF, Williams LM, et al. Monocytes induce STAT3 activation in human mesenchymal stem cells to promote osteoblast formation. *PLoS One* 2012;7(7): e398:e39871.
- [48] Champagne CM, Takebe J, Offenbacher S, Cooper LF. Macrophage cell lines produce osteoinductive signals that include bone morphogenetic protein-2. *Bone* 2002;30:26–31.
- [49] Honda Y, Anada T, Kamakura S, Nakamura M, Sugawara S, Suzuki O. Elevated extracellular calcium stimulates secretion of bone morphogenetic protein 2 by a macrophage cell line. *Biochem Biophys Res Commun* 2006;345:1155–60.
- [50] Takebe J, Champagne CM, Offenbacher S, Ishibashi K, Cooper LF. Titanium surface topography alters cell shape and modulates bone morphogenetic protein 2 expression in the J774A.1 macrophage cell line. *J Biomed Mater Res A* 2003;64:207–16.
- [51] Lohmann C, Schwartz Z, Köster G, Jahn U, Buchhorn G., MacDougall M., et al. Phagocytosis of wear debris by osteoblasts affects differentiation and local factor production in a manner dependent on particle composition. *Biomaterials* 2000;21:551–61.
- [52] Barradas AMC, Monticone V, Hulsman M, Danoux C, Fernandes H, Tahmasebi Birgani Z, et al. Molecular mechanisms of biomaterial-driven osteogenic differentiation in human mesenchymal stromal cells. *Integr Biol (Camb)* 2013;5:920–31.
- [53] Chen S, Jones JA, Xu Y, Low H-Y, Anderson JM, Leong KW. Characterization of topographical effects on macrophage behavior in a foreign body response model. *Biomaterials* 2010;31:3479–91.
- [54] Zhang W, Wang G, Liu Y, Zhao X, Zou D, Zhu C, et al. The synergistic effect of hierarchical micro/nano-topography and bioactive ions for enhanced osseointegration. *Biomaterials* 2013;34:3184–95.
- [55] Jäger M, Zilkens C, Zanger K, Krauspe R. Significance of nano- and microtopography for cell-surface interactions in orthopaedic implants. *J Biomed Biotechnol* 2007;2007:1–19.
- [56] Thomsen P, Gretzer C. Macrophage interactions with modified material surfaces. *Curr Opin Solid State Mater Sci* 2001;5:163–76.



CHAPTER 6

Osteoclast resorption of beta-tricalcium phosphate controlled by surface architecture

Noel L. Davison^{1,2}, Bas ten Harkel³, Ton Schoenmaker³,
Xiaoman Luo^{1,2}, Huipin Yuan^{1,2}, Vincent Everts³, Florence
Barrère-de Groot², Joost D. de Brujin^{1,2,4}

- 1 MIRA Institute for Biomedical Technology and Technical Medicine, University of Twente, Enschede, Netherlands
- 2 Xpand Biotechnology BV, Bilthoven, Netherlands
- 3 Departments of Oral Cell Biology and Periodontology, Academic Centre for Dentistry Amsterdam (ACTA), MOVE Research Institute, University of Amsterdam and VU University Amsterdam, Amsterdam, Netherlands
- 4 School of Engineering and Materials Science (SEMS), Queen Mary University of London, London, United Kingdom

A B S T R A C T

A resorbable bone graft substitute should mimic native bone in its capacity to support bone formation and be remodeled by osteoclasts (OCI) or other multinucleated cells such as foreign body giant cells (FBGC). We hypothesize that by changing the scale of surface architecture of beta-tricalcium phosphate (TCP), cellular resorption can be influenced. CD14+ monocyte precursors were isolated from human peripheral blood ($n = 4$ independent donors) and differentiated into OCI or FBGC on the surface of TCP discs comprising either submicron- or micron-scale surface topographical features (TCPs and TCPb, respectively). On submicrostructured TCPs, OCI survived, fused, differentiated, and extensively resorbed the substrate; however, on microstructured TCPb, OCI survival, TRAP activation, and fusion were attenuated. Importantly, no resorption was observed on microstructured TCPb. By confocal microscopy, OCI formed on TCPs contained numerous actin rings allowing for resorption, but not on TCPb. In comparison, FBGC could not resorb either TCP material, suggesting that osteoclast-specific machinery is necessary to resorb TCP. By tuning surface architecture, it appears possible to control osteoclast resorption of calcium phosphate. This approach presents a useful strategy in the design of resorbable bone graft substitutes.

1 INTRODUCTION

If a bone graft substitute is meant to be replaced by new bone tissue in a bony defect, then it must be resorbable. Unlike non-resorbable materials, resorbable materials avoid the local loss of bone density associated with stress shielding that stems from the disproportionately high loadbearing of an implant versus the surrounding bone. Moreover, resorbable bone graft substitutes, such as calcium phosphate (CaP), should allow for remodeling by bone resorbing osteoclasts [1], important for normal bone homeostasis, bone coupling, and osteogenesis [2–5].

The modes by which a CaP bone graft substitute can be resorbed in the body are generally categorized as cell-mediated (often termed bioresorption or biodegradation) or passive, such as dissolution, erosion, and mechanical fragmentation [6]. Related to these, two primary strategies for controlling the resorption rate of CaP include modifying the physical architecture and tuning the ceramic chemistry [7]. The first strategy is to incorporate an interconnected network of pores or channels large enough for cell infiltration ($> 20 \mu\text{m}$) to promote blood perfusion and capillary ingrowth to supply and sustain cells needed for bioresorption and osteogenesis. Additionally, increasing the pore area enhances the surface area allowing faster dissolution. The second strategy is to alter the ceramic crystalline chemistry to thermodynamically favor dissolution in the body. For instance, CaP composed of beta-tricalcium phosphate (TCP) tends to dissolve more readily than hydroxyapatite (HA) and is therefore preferred where resorbability is desired [1].

Other material properties may also determine CaP resorbability such as the physical surface architecture, i.e., the size and amount of surface micropores (0.1–10 μm) and grains [8,9]. However, Bohner (2012) recently emphasized that no studies have evaluated these factors while maintaining other material properties equal to clearly determine their effects on bioresorption or if there is an optimal design criterion [1]. More recently, results reported by our group described that despite possessing equivalent ceramic chemistry, macropores, and total porosity, TCP with submicron-scale surface grains and pores was shown to be resorbed by ~24% after implantation for 12 weeks in the dorsal muscle of dogs (an osteoinduction model) but TCP with micron-scale surface grains and pores was appreciably un-resorbed (Chapter 4). Multinucleated osteoclast-like cells were substantially identified on TCP with submicron-scale surface architecture, whereas multinucleated cells could scarcely be found on the un-resorbed TCP with micron-scale surface architecture. *In vitro*, neither TCP passively dissolved in culture medium containing serum, suggesting that multinucleated cell-mediated resorption is likely the principal mode by which these materials are degraded

in vivo. However, no resorption was observed in vitro, most likely due to the limitations of using the RAW264.7 osteoclast model cell line. These materials induced ectopic bone formation to similar extents that they were resorbed: TCPs formed ~20% in the free area while TCPb induced none (Chapter 4), suggesting that TCP resorption and bone induction may go hand in hand in a mechanism akin to bone coupling, as others have previously postulated [10,11].

The identity and function of such multinucleated cells surrounding CaP in vivo is the subject of debate with some groups speculating that they are fused macrophages (i.e., foreign body giant cells - FBGC) [12,13], while other groups asserting that they are specialized bone-resorbing osteoclasts (OCI) [14,15]. Actually, it is plausible that both cell types are present depending the chemical composition of the material, how it was fabricated (i.e., sintering temperature), and where it is implanted [6,15,16]. Following the host response, monocyte/macrophages will normally infiltrate the implantation site and adhere to the implant, providing a common precursor pool for both FBGC and OCI on the material surface [17,18]. Though many groups have demonstrated in vitro that OCI possess the cellular machinery necessary for resorption of CaP [19–22] and that a bony surface is not necessary for osteoclast activation [23], whether different surface structure can substantially influence this process and whether FBGC can also resorb CaP is unclear.

Beyond material resorption, multinucleated cells such as OCI may be important for the osteogenic properties of CaP in particular a class of microstructured CaP that can induce ectopic bone formation without exogenous stem cells or growth factors. For instance, depleting OCI by bisphosphonates has been repeatedly shown to obstruct ectopic bone formation by osteoinductive CaP [11,24]. The reason for this may be due to the powerful osteogenic signals that OCI express and secrete (e.g., S1P, Wnts, BMPs, and CTHRC1) [3,25–27]. Therefore, characterizing what material parameters are promotive of OCI formation, survival, and function may also bear impact on the osteogenic capacity of a CaP bone graft substitute.

Following up on our previous findings that the scale of surface architecture plays a determinant role in both the resorbability of TCP and the presence of multinucleated cells in vivo (Chapter 4), we speculated that surface architecture might directly affect the formation and resorative function of these cells. In essence, we hypothesized that it might be possible to control multinucleated cell formation and resorption by changing the scale of surface structure. To test this, we cultured human peripheral blood monocytes on the surface of the same two TCP with either submicron- or micron-scale surface features and differentiated

them into either OCl or FBGC by adding specific cytokines. The effects of different TCP surface architecture on multinucleated cell formation, survival, and resorption were analyzed using a variety of in vitro assays and techniques.

2 MATERIALS AND METHODS

2.1 Preparation and characterization of TCP with micron- and submicron-scale surface architecture

Dense TCP discs were fabricated and characterized as previously described (Chapter 4). TCP powders were synthesized by mixing calcium hydroxide and phosphoric acid (Sigma-Aldrich) at a Ca/P ratio of 1.50. TCP powders with small (TCPs) or big (TCPb) grains and micropores in the final ceramics were prepared by wet precipitation. The powders were foamed with diluted H_2O_2 (0.1%) (Merck) at 60 °C to form microporous green bodies and then dried. The dry green bodies were subsequently sintered at 1050 °C or 1100 °C for 8 hours to achieve small or big grains for TCPs and TCPb, respectively. Microporous discs ($Ø9 \times 1$ mm) were machined from the ceramic bodies using a lathe and a diamond saw microtome (Leica SP1600). Discs were ultrasonically cleaned in successive baths of acetone, ethanol, and deionized water, dried at 60 °C, and then heat sterilized at 160 °C for 2 hours for cell culture. Crystal chemistry of the materials was analyzed by X-ray diffraction (Rigaku Miniflex II) scanning the range $2\theta = 25\text{--}45^\circ$ (step size = 0.01°, rate = 1° min⁻¹) and confirmed to be TCP.

Table 1. Physical characterization of TCP .

Physical parameters	TCPs	TCPb
Average grain diameter (μm)	0.95 ± 0.27	3.66 ± 1.05
Average pore diameter (μm)	0.63 ± 0.33	1.78 ± 0.85
Average roughness, R_a (μm)	0.126 ± 0.003	1.287 ± 0.011
Root-mean-square roughness, R_{rms} (μm)	0.158 ± 0.003	1.597 ± 0.011
Porosity (%)	69.6	72.0
Total pore area (m ² /g)	1.477	0.769

Surface topography of the materials was analyzed using scanning electron microscopy (SEM) (JEOL JSM-5600 microscope) after sputter coating them with gold for 90 s (JEOL JFC 1300). For grain and pore size analysis, at least 50 grains and pores were measured across their vertical diameter using ImageJ software

(NIH, USA). Porosity and total pore area (analogous to specific surface area) were determined by mercury intrusion testing (Micromeritics, USA). Surface roughness was computed using MeX v5.1 software (Alicona Imaging, Austria). Briefly, SEM stereo-micrographs of the same location were captured at two different tilt angles (2500 \times , $\pm 5^\circ$) and then digitally reconstructed into three-dimensional surfaces for surface roughness calculations by the software. These material properties are all reported in Table 1, as previously reported (Chapter 4).

2.2 Isolation of human monocytes and differentiation into osteoclasts (OCi) and foreign body giant cells (FBGC)

CD14+ monocytes were isolated from human peripheral blood mononuclear cells (PBMC) and then cultured on TCP discs. Briefly, human buffy coats ($n = 4$ donors) were acquired from San Quinn Blood Bank (Amsterdam), diluted with PBS containing 1% citrate (1:1), and then spun down (800 g, 30 minutes, without brake) in Ficoll gradient solution. The interphase containing the PBMC was carefully collected and washed 4 times in 0.5% bovine serum albumin buffer (2 mM EDTA, phosphate-buffered saline), then passed through a cell strainer (40 μm) to ensure the recovery of a clean mononuclear cell population. Cells were counted using a Muse cell counter and incubated with CD14-antibody tagged microbeads (Miltenyi Biotec) (1×10^7 cells in 20 μL microbead solution) for 15 minutes at 4 °C, then sorted using a manual MACS magnetic cell sorter (Miltenyi Biotec) following the manufacturer's instructions. These microbeads did not affect cell behavior or morphology, nor do they need to be removed due to their extremely small size (~50 nm). Because such a low concentration is used, they do not saturate the CD14 epitopes on the cell membrane, which makes CD14 labeling for FACs analysis after isolation possible. This method is commonly used to isolate CD14+ monocytes for use as osteoclast precursors in the literature [28]. Purified CD14+ cells were resuspended in basic culture medium consisting of αMEM (Life Technologies) supplemented with 10% fetal calf serum (HyClone I) and 1% penicillin-streptomycin (Sigma-Aldrich). The purity of the cells was confirmed to be $83 \pm 4\%$ by flow cytometry (Accuri C6, Becton Dickinson) using a CD14 antibody label and mouse IgG2a isotype antibody (both Miltenyi Biotec) as control.

CD14+ monocytes were seeded on TCP discs placed in 48-well tissue culture plates (Greiner Bio-One) at a cell density of ~500,000 cells/cm². Immediately prior to seeding, discs were incubated with 1 mL basic medium for 2 hours to equilibrate them. Cytokines were added to the culture medium in order to differentiate the cells into either OCi or FBGC. OCi cultures received macrophage colony-stimulating factor (M-CSF, 10 ng/mL) and receptor activator of nuclear

factor kappa-B ligand (RANKL, 2 ng/mL) to induce osteoclast differentiation. FBGC cultures received M-CSF, interleukin-4 (IL-4), and interleukin-13 (IL-13) (both 5 ng/mL) to induce foreign body giant cell differentiation, similar to previously described [29]. Cells were cultured in 5% CO₂ and 37 °C with medium refreshment every 3-4 days throughout the culture duration of 25 days. All cytokines were purchased from R&D Systems.

2.3 Cell viability and proliferation

The AlamarBlue (AB) fluorescent assay (Life Technologies) was used to measure cell viability and proliferation [30]. AB measures the reductive activity inside living cells, and is commonly used in the literature as a more sensitive alternative to formazan-based cell viability assays such as MTT and XTT [31,32]. To measure the viability of disc-adherent cells, discs seeded with cells were removed from their culture wells and placed in fresh wells containing pre-warmed culture medium containing 5% AB reagent. Medium was gently aspirated from the vacated culture wells and replaced with AB reagent to also measure the viability of cells cultured on tissue culture plastic adjacent to the discs. Cells were incubated with reagent for 2 hours in culture conditions and then media samples were collected in an opaque 96-well plate for fluorescent detection (excitation = 530 nm, emission = 590 nm) using a Synergy spectrophotometer. For time course study of cell proliferation, the same procedure was followed except that AB-containing culture medium was removed and refreshed with normal culture medium, and then continuously cultured until the next time point. Viability and proliferation assays were conducted using 3 independent donors and 2-4 culture replicates per donor.

2.4 Biochemical assays: DNA, total protein, and tartrate resistant acid phosphatase (TRAP)

For biochemical analysis, discs cultured with cells were rinsed with PBS, placed in fresh wells containing lysis buffer (0.1 M sodium acetate, 0.1% Triton X-100, pH 5.8), and then frozen at -80 °C and thawed to aid lysis. DNA in the lysate was quantified using a CyQuant assay kit (Life Technologies). Briefly, sample lysate was incubated with GR dye reagent (1x) following the manufacturer's instructions. Fluorescence (excitation = 480 nm, emission = 520 nm) was detected using a Zenyth Multimode Plate Reader. Total protein was quantified using a commercial Micro BCA Protein assay kit (Pierce) following the manufacturer's instructions. Absorbance at 405 nm was detected using a Synergy spectrophotometer. Last, tartrate resistant acid phosphatase (TRAP) activity in the lysate was quantified by conversion of p-nitrophenyl phosphate (pNPP) to p-nitrophenol (pNP), as

described by Ljusberg et al. (1999) [33]. Cell lysate sample (20 µL) was collected to a 96-well plate containing assay reagent (130 µL) composed of 10 mM PNPP, 0.1 M sodium acetate (pH 5.8), 0.15 M KCl, 0.1% Triton X-100, 10 mM sodium tartrate, 1 mM ascorbic acid, and 0.1 mM FeCl₆. The reaction was incubated for 1 hour at 37 °C and then finally converted to pNP (chromogen) by adding 0.3 M NaOH (100 µL). Absorbance at 405 nm was detected using a Synergy spectrophotometer and values were converted to mM pNP using a standard curve of pNP (Sigma-Aldrich). TRAP activity was normalized to total protein in the same sample lysate. Biochemical assays were conducted using 3 independent donors and 2-4 culture replicates per donor.

2.5 TRAP staining

TRAP enzyme was visually detected using a commercial staining kit (Leukocyte Acid Phosphatase Staining Kit, Sigma-Aldrich). Discs seeded with cells were first rinsed with PBS and fixed in 2.5% gluteraldehyde overnight at 4 °C. The following day, discs were rinsed once with PBS and stained following the manufacturer's instructions. Staining was visualized using a Nikon SMZ800 stereomicroscope equipped with a Nikon camera. TRAP staining was conducted using 3 independent donors and 2 culture replicates per donor.

2.6 Cell morphology and resorption

Cell morphology was evaluated using SEM (JEOL JSM-5600 microscope). After 25 days culture, discs cultured with cells were rinsed with PBS and fixed in 2.5% gluteraldehyde for up to 1 week. Cells were dehydrated in a graded ethanol series (60, 70, 80, 90, 95, and 100% x 2) and finally dried in HMDS (Sigma-Aldrich). Discs were then mounted on metal stubs and sputter coated with gold for enhanced imaging resolution.

To analyze TCP resorption after 25 days of culture, adherent cells were removed for qPCR analysis using RLT lysis buffer (Qiagen), and the discs were rinsed once in 70% ethanol then dried at 60 °C. Discs not seeded with cells were similarly cultured for 25 days and served as control references. Samples were mounted on metal stubs and sputter coated with gold for SEM. Cell morphology and resorption assays were conducted using cells from 4 independent donors and 2 culture replicates per donor.

2.7 Fluorescent Laser Scanning Confocal Microscopy

Cell fusion and actin ring formation were analyzed using fluorescent laser

scanning confocal microscopy. After culture for 25 days, cells seeded on discs were rinsed with PBS, fixed in 4% formaldehyde, blocked with 20% normal goat serum, then sequentially incubated with rat anti-mouse monoclonal primary antibody CD44 targeting the osteoclast plasma membrane (1:100 dilution) (Cedarlane, USA), goat anti-rat Alexa467-conjugated secondary antibody (1:400) (Invitrogen), Alexa488-conjugated phalloidin targeting F-actin (1:400) (Invitrogen), and Hoechst 33342 dye (1:500) (Sigma-Aldrich) to stain nuclei, as previously described [34]. Fluorescence was visualized using a Leica TCS-SP8-SMD DMI6000 laser scanning confocal microscope and overlaid image stacks were generated by scanning from the apical to basal surface of the cell (Leica LAS AF software). Confocal microscopy analysis was conducted using 2 independent donors.

2.8 Quantitative PCR (qPCR)

Total RNA was isolated using a commercial spin-column kit (Qiagen) following the manufacturer's instructions. Discs seeded with cells were removed from the culture wells and immediately lysed in RLT lysis buffer. The cells cultured adjacent to the discs on tissue culture plastic in the same wells were lysed separately. After column purification of total RNA in the cell lysate, RNA concentration was measured using a Synergy spectrophotometer. Reverse transcription of RNA was performed using the MBI Fermentas cDNA synthesis kit (Fermentas, Lithuania), using both the Oligo(dT)18 and the D(N)6 primers.

Quantitative PCR (qPCR) was performed on an ABI PRISM 7000 Sequence Detection System. The PCR reactions were performed with 60 ng cDNA in a total volume of 15 μ L containing SYBR GreenER qPCR SuperMix (consisting of SYBR Green 1 Dye, AmpliTaq Gold DNA polymerase, dNTPs, passive reference and buffer) (Life Technologies), and 300 nm of primer. For gene targets, the protocol consisted of an activation step (10 minutes, 94 °C) and 40 cycles of two-step PCR (95 °C for 15 seconds, 60 °C for 1 minute). TATA_b and UBC housekeeping genes were tested using a three-step protocol (95 °C for 10 seconds, 55 °C for 30 seconds, 72 °C for 30 seconds). All genes were subjected to melt curve analysis to test if any unspecific PCR products were generated. Expression of gene targets was normalized by endogenous expression of 5 housekeeping genes (TATA_b, UBC, GAPDH, cycloB, and HPRT) following the comparative CT method [35] and presented as fold expression ($2^{\Delta\text{CT}}$). These housekeeping genes were shown to be stable using GeNorm software (v. 3) and their geometric mean expression was calculated for normalization of gene targets. To account for variability between donors, fold expression levels were further normalized to those of cells cultured on TCP_b and presented as relative fold expression

CHAPTER 6

($2^{-\Delta\Delta CT}$). QPCR Primers were designed using Primer Express 2.0 software (Life Technologies) (Table 2), spanning at least 1 intron to avoid amplification of genomic DNA. QPCR analysis was conducted using 4 independent donors and 2-3 culture replicates per donor.

Table 2. qPCR primer sequences

Gene Target	Sequence (5' -> 3')	Product size (bp)	Accession ID
UBC	gcggtaacgccatgattat ttgcctgacattctcgatgg	202	ENSG00000150991
TATAb	ggctggaaaatggtgtgc gctggaaaacccaacttctg	100	ENSG00000112592
HPRT	tgacctgattttgcatacc cgagcaagacgttcagtct	101	ENSG00000165704
Cyc1	gcatgggtgaggactacg ggccaggaaagttagggttg	106	ENSG00000179091
GAPDH	tgggtgtgaaccatgagaagtatg ggtcaggaggcattgct	61	ENSG00000111640
CATK	ccatatgtggacaggaagagat tgcataatggccacagaga	149	ENSG00000143387
TRAP	cacaatctgcagttacactgcaagat cccatagtggaaagcgcagata	128	ENSG00000102575
CAII	tggactggccgttcttaggtatt tcttgcccttggtaatggaa	100	ENSG00000104267
AE2	ttgtgggcctccatagttatc gatcccgttaaggaggtgact	103	ENSG00000164889
TCIRG1	gctgccaaccacttgagctt caaagtgcacgtggtaaga	114	ENSG00000110719
DC-STAMP	attttctcagtgagcaagcagttc agaatcatggataatatcttgagttcctt	101	ENSG00000164935
VCAM-1	acaaagtggctcacaattaagaagtt tgaaaaatagagcagcagaagct	100	ENSG00000162692
ITGB1	tttccattggagatgagggtca cgtaaagcccagaggcctaa	100	ENSG00000150093

ITGB2	cgacggccgctgtca tgttgtttcagccagcttgt	100	ENSG00000160255
ITGB3	aggctggcaggcattgtc agccccaaagagggataatcc	100	ENSG00000259207
ITGA4	cttccagacagccaggagaa gggcactccatagcaacca	116	ENSG00000115232
ITGAV	tacagcaggcccagaact aattcagattcatcccgcatat	100	ENSG00000138448

2.9 Statistics

Statistical comparisons between TCPs and TCPb were performed using One-Way ANOVA and Tukey's multiple comparisons when comparing more than 2 groups in GraphPad Prism 6.0. P values < 0.05 were considered significant.

3 RESULTS

3.1 Cell viability and proliferation

After culture for 25 days on TCP, OCI and FBGC viability was roughly 100% higher on TCPs than on TCPb ($P = 0.0329$ and $P = 0.0074$, respectively) (Figure 1A). In contrast, there was no difference in viability of either OCI or FBGC cultured adjacent to the TCP discs on tissue culture plastic of the same culture well (Figure 1B), indicating that the differences in disc-adherent cell viability were due to the direct interaction with the TCP surface structure rather than soluble effects in the medium. In concert with these results, DNA content in the adherent cell lysate was measured and followed the same trends – ~2 to 3 times more DNA from cells on TCPs than on TCPb (Figure 1C).

To rule out the possibility that initial cell attachment was lower on TCPb or that it was cytotoxic, monocyte precursors were cultured for 25 days in the presence of only M-CSF for survival, and cell proliferation was assayed by measuring cell viability over time (Fig. 1D). The viability of adherent cells one day after seeding was equivalent between the materials, indicating that the initial cell attachment efficiency was equivalent. Moreover, viability increased through 14 days equivalently between the materials, indicating that neither material was cytotoxic and that cells were able to proliferate. However, as time progressed, cell viability sharply decreased on TCPb versus TCPs resulting in 38% less metabolic activity at day 21 ($P = 0.0003$) and 50% less at day 25 ($P = 0.0016$). These data indicate

that long-term cell survival was reduced on TCPb although initial cell attachment and proliferation were unhindered.

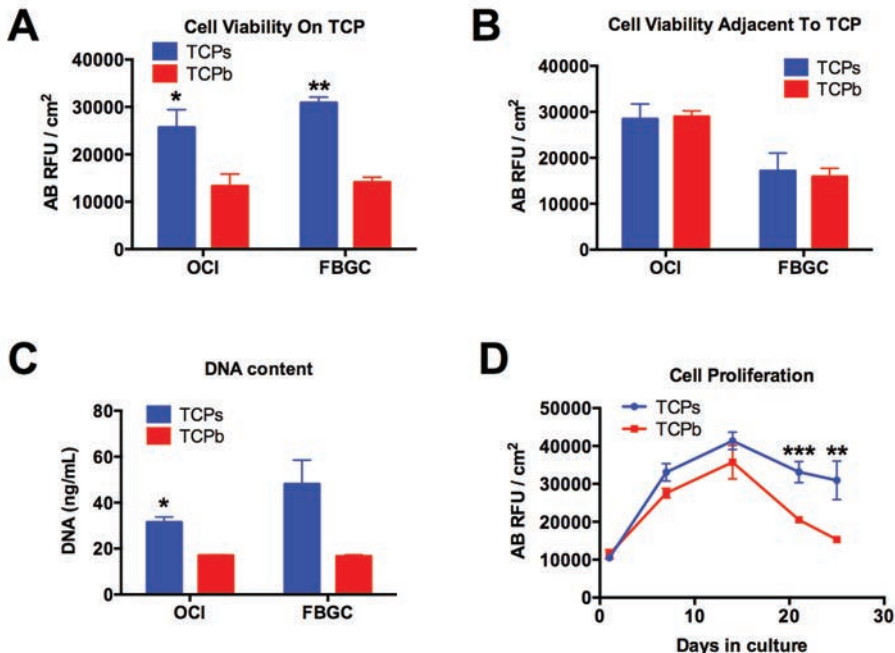


Figure 1. Cell viability (A,B), DNA content (C), and Proliferation (D). Viability of osteoclasts (OCI, induced with M-CSF and RANKL) and foreign body giant cells (FBGC, induced with M-CSF, IL-4, and IL-13) cultured directly on TCP was roughly double on submicrostructured TCPs than on microstructured TCPb at day 25 (A). However, there was no difference in viability in either cell type cultured on tissue culture plastic adjacent to TCPs or TCPb in the same well (B). DNA content from the lysate of TCP-adherent cells at day 25 mimicked the viability data and reflected less cells present on TCPb than on TCPs (C). Proliferation of monocyte/macrophage precursors (cultured only with M-CSF), as measured by viability over time, proceeded similarly on TCPs and TCPb through day 14 but sharply decreased by day 21 and 25 on TCPb versus TCPs (D). Cell viability and proliferation data are given in AlamarBlue relative fluorescent units normalized by the cell culture surface area (AB RFU cm⁻²). Data represent the mean \pm s.d. of n = 4 replicates from 3 independent donors. * P < 0.05, ** P < 0.01, *** P < 0.001.

3.2 TRAP activity

TRAP, an enzymatic marker of OCI [36,37] and macrophage activation [38,39], was both biochemically assayed and cytochemically stained after 25 days of culture. TRAP activity per total protein in OCI was more than 7 times higher after culture on TCPs than on TCPb (P = 0.0065). Similarly, TRAP activity in FBGC was

2.5 times higher after culture on TCPs than on TCPb ($P = 0.0161$), indicating that both OCI and FBGC activation was promoted by TCPs (Figure 2A). These results were confirmed by TRAP staining, which showed more intensely stained, massive multinucleated cells in an interconnected network on TCPs, but less intensely stained, smaller and unconnected cells on TCPb. TRAP staining of FBGC was also more intense on TCPs versus TCPb (Figure 2B). For both cell types, substantially more cells were present on TCPs than on TCPb, confirming the cell viability and DNA assays.

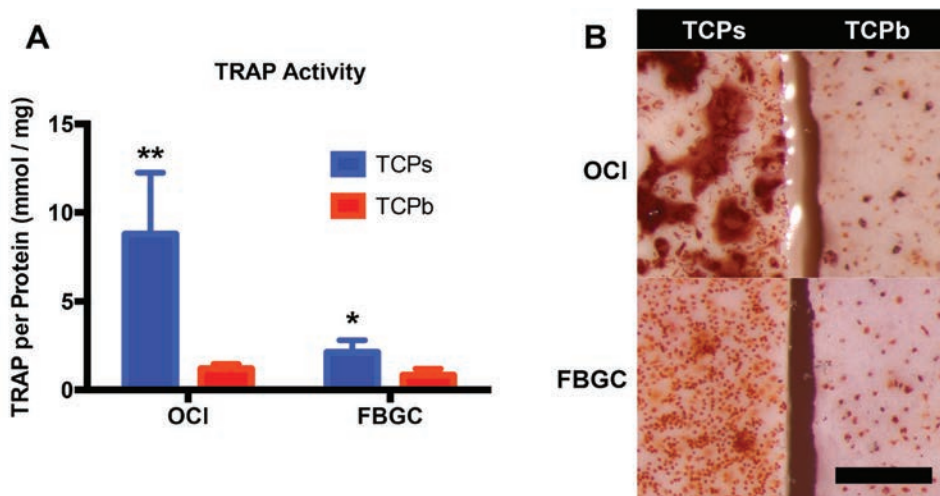


Figure 2. Tartrate resistant acid phosphatase (TRAP) activity (A) and staining (B). TRAP activity measured at day 25 in the cell lysate was 7 times and 2.5 times higher in OCI and FBGC, respectively, when formed on submicrostructured TCPs versus microstructured TCPb. TRAP activity was normalized per total protein in the lysate and given as mmol p-nitrophenol per mg total protein (mmol mg^{-1}) (A). Representative light micrographs of TCP discs stained for TRAP at day 25 showed intensely stained, interconnected OCI measuring greater than 500 μm across on the surface of TCPs versus weaker stained, sparse, smaller ($< 50 \mu\text{m}$) OCI on TCPb. Scale = 500 μm . TRAP activity represents the mean \pm s.d. of $n = 4$ replicates from 2 independent donors. * $P < 0.05$, ** $P < 0.01$.

3.3 Cell Morphology and TCP Resorption

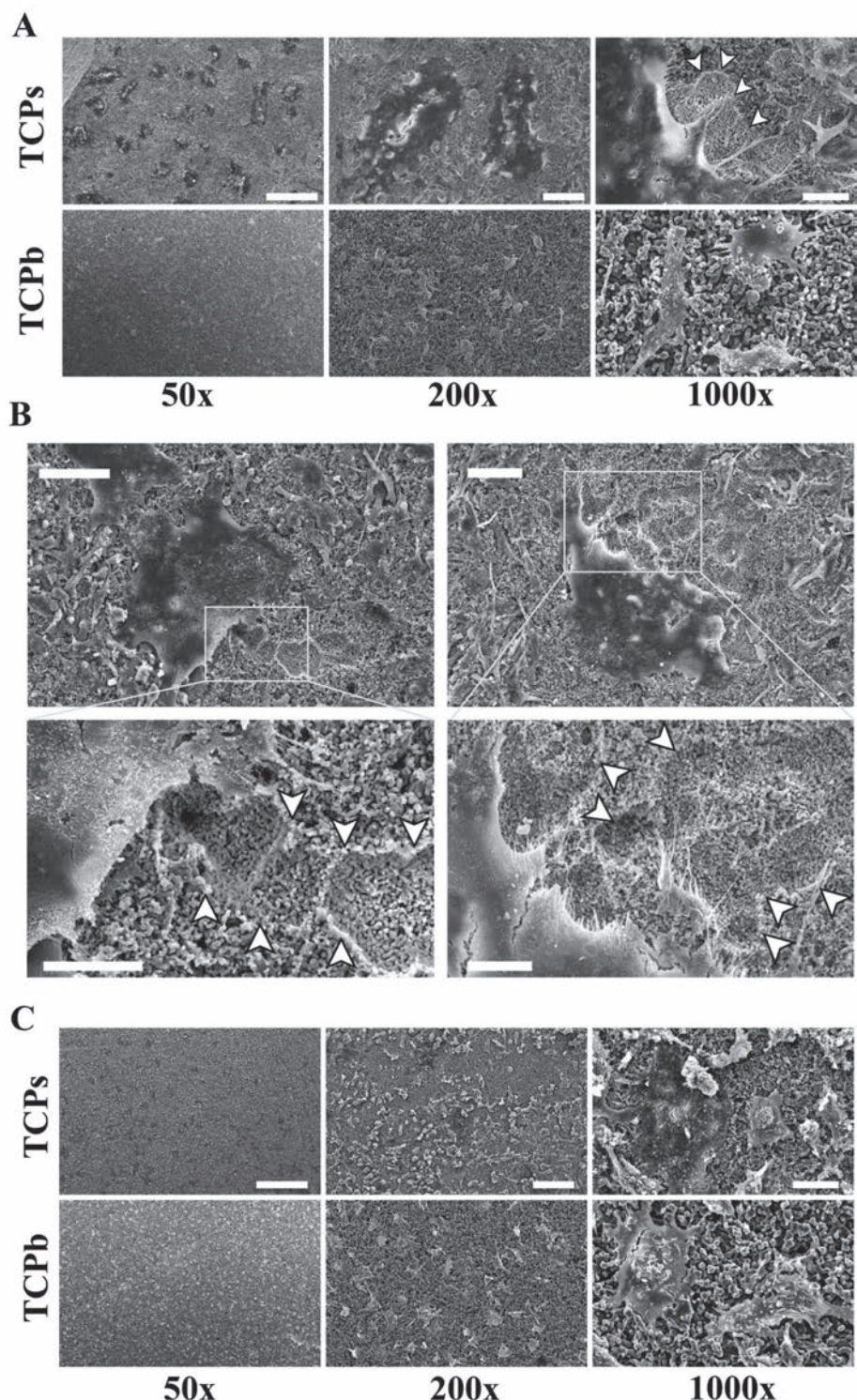
Cell morphology and TCP resorption were analyzed by SEM. On TCPs, fused OCI ($> \sim 200 \mu\text{m}$ across) extensively populated the submicrostructured surface and resided in prominent resorption lacunae. Cellular processes frequently connected adjacent OCI in a massive cell network. Numerous finger-like filopodia decorated the perimeter of the membrane, extending from the cell to the material surface. Non-fused mononuclear cells were also observed in and outside of the resorption lacunae. On TCPb, OCI were sparsely distributed and

smaller in comparison. No resorption lacunae were identified on TCPb. Fewer cells were present on TCPb than on TCPs, which confirmed the cell viability, DNA content, and TRAP staining results (Figure 3a-b).

In comparison, FBGC appeared substantially smaller than OCI on TCPs. On TCPb, FBGC appeared apoptotic or necrotic similar to OCI cultured on the material. No resorption lacunae created by FBGC could be identified on either material (Figure 3c).

TCP resorption was further analyzed after removing adherent OCI and FBGC after 25 days using cell lysis buffer without altering the native surface structure (Figure 4). Prodigious resorption pits ranging from ~10 – 500 µm covered the surface of TCPs cultured with OCI. In the resorption pits, the surface structure was visibly altered resulting in smaller grains, narrower inter-grain boundaries, and a more polygonal grain shape (Figure 3b, Figure 4). In contrast, no resorption lacunae were seen on TCPb cultured with OCI; the surface structure appeared identical to the control discs cultured without cells. Unlike OCI, no signs of resorption could be identified on either TCP cultured with FBGC. The ability of OCI to resorb TCPs, resulting in large resorption pits, but not TCPb was robustly confirmed across all 4 donors (Supplementary Figure).

Figure 3, opposite. Scanning electron micrographs of OCI cultured on TCP discs at day 25. (A) Representative images at low magnification (left) show massively fused OCI (~200 – 500 µm) homogenously populate the surface of TCPs but are less evident on TCPb (50x, scale = 500 µm). At higher magnification (middle), large fused OCI (dark cells, ~ 300 µm across) can be seen in close proximity to one another resorbing TCPs, surrounded by unfused precursors. Fused OCI on TCPb (light spots) are markedly smaller in comparison (< 100 µm) (200x, scale = 100 µm). At high magnification for detail (right), OCI actively resorb TCPs with filopodia extending to the border of the resorption lacunae (marked by white arrow heads). Small cells and no resorption lacunae are found on TCPb (1000x, scale = 20 µm). (B) OCI formed on TCPs create extensive networks of resorption pits and migrate toward unresorbed material (white arrows) (top row scale = 50 µm; bottom row scale = 20 µm). (C) Representative scanning electron micrographs of FBGC formed on TCP at day 25. Cells fuse to form large FBGC on TCPs (dark spots) ranging from ~40–100 µm across. On TCPb, cells are smaller and sparser, appearing necrotic (detail). No resorption is evident from FBGC on either material. 50x scale = 500 µm; 200x scale = 100 µm; 1000x scale = 20 µm.



6

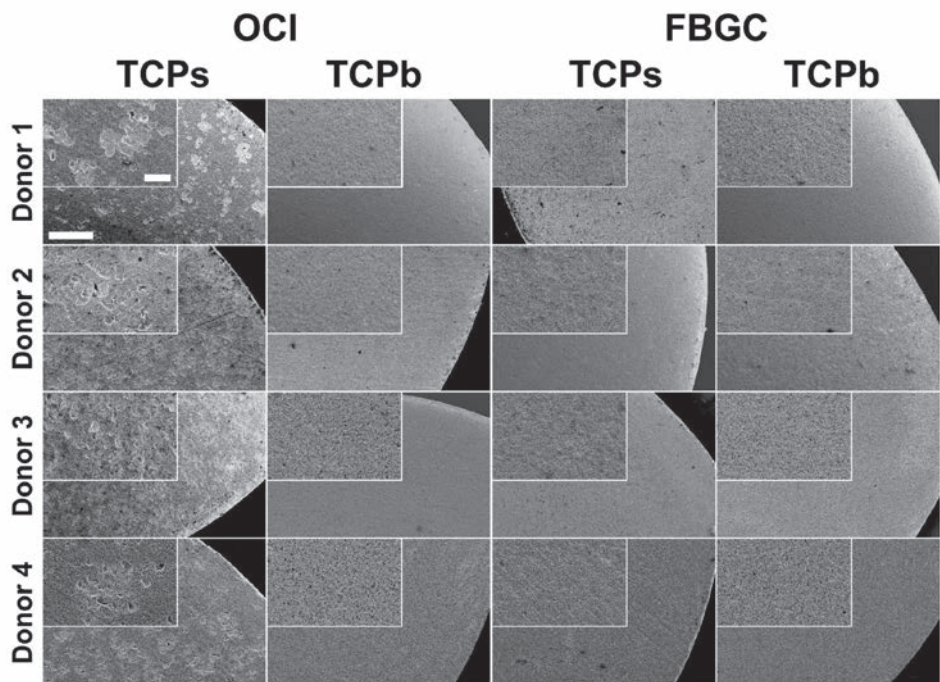
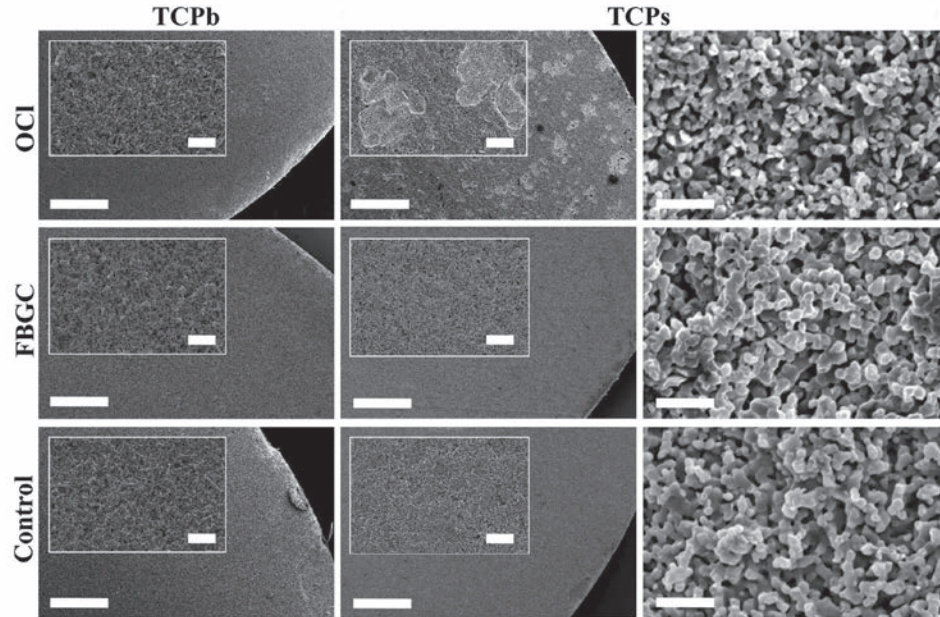


Figure 4, opposite top. Scanning electron micrographs of TCP resorption after removal of OCI and FBGC After 25 days, no resorption lacunae were detected on TCPb cultured with either cell type; discs were identical to the control reference incubated without cells (left column). Prominent resorption lacunae spanning ~100-200 μm across were evident on TCPs cultured with OCI but no resorption was evident from FBGC versus the control reference. High magnification micrographs of TCPs (right column) showed alteration of surface microstructure due to osteoclast resorption, specifically smaller grains and increased microporosity. Overview scale (50x) = 500 μm ; inset scale (500x) = 50 μm ; detail scale (5000x) = 5 μm .

Supplementary Figure, opposite bottom. Osteoclast resorption of TCPs by 4 independent human monocyte donors. Note that OCI were unable to resorb TCPb and FBGC were unable to resorb either TCPs or TCPB. Overview scale (50x) = 500 μm ; inset scale (250x) = 100 μm .

3.4 Cell fusion and Actin Ring Formation

Cell fusion, multinucleation, and actin ring formation were visualized using laser confocal microscopy. Fluorescent membrane and nuclei staining clearly showed that the large OCI seen on TCPs by TRAP staining and SEM contained many nuclei (Figure 5). Fluorescent staining targeting F-actin revealed numerous actin rings (~20 μm across) generally near the edge of the membrane of the multinucleated OCI. On TCPb, OCI were also fused and multinucleated, although to a lesser extent than on TCPs; however, clear actin ring structures were not found in OCI on TCPb. No actin ring structures were observed in FBGC on either material (data not shown).

3.5 Gene expression

The expression of genes related to substrate adhesion, cell-cell adhesion, and osteoclast differentiation and function was analyzed in order to explain the observed differences in osteoclast viability and resorption between the two materials. RNA was separately isolated from both the fraction of cells adhered to the discs and the fraction of cells adhered to the tissue culture plastic adjacent to the discs to isolate the effects of TCP surface structure from potential differences induced by dissolved material present in the media.

After 25 days culture, there was no significant difference in the expression of key osteoclast gene markers TRAP, CATK, CAII, AE2, TCIRG1, or DC-STAMP nor were there differences in expression of important integrins such as ITGB1, ITGB2, ITGB3, ITGAV, or ITGA4 (Figure 6). Only VCAM-1 (vascular cell adhesion molecule) was expressed differently on the two materials, ~12 times higher on

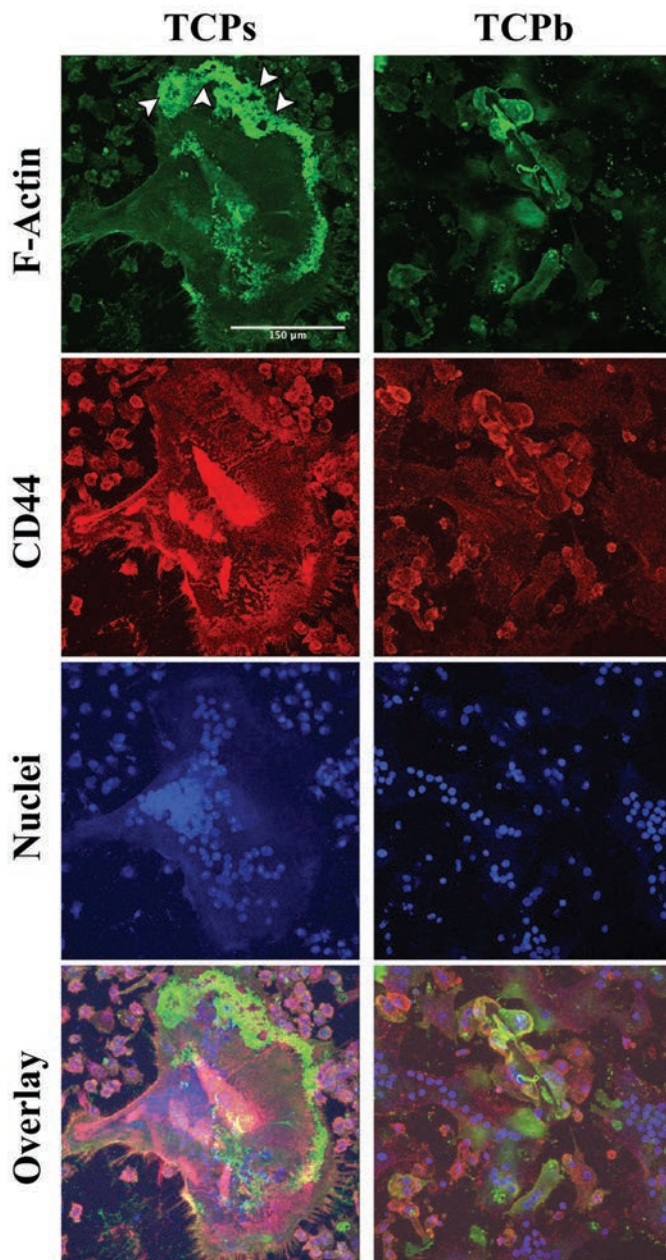


Figure 5. Representative laser scanning confocal micrographs of OCL formed on TCP. Actin ring structures (white arrows) are evident at the membrane border of OCL cultured on TCPs but not TCPb (Green = phalloidin targeting F-actin). The osteoclast membrane extends > 300 μm across on TCPs but remains small in comparison on TCPb (Red = CD44 antibody targeting cell membrane). Inside the membrane of a single osteoclast on TCPs, many nuclei are evident (Blue = Hoechst nuclei stain). Scale = 150 μm.

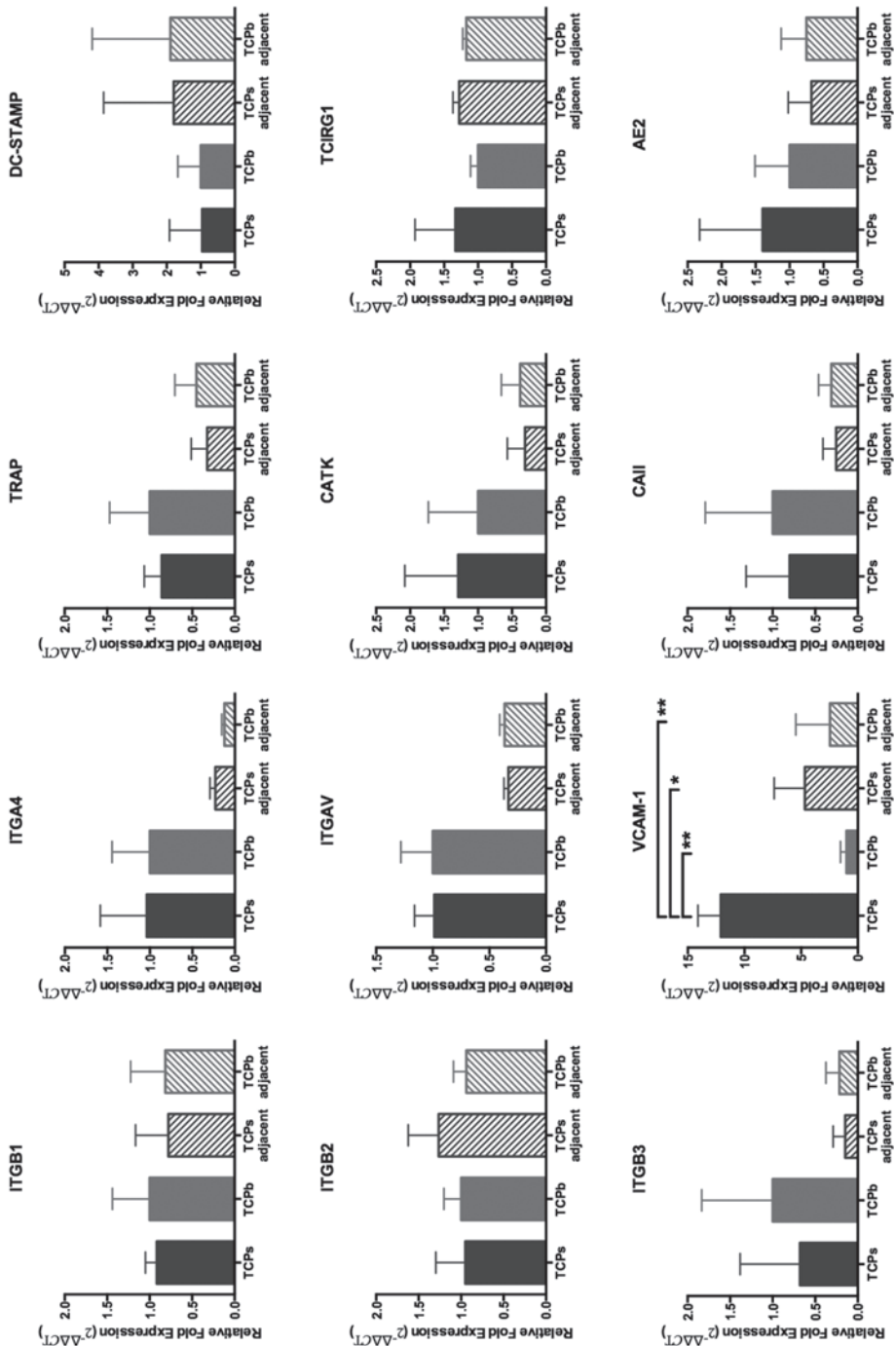
TCPs than on TCPb ($P = 0.002$). OCI expression of VCAM-1 on TCPs was also significantly higher than either cells cultured adjacent to TCPs or TCPb on tissue culture plastic ($P = 0.017$ and 0.004 , respectively) suggesting that this effect was due to direct interactions with the surface structure (Figure 6).

We speculated that gene expression may have followed a dynamic pattern over time similar to cell viability patterns, so we measured the time-course expression of the same genes in one additional donor. Only ITGB1, DC-STAMP, and VCAM-1 were differentially expressed between OCI cultured on TCPs and TCPb at time points earlier than day 25 (Figure 7). OCI cultured on TCPb expressed twice as much ITGB1 than TCPs at days 6 and 11 ($P = 0.042$ and 0.042 , respectively). Conversely, OCI expressed roughly 3 times as much DC-STAMP, the membrane protein responsible for osteoclast and macrophage fusion, on TCPs than on TCPb at day 6 ($P = 0.032$). VCAM-1 expression was significantly higher in OCI cultured on TCPs versus TCPb at day 6 (~50 fold, $P < 0.0001$), day 11 (~13 fold, $P = 0.0003$), day 18 (~12 fold, $P = 0.0430$) and day 25 (~2.6 fold, $P = 0.015$). Donor variability was evident in DC-STAMP expression at day 25, which was significantly higher on TCPs than on TCPb ($P = 0.042$) (Figure 7) although it was equivalent for the other 3 donors in aggregate (Figure 6).

4 DISCUSSION

Although modification of material physicochemistry [40] and macroporosity [41] have both been shown to enhance cellular resorption of CaP, little prior literature exists on the role of surface architecture in this process [1]. Previously, our group reported that in an intramuscular model of osteoinduction TCPs with submicron-scale surface structure directed the formation of multinucleated cells and was substantially resorbed but TCPb with micron-scale surface structure contained few multinucleated cells and was not resorbed (Chapter 4). Whether these multinucleated cells actively resorbed TCPs and why so few were present on TCPb were crucial questions left unanswered. Here, by differentiating human peripheral blood monocytes from multiple independent human donors into the two major types of multinucleated cells that reportedly form on CaP – OCI and FBGC – TCPs was found to promote the survival, differentiation, and resorbing function of OCI, while TCPb did not. These results reinforce our assertion that the scale of surface architecture may influence cellular resorption of CaP.

Whether multinucleated cells that resorb implanted CaP are phenotypically OCI or FBGC (or both) continues to be a topic of controversy. During subcutaneous implantation, both multinucleated OCI (TRAP+ and F4/80-) and FBGC (TRAP- and F4/80+) are distinctly present on the surface of submicrostructured TCPs



whereas only FBGC are found on the surface of microstructured TCP (Chapter 5); in the muscle tissue, only TCPs was resorbed (Chapter 4). Taken together, we speculated that the unique presence of OCI might be directly performing this resorption. The present in vitro results support this hypothesis because only OCI – not FBGC – resorbed TCP. Moreover, because OCI only resorbed TCPs and not TCPb, it can be concluded that osteoclast resorption is highly sensitive to the scale of TCP surface architecture, similar to what occurred *in vivo*.

In this study, the effects of surface structure on osteoclast formation and function were clear with respect to osteoclast survival, TRAP activity, multinucleation and fusion, actin ring assembly, and resorption pit creation – all of which strongly favored the submicrostructured, osteoinductive TCPs versus microstructured, non-osteoinductive TCPb. Most prior research on the cellular effects of surface structure – including surface roughness, a parameter that stems from it – is geared at improving osseointegration of an implant [42–44] with a focus on osteoblast differentiation and mineralization [45,46]. Recognizing that osteoclast resorption and osteoblast bone-secretion physiologically go hand in hand due to bone coupling mechanisms, Webster et al. (2001) were possibly the first to investigate ceramic surface nano/microstructure on osteoclast function [9]. By imparting surface grains and pores < 100 nm to alumina and HA ceramics, osteoclast activation and resorption were stimulated, particularly interesting findings since both materials are considered to be mainly non-resorbable. Conversely, starting with TCP, which is generally considered to be highly bioactive and soluble, our data suggests that not only does submicron-scale surface structure promote osteoclast activation and resorption, but on the other hand, larger micron-scale surface structure may block osteoclast activation and resorption, thus rendering TCP appreciably non-resorbable in these experimental conditions. Taken together, we speculate that surface nano/microstructure may be important in stimulating osteoclastogenesis irrespective of the chemical composition or solubility of the material. Indeed, other groups have shown that varying the surface roughness of other materials such as titanium substantially influences osteoclast activity and differentiation [47,48].

Figure 6, opposite. OCI RNA expression of key integrins and osteoclast markers at day 25 by qPCR. VCAM-1 was the only detectable difference in gene expression between OCI formed on TCPs and TCPb. Comparison to OCI formed on tissue culture plastic adjacent to TCP discs emphasizes the direct effect of microstructure on gene expression. Expression levels were normalized to OCI cultured on TCPb. Data represents the mean \pm s.d. of n = 6 replicates from 3 independent donors. * P < 0.05, ** P < 0.01.

VCAM-1 is an adhesion molecule typically associated with vascular stromal cells and under certain conditions also expressed by blood monocytes [49]. Its upregulation has been shown to greatly increase osteoclast fusion in bone metastases when it binds VLA-4 expressed by pre-OCI [50]. VCAM-1 expression was strongly and robustly upregulated in OCI cultured on TCPs as early as day 6, so we speculated that pre-osteoclast expression of VCAM-1 might promote osteoclast differentiation in an autocrine loop. However, the results of a VCAM-1 antibody blockade on OCI size were inconclusive (data not shown). Considering there was some donor variability, further experiments with additional donors should be conducted to block these early differentially expressed genes to elucidate what role they may play in osteoclast behavior on TCP such as survival, fusion, and resorption.

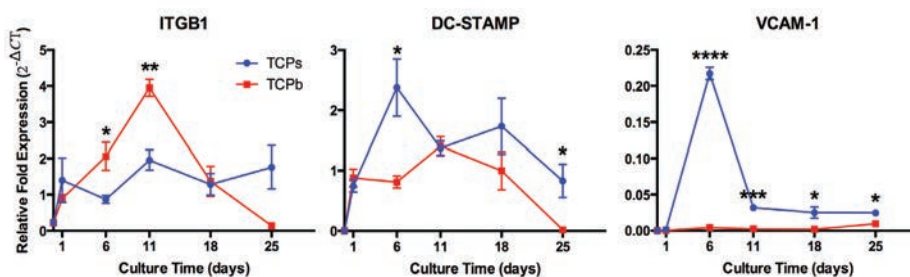


Figure 7. OCI RNA expression of differentially expressed gene targets over the culture period. Data represents the mean \pm s.d. of $n = 3$ replicates from 1 representative donor.
 $* P < 0.05$, $** P < 0.01$, $*** P < 0.001$, $**** P < 0.0001$.

These results show that different scales of surface architecture can differentially affect the formation and function of OCI and thus control their resorption of CaP. In the future, more material chemistries should be similarly tested to ascertain if these osteoclast-promotive effects are exclusively due to the material surface topography – that is the physical grain and pore shape and size – or if material physicochemistry also plays a role. Moreover, smaller surface architecture should be tested to find if there is an optimum scale for promoting osteoclast resorption. Although several groups have attempted to deter the formation of OCI on the surface of CaP by incorporating various inhibitory factors such as bisphosphonates [51–53], the influence of surface structural scale on osteoclast function may also bear significant impact on subsequent bone formation through bone coupling mechanisms. It is possible then that the key to designing an osteoinductive CaP is first to design a material surface that promotes the formation and function of OCI, such as submicrostructured TCPs investigated here.

5 CONCLUSION

The submicron-scale surface structure of TCP was found to promote the survival, differentiation, and resorption of OCI derived from human peripheral blood monocytes; however, micron-scale surface structure impeded OCI survival and resorption. FBGC were unable to resorb TCP irrespective of surface structure.

A C K N O W L E D G E M E N T S

The authors gratefully acknowledge the support of the TeRM Smart Mix Program of the Netherlands Ministry of Economic Affairs and the Netherlands Ministry of Education, Culture and Science. This research forms part of the Project P2.04 BONE-IP of the research program of the Biomedical Materials Institute, co-funded by the Dutch Ministry of Economic Affairs. This work was also supported by funding under the Seventh Research Framework Program of the European Union, through the project REBORNE under Grant agreement no. 241879. Special thanks are due to Dr. Teun de Vries and Dr. Behrouz Zandieh Doulabi (ACTA) for their enriching discussion, and Daisy Picavet (AMC) for her help with confocal microscopy.

6

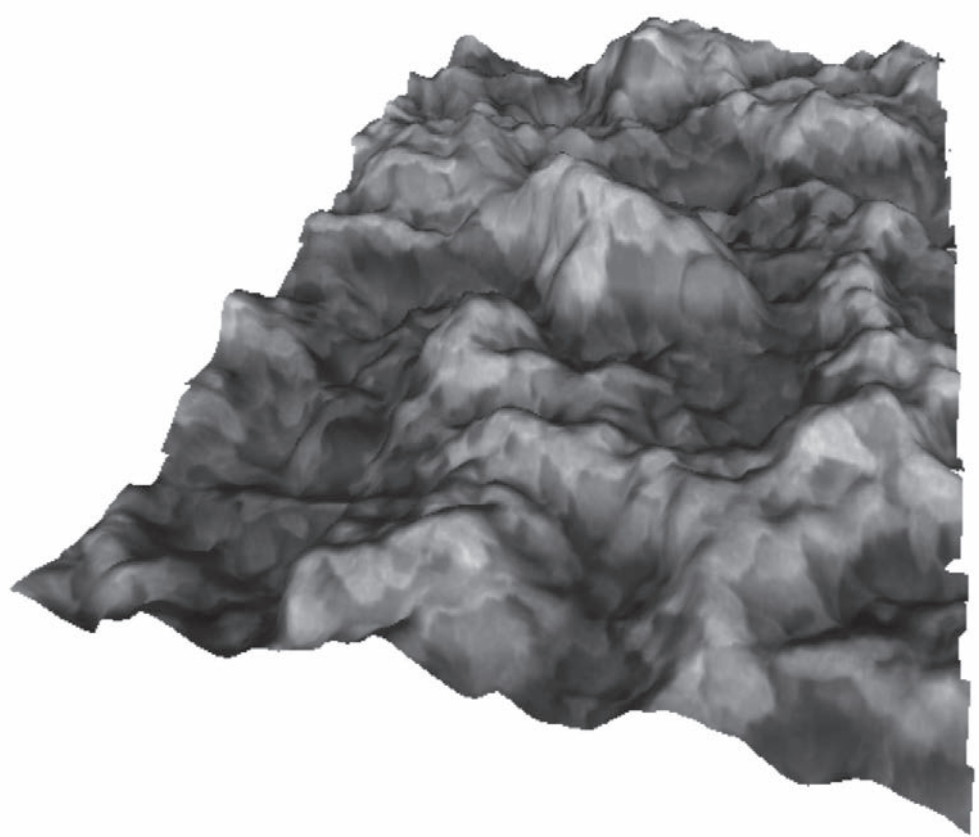
R E F E R E N C E S

- [1] Bohner M, Galea L, Doebelin N. Calcium phosphate bone graft substitutes: failures and hopes. *J Eur Ceram Soc* 2012;32:2663–71.
- [2] Nakahama K-I. Cellular communications in bone homeostasis and repair. *Cell Mol Life Sci* 2010;67:4001–9.
- [3] Takeshita S, Fumoto T, Matsuoka K, Park K, Aburatani H, Kato S, et al. Osteoclast-secreted CTHRC1 in the coupling of bone resorption to formation. *J Clin Invest* 2013;123:3914–24.
- [4] Zhao C, Irie N, Takada Y, Shimoda K, Miyamoto T, Nishiwaki T, et al. Bidirectional ephrinB2-EphB4 signaling controls bone homeostasis. *Cell Metab* 2006;4:111–21.
- [5] Sims NA, Gooi JH. Bone remodeling: Multiple cellular interactions required for coupling of bone formation and resorption. *Semin Cell Dev Biol* 2008;19:444–51.
- [6] Lu J, Descamps M, Dejou J, Koubi G, Hardouin P, Lemaitre J, et al. The biodegradation mechanism of calcium phosphate biomaterials in bone. *J Biomed Mater Res* 2002;63:408–12.
- [7] Eggli PS, Müller W, Schenk RK. Porous hydroxyapatite and tricalcium phosphate cylinders with two different pore size ranges implanted in the cancellous bone of rabbits. A comparative histomorphometric and histologic study of bony ingrowth and implant substitution. *Clin Orthop Relat Res* 1988;127–38.
- [8] Okuda T, Ioku K, Yonezawa I, Minagi H, Kawachi G, Gonda Y, et al. The effect of the microstructure of beta-tricalcium phosphate on the metabolism of subsequently formed bone tissue. *Biomaterials* 2007;28:2612–21.
- [9] Webster TJ, Ergun C, Doremus RH, Siegel RW, Bizios R. Enhanced osteoclast-like cell

C H A P T E R 6

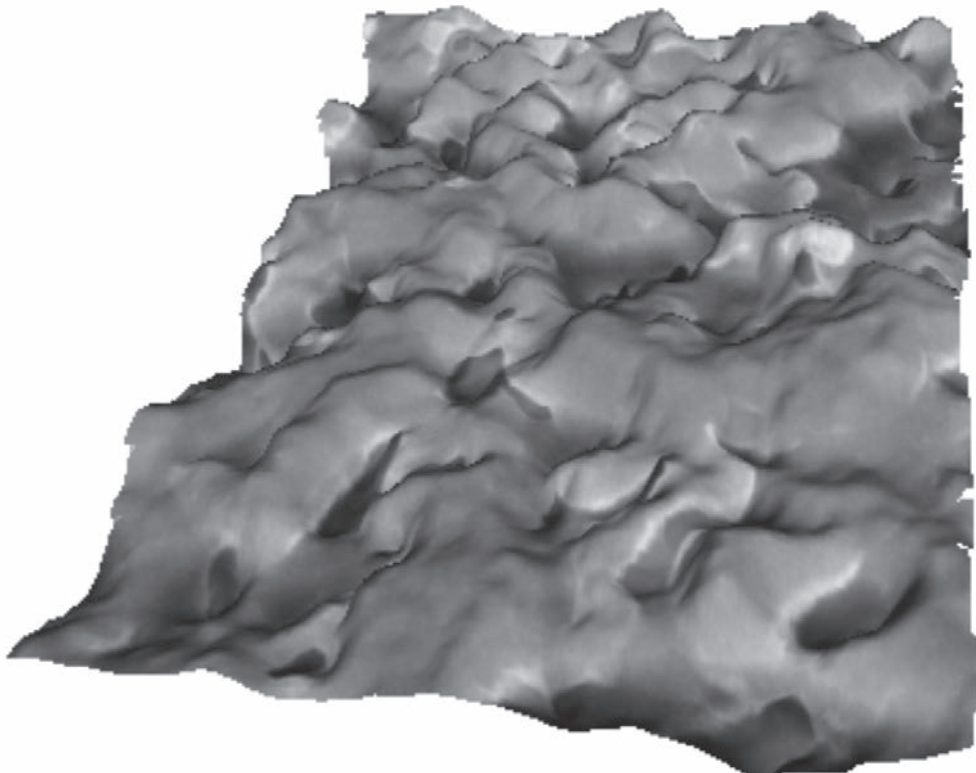
- functions on nanophase ceramics. *Biomaterials* 2001;22:1327–33.
- [10] Kondo N, Ogose A, Tokunaga K, Umezawa H, Arai K, Kudo N, et al. Osteoinduction with highly purified beta-tricalcium phosphate in dog dorsal muscles and the proliferation of osteoclasts before heterotopic bone formation. *Biomaterials* 2006;27:4419–27.
- [11] Tanaka T, Saito M, Chazono M, Kumagae Y, Kikuchi T, Kitasato S, et al. Effects of alendronate on bone formation and osteoclastic resorption after implantation of beta-tricalcium phosphate. *J Biomed Mater Res A* 2010;93:469–74.
- [12] Wada T, Hara K, Ozawa H. Ultrastructural and histochemical study of beta-tricalcium phosphate resorbing cells in periodontium of dogs. *J Periodontal Res* 1989;24:391–401.
- [13] Dersot JM, Colombier ML, Lafont J, Baroukh B, Septier D, Saffar JL. Multinucleated giant cells elicited around hydroxyapatite particles implanted in craniotomy defects are not osteoclasts. *Anat Rec* 1995;242:166–76.
- [14] Baslé MF, Chappard D, Grizon F, Filmon R, Delecrin J, Daculsi G, et al. Osteoclastic resorption of Ca-P biomaterials implanted in rabbit bone. *Calcif Tissue Int* 1993;53:348–56.
- [15] Wenisch S, Stahl J-P, Horas U, Heiss C, Kilian O, Trinkaus K, et al. In vivo mechanisms of hydroxyapatite ceramic degradation by osteoclasts: fine structural microscopy. *J Biomed Mater Res A* 2003;67:713–8.
- [16] Heymann D, Pradal G, Benahmed M. Cellular mechanisms of calcium phosphate ceramic degradation. *Histol Histopathol* 1999;14:871–7.
- [17] Anderson J, Rodriguez A, Chang D. Foreign body reaction to biomaterials. *Semin Immunol* 2008;20:86–100.
- [18] Vignery A. Macrophage fusion: the making of osteoclasts and giant cells. *J Exp Med* 2005;202:337–40.
- [19] Schilling AF, Linhart W, Filke S, Gebauer M, Schinke T, Rueger JM, et al. Resorbability of bone substitute biomaterials by human osteoclasts. *Biomaterials* 2004;25:3963–72.
- [20] Gomi K, Lowenberg B, Shapiro G, Davies JE. Resorption of sintered synthetic hydroxyapatite by osteoclasts in vitro. *Biomaterials* 1993;14:91–6.
- [21] Xia Z, Grover LM, Huang Y, Adamopoulos IE, Gbureck U, Triffitt JT, et al. In vitro biodegradation of three brushite calcium phosphate cements by a macrophage cell-line. *Biomaterials* 2006;27:4557–65.
- [22] Yamada S, Heymann D, Bouler JM, Daculsi G. Osteoclastic resorption of biphasic calcium phosphate ceramic in vitro. *J Biomed Mater Res* 1997;37:346–52.
- [23] Fuller K, Ross JL, Szewczyk KA, Moss R, Chambers TJ. Bone is not essential for osteoclast activation. *PLoS One* 2010;5(9): e128.
- [24] Ripamonti U, Klar RM, Renton LF, Ferretti C. Synergistic induction of bone formation by hOP-1, hTGF-beta3 and inhibition by zoledronate in macroporous coral-derived hydroxyapatites. *Biomaterials* 2010;31:6400–10.
- [25] Karsdal MA, Neutzsky-Wulff AV, Dziegiele MH, Christiansen C, Henriksen K. Osteoclasts secrete non-bone derived signals that induce bone formation. *Biochem Biophys Res Commun* 2008;366:483–8.
- [26] Pederson L, Ruan M, Westendorf JJ, Khosla S, Oursler MJ. Regulation of bone formation by osteoclasts involves Wnt/BMP signaling and the chemokine sphingosine-1-phosphate. *Proc Natl Acad Sci U S A* 2008;105:20764–9.
- [27] McCullough KA, Waits CA, Garimella R, Tague SE, Sipe JB, Anderson HC. Immunohistochemical localization of bone morphogenetic proteins (BMPs) 2, 4, 6, and 7 during induced heterotopic bone formation. *J Orthop Res* 2007;25:465–72.
- [28] Bradley E, Oursler M. Osteoclast Culture and Resorption Assays. In: Westendorf J, editor. *Osteoporos. SE - 2*, vol. 455, Humana Press; 2008, p. 19–35.
- [29] McNally AK, Anderson JM. Interleukin-4 induces foreign body giant cells from human monocytes/macrophages. Differential lymphokine regulation of macrophage fusion leads to morphological variants of multinucleated giant cells. *Am J Pathol* 1995;147:1487–99.
- [30] Nakayama GR, Caton MC, Nova MP, Parandoosh Z. Assessment of the Alamar Blue assay for cellular growth and viability in vitro. *J Immunol Methods* 1997;204:205–8.
- [31] Ahmed SA, Gogal RM, Walsh JE. A new rapid and simple non-radioactive assay to monitor and determine the proliferation of lymphocytes: an alternative to [³H]thymidine incorporation assay. *J Immunol Methods* 1994;170:211–24.

- [32] Gloeckner H, Jonuleit T, Lemke HD. Monitoring of cell viability and cell growth in a hollow-fiber bioreactor by use of the dye Alamar Blue. *J Immunol Methods* 2001;252:131–8.
- [33] Ljusberg J, Ek-Rylander B, Andersson G. Tartrate-resistant purple acid phosphatase is synthesized as a latent proenzyme and activated by cysteine proteinases. *Biochem J* 1999;343 Pt 1:63–9.
- [34] Jansen IDC, Vermeer JAF, Bloemen V, Stap J, Everts V. Osteoclast fusion and fission. *Calcif Tissue Int* 2012;90:515–22.
- [35] Livak KJ, Schmittgen TD. Analysis of relative gene expression data using real-time quantitative PCR and the 2(-Delta Delta C(T)) Method. *Methods* 2001;25:402–8.
- [36] Alatalo SL, Halleen JM, Hentunen TA, Mönkkönen J, Väänänen HK. Rapid screening method for osteoclast differentiation in vitro that measures tartrate-resistant acid phosphatase 5b activity secreted into the culture medium. *Clin Chem* 2000;46:1751–4.
- [37] Väänänen HK, Zhao H, Mulari M, Halleen JM. The cell biology of osteoclast function. *J Cell Sci* 2000;113 (Pt 3):377–81.
- [38] Bianco P, Costantini M, Dearden LC, Bonucci E. Expression of tartrate-resistant acid phosphatase in bone marrow macrophages. *Basic Appl Histochem* 1987;31:433–40.
- [39] Hayman AR. Tartrate-resistant acid phosphatase (TRAP) and the osteoclast/immune cell dichotomy. *Autoimmunity* 2008;41:218–23.
- [40] Egli RJ, Gruenenfelder S, Doebelein N, Hofstetter W, Luginbuehl R, Bohner M. Thermal treatments of calcium phosphate biomaterials to tune the physico-chemical properties and modify the in vitro osteoclast response. *Adv Eng Mater* 2011;13:B102–B107.
- [41] Takagi S, Chow LC. Formation of macropores in calcium phosphate cement implants. *J Mater Sci Mater Med* 2001;12:135–9.
- [42] Zhang W, Wang G, Liu Y, Zhao X, Zou D, Zhu C, et al. The synergistic effect of hierarchical micro/nano-topography and bioactive ions for enhanced osseointegration. *Biomaterials* 2013;34:3184–95.
- [43] Cooper LF. A role for surface topography in creating and maintaining bone at titanium endosseous implants. *J Prosthet Dent* 2000;84:522–34.
- [44] Mendonça G, Mendonça DBS, Aragão FJL, Cooper LF. Advancing dental implant surface technology--from micron- to nanotopography. *Biomaterials* 2008;29:3822–35.
- [45] Gittens RA, McLachlan T, Olivares-Navarrete R, Cai Y, Berner S, Tannenbaum R, et al. The effects of combined micron-/submicron-scale surface roughness and nanoscale features on cell proliferation and differentiation. *Biomaterials* 2011;32:3395–403.
- [46] Jäger M, Zilkens C, Zanger K, Krauspe R. Significance of nano- and microtopography for cell-surface interactions in orthopaedic implants. *J Biomed Biotechnol* 2007;2007:1–19.
- [47] Brinkmann J, Hefti T, Schlottig F, Spencer ND, Hall H. Response of osteoclasts to titanium surfaces with increasing surface roughness: an in vitro study. *Biointerphases* 2012;7:34.
- [48] Makihira S, Mine Y, Kosaka E, Nikawa H. Titanium surface roughness accelerates RANKL-dependent differentiation in the osteoclast precursor cell line, RAW264. 7. *Dent Mater J* 2007;26:739–45.
- [49] Thomas-Ecker S, Lindecke A, Hatzmann W, Kaltschmidt C, Zänker KS, Dittmar T. Alteration in the gene expression pattern of primary monocytes after adhesion to endothelial cells. *Proc Natl Acad Sci U S A* 2007;104:5539–44.
- [50] Lu X, Mu E, Wei Y, Riethdorf S, Yang Q, Yuan M, et al. VCAM-1 promotes osteolytic expansion of indolent bone micrometastasis of breast cancer by engaging $\alpha 4\beta 1$ -positive osteoclast progenitors. *Cancer Cell* 2011;20:701–14.
- [51] Fukuda C, Norihiro A, Mitsuru T, Shunsuke F, Masahi N, Takahashi N. Local application of alendronate on β -tricalcium phosphate accelerated induction of osteogenesis with formation of giant osteoclast-like cell. *J Biomater Nanobiotechnol* 2012;03:169–77.
- [52] Faucheu C, Verron E, Soueidan A, Josse S, Arshad MD, Janvier P, et al. Controlled release of bisphosphonate from a calcium phosphate biomaterial inhibits osteoclastic resorption in vitro. *J Biomed Mater Res A* 2009;89:46–56.
- [53] Denissen H, van Beek E, Löwik C, Papapoulos S, van den Hooff A. Ceramic hydroxyapatite implants for the release of bisphosphonate. *Bone Miner* 1994;25:123–34.



CHAPTER 7

General discussion



In the pursuit of designing better CaP bone graft substitutes, the aim of this work was to more clearly understand what material requirements and parameters are necessary to achieve both osteoinduction and resorption from the standpoint of the cell and tissue response. As discussed in Chapter 1, the starting point of this work as a whole was the general knowledge that certain material specifications such as macrostructure, microstructure, and chemical composition may all influence the osteoinductive and resorbable performance of CaPs. The cell and tissue responses necessary to bring about these biological processes were, however, less clear. Throughout the experimental chapters of this thesis, the overarching finding was that surface microstructure modulates the formation and activity of multinucleated osteoclasts and that these cells and their precursors appear to play a pivotal role in both osteoinduction and material resorption. Moreover, the results herein point to the innate inflammatory reaction to osteoinductive surface microstructure in directing these outcomes.

While the findings of Chapters 2 – 6 stand on their own, they also come together to address broader questions posed in Chapter 1, which will be discussed here. And beyond this thesis, this chapter will consider how the findings herein coalesce and relate to what was reported in the literature at the start.

1 PHYSICOCHEMICAL PARAMETERS FOR OSTEOINDUCTION: MICROSTRUCTURE, MACROSTRUCTURE, AND CHEMICAL COMPOSITION

Because osteoinductive CaPs do not contain osteogenic cells or osteoinductive growth factors like BMPs, how they stimulate de novo bone formation must relate to their intrinsic material properties such as chemical composition and physical structure. CaPs composed of various chemistries (e.g. HA, BCP, and TCP) and some non-CaPs like alumina [1] and titanium [2] have all been shown to be osteoinductive – albeit to varying degrees – depending on their physical architecture, underscoring this material parameter as the driving factor in de novo bone formation [3,4]. Surface architecture specifically on the microscale has been shown to be a key material parameter in osteoinduction – first by Yamasaki and Sakai (1992) who demonstrated that microporous HA was osteoinductive in dog muscle but dense HA was not [5]. This strategy of incorporating microporosity (and also micro-scale surface grains) was further developed by Yuan and Habibovic who showed through numerous studies that CaPs with identical chemistry and macrostructure could form de novo bone in the muscle of sheep, goats, and dogs if they had surface microstructure but not without it [6–11]. Similarly, macroporous titanium implants were osteoinductive in the muscle of

dogs only after they were thermo-chemically treated to impart nano/microphase surface structure [2,12]. Still, compositional chemistry may also play a role in the extent of osteoinduction in that the amount of bone formed by nano/microphase titanium was far less than what was reported for microstructured BCP or TCP [11]. Moreover, Habibovic et al. (2005) and Yuan et al. (2010) both showed by comparing two CaPs with similar microstructure but different solubilities (e.g., HA vs. BCP and BCP vs. TCP) that the more soluble CaP induced significantly more bone formation [10,11].

In addition to microstructure and chemical composition, macrostructural features such as concavities, macropores, and interparticle space have also been described as essential for osteoinduction. For instance, Ripamonti et al. (1999) and Habibovic et al. (2005) independently speculated that concavities or macropores were prerequisite for de novo bone formation because bone always formed in these features but never on a planar surface or on the edge of an implant [10,13]. However, in their U.S. patent, Yuan and de Bruijn (2009) clearly demonstrated and specified that microporous CaP particles, without macropores or concavities, powerfully induce de novo bone formation between the particles [14]. In their review of osteoinductive biomaterials, Barradas and colleagues (2011) distilled and interpreted some of these findings to mean that osteoinduction requires some sort of “sheltered” macroenvironment for the accumulation of $\text{Ca}^{2+}/\text{P}_i$ ions or circulating BMPs from the body fluid, whether it is created by macropores, concavities, channels, or interparticle space. To reinforce the importance of this, the authors went on to say that at the time of writing, no non-degradable material has been shown to be osteoinductive without one of these macrostructural characteristics [4]. Given these theories as a starting point to this work, it stood to reason that if surface microstructure was the only essential parameter to trigger de novo bone formation then a planar, microstructured surface without macropores, concavities, or interparticle space (i.e., macroscopically flat) could also be osteoinductive.

The results of Chapter 3 more clearly isolated surface microstructure, irrespective of macrostructure or surface chemistry, to be the primary factor necessary for osteoinduction. Specifically, macroscopically flat BCP discs, composed of either small or large surface microstructure, were fixed together with a central gap and implanted in the muscle of dogs. Based on the geometry of the constructs, bone was permitted to form on the outer surface of the constructs, where there was no macrostructural, sheltered environment, or it could form in the central gap similar to the space between granules. De novo bone was formed in 4 out of 5 BCP1150 implants with small microstructure, but no bone was formed in any of the 5 BCP1300 implants with larger microstructure. Surprisingly, bone

mostly formed on the outer surface of the microstructured discs, not in the inner gap, proving that macrostructural features are not essential for osteoinduction. Additionally, BCP1150 discs coated with a thin layer of titanium (BCP1150Ti), thus preserving the microstructure and chemical reactivity but changing the surface chemistry, still triggered bone formation in 3 out of 5 dogs, suggesting that surface chemistry is a flexible parameter in osteoinductive materials.

Still, in terms of bone area, the amount of bone formed on the planar BCP1150 discs was less than previously described for a similar microstructured BCP granules with interconnected macropores [11], so it is possible that macrostructural features promote de novo bone formation by osteoconduction after it has already been triggered by osteoinductive microstructure. For instance, macropores are thought to increase blood vessel infiltration, nutrients, and local concentrations of $\text{Ca}^{2+}/\text{P}_i$ ions – all biological factors that are known to promote bone growth [4,15].

2 MICROSTRUCTURAL DIMENSIONS FOR OSTEINDUCTION

Although surface microstructure has already been highlighted by many other groups [5,6,10,11,16–18], thorough surface characterization – such as grain and pore size distributions, surface profile, and roughness – is rarely reported in the literature [4]. The most specific surface microstructure requirements for osteoinduction comes from the patent of Yuan and de Bruijn (2009), who demonstrate through intramuscular implantation that surface grains and micropores should both be $< 1.5 \mu\text{m}$ to form de novo bone [14].

The results of Chapter 3 confirmed that the dimensions of surface microstructure are critical for de novo bone formation, because unlike other non-inductive controls used in the literature [9,19] BCP1300 was not completely dense. However, its surface grains and micropores were significantly larger than osteoinductive BCP1150 (e.g., 3–5 μm versus $\sim 1 \mu\text{m}$). Thus, these results were in agreement with the previous patent by Yuan and de Bruijn that microstructure must be $< 1.5 \mu\text{m}$ for osteoinduction to occur [14].

In Chapters 4 and 5, the importance of surface microstructure size for osteoinduction was further validated using TCP in different ectopic models of osteoinduction. Similar to BCP1150 and BCP1300, TCPs with surface micropores and grains sized roughly $\leq 1 \mu\text{m}$ was shown to be potently osteoinductive but TCPb with micropores and grains sized 3–5 μm was completely non-inductive, both intramuscularly in dogs and subcutaneously in mice.

Understanding why microstructure on such a narrow range of sizes is critical for osteoinduction remains a challenge because microstructure is inextricably linked with a whole host of other material characteristics – e.g., topography, roughness, wettability, zeta potential, specific surface area – that in turn dictate a variety of material functionalities – e.g., fluid uptake, protein adsorption, ion release, ion precipitation, cell behavior (adhesion, proliferation, differentiation), and tissue response. Thus, changing one factor in order to isolate its biological effect while maintaining the others constant is likely impossible.

Still, some theories have been presented to explain how CaP physical serves to induce *de novo* bone formation. Ripamonti and colleagues (1991) first suggested that (macro-) geometric features of osteoinductive CaPs act as a collector of endogenous BMPs [20], which de Groot (1998) later speculated may occur through the dissolution/reprecipitation of carbonate apatite at the material surface [21]. As Daculsi et al. (1990) showed, CaPs will invariably form a mineralized layer of carbonate apatite *in vivo* irrespective of their composition or architecture [22], so Habibovic proposed that microstructure may augment the precipitation of carbonated apatite and adsorption of anabolic proteins past a certain threshold necessary for bone induction. In contrast, other groups have proposed that increased $\text{Ca}^{2+}/\text{P}_i$ ion release rather than precipitation, due to the higher specific surface area of microstructured CaP, is the biological trigger for osteoblast differentiation [5,23–26]. The solubility of CaPs is believed to add to this effect, again implicating chemical composition in osteoinduction [23].

What may be missing from both of these physicochemical theories – reprecipitation of a carbonate apatite layer or $\text{Ca}^{2+}/\text{P}_i$ release – is the influence of the cellular response on these dissolution/degradation processes *in vivo* [27]. For instance, during the foreign body reaction, neutrophils and monocyte/macrophages will rapidly home to the surface of a CaP implant in order to break it down and clear it from the body through phagocytosis [28]. After differentiation from their monocyte/macrophage precursors, osteoclasts can resorb CaP and secrete the internalized degradation products from their apical functional secretory domain via transcytosis [29]. Based on this, osteoclast resorption of microstructured CaPs would conceivably increase local $\text{Ca}^{2+}/\text{P}_i$ concentrations available for both reprecipitation of carbonate apatite as well as cell signaling. In this way, the cellular response to CaPs may be an important initial biological process in explaining how the physicochemical aspects of surface microstructure translate to osteoinduction [30].

3 OSTEOCLASTOGENESIS AND OSTEOINDUCTION

Osteoclastogenesis has been shown to precede de novo bone formation by microstructured CaPs and is thought to be an important cellular response for osteoinduction. In the seminal study by Kondo et al. (2006), TRAP positive / cathepsin K positive multinucleated osteoclasts formed on the surface of microstructured TCP up to 4 weeks before de novo bone formation in the muscle of dogs [16]. Akiyama et al. (2011) independently corroborated this finding by showing that TRAP positive multinucleated cells were present after 2 weeks on the surface of microstructured calcium-deficient HA (CDHA) implanted in dog muscle, but de novo bone was not present until 2 weeks later [31].

To explain why osteoclasts may be important for osteoinduction, Klar, Ripamonti, and coworkers (2013) speculated that osteoclast resorption and subsequent release of Ca^{2+} ions into the microenvironment could be the physiologic trigger for osteoblast differentiation [30]. To substantiate this, both Klar et al. (2013) and Tanaka et al. (2010) showed that bisphosphonates such as zoledronate and alendronate, which antagonize osteoclast survival and activity, reduced both ectopic and orthotopic bone formation by different CaPs [30,32]. However, Fukuda and coworkers (2012) attempted to show the opposite – that alendronate-loaded TCP increased de novo bone formation. The results of this study are inconclusive, however, because the treatment did not significantly reduce the number of TRAP positive cells or osteoclast gene markers [33].

Despite this evidence to suggest that osteoclasts are somehow involved with osteoinduction, none of these previous studies incorporated non-inductive CaP controls to evaluate if osteoclastogenesis in ectopic locations was unique to osteoinductive CaPs. Moreover, none of the studies included in vitro investigation of why these particular CaPs promoted osteoclastogenesis *in vivo*. Thus, in view of the limitations of these prior findings at the start of this thesis, the theory that osteoclasts play a direct role in osteoinduction deserved more investigation particularly from the standpoint of how osteoclastogenesis may be affected by surface microstructure.

Throughout the experimental chapters of this thesis, osteoclastogenesis was consistently and robustly correlated with de novo bone formation by microstructured CaPs. Conversely, osteoclast formation was consistently attenuated on non-inductive CaPs. This relationship held true for both slow-resorbing BCP and fast-resorbing TCP, as well as in different animal models. For instance, in Chapters 3 and 4, (sub)microstructured BCP1150 and TCPs promoted osteoclast-like cell formation *in vitro* and *in vivo*, which correlated with their de novo bone formation in dog muscle. In contrast, non-inductive

BCP1300 and TCPb with larger microstructure stunted osteoclast formation in vitro and few osteoclast-like cells were observed in vivo. In Chapter 5, multinucleated osteoclasts (TRAP positive, F4/80 negative) were uniquely present on osteoinductive TCPs adjacent to de novo bone subcutaneously in mice, while only multinucleated foreign body giant cells (TRAP negative, F4/80 positive) formed on non-inductive TCPb. Thus, for the first time, osteoclast formation was analytically compared on both osteoinductive and non-inductive CaPs in vivo and in vitro and found to be uniquely present on osteoinductive CaP in vivo. Based on the fact that the materials only differed in their surface microstructure, we can conclude that microstructure was the regulator of this biological response.

However, these findings alone did not unequivocally prove the role of osteoclastogenesis in osteoinduction. With respect to the osteoinductive CaPs investigated herein, what comes first, the Osteoclast or the Osteoblast? Which cell type is driving the other's differentiation? To specifically address this, the aim of Chapter 5 was to deplete osteoclasts and their monocyte/macrophage precursors to find out if they are indeed essential for de novo bone formation. Using liposomal clodronate treatment to specifically deplete phagocytes like osteoclasts and their monocyte/macrophage precursors, it was shown that osteoclast depletion, verified by (immuno)histochemical staining and gene expression, blocked osteoinduction by TCPs despite the fact that Osterix positive stromal cells and F4/80 positive macrophages were still present in the implants. The reason for this could be due to inhibition of osteoclast-secreted anabolic factors such as CTHRC1, C3a, CT-1, S1P, and even TRAP – all shown in the literature to stimulate osteoblast differentiation from uncommitted precursors in vitro and in vivo [34]. Moreover, in Chapter 4, we further demonstrated osteoclast-secreted factors to be a novel mechanism by which osteoclastogenesis on microstructured CaPs may stimulate osteogenesis. Specifically, the conditioned medium of osteoclasts generated on osteoinductive TCPs potently stimulated osteoblast differentiation of hMSCs in the absence of osteogenic medium supplements; however the control culture medium of TCPs alone without osteoclasts had no effect on hMSC differentiation, nor were $\text{Ca}^{2+}/\text{P}_i$ ions elevated in the osteoclast-conditioned culture medium. So, the observed anabolic effects were attributed to osteoclast-secreted factors and not physicochemical aspects of TCPs itself.

Alternatively, other groups have shown that surface microstructure may also influence the differentiation of osteoblasts and their precursors directly. For instance, submicron scale surface roughness of ceramics, titanium, and tissue culture plastic promotes osteoblast differentiation [35–37]. Micropore size may also direct osteoblast differentiation – for instance, Lee et al. (2004) showed

that differentiation of osteoblast-like cells was promoted on polycarbonate membranes with larger pores ($\sim 8 \mu\text{m}$) rather than smaller ones ($0.2 \mu\text{m}$) [38]. Concerning osteoinductive CaPs specifically, Barradas et al. (2013) and Yuan et al. (2010) both showed that MSCs cultured on osteoinductive, microstructured TCP in osteogenic medium expressed upregulated osteoblast markers versus non-inductive, non-microstructured HA [11,23].

More studies should be done to exclusively deplete osteoclasts, leaving their monocyte/macrophage precursors intact, in order to specifically investigate whether osteoclasts are directing de novo bone formation or if macrophage-mediated inflammation is the osteogenic inductor. For instance, a useful experiment would be to implant osteoinductive CaP subcutaneously in FVB mice and then locally inject osteoprotegerin (OPG) to block osteoclastogenesis. Because according to the current knowledge OPG only disrupts RANK-RANKL signaling by specifically binding RANKL, macrophages and their related inflammatory signals would remain intact. For instance, human recombinant OPG has been investigated for use as a treatment for osteopenia, bone density loss because it targets osteoclast resorption [39]. If osteoclasts are essential for osteoinduction, then the successful OPG blockade of RANK-RANKL signaling would block de novo bone formation. Conversely, locally injecting RANKL in a non-osteoinductive TCP implant may be an intriguing way to generate osteoclasts where they normally would not form and perhaps ultimately stimulate de novo bone formation.

4 OSTEOCLAST RESORPTION AND OSTEOGENESIS

The main functional characteristic of mature osteoclasts is their ability to resorb mineralized substrates such as bone as well as CaPs [27,40–43], which can be influenced by the nano/microtopography of the substrate [44]. For instance, the pioneering work of Gomi et al. (1993) and Webster et al. (2001) showed that surface nano-/microroughness strongly promotes osteoclast formation and resorption of HA in vitro, despite its low solubility [45,46]. Still, an ideal micropore and surface grain size (i.e., microstructure) for controlling (cellular) resorption in vivo is currently unknown [47]. More to the point, at the start of this thesis, it was unclear if osteoclast resorption and osteoinduction by microstructured CaPs are linked, similar to how bone resorption and formation are coupled. Understanding this would be useful for designing osteoinductive CaPs in order to match their resorption profile with the rate of bone formation.

In the present work, the *in vivo* results of Chapter 4 showed that microstructural dimensions play a role in how osteoclasts form and resorb CaPs ectopically. Specifically, after 12 weeks in the muscle TCP was not degraded with surface grains and pores sized $\sim 3\text{--}5 \mu\text{m}$ (TCPb) but was highly resorbed with grains and pores sized $\leq 1 \mu\text{m}$ (TCPs). Although the long-term resorption profile of the materials was not investigated and may be different in orthotopic sites, the disparate presence of multinucleated osteoclast-like cells on TCPs but not on TCPb strongly suggested that they were responsible for the resorption of the material in the muscle. In Chapter 6, these *in vivo* findings were recapitulated *in vitro* using a human monocyte-derived osteoclast model – notably, in 4 independent human donors, osteoclasts survived on the surface of TCPs and readily resorbed it but hardly survived on TCPb and were completely unable to resorb it. Although the mechanism for this was unclear, osteoclasts formed actin rings, the cytoskeletal boundaries of sealing zones where substrate resorption occurs, on TCPs but not on TCPb. Indeed, Geblinger and colleagues (2010, 2012) repeatedly showed that osteoclasts can sense the nano-/microtopography of their substrate, and surface roughness can directly influence actin ring assembly and integrity [44,48]. Not limited to just that, osteoclast viability, TRAP activation, and fusion were also promoted by the microstructure of TCPs and stunted by the structure of TCPb, although initial cell attachment and proliferation of pre-osteoclasts were similar between the materials.

The biomolecular basis for these differences was probed further using a large panel of osteoclast genes regulating substrate adhesion, differentiation, fusion, and resorption. Of these gene targets, VCAM-1 and DC-STAMP were both found to be significantly upregulated and ITGB1 was significantly downregulated at early time points on TCPs. Of these genes, upregulation of VCAM-1 may best explain the observed differences in osteoclast differentiation, fusion, and size in view of the findings of Lu et al. (2011) who showed that RAW264.7 cells cultured on a VCAM-1 coated surface fused substantially more along with upregulated osteoclast gene markers [49]. In this model, the VCAM-1 coating represented VCAM-1 expression by osteosarcoma cells; however, in our model VCAM-1 was directly expressed by the (pre-)osteoclasts themselves, suggesting that VCAM-1 binding could also occur in a paracrine manner. Importantly, foreign body giant cells (FBGC) could not resorb either TCPs or TCPb, indicating that osteoclast-specific machinery is necessary to cellularly degrade these CaPs.

The question remains, is osteoclast resorption and de novo bone formation by osteoinductive CaPs coupled? In Chapter 4, de novo bone formation by TCPs appeared to be linked with its resorption because average bone formation and material resorption occurred to similar extents (Chapter 4). However, closer

analysis of these same data later indicated there was no relationship between resorption and bone induction on a per subject basis (Figure 1, $P = 0.84$).

As it stands, the relationship between osteoclast resorption and osteoinduction by microstructured CaPs is still unclear. But, because it is an important aspect of the performance of CaP bone graft substitutes, this topic will be discussed in more detail in the next chapter.

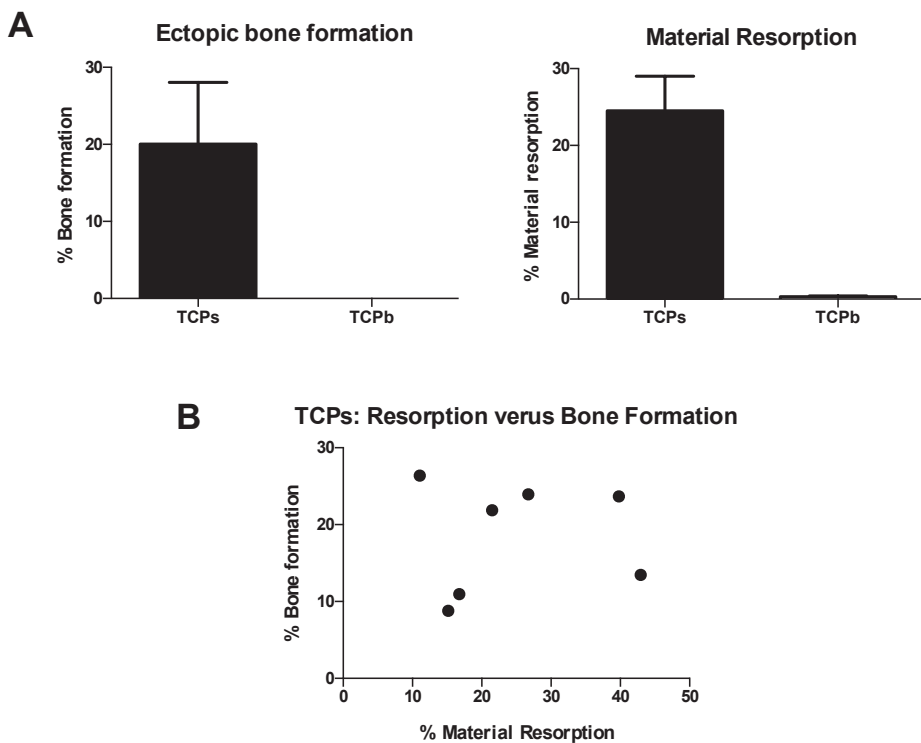


Figure 1. The relationship between material resorption and osteoinduction of TCP in the muscle of dogs after 12 weeks. (A) In aggregate, bone formation and material resorption of osteoinductive TCPs appear to be linked (histomorphometric data represents the mean \pm S.D of $n = 8$ implants, 1 per animal). (B) However, on a per subject basis of the same TCPs implants, there is no relationship between bone formation and material resorption. Spearman's test of correlation: $r = 0.095$, $P = 0.84$. Data taken from the in vivo study presented in Chapter 4.

5 THE INFLAMMATORY RESPONSE AND OSTEOINDUCTION

In addition to osteoclastogenesis, another cellular theory on osteoinduction based on inflammation was also presented in the literature. In multiple articles, Le Nihuouannen et al. (2005) suggested that microporosity may serve to stimulate de novo bone formation by releasing inflammatory microparticles that activate macrophage phagocytosis and secretion of osteogenic cytokines like TNF α [17,50]. Later, Fellah et al. (2007) of the same group showed that BCP microparticles sized < 20 μm provoked the strongest inflammatory reaction *in vivo* compared with larger particles sized 40-80 and 80-200 μm . They later (2010) explored this further *in vitro*, showing that microparticles sized < 20 μm activated the strongest inflammatory response in macrophages in terms of TNF α and IL-6 protein secretion, and that similar concentrations of these cytokines added to the culture medium of MC3T3 cells upregulated their expression of osteoblast genes [51,52]. However, it was not shown if these same cytokines were indeed expressed *in vivo* or if changing the inflammatory response would have any effect on de novo bone formation. Moreover, without other CaP surface structures to compare these *in vivo* and *in vitro* inflammatory responses to de novo bone formation, any link between inflammation and osteoinduction was mainly speculative.

Although Chapter 2 undertook the practical challenge of designing a moldable, osteoinductive CaP putty to aid surgical handling, it also revealed important biological insight into the importance of the early implantation period on osteoinduction. Specifically, the less time it took for a carrier to dissolve, the greater de novo bone formation by the constituent TCP particles. This finding suggested that whatever biological processes were taking place necessary for de novo bone formation were likely occurring in roughly the first 2-3 days after implantation, implicating the innate inflammatory response.

In Chapter 5, by depleting the invading tissue macrophages (and their multinucleated relatives, osteoclasts), osteoinduction was blocked suggesting that inflammation may be specifically activated by surface microstructure to direct subsequent de novo bone formation. However, more *in vivo* studies should be conducted, particularly with earlier time points and the local administration of anti-inflammatory molecules, to investigate how inflammation specifically directs bone formation. A multiplexed ELISA targeting a panel of pro- and anti-inflammatory cytokines present in the soft tissue of the implant would be a useful tool to measure the effects of this treatment.

6 OSTEOIMMUNOLOGY: THE LINK BETWEEN INFLAMMATION, OSTEOCLASTOGENESIS, AND OSTEOINDUCTION?

In view of the apparent importance of CaP surface microstructure in influencing inflammation, osteoclastogenesis, and subsequent osteoinduction, is it possible that all these processes are linked and regulated by an overarching mechanism? Osteoimmunology describes the crosstalk between the bone organ and the immune system – in particular, the relationship between osteoclasts and the immune cells that produce cytokines to regulate them [53]. Because CaPs are immediately subjected to the innate immune system after implantation due to the foreign body response, and because this immune reaction can dictate the formation of osteoclasts and bone through osteoimmunological crosstalk, it is plausible. Based on this paradigm and the results presented in this thesis, we propose a new mechanism for how surface microstructure regulates osteoclastogenesis and subsequent osteoinduction by modulating the initial inflammatory reaction (Figure 2).

Theoretically, inflammation may act in at least two distinct ways to stimulate de novo bone formation. On one hand, it may be that macrophage-mediated inflammation in response to osteoinductive microstructure is the key event in stimulating osteoclastogenesis. For instance, when macrophages interact with osteoinductive microstructure they may be uniquely activated to secrete a particular family of cytokines to stimulate osteoclast differentiation from the invading mononuclear precursors. Indeed, in unpublished *in vitro* results, we have found that macrophages secrete significantly more IL-6 when cultured on cultured on osteoinductive CaP surfaces versus non-inductive CaPs or tissue culture plastic, and IL-6 is known to stimulate osteoclastogenesis through RANK-RANKL signaling [54]. As shown in Chapter 5, the host response to osteoinductive surface microstructure resulted in osteoclast formation, but not in response to non-inductive surface structure; however, when the inflammatory reaction was modulated by liposomal clodronate, osteoclast formation was blocked as was bone formation (Figure 3).

Thus, inflammation in response to surface microstructure may supply the necessary cytokines to stimulate osteoclastogenesis in ectopic locations. In turn, osteoclast formation and survival is strongly promoted by osteoinductive surface structure (Chapters 3, 4, 5, 6), and can also stimulate their secretion of powerful osteoblast-differentiating factors (Chapter 4), similar to bone coupling mechanisms.

On the other hand, macrophage-mediated inflammation may act directly in stimulating osteoblast differentiation through their secretion of osteogenic cytokines such as TNF α and OSM [55–57]. Indeed, in Chapter 4, it was shown that macrophages cultured on osteoinductive TCPs also secreted anabolic factors capable of inducing osteoblast differentiation of MSCs, albeit to a lesser extent than osteoclasts.

In summary, the biological responses of inflammation, osteoclastogenesis, and osteoinduction appear to all be regulated by surface microstructure. To provide a starting point for further research, we present a new hypothesis based on an osteoimmunological paradigm to explain how surface microstructure confers osteoinductivity to CaPs by:

- (1) stimulating the inflammatory response along with osteoclast-inducing cytokines,
- (2) providing an instructive substrate for osteoclast formation and resorption, and
- (3) promoting osteoclast secretion of bone coupling factors leading to osteoblast differentiation and de novo bone formation (Figure 2).

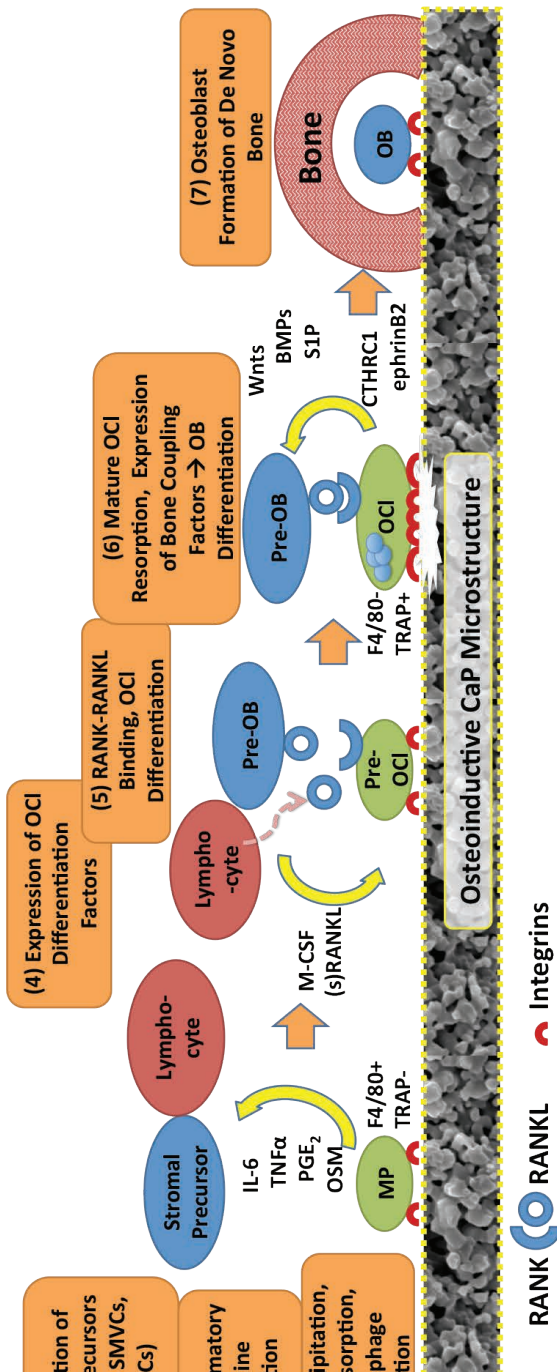


Figure 2. Proposed biological mechanism for osteoinduction. Shortly after implantation of microstructured CaP, macrophages (MP) (characterized by F4/80+ phenotype) adhere to the surface via integrin binding to surface-adsorbed proteins. Surface microstructure activates MP secretion of osteoclast-promotive inflammatory cytokines, some of which may also stimulate osteoblast differentiation directly (e.g., OSM, TNF α). Neighboring lymphocytes and stromal precursors, including pericytes, smooth muscle vascular cells (SMVCs), and MSCs respond to inflammatory MP cytokines by expressing osteoclast differentiation factors M-CSF and RANKL. RANKL is expressed on the surface of (pre-) osteoblasts (pre-OB) and secreted by lymphocytes, in particular T-cells, underscoring the importance of the immune system on the bone organ. When RANK, expressed by pre-osteoclasts (pre-OC), binds its ligand RANKL, osteoclast differentiation is induced. Osteoclast differentiation, fusion, and resorption, and secretion of anabolic coupling factors are further promoted by osteoinductive microstructure. Osteoclast-secreted coupling factors differentiate OB from surrounding pre-OB resulting in bone formation.

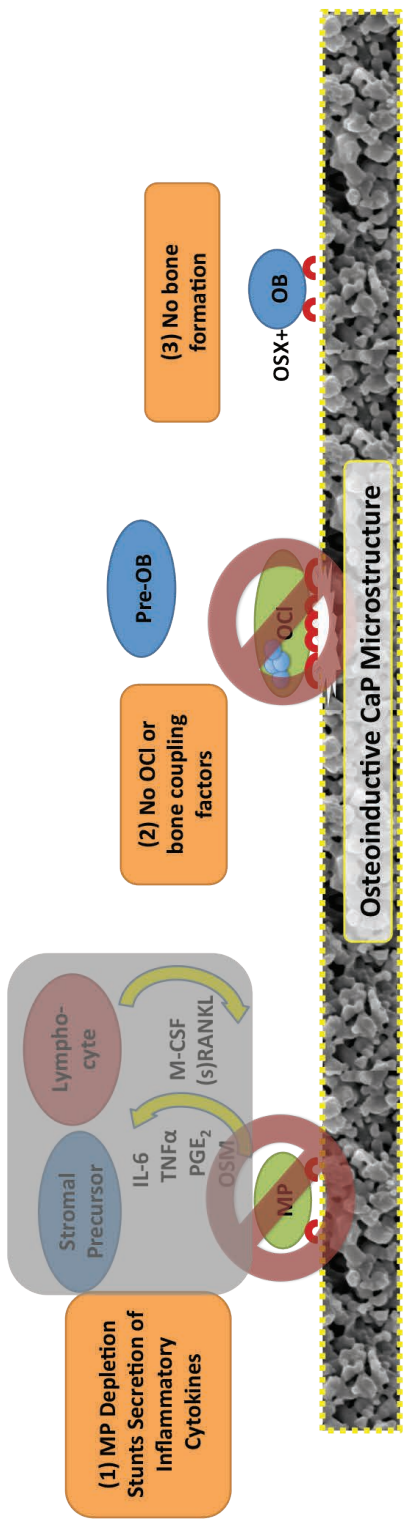


Figure 3. Biological effects of liposomal clodronate treatment. In Chapter 5, liposomal clodronate (LipClod) partially depleted MP and completely blocked osteoclast formation. Consequently no bone formation was observed although Osterix (OSX) positive pre-OB were still present on the surface of TCPs + LipClod. In contrast, no OSX+ cells were present in non-inductive TCPb control samples.

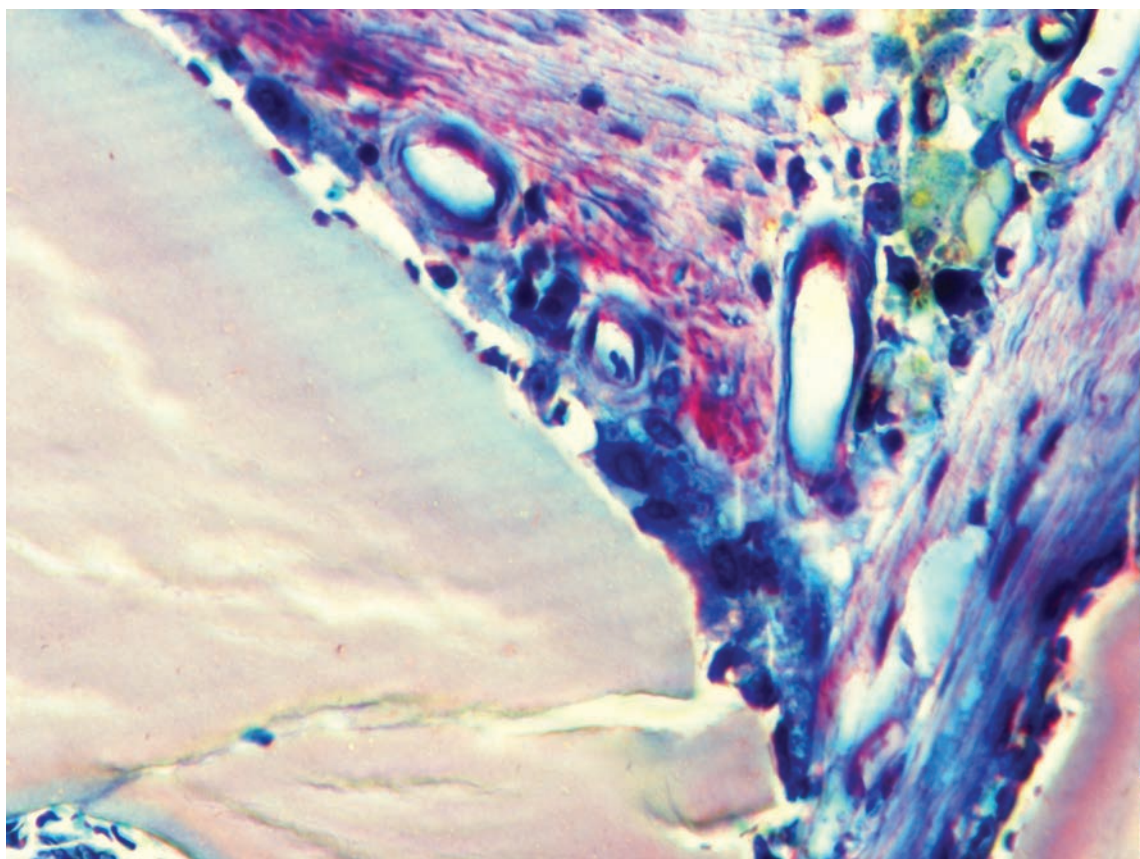
R E F E R E N C E S

- [1] Yuan H, de Bruijn JD, Zhang X, van Blitterswijk CA, de Groot K. Osteoinduction by porous alumina ceramic. *Eur Conf Biomater*, London, UK: 2001, p. 209.
- [2] Fujibayashi S, Neo M, Kim H-M, Kokubo T, Nakamura T. Osteoinduction of porous bioactive titanium metal. *Biomaterials* 2004;25:443–50.
- [3] LeGeros RZ. Calcium phosphate-based osteoinductive materials. *Chem Rev* 2008;108:4742–53.
- [4] Barradas AMC, Yuan H, van Blitterswijk CA, Habibovic P. Osteoinductive biomaterials: current knowledge of properties, experimental models and biological mechanisms. *Eur Cell Mater* 2011;21:407–29.
- [5] Yamasaki H, Sakai H. Osteogenic response to porous hydroxyapatite ceramics under the skin of dogs. *Biomaterials* 1992;13:308–12.
- [6] Yuan H, Kurashina K, de Bruijn JD, Li Y, de Groot K, Zhang X. A preliminary study on osteoinduction of two kinds of calcium phosphate ceramics. *Biomaterials* 1999;20:1799–806.
- [7] Yuan H, De Bruijn JD, Li Y, Feng J, Yang Z, De Groot K, et al. Bone formation induced by calcium phosphate ceramics in soft tissue of dogs: a comparative study between porous alpha-TCP and beta-TCP. *J Mater Sci Mater Med* 2001;12:7–13.
- [8] Habibovic P, Sees TM, van den Doel MA, van Blitterswijk CA, de Groot K. Osteoinduction by biomaterials--physicochemical and structural influences. *J Biomed Mater Res A* 2006;77:747–62.
- [9] Habibovic P, Yuan H, van den Doel M, Sees TM, van Blitterswijk CA, de Groot K. Relevance of osteoinductive biomaterials in critical-sized orthotopic defect. *J Orthop Res* 2006;24:867–76.
- [10] Habibovic P, Yuan H, van der Valk CM, Meijer G, van Blitterswijk CA, de Groot K. 3D microenvironment as essential element for osteoinduction by biomaterials. *Biomaterials* 2005;26:3565–75.
- [11] Yuan H, Fernandes H, Habibovic P, de Boer J, Barradas AMC, de Ruiter A, et al. Osteoinductive ceramics as a synthetic alternative to autologous bone grafting. *Proc Natl Acad Sci U S A* 2010;107:13614–9.
- [12] Fukuda A, Takemoto M, Saito T, Fujibayashi S, Neo M, Pattanayak DK, et al. Osteoinduction of porous Ti implants with a channel structure fabricated by selective laser melting. *Acta Biomater* 2011;7:2327–36.
- [13] Ripamonti U, Crooks J, Kirkbride AN. Sintered porous hydroxyapatites with intrinsic osteoinductive activity: geometric induction of bone formation. *South African J Sci* 1999;335–43.
- [14] Yuan H, de Bruijn JD. Osteoinductive calcium phosphates. U.S. Patent 7,942,934, 2009.
- [15] Carano RA, Filvaroff EH. Angiogenesis and bone repair. *Drug Discov Today* 2003;8:980–9.
- [16] Kondo N, Ogose A, Tokunaga K, Umezawa H, Arai K, Kudo N, et al. Osteoinduction with highly purified beta-tricalcium phosphate in dog dorsal muscles and the proliferation of osteoclasts before heterotopic bone formation. *Biomaterials* 2006;27:4419–27.
- [17] Le Nihouannen D, Daculsi G, Saffarzadeh A, Gauthier O, Delplace S, Pilet P, et al. Ectopic bone formation by microporous calcium phosphate ceramic particles in sheep muscles. *Bone* 2005;36:1086–93.
- [18] Daculsi G, Layrolle P. Osteoinductive Properties of Micro Macroporous Biphasic Calcium Phosphate Bioceramics. *Key Eng Mater* 2004;254–256:1005–8.
- [19] Yuan H, Van Den Doel M, Li S, Van Blitterswijk CA, De Groot K, De Bruijn JD. A comparison of the osteoinductive potential of two calcium phosphate ceramics implanted intramuscularly in goats. *J Mater Sci Mater Med* 2002;13:1271–5.
- [20] Ripamonti U. The morphogenesis of bone in replicas of porous hydroxyapatite obtained from conversion of calcium carbonate exoskeletons of coral. *J Bone Joint Surg Am* 1991;73:692–703.
- [21] Groot K De. Carriers That Concentrate Native Bone Morphogenetic Protein in Vivo. *Tissue Eng* 1998;4:337–41.
- [22] Daculsi G, LeGeros RZ, Heughebaert M, Barbieu I. Formation of carbonate-apatite crystals after implantation of calcium phosphate ceramics. *Calcif Tissue Int* 1990;46:20–7.
- [23] Barradas AMC, Monticone V, Hulsman M, Danoux C, Fernandes H, Tahmasebi Birgani Z,

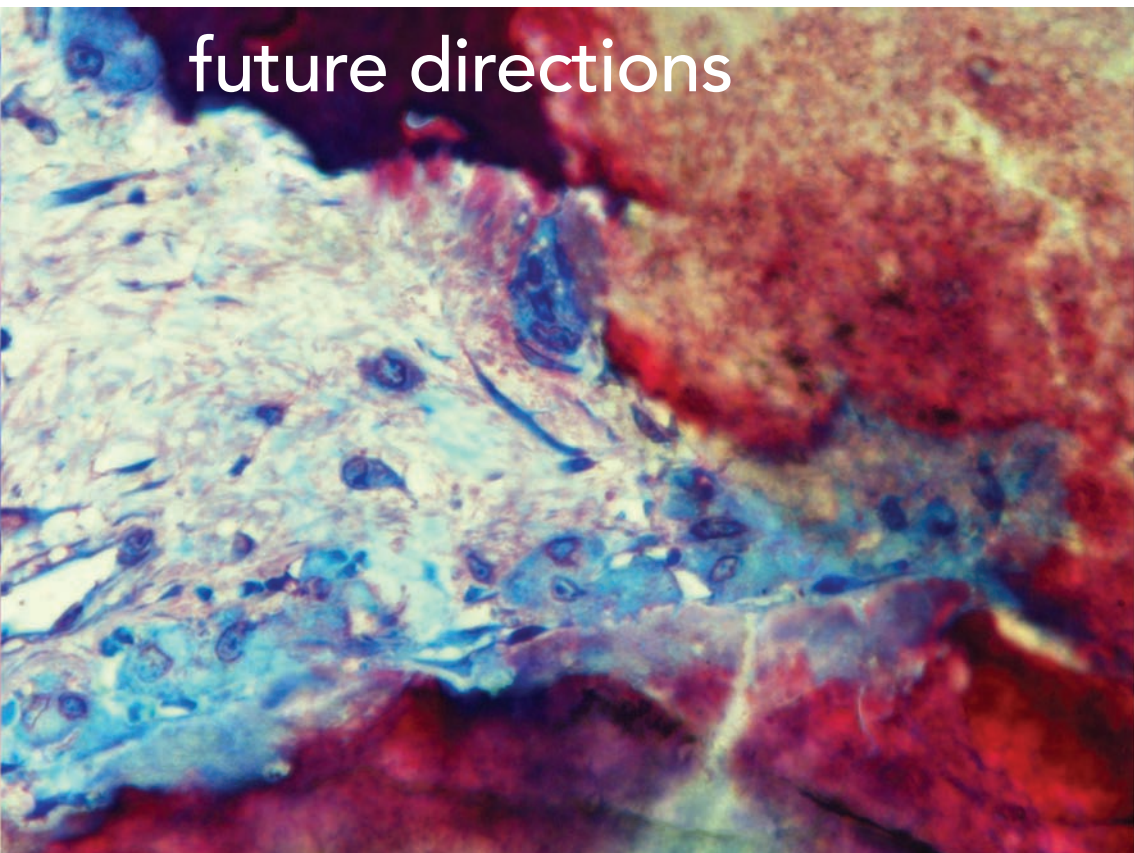
- et al. Molecular mechanisms of biomaterial-driven osteogenic differentiation in human mesenchymal stromal cells. *Integr Biol (Camb)* 2013;5:920–31.
- [24] Eyckmans J, Roberts SJ, Bolander J, Schroten J, Chen CS, Luyten FP. Mapping calcium phosphate activated gene networks as a strategy for targeted osteoinduction of human progenitors. *Biomaterials* 2013;34:4612–21.
- [25] Chai YC, Roberts SJ, Desmet E, Kerckhofs G, van Gastel N, Geris L, et al. Mechanisms of ectopic bone formation by human osteoprogenitor cells on CaP biomaterial carriers. *Biomaterials* 2012;33:3127–42.
- [26] Beck GR. Inorganic phosphate as a signaling molecule in osteoblast differentiation. *J Cell Biochem* 2003;90:234–43.
- [27] LeGeros RZ. Biodegradation and bioresorption of calcium phosphate ceramics. *Clin Mater* 1993;14:65–88.
- [28] Anderson J, Rodriguez A, Chang D. Foreign body reaction to biomaterials. *Semin Immunol* 2008;20:86–100.
- [29] Salo J, Lehenkari P, Mulari M, Metsikkö K, Väänänen HK. Removal of osteoclast bone resorption products by transcytosis. *Science* 1997;276:270–3.
- [30] Klar RM, Duarte R, Dix-Peek T, Dickens C, Ferretti C, Ripamonti U. Calcium ions and osteoclastogenesis initiate the induction of bone formation by coral-derived macroporous constructs. *J Cell Mol Med* 2013;17:1444–57.
- [31] Akiyama N, Takemoto M, Fujibayashi S, Neo M, Hirano M, Nakamura T. Difference between dogs and rats with regard to osteoclast-like cells in calcium-deficient hydroxyapatite-induced osteoinduction. *J Biomed Mater Res A* 2011;96:402–12.
- [32] Tanaka T, Saito M, Chazono M, Kumagae Y, Kikuchi T, Kitasato S, et al. Effects of alendronate on bone formation and osteoclastic resorption after implantation of beta-tricalcium phosphate. *J Biomed Mater Res A* 2010;93:469–74.
- [33] Fukuda C, Norihiro A, Mitsuru T, Shunsuke F, Masahi N, Takahashi N. Local application of alendronate on β -tricalcium phosphate accelerated induction of osteogenesis with formation of giant osteoclast-like cell. *J Biomater Nanobiotechnol* 2012;03:169–77.
- [34] Charles JF, Aliprantis AO. Osteoclasts: more than “bone eaters.” *Trends Mol Med* 2014;1–11.
- [35] Zinger O, Zhao G, Schwartz Z, Simpson J, Wieland M, Landolt D, et al. Differential regulation of osteoblasts by substrate microstructural features. *Biomaterials* 2005;26:1837–47.
- [36] Gomi K, Davies JE. Guided bone tissue elaboration by osteogenic cells in vitro. *J Biomed Mater Res* 1993;27:429–31.
- [37] Webster T. Enhanced functions of osteoblasts on nanoporous ceramics. *Biomaterials* 2000;21:1803–10.
- [38] Lee SJ, Choi JS, Park KS, Khang G, Lee YM, Lee HB. Response of MG63 osteoblast-like cells onto polycarbonate membrane surfaces with different micropore sizes. *Biomaterials* 2004;25:4699–707.
- [39] Kostenuik PJ, Bolon B, Morony S, Daris M, Geng Z, Carter C, et al. Gene therapy with human recombinant osteoprotegerin reverses established osteopenia in ovariectomized mice. *Bone* 2004;34:656–64.
- [40] Wenisch S, Stahl J-P, Horas U, Heiss C, Kilian O, Trinkaus K, et al. In vivo mechanisms of hydroxyapatite ceramic degradation by osteoclasts: fine structural microscopy. *J Biomed Mater Res A* 2003;67:713–8.
- [41] Yamada S, Heymann D, Bouler JM, Daculsi G. Osteoclastic resorption of calcium phosphate ceramics with different hydroxyapatite/beta-tricalcium phosphate ratios. *Biomaterials* 1997;18:1037–41.
- [42] Heymann D, Pradal G, Benahmed M. Cellular mechanisms of calcium phosphate ceramic degradation. *Histol Histopathol* 1999;14:871–7.
- [43] Klein CP, Patka P, den Hollander W. Macroporous calcium phosphate bioceramics in dog femora: a histological study of interface and biodegradation. *Biomaterials* 1989;10:59–62.
- [44] Geblinger D, Addadi L, Geiger B. Nano-topography sensing by osteoclasts. *J Cell Sci* 2010;123:1814–1814.
- [45] Gomi K, Lowenberg B, Shapiro G, Davies JE. Resorption of sintered synthetic hydroxyapatite by osteoclasts in vitro. *Biomaterials* 1993;14:91–6.

C H A P T E R 7

- [46] Webster TJ, Ergun C, Doremus RH, Siegel RW, Bizios R. Enhanced osteoclast-like cell functions on nanophasic ceramics. *Biomaterials* 2001;22:1327–33.
- [47] Bohner M, Galea L, Doebelin N. Calcium phosphate bone graft substitutes: failures and hopes. *J Eur Ceram Soc* 2012;32:2663–71.
- [48] Geblinger D, Zink C, Spencer ND, Addadi L, Geiger B. Effects of surface microtopography on the assembly of the osteoclast resorption apparatus. *J R Soc Interface* 2012;9:1599–608.
- [49] Lu X, Mu E, Wei Y, Riethdorf S, Yang Q, Yuan M, et al. VCAM-1 promotes osteolytic expansion of indolent bone micrometastasis of breast cancer by engaging $\alpha 4\beta 1$ -positive osteoclast progenitors. *Cancer Cell* 2011;20:701–14.
- [50] Le Nihouannen D, Guehennec L Le, Rouillon T, Pilet P, Bilban M, Layrolle P, et al. Micro-architecture of calcium phosphate granules and fibrin glue composites for bone tissue engineering. *Biomaterials* 2006;27:2716–22.
- [51] Fellah BH, Josselin N, Chappard D, Weiss P, Layrolle P. Inflammatory reaction in rats muscle after implantation of biphasic calcium phosphate micro particles. *J Mater Sci Mater Med* 2007;18:287–94.
- [52] Fellah BH, Delorme B, Sohier J, Magne D, Hardouin P, Layrolle P. Macrophage and osteoblast responses to biphasic calcium phosphate microparticles. *J Biomed Mater Res A* 2010;93:1588–95.
- [53] Nakashima T, Takayanagi H. Osteoimmunology: crosstalk between the immune and bone systems. *J Clin Immunol* 2009;29:555–67.
- [54] Steeve KT, Marc P, Sandrine T, Dominique H, Yannick F. IL-6, RANKL, TNF-alpha/IL-1: interrelations in bone resorption pathophysiology. *Cytokine Growth Factor Rev* 2004;15:49–60.
- [55] Glass GE, Chan JK, Freidin A, Feldmann M, Horwood NJ, Nanchahal J. TNF-alpha promotes fracture repair by augmenting the recruitment and differentiation of muscle-derived stromal cells. *Proc Natl Acad Sci U S A* 2011;108:1585–90.
- [56] Nicolaïdou V, Wong MM, Redpath AN, Ersek A, Baban DF, Williams LM, et al. Monocytes induce STAT3 activation in human mesenchymal stem cells to promote osteoblast formation. *PLoS One* 2012;7(7): e398:e39871.
- [57] Guihard P, Danger Y, Brounais B, David E, Brion R, Delecrin J, et al. Induction of osteogenesis in mesenchymal stem cells by activated monocytes/macrophages depends on oncostatin m signaling. *Stem Cells* 2012;30:762–72.



Perspectives and future directions



1 TUNING RESORPTION AND OSTEOINDUCTION OF CAPS

In view of the findings of this thesis, is it possible to tune CaP surface architecture to maximize osteoinduction and control its resorption at a similar rate? From the standpoint of osteoinduction, there may be a more optimal surface architecture that maximizes bone formation in terms of both volume and kinetics. Based on the current findings that surface grains and pores $\leq 1 \mu\text{m}$ are more osteoinductive than larger grains and micropores, would even smaller surface structure (e.g., $\leq 0.5 \mu\text{m}$) stimulate more bone formation or form it at a faster rate?

With respect to the resorption profile of osteoinductive CaPs, optimizing the surface structure will change the way osteoclasts differentiate and resorb the material based on the results of this thesis and the findings of others [1–3]. Additionally, smaller surface architecture will also increase solution-mediated degradation by increasing the surface area exposed to the body fluid. Because surface structure will simultaneously influence both the osteoinductivity as well as resorption rate, it may also be necessary to tune the solubility of the chemical composition, for instance by changing the HA/TCP ratio of BCP, in order to match the resorption rate with the rate of new bone formation. For instance in Chapter 3, BCP1150 promoted substantial osteoclast formation in dog muscle versus BCP1300 with larger microstructure, but still little resorption was observed probably owing to the high HA content (80%) in the materials.

At the same time, if future studies can definitively prove that osteoclastogenesis is crucial for osteoinduction by CaPs, then tuning surface microstructure to increase osteoclast formation may be a promising strategy to improve their osteoinductive performance. If this is the case, is the resorption of osteoinductive CaPs by osteoclasts synchronized to their anabolic effects on bone formation, similar to bone coupling? In other words, do osteoclast need to be resorbing the material to also secrete osteoblast-differentiating factors? Or is their differentiation and activation (specifically, multinucleation, loss of macrophage-specific markers, formation of actin rings, and TRAP synthesis) without resorption enough to signal differentiation and bone formation by osteoblasts? From the literature on osteoclast biology, this is difficult to answer. For instance, Kreja et al. (2010) and Pederson et al. (2008) independently showed that non-resorbing osteoclasts cultured on tissue culture plastic can secrete osteoblast differentiating factors [4,5], and Karsdal et al. (2007) argued that non-resorbing osteoclasts are actually the source of anabolic factors in certain bone metabolic imbalances such as osteopetrosis [6]. On the other hand, Takeshita et al. (2013) convincingly showed that in normal bone metabolism, osteoclast resorption and bone formation are

coupled through osteoclast expressed CTHRC1, which is strongly up-regulated during resorption of bone or hydroxyapatite but attenuated when resorption is inhibited by alendronate treatment [7].

The relationship between CaP resorption and osteogenesis is also at odds in the biomaterials literature. For instance, Kurashina and colleagues (2002) showed that out of BCPs with three different HA/TCP ratios, only the least resorbed material with the highest HA content was osteoinductive in the muscle of rabbits (there were still, however, multinucleated cells present) [8]. Moreover, Zerbo et al. (2005) showed that TRAP-positive multinucleated cells were hardly present where TCP particles were degraded and bone was formed in sinus lift implantations [9]. On the other hand, Okuda and coworkers (2007) showed that TRAP positive osteoclast-like cells were present in TCP implanted in rabbit femurs and related to subsequent bone formation and material resorption; however, for a fast-resorbing TCP, bone formation was remodeled and replaced by bone marrow, actually decreasing the bone volume suggesting an optimal balance between resorption and osteogenesis [10]. Similarly, Chazono et al. (2004) also showed a time-dependent relationship between the peak number of TRAP-positive multinucleated osteoclast-like cells and osteogenesis by TCP-hyaluronate complexes in rabbit femur defects and suggested that bone coupling mechanisms were at play [11]. At least in the case of osteoinduction, de novo bone formation by nonresorbable microstructured titanium proves that material resorption is not necessary for de novo bone formation [12,13].

A useful study to clarify this relationship between osteoclast resorption and secretion of osteogenic factors on osteoinductive CaPs would be to apply the human osteoclast model (Chapter 6) to both osteoinductive BCP and TCP with equivalent surface microstructure but different chemical composition and intrinsic dissolution rates (e.g., BCP1150 and TCPs). By collecting the osteoclast-conditioned media and applying it to hMSCs to stimulate their osteoblast differentiation (for instance, in terms of ALP activity and mineralization) while also measuring the osteoclast resorption of the materials, osteoclast secretion of osteogenic factors versus resorption could be quantitatively compared.

8

2 IN VITRO MODELS OF OSTEOINDUCTION

In this optimization process, are in vitro models useful to understand or predict osteoinduction by CaPs? Although a novel model was presented in Chapter 4 using the conditioned medium of osteoclasts cultured on osteoinductive Cap to stimulate osteoblast differentiation of hMSCs, this effect might be better demonstrated by co-culturing osteoclasts and hMSCs together on the materials

and evaluating in vitro mineralization – the truest biochemical marker of osteoblast differentiation. After all, some osteoclast-secreted osteogenic factors such as BMPs have a high binding affinity to CaP [14–16] so the most potent anabolic factors may be adsorbed to the material and thus not soluble in the conditioned medium. Of course, the role of osteoclasts in osteoinduction should first be elucidated *in vivo* to make this a worthwhile pursuit.

Other in vitro models of osteoinduction based on osteoblast differentiation of MSCs or related precursors have been proposed also [17–19]. For instance, Barradas et al. (2013) and Yuan et al. (2010) showed that at least on the gene level, osteoblast markers were upregulated in hMSCs cultured on osteoinductive CaPs in proportion to their *in vivo* osteoinductivity. However, one limitation of these studies is that no non-inductive TCP (e.g., TCPb) was tested in order to better discriminate the effects of microstructure versus chemical reactivity. For instance, based on Barradas' hypothesis that Ca^{2+} release plays a principal role in osteoblast differentiation [18], it would be interesting to know if hMSCs differentiate better on non-inductive TCPb than on osteoinductive BCP1150 due to differences in solubility. Moreover, because the defining attribute of a fully differentiated osteoblast is its ability to secrete and mineralize bone matrix, in vitro mineralization of hMSCs should be characterized to verify if these models functionally correlate with *in vivo* bone formation, the way that osteoclast formation was shown to consistently do here. Certainly, the role of microstructure in eventually inducing osteoblast differentiation may involve osteoclast-derived signals as well as direct signals to osteoblast precursors, including not only MSCs but also pericytes [20], smooth muscle vascular cells [21], myoblasts [22], or fibroblasts [23], which have all been shown to be capable of differentiating into osteoblasts given specific stimuli.

Nonetheless, the results of Chapters 3, 4, 5, and 6 support the conclusion that in vitro osteoclastogenesis on microstructured CaPs correlates with *in vivo* osteoinduction, potentially due to the role that osteoclasts play in directing de novo bone formation. Although this link has not been universally validated by the present work, in vitro osteoclastogenesis was consistently correlated with the *in vivo* osteoinductive performance for the two most investigated osteoinductive CaPs – microstructured BCP and TCP [14] – using both the RAW264.7 cell line as well as 4 human monocyte donors.

To supplement the work presented in this thesis and further validate the osteoclastogenesis assay with relation to de novo bone formation *in vivo*, RAW264.7 osteoclasts were cultured on TCP sintered at 1000, 1050, and 1150 °C (Figure 1). The increasing sintering temperature resulted in decreasing

microporosity and increasing microstructure dimensions. Dense cylinders made of the same materials with channels to allow de novo bone formation were also implanted in the muscle of dogs to evaluate their osteoinductive potential. In agreement with the findings of Chapters 3, 4, and 6, in vitro osteoclastogenesis increased with decreasing surface microstructure dimensions in concert with increasing de novo bone formation in vivo (Figure 1). Thus, in vitro osteoclastogenesis on CaPs may be a sensitive, robust indicator of osteoinductive capacity.

3 OSTEOCLASTOGENESIS AND OSTEOINDUCTIVE COMPOSITES

In the present work, it has been proposed that CaP microstructure is the primary trigger for osteoclastogenesis and subsequent de novo bone formation, but what about other materials without microstructure that have also been shown to be osteoinductive? Is there a relationship between osteoclastogenesis and osteoinduction with these materials as well? Recently, Barbieri et al. (2013) described how nano-apatite composites can form de novo bone depending on the molecular weight of their constituent polymer [24,25]. They did this by designing both low and high molecular weight composite pairs composed of 50% (w/w) nano-apatite and either poly(D,L-lactide) (PDL) or poly(L-lactide-co-D,L-lactide) copolymer (PLDL) [24,25]. Because of alkaline surface treatment to expose the apatite crystals, all materials possessed average surface roughness (R_a) ~ 100 nm but none were microporous. In dog and sheep intramuscular models of osteoinduction, both low molecular weight PDL and PLDL (PDL04 and PLDL38) composites formed consistent de novo bone in all implants whereas their high molecular weight counterparts (PDL 45 and PLDL60) formed no bone (Figure 2). These results suggested that polymer molecular weight was somehow promoting or inhibiting de novo bone formation through an unknown mechanism – potentially degradation rate and hydrophilicity. In the histology, prominent multinucleated osteoclast-like cells were observed in contact with the osteoinductive, low molecular weight composites similar to osteoinductive CaPs whereas less inductive, higher molecular weight composites were primarily surrounded by fibrous tissue and less multinucleated cells (Figure 2). To evaluate the universality of the in vitro osteoclastogenesis assay, RAW264.7 osteoclasts were differentiated in the presence of RANKL on these composites in a pilot study. Intriguingly, TRAP activity and cell fusion – markers of osteoclast differentiation – again correlated with relative levels of de novo bone formation in vivo (Figure 2). Because of the limitations of using the RAW264.7 cell line model as well as

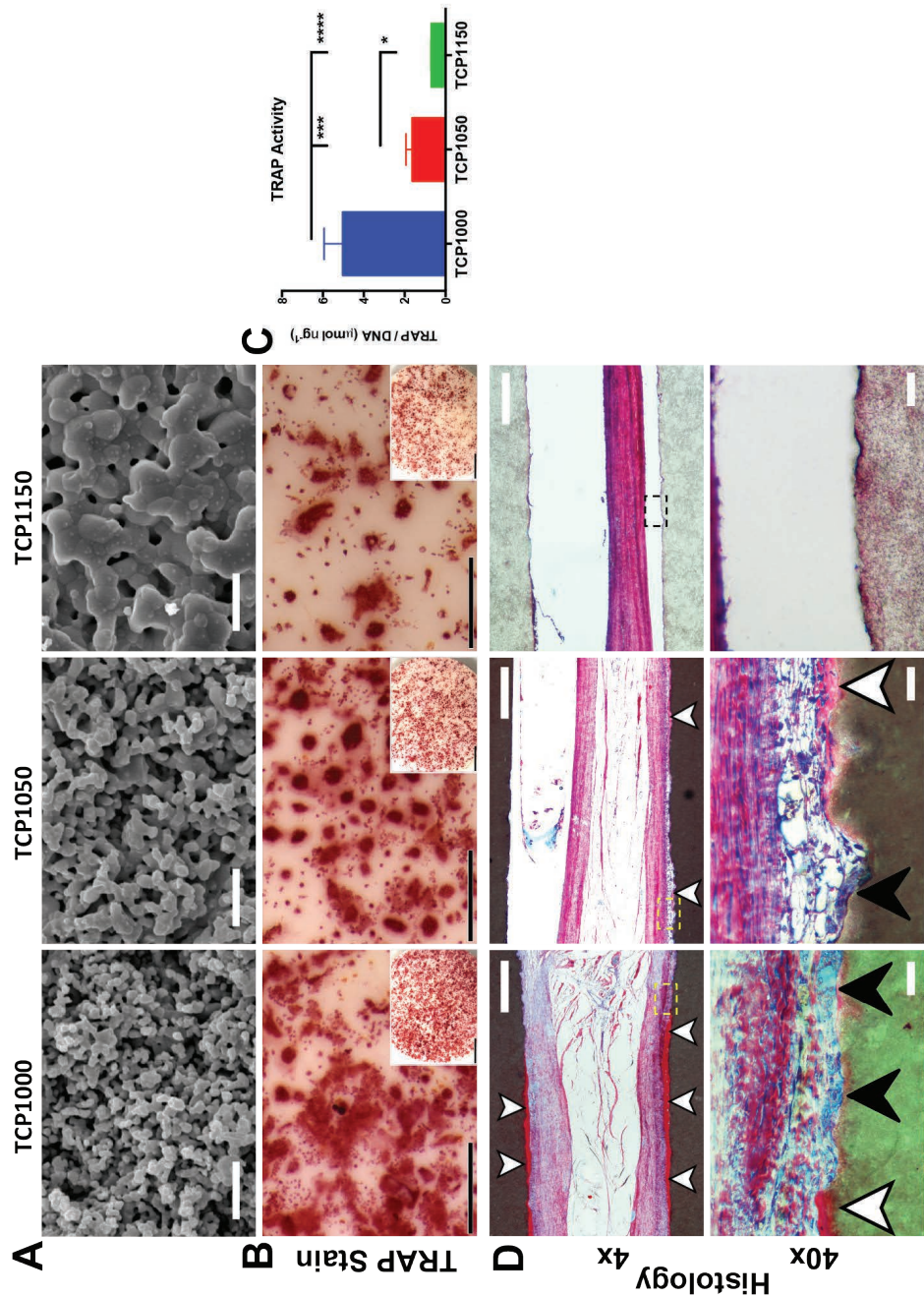
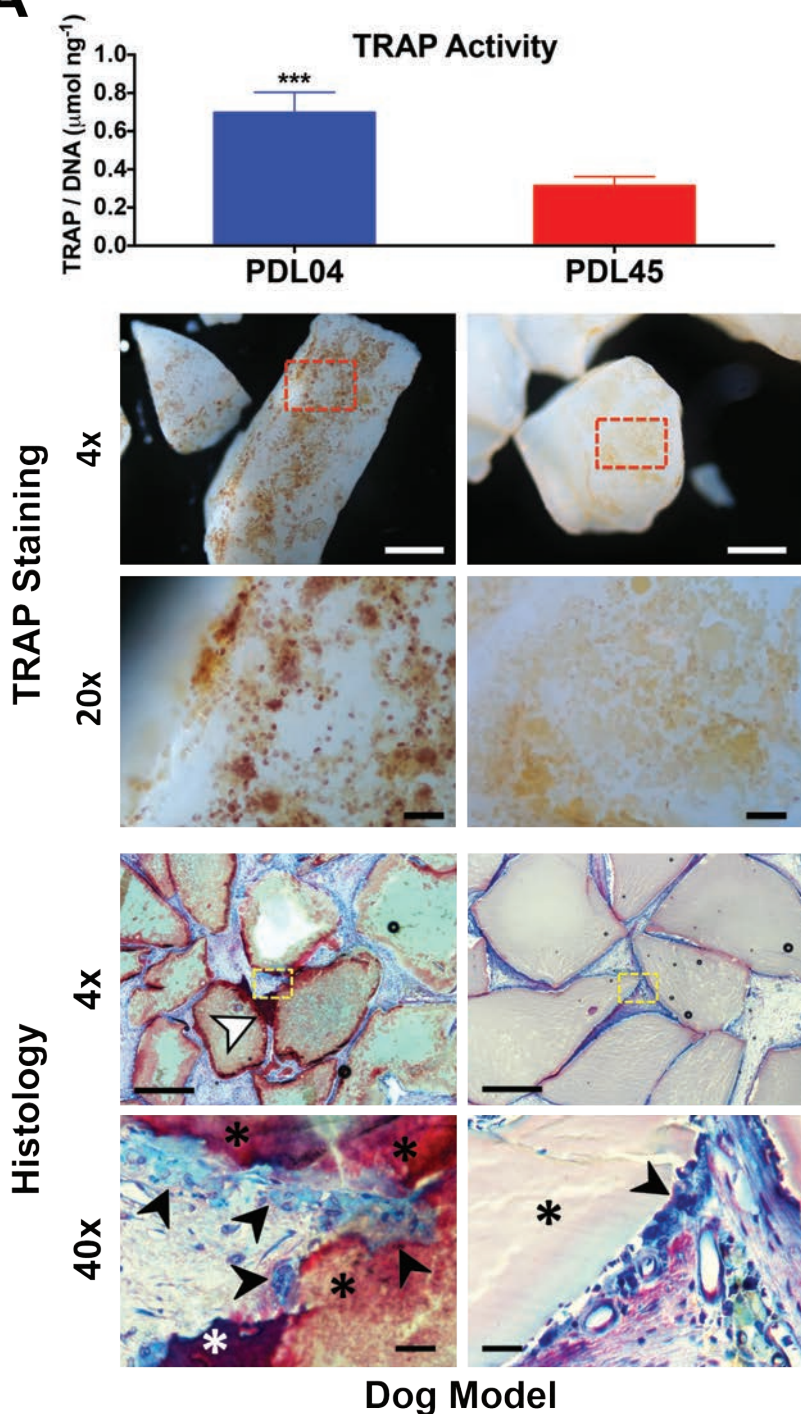


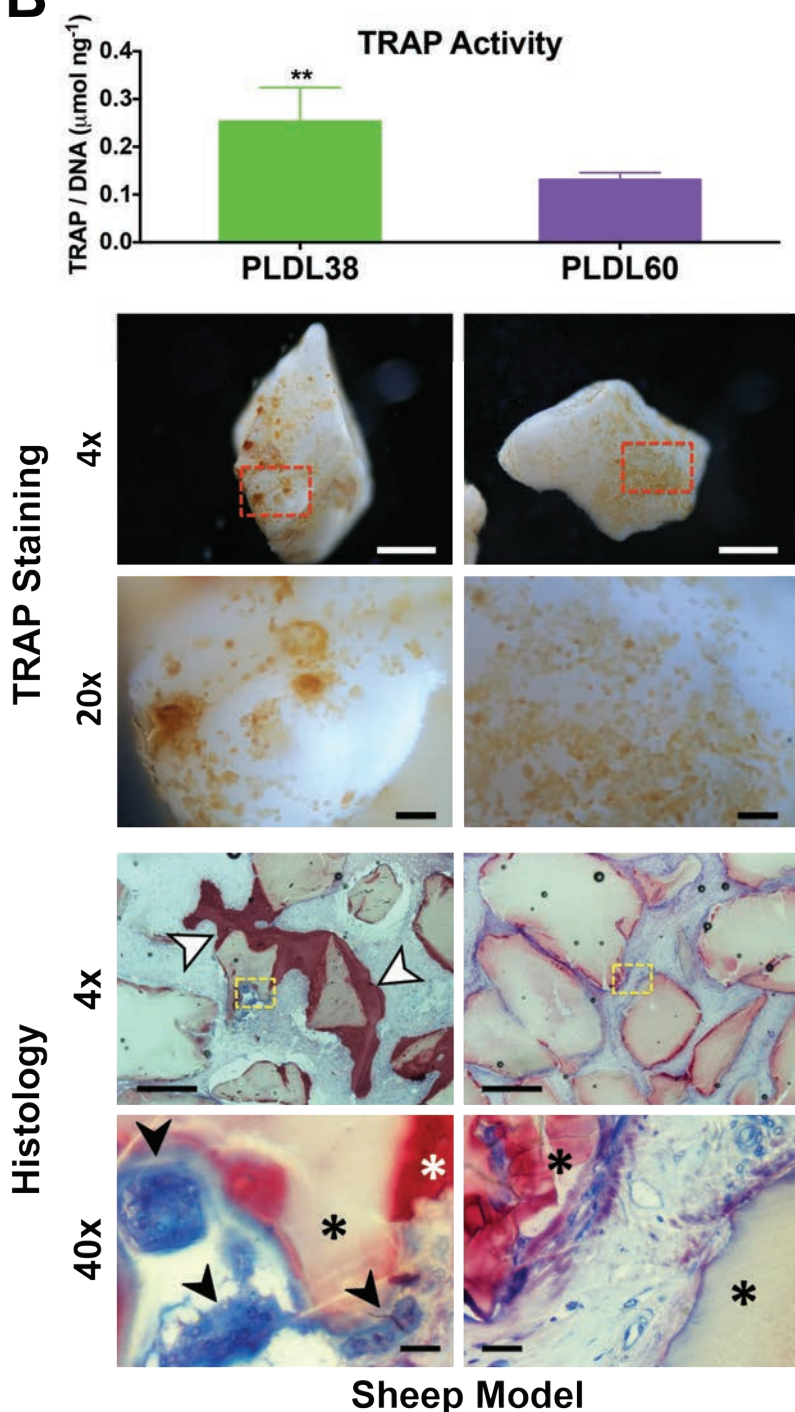
Figure 1, opposite. In vitro osteoclastogenesis on TCP sintered at 1000, 1050, and 1150 °C relates to de novo bone formation. (A) SEM of TCP1000, 1050, and 1150 shows that microstructure dimensions increases with sintering temperature, while microporosity decreases. Scale bar = 5 µm. (B) TRAP staining of RAW264.7 osteoclasts cultured on TCP discs for 5 days shows increasing osteoclast size with decreasing TCP sintering temperature (representative of n = 2 culture replicates). Scale bar = 500 µm, inset scale bar = 2 mm. (C) TRAP activity normalized to DNA in the cell lysate is highest on TCP1000 and decreases significantly with increasing sintering temperatures. Values represent the mean ± s.d. of n = 4 disc replicates; * P < 0.05, *** P < 0.001, **** P < 0.0001. (D) Representative histological sections of dog intramuscular implants after 12 weeks, stained for bone with basic fuchsin/methylene blue. Dense cylinders (brown/sand color) were machined with channels (~ 1 mm) to allow ectopic bone formation (red/pink color denoted by white arrows). De novo bone formation decreased with increasing sintering temperature: TCP1000 induced the most bone and TCP1150 induced none. Multinucleated cells (black arrows) formed prominently on the surface of TCP1000 but to a lesser extent on TCP1050, and few if any formed on TCP1150. Soft tissue did not bond strongly to TCP1150 and detached from the surface during processing (fuchsia/purple color). 4x scale bar = 250 µm; 40x scale = 25 µm. Materials courtesy of Dr. Huipin Yuan.

Figure 2, following pages. In vitro osteoclastogenesis on nano-apatite composites relates to multinucleated cell and de novo bone formation in vivo. RAW264.7 macrophages were cultured in the presence of RANKL on low and high molecular weight composite particles composed of nano-apatite (50% w/w) and either (A) poly(D,L-lactide), PDL or (B) poly(L-lactide-co-D,L-lactide), PLDL. After 4 days culture, osteoclastogenesis was assayed by measuring TRAP enzyme activity normalized to DNA in the cell lysate of particle-adherent cells (mean ± s.d. of n = 5 culture replicates) and staining the enzyme in cells fixated on the particles (representative of n = 2 culture replicates). TRAP staining scale bars: 4x = 250 µm; 20x = 50 µm. In vitro osteoclastogenesis was compared to in vivo multinucleated cell and de novo bone formation in the histology of (A) dog and (B) sheep intramuscular implantation. White arrows and white stars denote de novo bone (stained red), black arrows point to multinucleated cells, and black stars denote composite material. Histology scale bars: 4x = 250 µm; 40x = 25 µm. Materials courtesy of Dr. Davide Barbieri.

(A) TRAP activity was ~2x greater (***, P = 0.0002) in cells cultured on low molecular weight PDL04 than high molecular weight PDL45. TRAP staining showed more intensely stained red multinucleated osteoclast-like cells on PDL04 than PDL45, confirming the biochemical assay. In vivo, PDL04 consistently formed small amounts of de novo bone in all 6 samples implanted in 6 dogs after 12 weeks but no bone was detectable in any of the 6 PDL45 samples implanted in the same animals. Multinucleated osteoclast-like cells abundantly colonized PDL04 in close proximity to de novo bone but their formation on PDL45 was less evident.

(B) Similarly, TRAP activity was ~2x greater (**, P = 0.006) in cells cultured on low molecular weight PLDL38 than high molecular weight PLDL60. TRAP staining of multinucleated osteoclast-like cells was also more intense on PLDL38 than PLDL60. In vivo, PLDL38 formed substantial de novo bone (7.8 ± 2.3 , n = 5) in the muscle of 5 sheep after 24 weeks but no bone was detectable in any of the 5 PLDL60 samples implanted in the same animals. Large multinucleated giant cells and osteoclast-like cells prominently formed on the surface of PLDL38 whereas the PLDL60 surface was typically surrounded by fibrous tissue.

A

B

composite particles, these trends should be validated using the more robust primary human monocyte-derived osteoclast model (Chapter 6) cultured on composite discs.

The question remains how exactly osteoclastogenesis is promoted by osteoinductive materials. It may be due to increased protein absorption or augmented $\text{Ca}^{2+}/\text{P}_i$ signaling, following the theories on osteoinduction already in the literature. Surface microstructure could also promote osteoclastogenesis through mechanotransduction – the conversion of mechanical signals at the cell-substrate interface to gene transcription and lineage commitment in the nucleus. For instance, Dalby and colleagues (2007) elegantly showed that randomly arranged surface pits ($\varnothing 120 \times 100 \text{ nm}$) induced more hMSC differentiation than did pits arranged in an orderly grid, even without osteogenic medium supplements [26]. The molecular mechanism by which the mechanical stimulus from cell-adhesion to a specific topography is converted to transcriptional regulation of cell fate is complex and not fully understood [27]. It may be that the topography of osteoinductive microstructure uniquely changes the focal adhesions and cytoskeletal tension of adherent pre-osteoclasts, which in turn upregulates transcription of osteoclast genes. To explore the molecular mechanism by which osteoclasts differentiate better on osteoinductive versus non-inductive CaPs, a useful *in vitro* study would be to induce osteoclastogenesis on TCPs, TCPb, BCP1150, and BCP1300 then analyze stimulated signaling pathways using whole genome microarray analysis. Next, candidate pathways could be blocked at the gene or protein level using siRNA or antibodies, respectively, to evaluate if they are in fact regulating superior osteoclastogenesis on osteoinductive CaPs.

4 ECTOPIC AND ORTHOTOPIC MODELS OF OSTEINDUCTION

Ectopic models of osteoinduction, such as in the muscle (Chapters 2, 3, 4) or under the skin (Chapter 5), are useful to analyze de novo bone formation in soft tissue where no bone is already present or nearby. Historically, osteoinduction has been most reliably demonstrated in larger mammals such as dogs, goats, sheep, and non-human primates [14]. That is why the FVB mouse model for evaluating osteoinduction described by Barradas et al. (2012) was a valuable step forward in investigating the mechanism of osteoinduction because of the availability of antibodies, a well-sequenced genome, and the alleviated cost and ethical considerations of using large mammals [28]. The authors identified genetic differences between the FVB strain and 9 other strains tested that may have allowed it to form de novo bone in response to osteoinductive TCP.

Still, in both Barradas' study and the FVB mouse study here (Chapter 5), the amount of subcutaneous bone formation by osteoinductive TCP was tiny in comparison to the amount of bone formed by the same material implanted intramuscularly in dogs (Chapter 4 versus 5). If osteoclasts are directly related to de novo bone formation, species differences in osteoclastogenesis might explain why this is so. Intriguingly, Akiyama et al. (2010) showed that over the course of 6 weeks, on average ~600-1,100 TRAP positive osteoclast-like cells were present in histological sections of osteoinductive calcium deficient HA (CDHA) implanted in dog muscle but only ~10 of these cells were present rat muscle implants. Importantly, microporous CDHA formed no de novo bone in rats, but consistently formed bone in dogs. One limitation of the intramuscular dog studies reported in this thesis is that TRAP staining was not possible due to the embedding procedure because the high temperatures of MMA polymerization likely inactivated the enzyme. However, if we compare the small amount of TRAP staining present in TCPs in the FVB mouse model (Chapter 5) with the large amount of TRAP staining in a similarly osteoinductive TCP implanted in the muscle of dogs reported by Kondo et al. (2006), then it is possible that inferior osteoclast formation in FVB mice explains the small amount of de novo bone in comparison to what was observed in dogs.

Orthotopic models of osteoinduction also exist which serve to more directly explain how osteoinductive materials can be applied to repair critical sized bone defects in the clinic. For instance, Habibovic et al. (2006) and Yuan et al. (2010) both demonstrated that microstructured CaPs induce more bone in critical sized os ilium defects than non-microstructured CaPs, which they showed were at levels comparable to autologous bone or BMPs [19,29]. Posterolateral fusion can also be considered a critical sized defect model because osteoinductive stimulus is needed to form bone between the transverse processes of the vertebrae and make a bony bridge [30]. In these orthotopic sites, it is unclear how microstructure may affect osteoclastogenesis and cellular resorption because an immediate source of mature osteoclasts would already be present in the surrounding bone, rather than differentially induced by the microstructure as in the ectopic studies shown in this thesis (Chapter 5). Indeed, orthotopic studies to study the role of microstructure on osteoclastogenesis are the obvious next steps to translate the fundamental findings of this work to the bedside.

5 COMMERCIALIZATION OF INSTRUCTIVE BIOMATERIALS

At the moment, no FDA-approved bone graft substitutes strictly comprising

CaP made the claim of osteoinduction [31,32]. Instead, the approved bone graft substitutes making this claim contained either (1) demineralized bone matrix with intrinsic BMPs, (2) recombinant BMPs, (3) allogeneic stem cells, or (4) were combined with bone marrow aspirate during surgery. Of course, a CaP that is osteoinductive without bone marrow aspirate, expensive BMPs, allogeneic cells, or lot-to-lot variability of DBM would presumably be attractive for use in the clinic for a variety of reasons. Because there is no preexisting CaP bone graft substitute approved with an osteoinductive claim, FDA approval of an osteoinductive CaP via the “fast-tracked” 510(k) pathway based on a predicate device is likely not possible; instead, pre-market approval requiring clinical trials may be necessary. Still, microstructured TCP (CuriOs, Progentix Orthobiology B.V.) similar to TCPs used here is approved by the FDA for orthopaedic and craniomaxillofacial use without the claim of osteoinductivity.

Alternatively, it may be possible to apply the knowledge gained here to make other biomaterials that guide a specific tissue response through a specifically designed surface structure. For instance, material surfaces that modulate the innate immune reaction would be useful for applications where inflammation or fibrous tissue formation are key failure modes [33]. For instance, by applying the nearly inert microporous structure of TCPb to a biopolymer film, a “smart” surgical membrane or vascular graft could deter multinucleated cell formation and fibrous tissue encapsulation similar to the tissue response of TCPb (Chapter 4). According to the literature, this type of non-fibrotic tissue response would be beneficial to their purpose [34]. Indeed, companies already exist which produce polymer films to guide vascularization and mitigate the foreign body response by virtue of precise surface pore size that promotes angiogenesis [35] (e.g., Healionics, USA).

Might it also be possible to induce de novo cartilage formation instead of bone using surface microstructure? Engler et al. (2006) described how substrate stiffness is a critical parameter in the fate of adhered stem cells and a less stiff, more elastic substrate was shown to be conducive to chondrocyte differentiation [36]. Perhaps by imparting a specific surface microstructure to a biodegradable polymer matrix more elastic and far less stiff than CaP, “chondroinduction” could be achieved.

On the horizon, there are certainly wide-ranging possibilities, both in and outside the field of bone regeneration, for designing tissue-instructive biomaterials by tuning their surface microstructure. With more research, topographical control of tissue response could be a key biomaterial feature in the future of regenerative medicine.

R E F E R E N C E S

- [1] Gomi K, Lowenberg B, Shapiro G, Davies JE. Resorption of sintered synthetic hydroxyapatite by osteoclasts in vitro. *Biomaterials* 1993;14:91–6.
- [2] Webster TJ, Ergun C, Doremus RH, Siegel RW, Bizios R. Enhanced osteoclast-like cell functions on nanophasic ceramics. *Biomaterials* 2001;22:1327–33.
- [3] Geblinger D, Zink C, Spencer ND, Addadi L, Geiger B. Effects of surface microtopography on the assembly of the osteoclast resorption apparatus. *J R Soc Interface* 2012;9:1599–608.
- [4] Kreja L, Brenner RE, Tautzenberger A, Liedert A, Friemert B, Ehrnthal C, et al. Non-resorbing osteoclasts induce migration and osteogenic differentiation of mesenchymal stem cells. *J Cell Biochem* 2010;109:347–55.
- [5] Pederson L, Ruan M, Westendorf JJ, Khosla S, Oursler MJ. Regulation of bone formation by osteoclasts involves Wnt/BMP signaling and the chemokine sphingosine-1-phosphate. *Proc Natl Acad Sci U S A* 2008;105:20764–9.
- [6] Karsdal MA, Martin TJ, Bollerslev J, Christiansen C, Henriksen K. Are nonresorbing osteoclasts sources of bone anabolic activity? *J Bone Miner Res* 2007;22:487–94.
- [7] Takeshita S, Fumoto T, Matsuoka K, Park K, Aburatani H, Kato S, et al. Osteoclast-secreted CTHRC1 in the coupling of bone resorption to formation. *J Clin Invest* 2013;123:3914–24.
- [8] Kurashina K, Kurita H, Wu Q, Ohtsuka A, Kobayashi H. Ectopic osteogenesis with biphasic ceramics of hydroxyapatite and tricalcium phosphate in rabbits. *Biomaterials* 2002;23:407–12.
- [9] Zerbo IR, Bronckers ALJJ, de Lange G, Burger EH. Localisation of osteogenic and osteoclastic cells in porous beta-tricalcium phosphate particles used for human maxillary sinus floor elevation. *Biomaterials* 2005;26:1445–51.
- [10] Okuda T, Ioku K, Yonezawa I, Minagi H, Kawachi G, Gonda Y, et al. The effect of the microstructure of beta-tricalcium phosphate on the metabolism of subsequently formed bone tissue. *Biomaterials* 2007;28:2612–21.
- [11] Chazono M, Tanaka T, Komaki H, Fujii K. Bone formation and bioresorption after implantation of injectable beta-tricalcium phosphate granules-hyaluronate complex in rabbit bone defects. *J Biomed Mater Res A* 2004;70:542–9.
- [12] Fujibayashi S, Neo M, Kim H-M, Kokubo T, Nakamura T. Osteoinduction of porous bioactive titanium metal. *Biomaterials* 2004;25:443–50.
- [13] Fukuda A, Takemoto M, Saito T, Fujibayashi S, Neo M, Pattanayak DK, et al. Osteoinduction of porous Ti implants with a channel structure fabricated by selective laser melting. *Acta Biomater* 2011;7:2327–36.
- [14] Barradas AMC, Yuan H, van Blitterswijk CA, Habibovic P. Osteoinductive biomaterials: current knowledge of properties, experimental models and biological mechanisms. *Eur Cell Mater* 2011;21:407–29.
- [15] Ripamonti U. Osteoinduction in porous hydroxyapatite implanted in heterotopic sites of different animal models. *Biomaterials* 1996;17:31–5.
- [16] Yuan H, Kurashina K, de Brujin JD, Li Y, de Groot K, Zhang X. A preliminary study on osteoinduction of two kinds of calcium phosphate ceramics. *Biomaterials* 1999;20:1799–806.
- [17] Barradas AMC, Fernandes HAM, Groen N, Chai YC, Schrooten J, van de Peppel J, et al. A calcium-induced signaling cascade leading to osteogenic differentiation of human bone marrow-derived mesenchymal stromal cells. *Biomaterials* 2012;33:3205–15.
- [18] Barradas AMC, Monticone V, Hulsman M, Danoux C, Fernandes H, Tahmasebi Birgani Z, et al. Molecular mechanisms of biomaterial-driven osteogenic differentiation in human mesenchymal stromal cells. *Integr Biol (Camb)* 2013;5:920–31.
- [19] Yuan H, Fernandes H, Habibovic P, de Boer J, Barradas AMC, de Ruiter A, et al. Osteoinductive ceramics as a synthetic alternative to autologous bone grafting. *Proc Natl Acad Sci U S A* 2010;107:13614–9.
- [20] Doherty MJ, Ashton BA, Walsh S, Beresford JN, Grant ME, Canfield AE. Vascular pericytes express osteogenic potential in vitro and in vivo. *J Bone Miner Res* 1998;13:828–38.
- [21] Steitz SA, Speer MY, Curinga G, Yang H-Y, Haynes P, Aebersold R, et al. Smooth Muscle Cell Phenotypic Transition Associated With Calcification: Upregulation of Cbfa1 and Downregulation of Smooth Muscle Lineage Markers. *Circ Res* 2001;89:1147–54.

C H A P T E R 8

- [22] Katagiri T, Yamaguchi A, Komaki M, Abe E, Takahashi N, Ikeda T, et al. Bone morphogenetic protein-2 converts the differentiation pathway of C2C12 myoblasts into the osteoblast lineage. *J Cell Biol* 1994;127:1755–66.
- [23] Lin WL, McCulloch CA, Cho MI. Differentiation of periodontal ligament fibroblasts into osteoblasts during socket healing after tooth extraction in the rat. *Anat Rec* 1994;240:492–506.
- [24] Barbieri D, Yuan H, Luo X, Farè S, Grijpma DW, de Bruijn JD. Influence of polymer molecular weight in osteoinductive composites for bone tissue regeneration. *Acta Biomater* 2013;9:9401–13.
- [25] Barbieri D. Instructive composites for bone regeneration. Doctoral dissertation, University of Twente, 2012.
- [26] Dalby MJ, Gadegaard N, Tare R, Andar A, Riehle MO, Herzyk P, et al. The control of human mesenchymal cell differentiation using nanoscale symmetry and disorder. *Nat Mater* 2007;6:997–1003.
- [27] Ingber DE. Cellular mechanotransduction: putting all the pieces together again. *FASEB J* 2006;20:811–27.
- [28] Barradas AMC, Yuan H, van der Stok J, Le Quang B, Fernandes H, Chaterjea A, et al. The influence of genetic factors on the osteoinductive potential of calcium phosphate ceramics in mice. *Biomaterials* 2012;33:5696–705.
- [29] Habibovic P, Yuan H, van den Doel M, Sees TM, van Blitterswijk CA, de Groot K. Relevance of osteoinductive biomaterials in critical-sized orthotopic defect. *J Orthop Res* 2006;24:867–76.
- [30] Boden SD, Martin GJ, Morone MA, Ugbo JL, Moskovitz PA. Posterolateral lumbar intertransverse process spine arthrodesis with recombinant human bone morphogenetic protein 2/hydroxyapatite-tricalcium phosphate after laminectomy in the nonhuman primate. *Spine (Phila Pa 1976)* 1999;24:1179–85.
- [31] Greenwald AS, Boden SD, Goldberg VM, Yaszemski M, Heim CS. Bone-graft substitutes: facts, fictions, and applications. *Am. Acad. Orthop. Surg. 73rd Annu. Meet.*, Chicago, Illinois: 2006.
- [32] Miron RJ, Zhang YF. Osteoinduction: a review of old concepts with new standards. *J Dent Res* 2012;91:736–44.
- [33] Hubbell JA, Thomas SN, Swartz MA. Materials engineering for immunomodulation. *Nature* 2009;462:449–60.
- [34] Naito Y, Shinoka T, Duncan D, Hibino N, Solomon D, Cleary M, et al. Vascular tissue engineering: towards the next generation vascular grafts. *Adv Drug Deliv Rev* 2011;63:312–23.
- [35] Marshall AJ, Alvarez M, Maginness M. Implantable medical devices having microporous surface layers and method for reducing foreign body response to the same. U.S. Patent 8372423 B2, 2011.
- [36] Engler AJ, Sen S, Sweeney HL, Discher DE. Matrix elasticity directs stem cell lineage specification. *Cell* 2006;126:677–89.

S U M M A R Y

Calcium phosphate ceramics (CaPs) have been widely used in the clinics to repair bone defects for decades, and as such represent an important subset of biomaterials. Certain CaPs not only act as a template for bony ingrowth (i.e., osteoconductive) but can also stimulate bone formation where no bone previously existed (i.e. osteoinductive) without added stem cells or growth factors. Because of this capacity to form de novo bone tissue, osteoinductive CaPs hold particular promise as a clinically relevant alternative to harvesting the patient's own bone in order to repair large bone defects that will not heal on their own. Despite more than 20 years of research, the material parameters necessary to induce de novo bone formation are still unclear. Furthermore, how uncommitted precursor cells can differentiate into bone forming osteoblasts in non-bony (ectopic) locations can only be speculated.

Concerning the material properties necessary for osteoinduction by CaPs, surface microstructure has been repeatedly shown to be critical, although other parameters like concavities and macropores have also been deemed to be 'essential'. With respect to the biological response necessary for osteoinduction by CaPs, macrophages and their multinucleated relatives, osteoclasts, have been implicated with de novo bone formation but a mechanism has not been clearly explained. Thus, the goal of this thesis was to understand how osteoinductive surface microstructure in particular changes the cell and tissue response toward the eventual formation of de novo bone.

In the first experimental chapter (Chapter 2), unrestricted access of the host to osteoinductive surface microstructure was found to be crucial for de novo bone formation suggesting that the innate inflammatory reaction might play an important role in this process. Substantiating this hypothesis, it was later shown in Chapter 5 that by partially depleting invading macrophages, osteoinduction by the same microstructured CaP was blocked. Following this treatment, osteoclast formation was also completely blocked. Thus, an unencumbered innate inflammatory response was essential for both osteoclastogenesis and de novo bone formation in these experimental models.

In Chapters 3 and 4, osteoinductive surface microstructure of both biphasic calcium phosphate (BCP) and tricalcium phosphate (TCP) specifically augmented osteoclastogenesis *in vitro* (i.e., cell fusion, differentiation, and survival) versus chemically equivalent materials with larger non-inductive surface architecture. Moreover, osteoclasts formed on osteoinductive surface microstructure secreted powerful signals that induced osteoblast differentiation of mesenchymal stem cells without osteogenic supplements in the medium. Thus, surface microstructure was shown to promote osteoclast formation in a process that

could also consequently stimulate osteoblast formation.

Further in Chapters 3 and 4, osteoinductive surface microstructure stimulated osteoclast-like cell formation concurrent with de novo bone formation *in vivo*, correlating with the *in vitro* findings. Specifically, the osteoinductive surface microstructure of BCP and TCP promoted multinucleated osteoclast-like cell formation adjacent to de novo formed bone in the muscle of dogs. However, larger, non-osteoinductive surface architecture was neither populated by osteoclast-like cells nor bone forming osteoblasts. For osteoinductive TCP, the average resorption of the material likely due to disparate presence of osteoclast-like cells was correlated with the amount of de novo bone formation in the implants. In this way, a specific dimensionality of surface structure was shown to be crucial for osteoclast-like cell formation and osteoinduction in a coupled manner.

In Chapter 5, genuine osteoclasts (TRAP positive, F4/80 negative multinucleated cells) were uniquely present on TCP with osteoinductive surface microstructure under the skin of mice, but not on chemically equivalent TCP with larger microstructure. These results clearly showed that microstructure specifically induces osteoclastogenesis in concert with de novo bone formation *in vivo*. After liposomal clodronate treatment to deplete mono- and multinucleated phagocytes, some macrophages were still intact in the central areas of the implants but osteoclasts were completely depleted. Coupled with the lack of de novo bone formation by this treatment, it was concluded that the innate inflammatory reaction and concomitant osteoclastogenesis were essential for de novo bone formation.

In addition to its relationship with de novo bone formation, osteoinductive surface microstructure specifically modulated human osteoclast resorption *in vitro* - in particular, small microstructure ($\sim \leq 1 \mu\text{m}$) stimulated osteoclast resorption of TCP but larger, non-inductive structure decreased their survival and no resorption occurred (Chapter 6). Finally, osteoclastogenesis was also promoted *in vitro* and *in vivo* by nano-apatite composites concurrent with de novo bone formation in dogs and sheep (Chapter 8), proving that this particular cellular response may be a robust indicator of osteoinductive potential of a wide variety of biomaterials as well.

By better understanding the cell and tissue response to osteoinductive calcium phosphate architecture, this thesis lays a biological foundation for their improvement. For instance, in the future it may be possible to stimulate inflammation and osteoclast formation through a drug delivery approach or engineer even smaller surface microstructure in order to more powerfully stimulate osteoinduction by bone graft substitutes.

S A M E N V A T T I N G

Keramische calciumfosfaten (CaPs) worden al jaren in de kliniek gebruikt om botdefecten te repareren. CaPs maken dan ook een belangrijk deel uit van de grotere groep van biomaterialen. Sommige CaPs functioneren niet alleen als mal voor botingroei (osteoconductie), maar kunnen ook botvorming stimuleren op plaatsen waar geen bot is (osteoinductie), zonder de toevoeging van stamcellen of groefactoren. Vanwege deze capaciteit om nieuw botweefsel te vormen, zijn osteoinductieve CaPs een veelbelovend alternatief voor het gebruik van patiënt-eigen bot bij de behandeling van grote botbreuken die niet zelf kunnen helen. Ondanks meer dan 20 jaar onderzoek naar deze materialen, zijn de materiaaleigenschappen die nodig zijn om nieuw bot te vormen nog steeds niet duidelijk. We kunnen alleen maar speculeren over de cellulaire mechanismen die ervoor zorgen dat voorlopercellen differentiëren naar osteoblasten op plekken waar geen bot is.

Een van de materiaaleigenschappen die belangrijk is voor de osteoinductieve capaciteit van de CaPs is de oppervlakte microstructuur. Daarnaast zijn enkele andere parameters ook essentieel om botvorming te induceren. Met betrekking tot de biologische reactie die leidt tot botvorming, wordt gesuggereerd dat macrofagen en osteoclasten een rol spelen in osteoblastdifferentiatie en de daaropvolgende botdepositie. Desondanks is het mechanisme grotendeels onbekend. Het doel van dit proefschrift is dan ook om te begrijpen hoe een osteoinductieve microstructuur de cel- en weefselreactie kan sturen naar het vormen van nieuw bot.

Het eerste experimentele hoofdstuk duidde dat onbeperkte toegang van de gastheercellen tot de osteoinductieve microstructuur cruciaal is voor de vorming van nieuw bot. Dit suggereert dat de afweerreactie een belangrijke rol speelt in dit proces. Overeenkomstig met deze resultaten liet hoofdstuk 5 zien dat bij het decimeren van macrofagen de osteoinductie bij dezelfde microstructuur van CaPs nog verder geïnhibeerd was. Met dezelfde methode was de osteoclastvorming ook geïnhibeerd. Dit versterkt het bewijs dat de angeboren immuunreactie essentieel is voor zowel osteoclastvorming als het nieuw te vormen bot. Deze resultaten laten zien dat in deze experimentele modellen een onbelemmerde onstekingsreactie essentieel is voor het vormen van osteoclasten en het nieuw te vormen bot.

Hoofdstuk 3 en 4 lieten zien dat de osteoinductieve microstructuur van zowel bifasisch calciumfosfaat (BCP) als tricalcium fosfaat (TCP) osteoclast fusie, differentiatie en overleving faciliteert, in tegenstelling tot een chemisch vergelijkbaar materiaal met grotere non-inductieve microstructuur. Bovendien initieerden osteoclasten, gevormd op een osteoinductieve microstructuur, de differentiatie van mesenchymatische stamcellen naar osteoblasten zonder toediening van groefactoren in het medium. Uit deze resultaten kan opgemaakt worden dat de oppervlaktemicrostructuur osteoclastvorming bevordert in een

proces dat tegerlijkertijd osteoblastvorming stimuleert.

Verder toonde hoofdstuk 3 en 4 aan dat een osteoinductieve microstructuur osteoclastachtige celvorming en botvorming *in vivo* stimuleert, wat correleert met de *in vitro* resultaten. De osteoinductieve microstructuur van BCP en TCP stimuleerde meerkerige osteoclastachtige celvorming naast het nieuw gevormde bot in de spieren van honden. Een structuur met een non-osteoinductieve oppervlakte was daarentegen niet geïnfiltreerd met osteoclastachtige cellen en osteoblasten. De gemiddelde resorptie voor osteoinductief TCP was gecorreleerd met de hoeveelheid gevormd bot in de implantaten, waarschijnlijk ten gevolge van de aanwezigheid van osteoclastachtige cellen. Op deze manier werd aangetoond dat een specifieke dimensie van de oppervlaktestructuur cruciaal is voor het vormen van osteoclastachtige cellen en gekoppeld hieraan, osteoinductie.

Hoofdstuk 5 liet zien dat osteoclasten (TRAP postief, F4/80 negatief, meerkerig) aanwezig zijn op TCP met een osteoinductieve microstructuur onder de huid van muizen. Echter, op een chemisch gelijkwaardig TCP met een grotere microstructuur waren geen osteoclasten aanwezig. Deze resultaten laten duidelijk zien dat de microstructuur specifiek osteoclastvorming induceert samen met botvorming *in vivo*. Na de behandeling met liposomale clodronate, om mono- en meerkerige fagocyten te verminderen, waren enkele macrofagen nog steeds aanwezig rond het implantaat, maar de osteoclasten waren compleet afwezig. Door de behandeling met liposomal clodronate was er een gebrek aan botvorming waardoor geconcludeerd kan worden dat de aangeboren onstekingsreactie en osteoclastvorming essentieel zijn om nieuw bot te vormen.

Naast de relatie met het nieuw te vormen bot werd de *in vitro* resorptie door humane osteoclasten ook gemoduleerd door de osteoinductieve microstructuur. Een kleine microstructuur ($\sim \leq 1 \mu\text{m}$) stimuleerde osteoclast resorptie van TCP terwijl een grotere, non-inductieve structuur de overlevingskans van deze cellen verminderde en er geen resorptie plaatsvond (Hoofdstuk 6). Tenslotte werd osteoclastvorming *in vitro* en *in vivo* ook geïnduceerd door een composiet van nano-mineraal terwijl dat samenging met de novo botvorming in honden en schapen (Hoofdstuk 8). Dit wijst erop dat deze specifieke cellulaire reactie een robuuste indicatie kan zijn voor het aantonen van de osteoinductieve eigenschap van een grote verscheidenheid aan biomaterialen.

Dit proefschrift legt een biologische fundering voor het verbeteren van osteoinductieve calciumfosfaten middels het beter begrijpen van de cel en weefselreactie op deze materialen. In de toekomst wordt het misschien mogelijk om inflammatie en osteoclastvorming te stimuleren via een "drug delivery approach" of middels het creëren van een nog kleinere oppervlaktestructuur ter verbetering van de osteoinductieve eigenschappen van botvervangende materialen.

A C K N O W L E D G E M E N T S

This thesis represents an adventure of discovery both scientifically and personally. I still remember the excitement of arriving to my shared home in Utrecht with nothing but 2 duffel bags and a disassembled bike, exhausted from the transatlantic red-eye flight but completely charged to start exploring this city that would be my new home. Five years later, Utrecht is still a fairy-tale place, with a friendly, cozy energy that you can feel right away – perfectly encapsulating the Dutch ideal of “gezelligheid.” Utrecht, I owe you a great deal of gratitude for making the transition from American to European an easy one: always welcoming, continually fun, and forever memorable.

Florence, this adventure would have never begun were it not for you – and because of that, I am honored to thank you first. From our first conversations on Skype while I still lived in Baltimore, I immediately knew that despite the massive transition it would be for me to leave family, friends, and career options in the USA, you would help me succeed across the Atlantic in every way possible. You even convinced me to take the PhD position, something I swore to my colleagues at Hopkins that I would never do. From the first day, you gave me an inordinate amount of trust to do things the way I judged best, but still never ceasing to offer support, solid advice, and a pragmatic view. When I completed my first project and needed to change gears for the rest of my PhD, you again gave me the freedom to take on a far riskier, abstract topic – the cellular mechanism of osteoinduction – and linked up the collaborations that would later define my work and propel our collective success. For me, this was the most enjoyable, fruitful way to be managed. You are simultaneously intuitive and analytical, encouraging and pragmatic – I hope I have learned how to balance these traits like you! And, I hope our adventures in *in vitro* work have stimulated your interest in cell biology to compliment your considerable expertise in material science. Take this heartfelt encouragement from your first PhD student: you were the ideal manager, mentor, and friend that PhDs after me will be blessed to have.

Joost, as my promoter and CEO, this journey also would not have been possible without your guidance and support. You understood early on that my aspirations to earn a PhD in your company were based not only on a passion for science but also a keen interest in translating biomedical research to the clinic. With your success first as a scientist and then as an entrepreneur, I probably could not have learned this from anyone better than you. Although my work may never translate to more fiscal revenue, you were always just as eager as I was to uncover the mysterious biological basis of osteoinduction. I learned how to do world-class research with your expert criticism, innumerable revisions, and meticulous eye for detail and consistency. I’m still amazed at how you can read a 30-page manuscript and identify both a glaring hole in an argument as well as an extra comma where it did not belong. And, to have my English consistently corrected by a non-native speaker will always humble me and make me laugh!

Next, I’m thankful for the rest of my Xpand comrades who helped me along the way through friendship as well as solid scientific feedback. Davide and Xiaoman: As fellow PhDs at Xpand, we will always be able to laugh about the fun challenges of doing research at a company, and I doubt I could have found better scientists to bounce around crazy ideas or mull over difficult data. At conferences or playing pool in town, we shared a lot of good times and I hope our friendship and collegiality continues. To Ruud and Rens, my bioreactor buddies, I owe you thanks for your senses of humor, your patience hearing about my latest exciting but confusing data, and your help with nifty software that could

optimize my workflow. Vincent v. M., thanks for keeping things light, for teasing me when necessary (often), and for balancing out the dull taste of euro-house and stale Heineken with real jazz and Trappist ales. To Marieke and Jinyi, my hardworking students: you truly left a mark on this research and I'm grateful for your perserverance and commitment to our projects. To all of you at Xpand and Cellcotec, thank you for your patience with my atrocious Dutch at lunch and my compulsion to eat all of the cookies in the common pot – you made work a friendly, fun place.

To my lab mates at my 2nd home in Amsterdam, thank you for welcoming me to the 11th floor and making sure that I had just as much (if not more) fun as I did work. Ton, you had a massive impact on my research – lending your in vitro expertise and facilitating many of the experiments that defined this book. Bas, I owe you a special thanks for reminding me what a real love of science looks like while being a great friend. It was also a pleasure to (mostly) kick your ass at basketball and teach the Cloggies a thing or two about the U-S-A!

Vincent, you are my scientific mentor. I'm grateful for your poignant question during our first meeting: "Aren't you being a bit dogmatic, Noel?" and later for reminding me that, "Cells can do anything they want." Considering wild possibilities that challenge the dogma makes science (and life) worth doing. You opened the doors at ACTA wide for me and I hope you agree that it was as much fun as it was fruitful to work together.

Pierre, you also welcomed me to your lab in Nantes with open arms and let me do a dream experiment that would not have been possible otherwise. Plus, the homecooked meals with you and your family were worth the trips in themselves. The same goes for Jerome (mon ami!), Martine, Anne Laure, Meadhbh, and the rest of the INSERM team: thanks for making my stay there warm and fun.

To my friends and colleagues at U. Twente – Jingwei, Niloofar, Febriyani, Ana, Hugo, Ziryan – thanks for the camaraderie over the years. As frequently as the SEM broke down, I knew I had some smart, friendly folks around to lend a hand or grab a cup of coffee instead. Lorenzo, I owe you a special thanks for connecting me with Xpand in the first place while we were still at Hopkins. Were it not for that suggestion, I doubt I would have ever found this little company with big technology, or considered moving to this small but great country to have the time of my life. Thanks for the sage counsel on academia and life through the years – salute!

At the UMC Utrecht, I'd be remiss to not thank Stefan Nierkens for opening up your immunology lab to me and bouncing around ideas. And of course, to my favorite Brabantse buddy, Nard – you're a talented surgeon and a gifted connoisseur of Asian take-out. It's been stellar hanging out with you and Lon; I look forward to hosting you both for Carnival next year!

To my buitenaarder buddies in de 'Trecht – Alistair, Blaise, Kevin, Fraser, Tom, John and Pascale, Davide and Indre, Mike and Renate*, Niels* and Christel* (*honorary buitenaarders), Eleonora and Piero, Christian, Alice, Fiona, Helen – you know I couldn't forget you! From the yearly snow and cycle holidays, to the outrageous costume parties, the weddings, the festivals, Queen's Days followed by King's Days, summer BBQs in the park, learning to ice skate (kinda) with a brakelight on, impromptu dance contests at Hofman, forgetting where or what the Oude Gracht is, late night experiments with Dutch "cuisine", perfecting the Dutch "G," and so many other memories. You have made the last 5 years of my life hilarious, vivid, adventurous, exciting, and connected. I'm blessed to have you as friends and look forward to visits wherever in the world we all end up.

A C K N O W L E D G E M E N T S

And to all my lifelong friends back in the States – I know it hasn't been easy staying in touch when I took off across the Atlantic but thank you so much for continually updating me with your baby photos, the football scores, and the rest of the details that made me feel a part of your lives. If none of this book makes sense, I'll explain it at the next Crunkfest.

Karlijn, you have kept me sane in some of the most hectic times of my life and I'm so thankful for that. I hope that I encourage you as much as you support me! You've teased me that I'm always celebrating something...but the fact of the matter is, the publications, the thesis submission, and the victory of completing this thing simply wouldn't be as sweet without you to share it. Liefje, ik hoop dat wij nog lange, lange tijd samen pittige ontbijtjes zullen maken!

Momma, you always encouraged me to pursue my dreams even if they took me far away. And not just that, you've rooted for me every step of the way as though they were your own dreams. That's selfless love. Without your ceaseless nurturing and sacrifice, there would be no book at all. Now, let's celebrate with some champagne in Paris!

To Aria, my smarter, funnier, and better looking sibling: thanks for putting up with endless talk about science, research, bone, and other nerdy stuff that probably bored you unconscious over the years. That's why when you continually come to share European adventures together it means the world to me. I'm incredibly proud of your achievements just like you are of mine and soon we'll be celebrating more letters behind your name too.

Grandma and Grandpa, I don't have any bigger fans on this planet than you two. Grandma, in a different era I think you with your interest in medicine you would have made a great scientist. And Gramps, blowing that horn for as many decades as you have makes me awfully proud to have inherited your genes – a true legend. I should have gotten you in the lab to make some real discoveries! Thank you for cheering me on from the very start – this book is for you.

Dad: I miss you each and every day, but I know you're getting a great kick out of reading this – laughing, smiling, and beaming proud. And, that makes me proud too.

R E L E V A N T P U B L I C A T I O N S

JOURNAL ARTICLES

Davison N, Yuan H, de Bruijn JD, Barrère-de Groot F. In vivo performance of microstructured calcium phosphate formulated in novel water-free carriers. *Acta Biomater* 2012;8:2759–69.

Davison N, Luo X, Schoenmaker T, Everts V, Yuan H, Barrère-de Groot F, et al. Submicron-scale surface architecture of tricalcium phosphate directs osteogenesis in vitro and in vivo. *Eur Cell Mater* 2014;27:281–97; discussion 296–7.

Davison N, Gamblin A-L, Layrolle P, Yuan H, de Bruijn JD, Barrère-de Groot F. Liposomal clodronate inhibition of osteoclastogenesis and osteoinduction by submicrostructured beta-tricalcium phosphate. *Biomaterials* 2014;35:5088–97.

Davison N, ten Harkel B, Schoenmaker T, Luo X, Yuan H, Everts V, et al. Osteoclast resorption of beta-tricalcium phosphate controlled by surface architecture. *Biomaterials* 2014;35:7441–51.

Davison N, Su J, Yuan H, van den Beucken JJJP, de Bruijn JD, et al. Influence of surface microstructure and chemistry on osteoinduction and osteoclastogenesis by biphasic calcium phosphate discs. Submitted 2014.

Luo X, Barbieri D, Davison N, Yan Y, de Bruijn JD, Yuan H. Zinc in calcium phosphate mediates bone induction: in vitro and in vivo model. *Acta Biomater* 2014;10:477–485.

PATENTS

Yuan H, Barbieri D, de Bruijn JD, de Groot F, Davison N. Injectable and moldable osteoinductive ceramic materials. International Patent Application PCT/EP2010/004548, 2010.

TEXTBOOK CHAPTERS

Davison N, Barrère-de Groot F, Grijpma D. Degradation of biomaterials. In: van Blitterswijk CA, de Boer J, editors. *Tissue Engineering*. 2nd ed. Elsevier: in press.

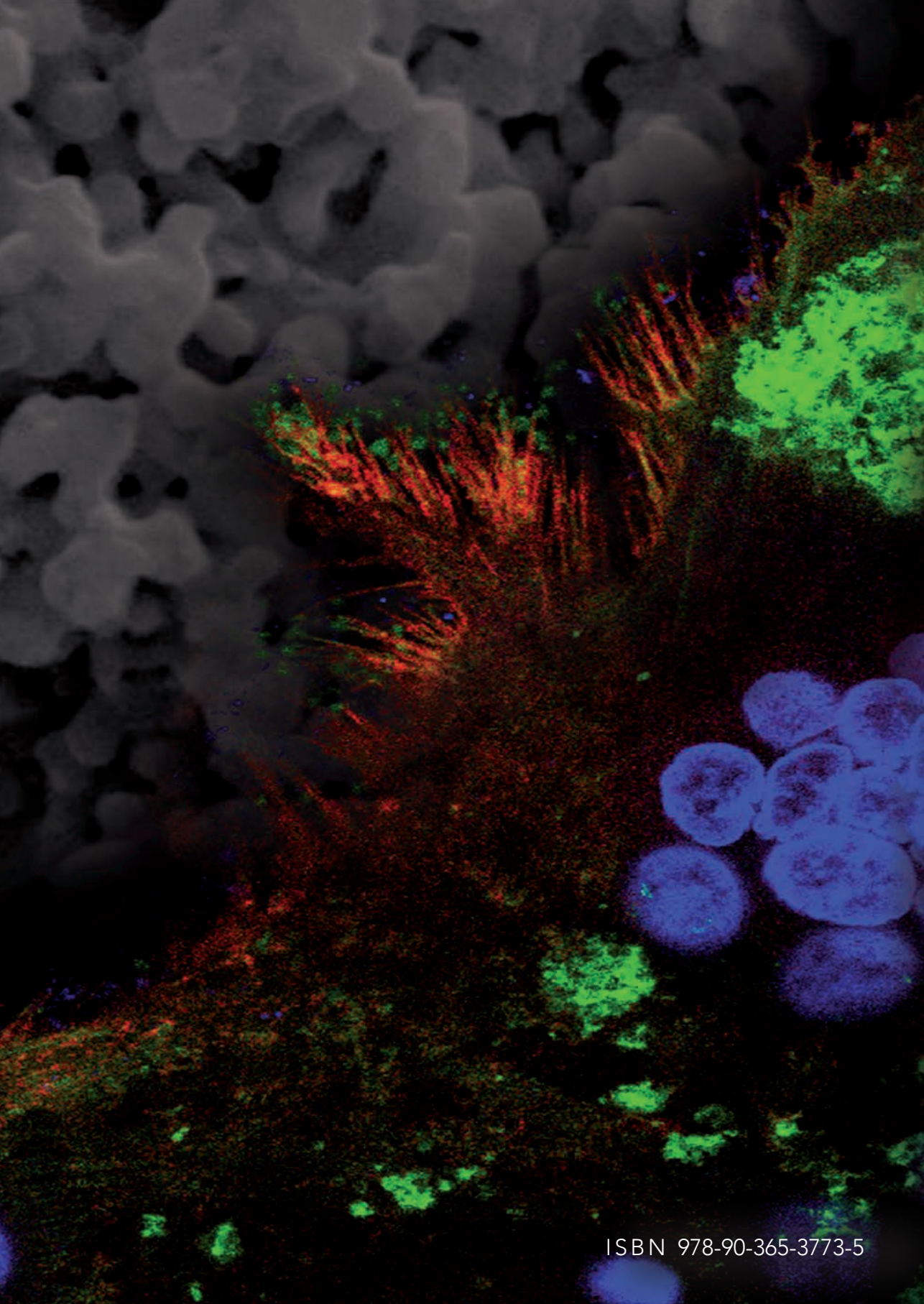
ABOUT THE AUTHOR



Noel was born to Mark and Michelle Davison in Portland, Oregon. Although he swore he would never do a PhD, he was surprised to find that he keenly enjoyed it.

Before the University of Twente, Noel earned his masters degree in biomedical engineering at Johns Hopkins University and his bachelors degree *summa cum laude* in bioengineering at the University of Florida.

He hopes that his love of science takes him to other corners of the globe as a good excuse to try the food.



ISBN 978-90-365-3773-5